The continental intraplate volcanism of Syria: Rift-related or plume-induced

Dissertation
zur Erlangung des Doktorgrades
der Mathematisch-Naturwissenschaftlichen Fakultät
der Christian-Albrechts-Universität
zu Kiel

vorgelegt von
Marc-Sebastian Krienitz

Kiel
2004

Referent/in: .....
Korreferent/in: .....
Tag der mündlichen Prüfung: .....
Zum Druck genehmigt: Kiel, ...

Der Dekan

Ich versichere an Eides statt, dass die vorliegende Abhandlung ausschließlich unter Verwendung der angegeben Hilfsmittel entstanden ist und, abgesehen von der Beratung durch meine akademischen Lehrer, nach Inhalt und Form meine eigene Arbeit darstellt.

Kiel, den .....

.....
Marc-Sebastian Krienitz

CHAPTER THREE
The Afro-Arabian Connection: Volcanism in Syria and the Role of the Afar Plume

Vorwort

Die vorliegende Dissertation besteht aus drei Kapiteln, die zwar unabhängig voneinander publiziert werden können, die in Umfang und innerer Kohärenz aber auch einer monographischen Dissertation entsprechen und denen eine Einführung und Zusammenfassung vorangestellt ist.

Meinem Betreuer Dr. habil. Karsten Haase, auf dessen Anregung hin dieses Projekt zustande kam, möchte ich für seine gute Betreuung meinen herzlichsten Dank aussprechen, ebenso für seinen Enthusiasmus, die vielen Denkanstösse und ausgiebigen Diskussionen während der Entstehung dieser Arbeit. Darüber hinaus bin ich ihm sehr dankbar, daß er mir die Möglichkeit zur Promotion gab, wofür ich ebenfalls Herrn Prof. Peter Stoffers herzlichst danke. Insbesondere gilt mein Dank Prof. Klaus Mezger für die Möglichkeit zur Durchführung der Isotopen-Messungen in Münster sowie für seine hervorragende Betreuung und all die kleinen Kniffe und Tricks bei den Aufschlüssen und während der Messungen. Prof. M. A. Shaikh-Mashail von der Universität Aleppo in Syrien sei für seine Organisation und seine Unterstützung während des Geländeaufenthaltes gedankt, ohne die wahrscheinlich nie eine so ausführliche Beprobung hätte durchgeführt werden können.

Bei Dieter Garbe-Schönberg und dem gesamten Team aus dem fünften Stock möchte ich mich für ihre Unterstützung während der ICP-MS Analytik und für die Messungen bedanken. Peter Appel, Barbara Mader sowie Astrid Weinkauf bin ich für Ihre Hilfe während der RFA und Mikrosondenanalytik dankbar. Paul van den Boogard sei für seine Hilfe und für die Durchführung der Altersdatierungen bedankt. All den Münsteranern, die mir während meines Aufenthaltes zur Seite standen, möchte ich ebenfalls meinen Dank aussprechen, insbesondere Heidi Baier aufgrund ihres Wissens im Labor und ihrer Hilfsbereitschaft.

Gerade im Anfangsstadium der Arbeit gilt mein Dank den „Old Guys“ Helge Möller und Gerald Maroske für Ihre eingehende Unterstützung bei der Internetrecherche, ebenso Christoph Beier und Martin Schodlok für aufmunternden Konversationen.

Außerdem möchte ich all jenen danken, die mir, sei es direkt oder indirekt, geholfen haben, das Projekt zum Abschluß zu bringen.

Für ihr Verständnis und Ihre Unterstützung sowie für das mir entgegen gebrachte Vertrauen und für ihre Liebe danke ich den wichtigsten Menschen in meinem Leben, Nicole und meinen Eltern.

Die vorliegende Arbeit wurde von der Deutschen Forschungsgemeinschaft im Rahmen des Projektes „Der kontinentale Intraplattenvulkanismus Syriens: Einblicke in 170 Millionen Jahre andauernde Magmengenese und Lithosphärenentwicklung“ gefördert (HA 2568/5-1 und HA 2568/5-4).

Einführung und Zusammenfassung

Syrien liegt am nordwestlichen Rand der Arabischen Halbinsel und ist von einer Vielzahl von Miozänen bis rezenten Vulkanfeldern bedeckt. Die Ursache dieses extensiven, intrakontinentalen Vulkanismus ist bis heute nicht geklärt. Im allgemeinen gibt es zwei Modelle zur Erklärung des intrakontinentalen Vulkanismus: (1) das passive Rifting und (2) das aktive Rifting Model. Im Falle des passiven Riftings wird der Vulkanismus durch Lithosphärendehnung, die zur adiabatischen Dekompression und Aufschmelzung von Mantel Material führt, verursacht (Sengör und Burke, 1978). Die Dehnung der Lithospäre ist durch die an den Plattengrenzen auftretenden Zugkräfte bedingt. Der Vulkanismus beim aktiven Rifting hingegen wird durch Mantleplumes initiiert. Mantelplumes bewirken eine regionale Aufdomung der Asthenosphäre, gefolgt von Vulkanismus und Rifting (Sengör und Burke, 1978). Im Detail sind folgende Modelle zur Erklärung der vulkanischen Aktivität im nördlichen Arabien vorgeschlagen worden: (1) die Existenz eine Mantleplumes unter der nördlichen Arabischen Halbinsel (Camp and Roobol, 1992), (2) eine nordwestwärts gerichtete Strömung von heißem asthenosphärischem Material vom Afar Mantelplume entlang der westlichen Arabischen Halbinsel (Camp and Roobol, 1992), (3) durch Lithosphärenrifting verursachte Mobilisierung von Material aus einem fossilen Plumekopf unterhalb der Lithosphäre (Stein and Hofmann, 1992), (4) eine fortschreitende Lithosphärenausdünnung durch die lithosphärische (fossiles Plumematerial) und asthenosphärische Mantelquellen angezapft werden (Bertrand et al., 2003; Shaw et al., 2003). In diesem Zusammenhang ist das Hauptziel dieser Arbeit, die Prozesse zu bestimmen, die den Vulkanismus in Syrien kontrollieren. Im Folgenden werden wir anhand von Haupt-, Spurenelement-, Isotopen- und Altersdaten sowie Aufschmelz-, Fraktionierungs- und Assimilationsmodellierungen zeigen, daß der syrische Vulkanismus hauptsächlich durch einen pulsierenden Mantelplume verursacht wird.

Das erste Kapitel behandelt hauptsächlich die Kontamination primärer Schmelzen durch Material der kontinentalen Kruste. Das Zusammenspiel zwischen Assimilation, fraktionierender Kristallisation (AFC) sowie Variationen in den Aufschmelzgraden führte zur Eruption von zwei verschiedenen Lavasuiten mit unterschiedlicher Haupt- und Spurenelementzusammensetzung und unterschiedlichen Isotopensignaturen. Anhand der P_2O_5 Gehalte konnten die untersuchten Magmen in zwei verschiedene Suiten eingeteilt werden. Die erste Suite ist durch hohe P_2O_5 Gehalte gekennzeichnet im Gegensatz zur zweiten Suite, die durch niedrige P_2O_5 Gehalte gekennzeichnet ist. Die AFC Prozesse, die zur Bildung dieser Suiten führte, sind durch unterschiedliche Isotopensignaturen während der Differentiation sowie durch erniedrigte Ce/Pb und Nb/U Verhältnisse und die Fraktionierung variabler Mengen an Olivin, Klinopyroxen, Plagioklas und Fe-Ti Oxiden in den beiden Suiten charakterisiert. AFC Modellierungen zeigen, daß die Laven mit hohen P_2O_5 Gehalten bis zu 50% an mafischer Unterkruste assimiliert haben, wohingegen die Laven mit niedrigen P_2O_5 Gehalten lediglich bis zu 10% einer mafischen Krustenkomponente assimilierten, die entweder zur Unterkruste oder zum mafischen Teil der Oberkruste gehört. Desweiteren hat die Modellierung der Aufschmelzprozesse gezeigt, daß die primitiven, unkontaminierten Laven mit hohen P_2O_5 Gehalten durch 8 bis 10% Aufschmelzung einer granathaltigen Mantelquelle entstanden sind, wohingegen die Laven mit geringen P_2O_5 Gehalten wahrscheinlich lediglich durch 2 bis 4% Aufschmelzung entstanden sind. Im zeitlichen Zusammenhang gesehen ist eine Abnahme des Aufschmelzgrades mit der Zeit zu beobachten,

wobei zuerst die Laven mit den niedrigen P_2O_5 Gehalten und danach die Laven mit den hohen P_2O_5 Gehalten gefördert wurden.

Im zweiten Kapitel wird die zeitlichen Entwicklung der eruptierten Magmen und damit der Mantelquellen im syrischen Teil des Harrat Ash Shamah, dem größten Vulkanfeld auf der Arabischen Halbinsel, eingehend untersucht. Die Hauptelementzusammensetzung dieser Magmen ist überwiegend durch die fraktionierende Kristallisation von Olivin, Klinopyroxen ±Plagioklas und ±Fe-Ti Oxide kontrolliert, wobei die höchst entwickelten Vulkanite zusätzlich Feldspat und Apatit fraktioniert haben. Neben der fraktionierenden Kristallisation ist die Genese der Harrat Ash Shamah Vulkanite durch Variationen in den Aufschmelzgraden und –tiefen sowie durch Unterschiede in der Quellzusammensetzung und durch Krustenkontamination beeinflusst worden. Die Assimilation von kontinentalem Krustenmaterial läßt sich anhand der hohen Sr und niedrigen Nd Isotopenverhältnisse gekoppelt mit niedrigen Ce/Pb und Nb/U Verhältnissen in den untersuchten Laven nachweisen. Die Fraktionierung der schweren Seltenen Erden sowie Unterschiede in den Spurenelement und SiO_2 Gehalten der unkontaminierten, primitiven Magmen zeigt, daß die Harrat Ash Shamah Vulkanite durch unterschiedliche Aufschmelzgrade von Granat Peridotit in verschiedenen Tiefen entstanden sind. Zusätzlich zeigt die relativ heterogene Isotopen- und Spurenelementzusammensetzung der untersuchten Laven, daß diese aus einer an Volatilen und inkompatiblen Elementen angereicherten lithosphärischen oder asthenosphärischen Mantelquelle stammen müssen. Desweiteren spricht die isotopische Zusammensetzung dieser Magmen für die Beteiligung eines Mantelplumes, mit einer maximalen Überschußtemperatur von circa 180°C, an deren Genese. Die zeitliche Entwicklung der Aufschmelzprozesse und der chemischen und isotopischen Zusammensetzung, die sich in den untersuchten Laven widerspiegelt sowie die diskontinuierliche vulkanische Aktivität zeigen, daß der Harrat Ash Shamah Vulkanismus durch einen unter nordwest Arabien liegenden, pulsierenden Mantelplume entstanden sein muß.

Im dritten Kapitel wird der Vulkanismus in Syrien unter Einbezug der vulkanischen Aktivität entlang der gesamten Arabischen Halbinsel und in Äthiopien/Djibuti betrachtet, um Rückschlüsse auf sowohl räumliche und zeitliche wie auch auf dynamische Mantelprozesse ziehen zu können. $^{40}Ar/^{39}Ar$ Alter von Mineralseparaten und Gesamtgesteinen bestätigen den Miozänen bis rezenten Vulkanismus in Syrien. Altersdaten von der gesamten Afro-Arabischen Region zeigen eine nach Norden gerichtete Progression des Vulkanismus seit der frühesten Aktivität des Afar Mantelplumes vor etwa 30 Millionen Jahren an. Die Zusammensetzung der arabischen und Afar Laven deutet auf signifikante Änderungen sowohl in der Aufschmelztiefe als auch im Aufschmelzgrad der Magmen, wobei relativ flaches Aufschmelzen bei hohen Aufschmelzgraden im Süden und geringe Aufschmelzung in größeren Tiefen im Norden stattfindet. Die Sr, Nd und Pb Isotopenzusammensetzung der syrischen Laven weisen sowohl auf eine relativ veramte, asthenosphärische als auch auf eine lithosphärische Mantelquelle und einen Mantelplume hin, die in deren Magmengenese involviert sind. Die Plumemantelquelle repräsentiert wahrscheinlich mitgerissenes Material aus dem oberen Mantel, welches aus dem Afar Mantelplume stammt. Der Trend zu höheren $^{206}Pb/^{204}Pb$ Verhältnissen, der in den syrischen Laven in den letzten 13 Millionen Jahren zu beobachten ist, deutet auf den verstärkten Einfluß des Afar Plumes. Die Verteilung der Laven mit hohen $^{206}Pb/^{204}Pb$ Verhältnissen zeigt, daß der Einfluß des Afar

Mantelplumes über 2.500km in nördlicher Richtung reicht.

Introduction and Summary

Syria, being situated on the northwestern edge of the Arabian peninsula, is covered by several volcanic fields of Miocene to recent age. The definite causes of volcanism being responsible for this extensive volcanic coverage still remain, up to now, unclear. In general, rift related volcanism in continental regions is explained by two different models, one including passive rifting and the other including active rifting of the continental lithosphere. In the case of passive rifting volcanism is induced by lithospheric extension being caused by plate boundary forces resulting in adiabatic decompression and melting of mantle material (Sengör and Burke, 1978). In the active rifting model volcanism is initiated by mantle plumes resulting in regional doming of the asthenosphere followed by volcanism and rifting (Sengör and Burke, 1978). In detail, the following models have been proposed to explain the Syrian intraplate volcanism: (1) a mantle plume existing underneath northern Arabia (Camp and Roobol, 1992), (2) northwestward channelling of material from the Afar plume along western Arabia (Camp and Roobol, 1992), (3) lithospheric rifting mobilising old fossile plume head material beneath the subcontinental lithosphere (Stein and Hofmann, 1992) and (4) progressive lithospheric thinning tapping lithospheric (fossil-plume material) to asthenospheric sources (Bertrand et al., 2003; Shaw et al., 2003). In this context the aim of this study is to deduce the processes, including mantle melting, fractionation and crustal assimilation, being responsible for the Syrian volcanism. Based on major and trace element compositions of lavas and their isotope geochemistry as well as on the modelling of melting, fractionation and assimilation processes we are going to show that the volcanic activity in Syria is caused by a pulsing mantle plume.

The first chapter of this thesis treads the processes of crustal contamination during magma genesis. The combined effects of assimilation and crystal fractionation (AFC) as well as different degrees of partial melting lead to the eruption of two lava suites being characterised by different major and trace element contents as well as variable isotope compositions. Based on their P_2O_5 concentrations lavas have been divided into a high-P and a low-P suite. The AFC process is indicated by variable isotopic compositions throughout the differentiation trend, by decreasing Ce/Pb and Nb/U ratios as well as variations in the amount of olivine, clinopyroxene, plagioclase and Fe-Ti oxides. AFC modelling shows that the high-P suite has assimilated up to 50% of mafic continental crust. In contrast, lavas of the low-P suite have assimilated only maximal 10% of a mafic crustal component being part of either lower crust or of a mafic upper crustal section. During the period of volcanism the degree of partial melting was reduced producing first low-P lavas followed by the eruption of high-P lavas. As shown by modelling of the partial melting processes the primitive uncontaminated lavas of the low-P suite can be produced by 8 to10% melting of a garnet-bearing mantle source, whereas those of the high-P suite were probably formed by 2 - 4% melting.

The second chapter focuses on the temporal evolution of lavas and their magmatic sources in the Syrian part of the Harrat Ash Shamah, the largest volcanic field on the Arabian peninsula. The lavas have undergone fractional crystallisation of olivine, clinopyroxene, ±plagioclase, and

±Fe-Ti oxides. The most differentiated lavas have also fractionated alkalifeldspar and apatite. High $^{87}Sr/^{86}Sr$ and low $^{143}Nd/^{144}Nd$ ratios of some lavas coupled with low Ce/Pb and Nb/U ratios indicate assimilation of continental crust during their genesis. Crustally uncontaminated, primitive lavas were formed by variable degrees of partial melting of a garnet peridotite at different depths, as indicated by major element variations and variably fractionated heavy rare earth elements. The large range of isotopic compositions and the variable trace element enrichment of the lavas imply that the magmas were generated in a volatile- and incompatible element-enriched lithospheric or asthenospheric mantle source and that a mantle plume with an maximum excess temperature of about 180°C also contributed to their origin. The temporal changes being observed in the partial melting process and in the chemical and isotopic compositions as well as the discontinuous volcanic activity suggest that volcanism was triggered by a pulsing mantle plume situated underneath northwestern Arabia.

In the third chapter Syrians volcanism is related to the magmatic activity in the whole Arabian peninsula and in Ethiopia/Djibouty in order to evaluate the spatial, temporal and dynamic implications for magmatism in the Afro-Arabian region. $^{40}Ar/^{39}Ar$ dating of mineral separates and whole rock samples establish Miocene to recent volcanic activity in Syria. The age data of lavas from the Afro-Arabian region suggest a northward progression of volcanism since the arrival of the Afar plume beneath Ethiopia/Djibouti some 30 Ma ago. The compositions of lavas from western Arabia and the Afar region indicate significant variations in both the depth and the extent of partial melting, varying from relatively shallow and high degree melting in the south to increasingly deeper regions coupled with lower extents of partial melting in the north. Sr, Nd, and Pb isotope compositions of Syrian lavas indicate that a relatively depleted asthenospheric mantle source, a lithospheric source, and a mantle plume have been involved in their formation. The plume end member contributing to Syrian volcanism may represent an entrained upper mantle component related to the Afar plume. Increasing $^{206}Pb/^{204}Pb$ ratios observed in the last 13 Ma in Syrian lavas point to an increasing influence of this plume component with time. The distribution of the high $^{206}Pb/^{204}Pb$ lavas in Arabia indicates a spatial influence of the Afar plume of about 2,500 km in northward direction.

References

Bertrand, H., Chazot, G., Blichert-Toft, J. and Thoral, S., 2003. Implications of widespread high-μ volcanism on the Arabian Plate for Afar mantle plume and lithosphere composition. Chemical Geology, 198: 47-61.

Camp, V.E. and Roobol, M.J., 1992. Upwelling asthenosphere beneath western Arabia and its regional implications. Journal of Geophysical Research, 97: 15,255-15,271.

Sengör, A.M.C. and Burke, K., 1978. Relative timing of rifting and volcanism on Earth and its tectonic implications. Geophysical Research Letters, 5: 419-421.

Shaw, J.E., Baker, J.A., Menzies, M.A., Thirlwall, M.F. and Ibrahim, K.M., 2003. Petrogenesis of the Largest Intraplate Volcanic Field on the Arabian Plate (Jordan): a Mixed Lithosphere-Asthenosphere Source Activated by Lithospheric Extension. Journal of Petrology, 44: 1657-1679.

Stein, M. and Hofmann, A.W., 1992. Fossil plume head beneath the Arabian lithosphere? Earth and Planetary Science Letters, 114: 193-209.

CHAPTER ONE

Constraints on Continental, Intra-Plate Volcanism in Northwestern Syria: Crustal Contamination Versus Subcontinental Lithospheric Mantle Sources

M.-S. Krienitz[1*], K. M. Haase[1], K. Mezger[2], V. Eckardt[2] , M. A. Shaikh-Mashail[3]
[1] Institut für Geowissenschaften der Universität Kiel, Olshausenstr. 40, 24118 Kiel, Germany
[2] Institut für Mineralogie der Universität Münster, Corrensstr. 24, 48149 Münster, Germany
[3] Faculty of Civil Engineering, University of Aleppo, PO-Box 5427, Aleppo, Syria
[*] Corresponding author. Telephone +49 (0) 431 880 3694. Fax +49 (0) 431 880 4376. E-mail: mk@gpi.uni-kiel.de

Abstract

Miocene to Quaternary lavas from northwestern Syria consist of basanites, alkali basalts and tholeiites as well as hawaiites, mugearites and basaltic andesites. Based on their P_2O_5 concentrations the lavas can be divided into two suites, a high-P and a low-P suite. The high-P lavas exhibit variable contents in major and trace element compositions, i. e. high TiO_2, Na_2O, K_2O, P_2O_5 and low SiO_2, Cr and Ni compared to the low-P lavas. The geochemical differences between both suites are caused by the combined effects of assimilation and crystal fractionation (AFC) as well as different degrees of partial melting of the mantle source. The AFC process is indicated by decreasing Ce/Pb and Nb/U ratios as well as variable isotopic compositions throughout the differentiation trend and variations in the amount of olivine, clinopyroxene, plagioclase and Fe-Ti oxides fractionation between the two suites. Only primitive lavas of both suites are free of contamination. AFC modelling shows that the high-P suite has assimilated up to 50% of mafic continental crust, whereas lavas belonging to the low-P suite have assimilated only maximal 10% of a mafic crustal component being a part of either lower crust or of a mafic upper crustal section. Even though plume material has been recognised in the investigated samples, indicating an enriched mantle source compared to the depleted mantle source of average mid-ocean ridge basalts being responsible for the generation of the NW Syrian lavas, influence of the Afar plume source with characteristically high $^3He/^4He$ ratios can be ruled out. During the period of volcanic activity the degree of partial melting was reduced producing first low-P lavas and high-P lavas at a later stage. Partial melting occurred in the garnet stability field and about 8 - 10% melting of the mantle source can have produced the primitive, uncontaminated tholeiites, whereas 2 - 4% melting can have lead to the formation of uncontaminated basanite and alkali basalts.

1.1 Introduction

The characterisation of magmatic sources of lavas erupting in intracontinental settings and potential processes of contamination during the ascent of the magmas are still a matter of debate in magmatic geochemistry. In general, rift related continental volcanism is induced by upwelling of the mantle, either due to a mantle plume (active rift model), or by the extension of the continental lithosphere triggered by plate boundary forces (passive rift model; Sengör and Burke, 1978). In both cases mantle material melts due to adiabatic ascent. Consequently, the geochemical composition of the magmas should be either characteristic for a mantle plume or for an asthenospheric/lithospheric source.

Trace element and isotope compositions of continental volcanic rocks often differ from lavas erupted in oceanic settings indicating that their petrogenesis does not only include mantle material. During the ascent of magmas, the primary geochemical signatures of the mantle sources, either plume-derived, asthenospheric, or lithospheric, may be modified by the assimilation of crustal wall rocks as well as by crystal fractionation processes. Several thermodynamic formulations have been developed to model these processes (DePaolo, 1981; Aitcheson and Forrest, 1994; Spera and Bohrson, 2001). Magmas originating in the asthenosphere may be contaminated by lithospheric melts or by crustal material as the magma rises to the surface. This crustal contamination may result in geochemical signatures similar to lavas originating directly in the subcontinental lithosphere. Magmas emanating from lithospheric sources may also assimilate continental crust.

The aim of this study is to evaluate the importance of crustal contamination during the magma genesis of the volcanic rocks of northwestern Syria and to characterise the potential mantle sources of the Syrian volcanic rocks.

1.2 Geological framework

Large parts of western Arabia are covered by Cenozoic alkali basalts belonging to different magmatic provinces (e. g. Coleman et al.,1983; Camp and Roobol, 1989; Camp et al., 1991). The widespread magmatic activity is related to the two-stage formation of the Red Sea, beginning in Miocene times and the development of the Miocene/Pliocene Dead Sea fault (DSF) system, running from the Red Sea/Gulf of Aqaba region in the south to the Taurus collision zone in the north (Bohannon et al., 1989; Nasir and Safarjalani, 2000). The evolution of the western Arabian rift system is accompanied by widespread magmatism, but the causes of the extensive intraplate volcanism in Syria, Israel, Jordan, and southern Turkey are unknown and several models have been proposed to account for this magmatic activity. For example, Stein and Hofmann (1992) suggested that an old plume head, not strong enough to reach the surface, was stored beneath the subcontinental lithosphere and that volcanism was triggered during subsequent periods of

lithospheric extension. In contrast, Camp and Roobol (1992) proposed that the volcanism was caused by hot asthenospheric material either channeled northwards from the Afar plume or that another mantle plume exists beneath western Arabia.

The territory of Syria is located at the northwestern flank of the Arabian peninsula and is covered by several volcanic fields of Miocene to Quaternary age (Fig. 1.1). Volcanic rocks are concentrated in the western part of Syria in the vicinity of the Dead Sea fault, but other volcanic fields are spread across the whole country. The present tectonic situation in Syria is the result of the interaction of the Cenozoic plate boundaries with older intraplate features (McBride et al., 1990). Based on Bouguer gravity anomalies Syria can be divided into three major areas: the Rutbah Uplift in the south is separated by the Palmyride Fold Zone from the northern Aleppo Plateau (Searle, 1994), which is covered by relatively undeformed Palaeozoic and Mesozoic sedimentary rocks (Best et al., 1990; Searle, 1994; Sharkov et al., 1994;). Seismic studies have shown that the depth to metamorphic basement beneath the plateau is about 6 km and that a crustal thickness of about 40 km is reached in Syria similar to Jordan and Saudi Arabia (Best et al., 1990; El-Isa et al., 1987; Sandvol et al., 1998; Walley, 1998; Kumar et al., 2002). Furthermore, geophysical and geochemical data indicate an upper crustal layer of presumably granitic rocks, ranging in depths from about 5 to 20 km and a lower crust, composed of mafic rocks with high feldspar contents, at depths of about 20 to 27 km for the northwestern Arabian plate and southern Syria (Nasir, 1992; Nasir and Safarjalani, 2000).

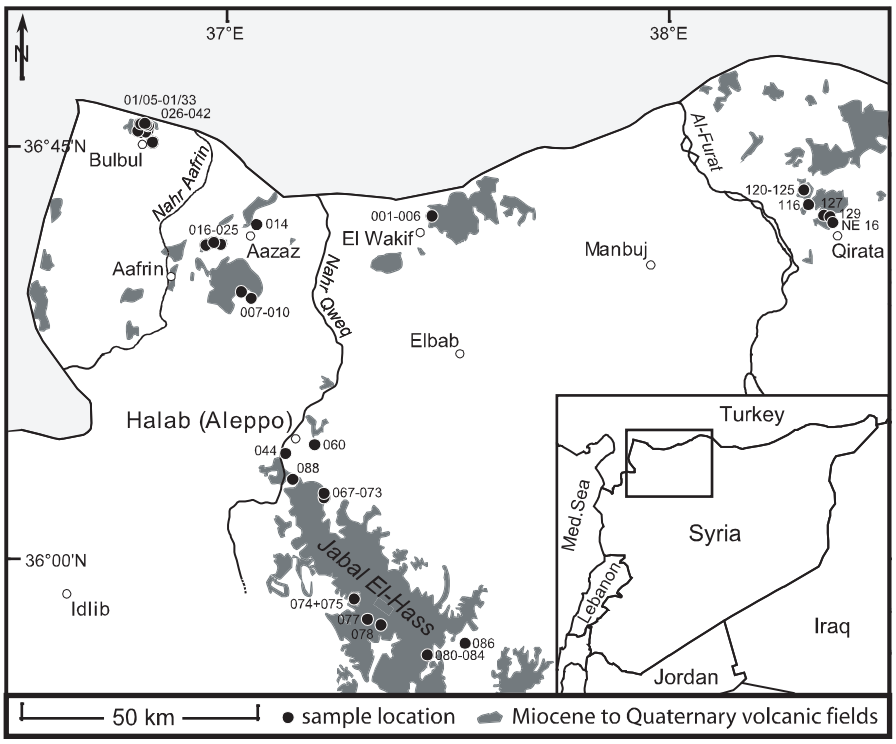

Fig. 1.1. Location map of northwest Syria showing volcanic fields from which samples were collected. The inset shows the northwestern part of the Arabian peninsula with Syria and surrounding countries. Numbers beneath sample locations refer to samples names listed in Table 2. The simplified map based on geological maps of Ponikarov et al. (1963).

The largest volcanic field located in the investigated area of NW Syria forms the mountain range Jabal El-Hass, with a maximum relief of 300 m and reaches altitudes of 640 m (Fig. 1.1). The volcanic field consists of several lava flows of Miocene age, reaching a total thickness of about

50 m and lying on Paleogene and Neogene sediments (Ponikarov et al., 1963). Single flows vary in thickness from one to ten metres and in some places are separated by thick layers of limestone. Other major volcanic fields, composed of several lava flows, are situated near the villages of Qirata on the eastern side of the Euphrates and around Aazaz and El Wakif. Detailed sampling of single flow units took place on a minor volcanic outcrop located north of the town of Bulbul (Fig. 1.1). Ponikarov et al. (1963) suggested that most of these volcanic units are of upper Pliocene age, but lower Quaternary volcanism occurs around Qirata as well and newly obtained Ar-Ar age determinations yield Miocene ages for volcanic rocks from the Bulbul region Krienitz et al. (Chapter III).

1.3 Analytical methods

After cutting the freshest parts from each sample, the pieces were washed with deionised water in an ultrasonic bath for 15 minutes, crushed to coarse sand size with a screw press and washed again. For chemical analysis samples containing fresh glass were handpicked under a binocular microscope. Whole rock samples were reduced to powder in an agate ball mill for major, trace, and isotope analyses. Several samples were studied petrographically in thin section and mineral phases were analysed with a JEOL JXA 8900 electron microprobe running in wavelength dispersive mode at a beam current of 15 mA (10 mA for glass measurements) and an accelerating voltage of 15 kV. The beam diameter for most analyses was 2 µm but was defocused for feldspar and glass analyses. The measurements were calibrated with mineral standards for the specific elements. Standard as well as representative mineral and glass analyses are listed in Table 1.

Major and selected trace (Cr, Ni, Zn, Rb, Sr) element analyses were carried out at the Universität Kiel with a Philips PW 1400 XRF using international rock standards for calibration and data quality control. 0.6g of sample powder were mixed with 3.6g of flux (lithiumtetraborate) and melted to glass tablets. The accuracy of standard analyses relative to reference values is generally better than 3% for most of the major and trace elements. Only Na_2O and P_2O_5 show higher deviations (8% and 3%, respectively). Replicate analyses of the BHVO-1 standard gave a precision better than 0.30% (SD) for all major elements and generally better than 7.5% (SD) for trace elements (Table 2).

100 mg of sample material were used for trace and rare earth element (REE) analyses. Measurements were made at the Universität Kiel with an upgraded PlasmaQuad PQ1 ICP-MS following the method of Garbe-Schönberg (1993). Comparison of duplicate digestions of the same sample yielded a precision generally better than 1% (SD). The accuracy of the data based on the international rock standard BHVO-1 is better than 7% except for Nb, Ta (<9%), Sc, Cs and Th (>9%) and can be estimated from the standard analyses given in Table 2.

Most analyses of Sr, Nd, and Pb isotopic ratios (Table 3) were made at the Zentrallaboratorium

Table 1. Representative microprobe analyses of glasses and minerals of Syrian lavas. Also given are the results of the VG-2 glas standard analyses.

Phase	plagioclase				clinopyroxene				olivine					magnetite	glas				glas standard	
Sample	SY-028			SY-069	SY-039			SY-127	SY-021			SY-088		SY-127	SY-023gl		SY-024gl		VG-2	
Host rock	mugearite			tholeiite	hawaiite			alkali basalt	basaltic andesite			tholeiite		alkali basalt	basaltic andesite		basaltic andesite			
															Mean	SD	Mean	SD	Mean	SD
	core	rim	matrix	matrix	core	rim	matrix	matrix	core	rim	matrix	core	rim	matrix	(n=13)		(n=11)		(n=9)	
SiO_2	52.95	53.60	58.26	53.34	51.95	49.43	50.03	46.03	39.06	38.35	37.87	38.26	36.97	0.07	55.26	0.27	55.28	0.39	50.87	0.16
TiO_2	-	-	0.29	0.10	0.82	1.83	1.84	3.85	-	-	-	0.08	0.11	28.46	2.05	0.04	2.04	0.06	1.88	0.03
Al_2O_3	29.76	28.97	25.25	28.74	1.47	3.25	2.80	6.81	0.07	0.06	0.07	-	-	2.83	14.67	0.09	14.65	0.21	14.02	0.10
FeO^T	0.48	0.59	1.11	0.79	8.55	10.19	10.54	8.20	17.01	21.41	23.94	22.82	30.69	64.65	10.30	0.15	10.31	0.13	11.76	0.16
MnO	-	-	0.02	0.02	0.22	0.24	0.27	0.13	0.21	0.25	0.34	0.27	0.45	0.61	0.12	0.04	0.12	0.05	0.19	0.06
MgO	-	-	0.17	0.05	14.21	12.87	12.67	11.36	42.37	38.57	36.71	38.04	31.68	2.08	4.72	0.08	4.74	0.11	6.81	0.06
CaO	12.56	11.53	7.31	10.96	21.55	20.83	21.07	21.99	0.16	0.22	0.29	-	-	0.06	8.07	0.08	8.02	0.08	11.08	0.09
Na_2O	4.15	4.60	6.60	4.99	0.38	0.46	0.45	0.56	-	-	-	-	-	0.04	3.26	0.17	3.40	0.09	2.64	0.06
K_2O	0.22	0.25	0.48	0.35	-	-	-	0.03	-	-	-	-	-	0.01	0.97	0.03	0.97	0.04	0.18	0.02
P_2O_5	-	-	-	-	-	-	-	-	-	-	-	-	-		0.32	0.04	0.31	0.02	0.28	0.03
Cr_2O_3	-	-	0.04	-	0.09	0.04	0.03	0.04	-	0.08	0.08	0.06	0.04	0.01	0.05	0.04	0.05	0.04	0.04	0.04
NiO	-	-	-	-	-	-	-	-	0.26	0.17	0.16	-	-	-	-		-		-	
Total	100.11	99.54	99.54	99.33	99.25	99.14	99.70	99.00	99.14	99.12	99.45	99.53	99.94	98.83	99.91		100.00		100.03	
Ab	37.0	41.3	60.3	44.3																
An	61.8	57.2	36.9	53.7																
Or	1.2	1.5	2.8	2.0																
En					41.2	38.4	37.6	35.8												
Fs					13.9	17.0	17.5	14.5												
Wo					44.9	44.6	44.9	49.7												
Fo									81.6	76.3	73.2	74.8	64.8							
Usp														82.7						

Table 2. Coordinates, rock type, major (XRF) and trace element (XRF, ICP-MS) analyses of the Syrian samples. Averages of analyses of the standard BHVO-1 (XRF n = 7; ICP-MS n = 9) are also given.

Sample	NE 16	SY 01/05	SY 01/08	SY 01/09	SY 01/10	SY 01/11	SY 01/12	SY 01/14	SY 01/15	SY 01/23	SY 01/24	SY 01/25
Lat. [°N]	36°36`55``	36°47`28``	36°47`34``	36°47`19``	36°47`13``	36°46`58``	36°46`57``	36°47`01``	36°47`08``	36°47`08``	36°47`20``	36°47`26``
Long. [°E]	38°22`50``	36°48`41``	36°49`04``	36°49`27``	36°49`27``	36°49`43``	36°49`48``	36°49`51``	36°49`55``	36°49`07``	36°48`56``	36°48`52``
Elevation [m]	454	1199	1163	1046	989	901	897	888	893	875	1004	1140
Rock type	AB	M	BA	H	H	M	M	H	T	T	H	T
SiO_2	47.00	50.06	50.54	49.84	49.43	50.86	50.80	49.85	50.67	49.96	49.41	49.44
TiO_2	1.96	2.01	1.93	1.90	2.23	1.97	2.02	2.20	1.97	1.90	2.21	2.17
Al_2O_3	13.06	15.56	15.52	15.14	14.73	15.99	16.16	16.20	15.91	15.79	16.27	14.76
$Fe_2O_3^T$	11.57	10.58	10.75	11.70	12.03	11.11	11.37	11.63	11.02	11.63	11.55	12.05
MnO	0.15	0.13	0.14	0.14	0.14	0.15	0.14	0.17	0.15	0.16	0.15	0.15
MgO	8.54	5.66	5.05	5.52	5.82	4.73	4.11	4.51	5.85	5.22	4.58	5.34
CaO	10.80	8.04	8.32	8.49	8.47	8.29	8.12	8.28	8.21	8.42	8.03	8.42
Na_2O	2.86	3.59	3.64	3.75	3.61	3.82	3.66	3.59	3.38	3.77	3.76	3.38
K_2O	1.09	1.36	1.24	1.26	1.33	1.28	1.31	1.36	1.22	1.00	1.49	1.27
P_2O_5	0.29	0.54	0.48	0.48	0.49	0.36	0.35	0.60	0.35	0.29	0.61	0.57
L.O.I.	1.06	1.39	0.72	0.48	0.75	0.33	0.70	0.37	0.76	0.51	0.15	1.31
Total	98.38	98.90	98.33	98.70	99.03	98.89	98.74	98.76	99.49	98.65	98.21	98.82
Mg-no.	0.61	0.53	0.50	0.50	0.50	0.47	0.43	0.45	0.53	0.48	0.45	48.2
Li	-	-	-	8.88	8.06	-	9.34	-	-	9.56	-	8.41
Sc	-	-	-	19.3	19.8	-	20.9	-	-	20.6	-	19.8
V	-	-	-	217	221	-	223	-	-	220	-	216
Cr	339	107	144	198	266	157	162	58	-	215	47	241
Co	-	-	-	40.7	40.0	-	35.6	-	-	38.2	-	39.6
Ni	259	8	44	97.1	114	33	40.9	17	-	63.8	10	94.3
Cu	-	-	-	31.2	35.4	-	26.2	-	-	32.9	-	36.3
Zn	97	102	109	113	126	103	111	117	-	113	116	118
Ga	-	-	-	37.0	35.2	-	34.1	-	-	30.5	-	36.3
Rb	18	49	50	28.5	28.6	38	26.5	47	-	14.1	46	29.0
Y	-	-	-	23.3	23.7	-	25.4	-	-	23.3	-	26.1
Cs	-	-	-	0.265	0.360	-	0.412	-	-	0.187	-	0.232
Sr	424	566	541	554	612	501	505	657	-	423	633	605
Ba	-	-	-	388	355	-	298	-	-	237	-	384
Zr	-	-	-	147	164	-	161	-	-	137	-	168
Hf	-	-	-	3.95	4.36	-	4.30	-	-	3.81	-	4.41
Nb	-	-	-	24.6	29.6	-	22.6	-	-	16.2	-	32.8
Ta	-	-	-	1.22	1.59	-	1.21	-	-	0.910	-	1.73
Pb	-	-	-	5.16	5.02	-	5.07	-	-	3.93	-	5.10
Th	-	-	-	4.59	4.48	-	4.03	-	-	2.97	-	4.65
U	-	-	-	1.18	1.06	-	1.02	-	-	0.646	-	1.12
La	-	-	-	31.1	30.8	-	24.9	-	-	16.8	-	34.9
Ce	-	-	-	63.1	60.4	-	48.3	-	-	35.5	-	66.7
Pr	-	-	-	7.56	7.65	-	6.37	-	-	4.57	-	8.92
Nd	-	-	-	30.1	31.3	-	26.4	-	-	19.6	-	36.4
Sm	-	-	-	6.39	6.81	-	6.06	-	-	4.90	-	7.81
Eu	-	-	-	1.96	2.13	-	1.91	-	-	1.62	-	2.42
Gd	-	-	-	6.08	6.48	-	6.12	-	-	5.14	-	7.36
Tb	-	-	-	0.900	0.953	-	0.943	-	-	0.817	-	1.07
Dy	-	-	-	5.04	5.20	-	5.37	-	-	4.76	-	5.83
Ho	-	-	-	0.943	0.953	-	1.03	-	-	0.923	-	1.06
Er	-	-	-	2.41	2.42	-	2.68	-	-	2.41	-	2.68
Tm	-	-	-	0.338	0.318	-	0.364	-	-	0.336	-	0.353
Yb	-	-	-	2.07	2.00	-	2.30	-	-	2.09	-	2.19
Lu	-	-	-	0.299	0.276	-	0.330	-	-	0.303	-	0.306

Major elements in wt.%, trace elements in ppm. gl - glas analyses, major elements determined by electron microprobe (cp. Table 1). BAS - basanite, AB - alkali basalt, BA - basaltic andesite, BAS - basanite, H - hawaiite, M - mugearite, T - tholeiite, LC - lower crust. Mg-no. = $Mg/(Mg + Fe^{2+})$, assuming FeO = $0.85Fe^T$.

Table 2. (continued)

Sample	SY 01/27	SY 01/28	SY 01/29	SY 01/32	SY 01/33	SY-001	SY-004	SY-005	SY-006	SY-007	SY-009	SY-010	SY-014
Lat. [°N]	36°47`03``	36°47`04``	36°47`03``	36°47`06``	36°47`27``	36°37`29``	36°37`29``	36°37`29``	36°37`29``	36°28`30``	36°29`03``	36°29`03``	36°36`34``
Long. [°E]	36°48`30``	36°48`32``	36°48`40``	36°48`49``	36°48`30``	37°28`09``	37°28`09``	37°28`07``	37°28`07``	37°03`50``	37°02`18``	37°02`18``	37°04`26``
Elevation [m]	974	1021	1121	1094	1133	530	530	528	528	462	488	488	603
Rock type	M	T	M	H	T	T	T	T	T	AB	AB	AB	BA
SiO_2	49.97	48.52	50.30	50.07	49.67	50.79	49.92	49.68	50.06	46.74	46.46	45.69	52.12
TiO_2	2.14	1.80	1.86	1.83	1.84	1.53	1.39	1.57	1.47	1.98	2.02	1.95	1.74
Al_2O_3	16.10	14.37	15.57	15.11	14.74	14.19	14.39	14.15	14.53	15.43	15.17	14.81	14.84
$Fe_2O_3^T$	11.33	12.41	11.37	11.61	11.57	11.47	11.64	12.18	11.93	11.89	11.89	11.53	10.73
MnO	0.14	0.15	0.15	0.15	0.14	0.15	0.14	0.15	0.15	0.16	0.16	0.15	0.13
MgO	4.24	8.21	4.84	5.61	6.41	7.36	7.74	6.76	7.50	5.73	5.39	5.22	5.17
CaO	8.29	8.63	8.41	8.19	8.20	9.30	9.28	9.87	9.72	11.72	11.92	11.48	9.61
Na_2O	3.85	3.28	3.89	3.68	3.48	3.22	3.21	3.20	3.15	3.40	3.47	3.50	3.31
K_2O	1.48	0.88	1.29	1.24	1.22	0.66	0.54	0.66	0.58	0.95	0.96	0.96	0.83
P_2O_5	0.57	0.26	0.49	0.48	0.44	0.21	0.17	0.20	0.19	0.48	0.49	0.47	0.22
L.O.I.	0.31	0.27	0.68	0.69	0.62	1.38	1.19	2.10	1.50	1.74	2.45	2.39	2.15
Total	98.42	98.78	98.85	98.66	98.33	100.26	99.61	100.52	100.78	100.22	100.38	98.15	100.85
Mg-no.	0.44	0.58	0.47	0.50	0.54	0.60	0.61	0.56	0.59	0.53	0.51	0.51	0.53
Li	-	-	8.97	8.95	-	-	8.84	-	-	-	-	10.7	2.35
Sc	-	23.3	19.0	18.9	-	-	19.4	-	-	-	-	20.6	12.3
V	-	248	213	210	-	-	-	-	-	-	-	-	109
Cr	50	330	172	196	221	284	283	260	263	206	214	211	176
Co	-	56.0	39.6	42.7	-	-	48.0	-	-	-	-	41.3	26.3
Ni	20	224	72.9	102	125	199	209	216	237	87	109	82.2	65.3
Cu	-	45.5	25.3	25.6	-	-	58.0	-	-	-	-	37.5	29.2
Zn	113	125	112	111	109	106	98.2	106	106	106	107	98.4	76.0
Ga	-	30.7	37.7	36.6	-	-	-	-	-	-	-	-	-
Rb	40	18.0	30.0	28.5	33	12	11.0	11	12	15	14	16.6	19.1
Y	-	22.2	24.0	23.4	-	-	16.8	-	-	-	-	20.3	19.6
Cs	-	0.190	0.454	0.360	-	-	0.265	-	-	-	-	0.191	0.654
Sr	654	454	563	555	517	286	279	329	283	652	617	589	301
Ba	-	215	408	393	-	-	365	-	-	-	-	712	568
Zr	-	137	148	144	-	-	86.1	-	-	-	-	127	114
Hf	-	3.60	3.94	3.85	-	-	2.57	-	-	-	-	3.77	3.68
Nb	-	19.6	22.9	24.0	-	-	9.01	-	-	-	-	22.6	12.6
Ta	-	0.990	1.14	1.20	-	-	0.625	-	-	-	-	1.36	0.956
Pb	-	2.70	5.41	4.84	-	-	1.54	-	-	-	-	2.95	3.56
Th	-	2.73	4.77	4.52	-	-	1.44	-	-	-	-	3.29	2.90
U	-	0.720	1.28	1.06	-	-	0.442	-	-	-	-	0.553	0.748
La	-	17.4	32.2	31.1	-	-	8.68	-	-	-	-	26.9	14.4
Ce	-	36.0	64.9	63.2	-	-	19.3	-	-	-	-	55.6	30.4
Pr	-	4.60	7.75	7.53	-	-	2.54	-	-	-	-	6.63	4.02
Nd	-	19.4	30.8	30.1	-	-	11.3	-	-	-	-	26.9	17.2
Sm	-	4.83	6.52	6.39	-	-	3.13	-	-	-	-	5.86	4.45
Eu	-	1.66	1.98	1.96	-	-	1.12	-	-	-	-	1.87	1.46
Gd	-	5.00	6.17	6.06	-	-	3.62	-	-	-	-	5.80	4.79
Tb	-	0.810	0.922	0.906	-	-	0.588	-	-	-	-	0.832	0.789
Dy	-	4.70	5.15	5.06	-	-	3.56	-	-	-	-	4.66	4.60
Ho	-	0.900	0.975	0.946	-	-	0.679	-	-	-	-	0.861	0.871
Er	-	2.40	2.48	2.42	-	-	1.75	-	-	-	-	2.20	2.28
Tm	-	0.330	0.347	0.329	-	-	0.235	-	-	-	-	0.300	0.309
Yb	-	2.00	2.17	2.05	-	-	1.52	-	-	-	-	1.88	1.92
Lu	-	0.300	0.304	0.300	-	-	0.217	-	-	-	-	0.269	0.274

Table 2. (continued)

Sample	SY-016	SY-017	SY-018	SY-019	SY-021	SY-023gl	SY-024gl	SY-025	SY-026	SY-027	SY-028	SY-029	SY-030
Lat. [°N]	36°34`20``	36°34`20``	36°34`40``	36°34`40``	36°34`11``	36°34`11``	36°34`11``	36°34`11``	36°45`30``	36°45`30``	36°46`44``	36°46`44``	36°46`44``
Long. [°E]	36°59`36``	36°59`36``	36°58`44``	36°58`44``	36°57`38``	36°57`38``	36°57`38``	36°57`38``	36°50`12``	36°50`12``	36°48`53``	36°48`53``	36°48`53``
Elevation [m]	580	580	600	600	700	700	700	700	680	680	1125	1105	1087
Rock type	AB	T	T	T	BA	BA	BA	BA	T	BAS	M	H	T
SiO_2	46.65	48.29	49.69	50.16	50.68	55.26	55.28	51.39	49.98	44.23	51.08	51.06	49.26
TiO_2	2.32	2.48	1.80	1.82	1.56	2.05	2.04	1.60	1.86	2.52	1.93	1.89	2.18
Al_2O_3	15.87	16.59	13.90	13.90	13.53	14.67	14.65	14.03	15.28	14.23	16.02	15.85	15.05
$Fe_2O_3^T$	11.73	12.35	12.31	12.24	11.55	11.45	11.46	11.69	11.95	13.45	11.72	11.56	12.58
MnO	0.16	0.16	0.15	0.14	0.14	0.12	0.12	0.14	0.15	0.18	0.14	0.13	0.14
MgO	5.51	4.97	8.76	8.47	8.46	4.72	4.74	8.26	6.70	9.34	4.85	5.83	5.64
CaO	9.40	9.43	8.00	8.07	7.69	8.07	8.02	7.93	8.74	9.35	8.14	8.28	8.92
Na_2O	3.35	3.30	2.95	2.96	2.86	3.26	3.40	2.84	3.51	3.48	3.82	3.71	3.62
K_2O	1.18	1.21	0.67	0.71	0.74	0.97	0.97	0.84	1.20	1.55	1.35	1.29	1.24
P_2O_5	0.50	0.53	0.27	0.28	0.19	0.32	0.31	0.19	0.47	1.10	0.49	0.51	0.59
L.O.I.	1.97	1.00	2.14	2.12	2.10	-	-	2.01	0.69	1.17	1.20	0.79	1.05
Total	98.62	100.31	100.64	100.87	99.50	99.91	100.00	100.92	100.53	100.60	100.74	100.90	100.27
Mg-no.	0.52	0.48	0.62	0.62	0.63	0.49	0.49	0.62	0.57	0.62	0.49	0.54	0.51
Li	-	-	-	-	4.88	11.5	11.1	-	-	8.20	6.72	-	8.48
Sc	-	-	-	-	18.1	20.3	19.5	-	-	17.7	20.4	-	16.2
V	-	-	-	-	166	-	-	-	-	185	205	-	-
Cr	33	40	284	280	264	257	286	281	221	242	171	188	268
Co	-	-	-	-	50.1	37.9	39.6	-	-	48.7	36.2	-	37.3
Ni	38	45	262	252	216	106	142	236	109	179	70.5	90	101
Cu	-	-	-	-	63.4	69.5	67.4	-	-	67.6	25.9	-	32.3
Zn	132	115	110	112	105	107	106	109	113	105	109	107	117
Ga	-	-	-	-	20.6	-	-	-	-	-	24.2	-	22.0
Rb	16	16	10	9	15.6	19.8	19.8	12	22	19.9	30.9	28	25.1
Y	-	-	-	-	19.3	20.1	19.7	-	-	21.8	24.5	-	24.5
Cs	-	-	-	-	0.572	0.706	0.683	-	-	0.328	0.470	-	0.313
Sr	633	652	348	354	263	280	276	259	551	980	589	558	680
Ba	-	-	-	-	124	176	154	-	-	458	371	-	331
Zr	-	-	-	-	104	105	105	-	-	230	158	-	150
Hf	-	-	-	-	2.42	3.11	3.09	-	-	5.93	3.48	-	3.56
Nb	-	-	-	-	10.7	11.0	10.9	-	-	59.7	23.8	-	30.0
Ta	-	-	-	-	0.627	0.521	0.709	-	-	3.51	1.18	-	1.66
Pb	-	-	-	-	2.61	2.99	3.00	-	-	4.43	5.10	-	5.27
Th	-	-	-	-	1.83	2.33	2.32	-	-	9.60	4.50	-	4.00
U	-	-	-	-	0.516	0.677	0.679	-	-	2.69	1.15	-	0.971
La	-	-	-	-	10.1	11.7	11.4	-	-	69.6	31.0	-	32.3
Ce	-	-	-	-	22.0	25.4	24.9	-	-	122	62.6	-	64.4
Pr	-	-	-	-	2.76	3.21	3.18	-	-	12.8	7.16	-	7.93
Nd	-	-	-	-	11.8	14.1	13.9	-	-	46.7	28.0	-	32.0
Sm	-	-	-	-	3.20	3.87	3.80	-	-	8.65	5.88	-	6.72
Eu	-	-	-	-	1.21	1.31	1.29	-	-	2.66	1.95	-	2.09
Gd	-	-	-	-	3.58	4.34	4.26	-	-	8.11	5.71	-	6.34
Tb	-	-	-	-	0.575	0.697	0.690	-	-	1.05	0.807	-	0.885
Dy	-	-	-	-	3.27	4.20	4.10	-	-	5.42	4.41	-	4.84
Ho	-	-	-	-	0.620	0.796	0.774	-	-	0.944	0.815	-	0.881
Er	-	-	-	-	1.61	2.06	2.02	-	-	2.31	2.16	-	2.17
Tm	-	-	-	-	0.246	0.282	0.277	-	-	0.297	0.320	-	0.288
Yb	-	-	-	-	1.48	1.75	1.70	-	-	1.79	1.93	-	1.76
Lu	-	-	-	-	0.198	0.247	0.245	-	-	0.254	0.264	-	0.242

Table 2. (continued)

Sample	SY-031	SY-032	SY-033	SY-034	SY-035	SY-036	SY-037	SY-038	SY-039	SY-040	SY-041	SY-042	SY-044
Lat. [°N]	36°46`44``	36°46`44``	36°46`39``	36°46`39``	36°46`39``	36°46`39``	36°46`39``	36°46`39``	36°46`39``	36°46`39``	36°46`39``	36°46`39``	36°11`37``
Long. [°E]	36°48`53``	36°48`53``	36°48`52``	36°48`52``	36°48`52``	36°48`52``	36°48`52``	36°48`52``	36°48`52``	36°48`52``	36°48`52``	36°48`52``	37°08`18``
Elevation [m]	1058	1039	1023	1037	992	988	988	977	976	969	938	924	-
Rock type	H	T	H	H	T	T	T	H	H	BA	T	T	BA
SiO_2	49.78	49.72	49.38	50.63	48.58	47.93	48.20	49.90	50.12	50.97	49.95	50.06	51.28
TiO_2	2.22	2.16	2.33	2.16	1.86	1.88	1.84	2.22	2.26	1.86	1.93	1.91	1.48
Al_2O_3	15.01	14.82	14.95	15.41	15.00	14.49	14.66	16.12	16.55	16.07	15.53	15.41	14.25
$Fe_2O_3^T$	12.47	11.96	11.91	11.87	12.88	12.88	12.57	11.74	12.02	11.63	11.48	13.33	11.48
MnO	0.17	0.15	0.14	0.14	0.15	0.16	0.16	0.15	0.14	0.13	0.14	0.16	0.14
MgO	5.48	6.55	5.96	5.73	7.55	8.74	9.10	4.31	4.37	4.88	6.70	5.61	7.05
CaO	8.82	8.80	8.51	8.06	8.12	8.51	8.49	8.25	8.21	8.06	8.42	7.21	8.77
Na_2O	3.67	3.46	3.78	3.75	3.25	3.22	3.11	3.85	3.76	3.76	3.24	3.53	3.10
K_2O	1.33	1.35	1.47	1.43	0.89	0.88	0.87	1.48	1.48	1.03	0.99	1.04	0.41
P_2O_5	0.61	0.53	0.48	0.44	0.27	0.27	0.26	0.57	0.58	0.27	0.26	0.28	0.16
L.O.I.	1.00	0.49	0.67	0.99	1.43	0.00	1.65	1.15	1.31	1.81	1.95	2.27	1.62
Total	100.56	99.99	99.58	100.61	99.98	98.96	100.91	99.74	100.80	100.47	100.59	100.81	99.74
Mg-no.	0.51	0.56	0.54	0.53	0.58	0.61	0.63	0.46	0.46	0.49	0.58	0.50	0.59
Li	7.58	6.52	11.6	-	6.31	-	6.58	9.82	11.3	7.59	-	7.69	-
Sc	16.5	15.9	17.6	-	18.6	-	16.7	13.9	16.1	18.3	-	16.2	-
V	-	-	-	-	-	-	-	-	-	-	-	-	-
Cr	258	263	304	246	321	315	317	63.0	64.0	230	218	291	287
Co	42.5	40.3	37.1	-	46.2	-	46.9	29.3	30.5	37.4	-	45.3	-
Ni	91	102	95.0	95	216	198	201	33.0	35.0	86.0	70	179	265
Cu	32.7	33.5	38.0	-	45.4	-	40.7	23.1	24.4	29.5	-	45.0	-
Zn	121	106	114	117	116	117	115	115	117	108	111	133	109
Ga	22.5	21.9	24.6	-	22.2	-	20.5	23.7	24.8	23.4	-	22.5	-
Rb	27.8	26.7	29.5	28	15.0	14	13.5	26.6	30.2	19.6	19	18.3	12
Y	26.6	24.3	25.2	-	22.2	-	19.3	24.4	27.3	24.8	-	21.1	-
Cs	0.293	0.389	0.254	-	0.134	-	0.284	0.286	0.243	0.325	-	0.304	-
Sr	670	626	632	586	399	399	387	670	656	412	388	411	280
Ba	360	318	351	-	185	-	153	333	366	207	-	203	-
Zr	164	155	180	-	115	-	107	159	169	125	-	119	-
Hf	4.04	3.96	4.49	-	3.08	-	2.77	4.06	4.29	3.38	-	3.15	-
Nb	31.7	30.5	31.6	-	17.7	-	16.5	29.6	30.9	15.1	-	14.9	-
Ta	1.76	1.76	1.82	-	1.10	-	1.01	1.57	1.66	0.909	-	0.950	-
Pb	4.88	4.73	6.13	-	2.31	-	2.33	5.29	6.53	3.49	-	3.16	-
Th	4.43	4.08	4.59	-	2.23	-	2.03	4.47	4.85	2.84	-	2.53	-
U	1.09	1.04	1.00	-	0.622	-	0.580	0.753	0.947	0.716	-	0.621	-
La	33.4	29.0	29.1	-	15.1	-	13.6	31.8	34.9	16.4	-	15.3	-
Ce	67.5	59.7	58.7	-	29.8	-	28.8	64.3	67.7	33.2	-	31.1	-
Pr	8.23	7.25	7.13	-	3.95	-	3.61	7.64	8.44	4.22	-	4.00	-
Nd	33.2	29.5	29.6	-	16.8	-	15.2	30.8	33.8	18.0	-	16.9	-
Sm	7.12	6.36	6.55	-	4.18	-	3.78	6.42	7.05	4.45	-	4.15	-
Eu	2.16	1.97	2.03	-	1.45	-	1.29	1.94	2.17	1.48	-	1.34	-
Gd	6.73	6.04	6.22	-	4.47	-	4.00	5.99	6.67	4.74	-	4.36	-
Tb	0.937	0.856	0.885	-	0.692	-	0.617	0.841	0.951	0.730	-	0.666	-
Dy	5.16	4.75	4.92	-	4.13	-	3.64	4.72	5.32	4.30	-	3.85	-
Ho	0.939	0.866	0.881	-	0.791	-	0.693	0.884	0.982	0.840	-	0.744	-
Er	2.35	2.20	2.28	-	2.07	-	1.82	2.26	2.54	2.20	-	1.89	-
Tm	0.312	0.298	0.302	-	0.284	-	0.250	0.302	0.342	0.297	-	0.256	-
Yb	1.91	1.81	1.85	-	1.77	-	1.53	1.87	2.13	1.86	-	1.62	-
Lu	0.265	0.255	0.265	-	0.253	-	0.217	0.265	0.300	0.271	-	0.229	-

Table 2. (continued)

Sample	SY-060	SY-067	SY-069	SY-072	SY-073	SY-074	SY-075	SY-077	SY-078	SY-080	SY-081	SY-082	SY-083
Lat. [°N]	36°12`32``	36°06`56``	36°07`00``	36°06`55``	36°06`54``	35°55`43``	35°55`43``	35°53`18``	35°52`58``	35°49`29``	35°49`29``	35°49`29``	35°49`26``
Long. [°E]	37°12`11``	37°13`40``	37°13`40``	37°13`39``	37°13`39``	37°17`49``	37°17`49``	37°19`32``	37°19`33``	37°19`34``	37°19`35``	37°19`36``	37°19`37``
Elevation [m]	-	538	538	526	522	424	424	474	518	479	505	-	525
Rock type	T	BA	T	T	T	T	T	T	T	BA	T	T	AB
SiO_2	50.35	50.16	49.62	49.31	50.22	49.62	48.98	50.03	50.30	51.39	49.83	49.84	48.94
TiO_2	1.77	1.66	1.68	1.70	1.73	1.62	1.82	1.86	1.94	1.87	1.74	1.66	1.67
Al_2O_3	14.08	13.87	13.34	13.72	13.62	14.04	14.07	13.42	14.44	15.36	13.68	13.89	13.70
$Fe_2O_3^T$	11.88	11.55	11.61	11.79	11.45	12.03	11.99	11.68	12.22	11.62	11.54	11.65	11.87
MnO	0.15	0.15	0.14	0.15	0.15	0.14	0.15	0.15	0.15	0.14	0.16	0.15	0.15
MgO	8.46	6.31	8.66	7.26	8.80	5.92	6.32	8.06	6.87	4.55	7.26	8.08	7.58
CaO	8.46	9.99	9.54	9.76	8.88	10.26	10.09	9.48	8.75	9.41	10.17	9.64	10.63
Na_2O	3.04	3.27	2.80	3.04	3.09	2.66	3.34	3.41	3.31	3.17	3.26	3.14	3.24
K_2O	0.62	0.45	0.64	0.57	0.68	0.50	0.66	0.68	0.86	0.41	0.69	0.62	0.63
P_2O_5	0.23	0.20	0.23	0.23	0.23	0.17	0.25	0.27	0.29	0.22	0.25	0.22	0.24
L.O.I.	1.55	2.47	1.39	2.02	1.21	3.55	2.15	1.39	1.16	1.76	1.79	1.27	2.02
Total	100.59	100.08	99.65	99.55	100.06	100.51	99.82	100.43	100.29	99.90	100.37	100.16	100.67
Mg-no.	0.62	0.56	0.63	0.59	0.64	0.53	0.55	0.62	0.57	0.48	0.59	0.62	0.60
Li	-	10.1	-	-	-	4.63	8.05	-	-	-	-	8.90	-
Sc	-	15.0	-	-	-	21.2	18.1	-	-	-	-	19.7	-
V	-	-	-	-	-	186	-	-	-	-	-	-	-
Cr	261	279	343	340	346	270	266	311	333	162	298	321	321
Co	-	44.5	-	-	-	45.0	47.2	-	-	-	-	47.5	-
Ni	252	233	296	318	288	193	202	278	296	111	216	233	252
Cu	-	74.2	-	-	-	88.7	77.3	-	-	-	-	71.7	-
Zn	106	112	109	108	111	104	102	109	111	110	108	100	113
Ga	-	20.4	-	-	-	20.7	-	-	-	-	-	-	-
Rb	5.0	6.74	10	11	8	6.43	11.8	13	10	9	11	12.2	11
Y	-	20.5	-	-	-	19.1	16.6	-	-	-	-	18.1	-
Cs	-	0.155	-	-	-	0.125	0.342	-	-	-	-	0.418	-
Sr	320	293	327	339	330	292	365	394	403	364	349	340	348
Ba	-	1533	-	-	-	120	156	-	-	-	-	216	-
Zr	-	86.7	-	-	-	97.4	107	-	-	-	-	106	-
Hf	-	2.43	-	-	-	2.36	3.19	-	-	-	-	3.13	-
Nb	-	9.97	-	-	-	8.71	13.6	-	-	-	-	11.7	-
Ta	-	0.608	-	-	-	0.519	0.945	-	-	-	-	0.792	-
Pb	-	1.69	-	-	-	1.57	2.08	-	-	-	-	2.82	-
Th	-	1.04	-	-	-	1.16	1.73	-	-	-	-	1.76	-
U	-	0.331	-	-	-	0.364	0.566	-	-	-	-	0.630	-
La	-	8.13	-	-	-	8.00	12.1	-	-	-	-	11.5	-
Ce	-	18.1	-	-	-	18.3	27.0	-	-	-	-	25.4	-
Pr	-	2.39	-	-	-	2.43	3.52	-	-	-	-	3.33	-
Nd	-	10.9	-	-	-	10.9	15.6	-	-	-	-	14.7	-
Sm	-	3.32	-	-	-	3.13	4.00	-	-	-	-	3.94	-
Eu	-	1.26	-	-	-	1.23	1.40	-	-	-	-	1.39	-
Gd	-	3.92	-	-	-	3.61	4.26	-	-	-	-	4.34	-
Tb	-	0.642	-	-	-	0.584	0.655	-	-	-	-	0.682	-
Dy	-	3.89	-	-	-	3.38	3.73	-	-	-	-	3.99	-
Ho	-	0.730	-	-	-	0.640	0.693	-	-	-	-	0.745	-
Er	-	1.85	-	-	-	1.68	1.74	-	-	-	-	1.87	-
Tm	-	0.244	-	-	-	0.248	0.233	-	-	-	-	0.253	-
Yb	-	1.48	-	-	-	1.50	1.43	-	-	-	-	1.56	-
Lu	-	0.203	-	-	-	0.202	0.204	-	-	-	-	0.226	-

Table 2. (continued)

Sample	SY-084	SY-086	SY-088	SY-116	SY-120	SY-123	SY-124	SY-125	SY-127	SY-129	SY-94-30	SY-94-31	SY-94-32
Lat. [°N]	35°49`26``	35°50`54``	36°08`55``	36°38`51``	36°40`11``	36°40`10``	36°40`09``	36°40`09``	36°37`35``	36°37`18``	32°56`43``	32°56`43``	32°56`43``
Long. [°E]	37°19`38``	37°19`39``	37°19`40``	37°19`41``	37°19`42``	37°19`43``	37°19`44``	37°19`45``	37°19`46``	37°19`47``	36°42`48``	36°42`48``	36°42`48``
Elevation [m]	-	406	387	443	564	562	548	525	392	440	1066	1066	1066
Rock type	T	BA	T	H	T	T	T	T	AB	AB	**LC** xenolith	**LC** xenolith	**LC** xenolith
SiO_2	49.52	51.00	48.47	45.43	48.35	49.94	49.55	49.58	44.29	43.79	41.49	45.72	46.1
TiO_2	1.72	1.71	1.86	2.61	2.09	2.05	2.11	2.06	2.68	2.66	1.5	1.65	3.43
Al_2O_3	14.13	13.77	13.04	13.21	14.73	15.71	15.16	15.00	12.59	12.30	15.25	15.7	16
$Fe_2O_3^T$	11.79	11.86	11.82	12.63	11.17	11.45	12.09	11.57	13.21	13.06	15.33	9.85	11.56
MnO	0.15	0.15	0.12	0.16	0.15	0.15	0.16	0.15	0.18	0.17	0.25	0.13	0.17
MgO	7.04	7.05	9.36	7.70	5.43	5.97	6.34	5.75	9.72	10.16	9.52	8.9	5.47
CaO	10.11	9.20	8.65	10.29	10.76	9.18	9.41	9.81	10.61	10.49	10.57	13.44	9.14
Na_2O	3.13	3.06	3.03	3.67	3.20	3.53	3.04	3.25	2.68	2.34	2.57	2.95	4.16
K_2O	0.59	0.59	0.81	1.24	0.82	0.86	0.59	0.85	1.38	1.43	0.3	0.28	0.62
P_2O_5	0.24	0.23	0.27	0.49	0.27	0.28	0.27	0.27	0.52	0.51	0.51	0.15	1.19
L.O.I.	1.93	1.49	2.28	1.84	3.04	0.44	1.37	1.74	1.95	2.10	1.88	0.55	1.27
Total	100.35	100.11	99.71	99.27	100.01	99.56	100.09	100.03	99.81	99.01	99.17	99.32	99.11
Mg-no.	0.58	0.58	0.65	0.59	0.53	0.55	0.55	0.54	0.63	0.64	59.1	67.8	52.4
Li	9.45	-	5.69	-	-	6.93	-	-	6.09	8.49	10.4	4.37	4.27
Sc	19.8	-	15.0	-	-	16.1	-	-	21.2	15.4	30.4	43.9	19.5
V	-	-	-	-	-	-	-	-	239	- -	-	-	
Cr	312	269	330	248	180	201	265	239	283	289	350	145	14
Co	46.4	-	48.9	-	-	37.9	-	-	56.4	53.6	58	35.7	36.4
Ni	221	236	301	217	82	86.0	131	111	211	221	112	58.9	72.4
Cu	67.6	-	80.9	-	-	38.2	-	-	57.8	55.8	9.87	13.7	62.4
Zn	98.1	107	108	119	104	102	114	109	108	113	165	55.8	83.1
Ga	-	-	20.3	-	-	22.5	-	-	21.9	22.2	-	-	-
Rb	13.3	13	11.3	23	16	9.26	8	14	19.3	17.0	2.38	1.75	2.31
Y	18.6	-	19.3	-	-	21.6	-	-	19.6	20.7	22.5	13.7	27.2
Cs	0.456	-	0.120	-	-	0.160	-	-	0.200	0.114	0.045	0.036	0.018
Sr	339	366	366	666	418	413	408	396	691	707	315	768	1327
Ba	204	-	123	-	-	171	-	-	308	1174	152	160	683
Zr	109	-	106	-	-	124	-	-	182	176	113	53.6	126
Hf	3.22	-	2.85	-	-	3.35	-	-	4.22	4.34	3.04	1.58	3.97
Nb	12.2	-	17.4	-	-	13.1	-	-	41.7	41.3	4.12	8.9	21.4
Ta	0.838	-	1.12	-	-	0.844	-	-	2.71	2.74	0.384	0.539	1.23
Pb	2.64	-	1.82	-	-	2.19	-	-	2.39	2.62	0.83	0.444	2.24
Th	1.85	-	1.62	-	-	1.90	-	-	2.96	2.99	0.318	0.275	0.307
U	0.647	-	0.502	-	-	0.462	-	-	0.789	0.897	0.125	0.057	0.163
La	11.9	-	12.6	-	-	13.2	-	-	25.6	25.4	13.7	12.1	40.2
Ce	26.4	-	26.9	-	-	28.8	-	-	54.1	52.3	33.7	25	83.3
Pr	3.46	-	3.43	-	-	3.76	-	-	6.35	6.36	4.73	3.1	10.4
Nd	15.1	-	15.2	-	-	16.5	-	-	25.9	26.7	21.5	13.5	43.5
Sm	4.04	-	3.93	-	-	4.23	-	-	5.84	6.02	4.96	3.21	8.81
Eu	1.41	-	1.39	-	-	1.42	-	-	2.01	1.97	1.7	1.4	2.91
Gd	4.46	-	4.28	-	-	4.52	-	-	5.65	5.73	5.18	3.46	8.38
Tb	0.706	-	0.654	-	-	0.708	-	-	0.799	0.812	0.788	0.512	1.138
Dy	4.08	-	3.78	-	-	4.17	-	-	4.20	4.34	4.75	3	6.23
Ho	0.754	-	0.705	-	-	0.787	-	-	0.737	0.762	0.96	0.578	1.16
Er	1.91	-	1.75	-	-	2.05	-	-	1.77	1.84	2.63	1.5	2.98
Tm	0.259	-	0.226	-	-	0.281	-	-	0.232	0.237	0.376	0.205	0.399
Yb	1.61	-	1.36	-	-	1.70	-	-	1.40	1.39	2.47	1.25	2.49
Lu	0.226	-	0.189	-	-	0.235	-	-	0.185	0.189	0.375	0.182	0.366

Table 2. (continued)

Sample	SY-94-34	SY-94-36	SY-94-38	BHVO-1 (XRF)	BHVO-1 (ICP-MS)
Lat. [°N]	32°56`43``	32°56`43``	32°56`43``		
Long. [°E]	36°42`48``	36°42`48``	36°42`48``		
Elevation [m]	1066	1066	1066		
Rock type	LC xenolith	LC xenolith	LC xenolith	standard	standard
SiO_2	46.26	42.09	40.54	50.00	-
TiO_2	0.59	4.54	1.09	2.79	-
Al_2O_3	17.99	15.15	14.08	13.86	-
$Fe_2O_3^T$	7.89	16.39	14.9	12.26	-
MnO	0.11	0.18	0.21	0.17	-
MgO	9.77	6.83	16.15	7.23	-
CaO	11.53	9.87	10.17	11.54	-
Na_2O	2.38	3.06	1.02	2.43	-
K_2O	0.15	0.56	0.11	0.53	-
P_2O_5	0.08	0.13	0.21	0.28	-
L.O.I.	1.76	0.83	0.25	-	-
Total	98.51	99.63	98.73	101.09	-
Mg-no.	74.3	49.3	71.6	-	-
Li	4.83	6.76	6.8	-	4.45
Sc	33.4	28.2	33	-	28.7
V	-	-	-	-	332
Cr	305	11	367	291	293
Co	56.2	52.6	74.1	-	43.9
Ni	240	57.2	339	119	115
Cu	56.1	17.2	22.4	-	132
Zn	62.9	105	118	104	101
Ga	-	-	-	-	22.2
Rb	0.904	4.33	1.54	11	9.56
Y	12	20.4	17	-	24.7
Cs	0.012	0.059	0.025	-	0.094
Sr	2376	1076	105	401	390
Ba	171	192	25	-	133
Zr	41.9	47.7	31.3	-	168
Hf	1.13	1.91	1.12	-	4.50
Nb	1	10	1.72	-	17.7
Ta	0.1	0.682	0.132	-	1.13
Pb	0.607	0.836	0.362	-	2.10
Th	0.098	0.025	0.08	-	1.22
U	0.052	0.04	0.036	-	0.425
La	4.63	3.31	4.38	-	15.2
Ce	8.86	12.8	12.6	-	37.9
Pr	1.32	2.6	2.05	-	5.34
Nd	6.13	15.4	10.9	-	24.4
Sm	1.65	4.61	3.14	-	6.16
Eu	0.718	1.91	1.17	-	2.03
Gd	1.96	4.87	3.67	-	6.11
Tb	0.329	0.747	0.587	-	0.933
Dy	2.09	4.38	3.55	-	5.30
Ho	0.426	0.846	0.702	-	0.979
Er	1.16	2.19	1.83	-	2.47
Tm	0.166	0.294	0.246	-	0.323
Yb	1.07	1.84	1.56	-	1.98
Lu	0.153	0.263	0.225	-	0.273

Table 3. Sr, Nd and Pb isotopic compositions of selected samples of the Syrian lavas and of lower crustal xenoliths.

	isotopic compositions						age corrected isotopic compositions						
Sample	$^{87}Sr/^{86}Sr$ (2s)	$^{143}Nd/^{144}Nd$ (2s)	$^{206}Pb/^{204}Pb$	$^{207}Pb/^{204}Pb$	$^{208}Pb/^{204}Pb$		Age* [m.y.]	$^{87}Sr/^{86}Sr_T$	$^{143}Nd/^{144}Nd_T$	$^{206}Pb/^{204}Pb_T$	$^{207}Pb/^{204}Pb_T$	$^{208}Pb/^{204}$ T
SY 01/09	0.704749 (10)	0.512732 (13)					12.3	0.70472	0.512721			
SY 01/10	0.704592 (11)	0.512749 (12)					12.3	0.70457	0.512738			
SY 01/12	0.704882 (14)	0.512699 (14)	18.844	15.686	38.974		12.3	0.70486	0.512688	18.820	15.685	38.943
SY 01/23	0.704878 (18)	0.512706 (7)					12.3	0.70486	0.512694			
SY 01/25	0.704526 (22)	0.512752 (5)					12.3	0.70450	0.512741			
SY 01/28	0.704378 (12)	0.512819 (11)					12.3	0.70436	0.512807			
SY 01/29	0.704855 (13)	0.512732 (14)	18.952	15.704	39.050		12.3	0.70483	0.512721	18.924	15.703	39.016
SY 01/32	0.704745 (22)	0.512749 (6)					12.3	0.70472	0.512738			
SY-010	0.704066 (3)	0.512803 (3)	18.975	15.671	39.057		2.0	0.70406	0.512802	18.971	15.671	39.050
SY-028	0.704843 (16)	0.512703 (15)					12.3	0.70482	0.512693			
SY-033	0.704570 (17)	0.512721 (11)					12.3	0.70455	0.512710			
SY-037	0.704310 (11)	0.512895 (17)	18.935	15.691	39.036		12.3	0.70429	0.512883	18.906	15.690	39.002
SY-038	0.704600 (19)	0.512799 (11)					9.8	0.70458	0.512791			
SY-067	0.704215 (10)	0.512899 (12)	18.605	15.656	38.547		5.0	0.70421	0.512893	18.596	15.655	38.537
SY-074	0.704747 (10)	0.512781 (13)	18.987	15.648	38.818		5.0	0.70474	0.512775	18.976	15.648	38.806
SY-082	0.704276 (3)	0.512786 (3)	18.666	15.675	38.516		5.0	0.70427	0.512781	18.656	15.675	38.506
SY-088	0.703947 (13)	0.512899 (10)	18.828	15.657	38.724		5.0	0.70394	0.512894	18.815	15.656	38.709
SY-123	0.704223 (12)	0.512795 (11)	18.784	15.652	38.875		2.0	0.70422	0.512792	18.780	15.652	38.869
SY-127	0.703697 (10)	0.512909 (15)	18.843	15.622	38.767		2.0	0.70370	0.512907	18.836	15.622	38.759
SY-129	0.703882 (11)	0.512940 (11)	18.778	15.610	38.667		2.0	0.70388	0.512938	18.771	15.610	38.660
SY-94-30	0.70355 (15)	0.512758 (12)	18.795	15.609	38.597							
SY-94-32	0.70446 (12)	0.512709 (13)	18.582	15.638	38.450							
SY-94-38	0.70329 (8)	0.512850 (9)	18.751	15.566	38.589							

*correction age depends on geological map of Ponikarov et al. (1963) and Ar-Ar data of Krienitz et al. (in preparation)

für Geochronologie in Münster using a VG Sector 54 multicollector mass spectrometer. A few samples were analysed at the GEOMAR Forschungszentrum für marine Geowissenschaften in Kiel for Pb on a Finnigan MAT 262 RPQ2+ and for Sr and Nd on a Finnigan Triton mass spectrometer. For isotope determinations, 100 mg of powdered sample were used. Sr, Nd and Pb were separated from the matrix using standard ion exchange techniques. Sr and Nd isotope ratios were analysed in dynamic mode and corrected for isotope fractionation using $^{86}Sr/^{88}Sr$ = 0.1194 and $^{146}Nd/^{144}Nd$ = 0.7219, respectively. In Münster, standard runs for Sr isotopes gave NBS 987 (n = 16): 0.710299 (2SD = 0.000026) and all Sr isotope analyses were normalised to NBS 987 = 0.710250. Standard runs for $^{143}Nd/^{144}Nd$ gave La Jolla (n=14): 0.511862 (2SD = 0.000024). Pb isotopes were measured in static mode and the NBS 982 standard was used to correct Pb isotopic ratios for mass fractionation. Correction factors are $^{206}Pb/^{204}Pb$ = 0.02%, $^{207}Pb/^{204}Pb$ = 0.03% and $^{208}Pb/^{204}Pb$ = 0.04% and standard runs (n=10) gave $^{206}Pb/^{204}Pb$ = 36.646, $^{207}Pb/^{204}Pb$ = 17.101 and $^{208}Pb/^{204}Pb$ = 36.593 with a precision of ±0.022, ±0.014 and ±0.038 (2SD) respectively. In Kiel, the NBS 987 (n=8) gave 0.710273 (2SD = 0.000010) and all Sr isotope analyses were normalised to NBS 987 = 0.710250. Standard runs for $^{143}Nd/^{144}Nd$ gave 0.511710 (2SD = 0.000010) for the Nd Spex standard (n=5) corresponding to a La Jolla value of 0.511828. The Nd isotope analyses were normalised to the La Jolla standard measured in Münster. The NBS 981 standard was used to correct Pb isotopic ratios for mass fractionation. Correction factors are $^{206}Pb/^{204}Pb$ = 0.02%, $^{207}Pb/^{204}Pb$ = 0.03% and $^{208}Pb/^{204}Pb$ = 0.04% and standard runs (n = 28) gave $^{206}Pb/^{204}Pb$ = 16.903, $^{207}Pb/^{204}Pb$ = 15.447 and $^{208}Pb/^{204}Pb$ = 36.558 with a precision of ±0.018, ±0.024 and ±0.075 (2SD) respectively. Procedural blanks in both laboratories were generally better than 0.2ng, 0.1ng and 0.04ng for Sr, Nd and Pb. Isotopic compositions of all samples were age-corrected using the age of the different locations as defined by the geological maps of Ponikarov et al. (1963) and new Ar-Ar data of Krienitz et al. (Chapter III). The age-corrected isotopic data were used in the figures.

1.4 Results

1.4.1 Classification

According to the total alkali-silica diagram samples of NW Syria can be classified as basalts, one basanite, basaltic andesites, hawaiites and mugearites (Fig. 1.2). Basaltic samples include both nepheline- and hypersthene-normative compositions and thus can be further classified as alkali basalts and tholeiites.

1.4.2 Petrography

Alkali basalts and basanite

All studied undersaturated samples have porphyritic textures and phenocrysts make up to 20 vol.%. The groundmass of alkali basalts and the basanite consists of plagioclase (An_{65-44}),

clinopyroxene (Wo_{50-47}-En_{41-36}), olivine (Fo_{60-56}) and Ti-magnetite. Some samples show calcite vesicle fillings and quartz xenocrysts were observed in sample SY-028. Olivine is the most common phenocryst phase and dominates over clinopyroxene. Olivine phenocrysts are often subhedral to skeletal and always show iddingsite rims or are totally altered. One sample includes a clinopyroxene cumulate with resorbed and abundant broken crystals. An agglomerate of rounded olivine crystals (Fo_{85-82}) occurs in sample SY-127 and is interpreted as xenocrysts.

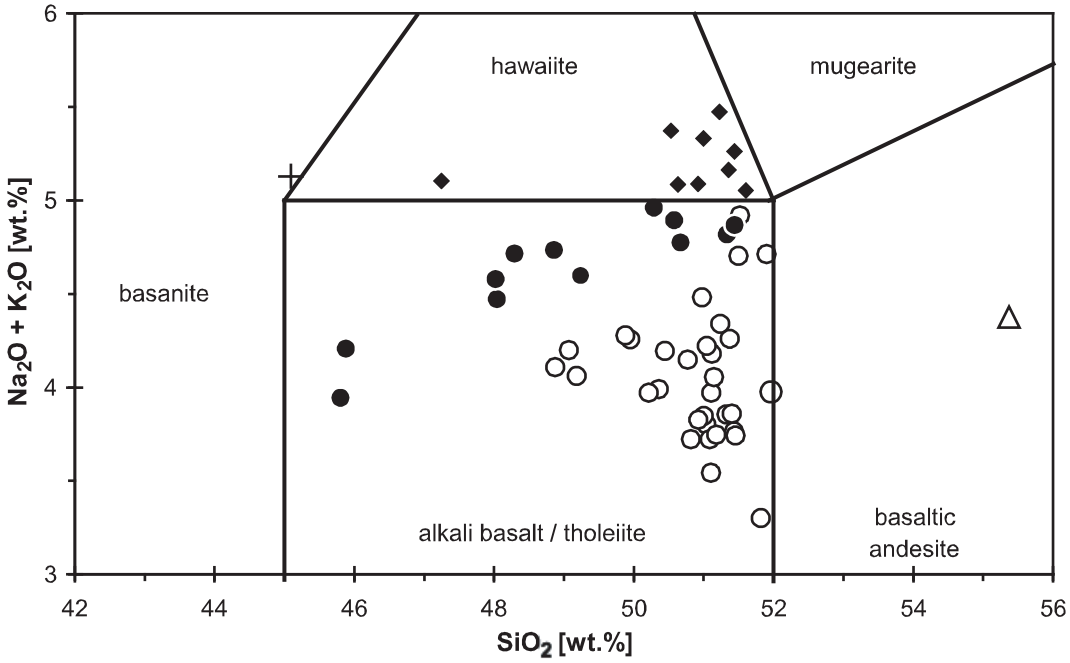

Fig. 1.2. Total-alkali-silica diagram of Le Bas et al. (1986) with rock type discrimination after Le Maitre et al. (1989) for the classification of northwestern Syrian samples. Filled symbols refer to high-P suite and open symbols to low-P suite samples (see text for details).

Tholeiites and basaltic andesites

Plagioclase ($An_{64-(12)}$), clinopyroxene (Wo_{44-30}-En_{52-41}), Ti-magnetite and rarely olivine (Fo_{75-73}) occur in the groundmass of tholeiites and basaltic andesites. Occasionally calcite fillings are found. Samples contain varying amounts of olivine (Fo_{82-55}), clinopyroxene (tholeiite Wo_{45-44}-En_{44-46}) and plagioclase (An_{65-29}) phenocrysts. Olivines are often altered and make up to 10 vol.% and are the most abundant phenocryst phase in the tholeiites. Olivine phenocrysts, occurring up to 5 vol.% in basaltic andesites, are altered and often show resorption. Plagioclase phenocrysts (5-10 vol.%) are more common in basaltic andesites and dominate in most cases over olivine. Aggregates of plagioclase, clinopyroxene and minor amounts of olivine are observed in both the tholeiites and the basaltic andesites.

Hawaiites and mugearites

The groundmass of hawaiites and mugearites is composed of plagioclase laths (An_{62-20}), clinopyroxene (Wo_{45-42}-En_{41-38}), Ti-magnetite and rare olivine (Fo_{60-42}). Resorbed quartz

crystals occur as xenocrysts in a few samples. Plagioclase phenocrysts (An_{65-48}) are euhedral to subhedral laths- and make up 5-20 vol.% and in most samples dominate over olivine (Fo_{83-50}) and clinopyroxene (Wo_{46-41}-En_{48-38}), both 5-10 vol.%. The subhedral to skeletal olivine phenocrysts always show iddingsite rims or are totally altered. Rare calcite fillings are observed as well and in some cases aggregates of clinopyroxene and plagioclase crystals.

1.4.3 Chemical alteration

Weathering causes chemical alteration of rocks affecting especially the mobile elements (Cs, Rb, K, and U) leading to a loss of these elements and to elevated H_2O (i.e. LOI) contents. The concentrations of mobile elements of the whole sample suite show no correlation with their respective MgO and LOI contents. Some alkali basalts, tholeiites and basaltic andesites have LOI values >2wt.% (up to 3.55wt.%) and show the lowest K_2O and U concentrations. If alteration processes have affected these samples, they should have high Nb/U ratios compared to fresh lavas. However, samples with low U concentrations are indistinguishable from the rest of the samples suite. Thus, chemical alteration plays no important role and generally did not affect the mobile elements of the analysed rocks and has no significant influence on variations of other major and trace elements.

1.4.4 Major and trace elements

Based on their P_2O_5 contents (Fig. 1.3a) the samples can be divided into two suites: (1) a high-P($_2O_5$) suite containing most of the alkali basalts and mugearites, the basanite, hawaiites and some of the tholeiites, and (2) a low-P($_2O_5$) suite consisting of most of the tholeiites and basaltic andesites and some of the alkali basalts and mugearites (cp. Fig. 1.2). Samples of the high-P suite are enriched in TiO_2 and K_2O, but most have lower SiO_2 and Ni at similar MgO concentrations with compared to the low-P suite (Fig. 1.3).

MgO concentrations of the samples range from 10.2 to 4.1 wt.%. TiO_2, Al_2O_3 and Na_2O in the low-P suite exhibits clear negative correlations with MgO (Fig. 1.3). FeO^T concentrations are approximately constant over the whole MgO range. Positively correlated with decreasing MgO are the compatible trace elements Cr and Ni (Figs. 1.3i and f). CaO scatters widely and shows no correlation with MgO. K_2O and P_2O_5 are constant over the whole MgO range and Cr contents decreases sharply at 6 wt.% MgO (Fig. 1.3i). Samples of the high-P suite show similar trends with respect to most of the major elements, but display a distinct positive correlation between TiO_2 and MgO.

Samples of the high-P suite are relatively enriched in highly incompatible elements and, for example, Ba, Nb, and Zr concentrations are twice as high in high-P lavas compared to the low-P suite (Figs. 1.4a - c). Both suites contain some samples enriched to variable amounts in Ba. Heavy rare earth element contents are similar in the high and low-P suite and increase with decreasing MgO (Fig. 1.4d). Samples of the high-P suite show chondrite-normalised La/Sm

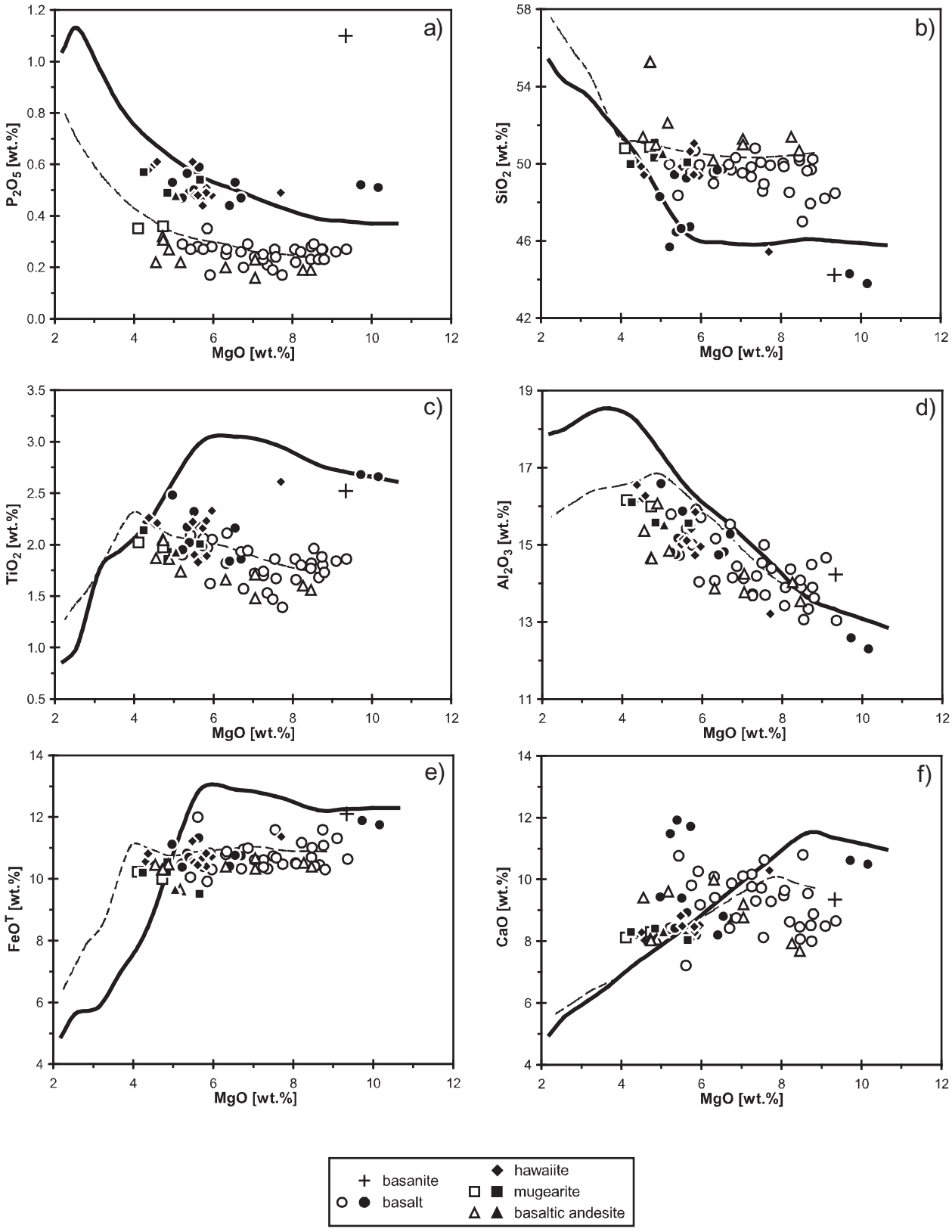

Fig. 1.3. (a - j) Selected major and compatible trace element variation diagrams versus MgO for the Syrian lavas. Also shown are the results for fractional crystallisation modeling using the software program MELTS of Ghiorso and Sack (1995) with input values listed in Table 4. Fractional crystallisation trends for high-P suite samples are given by continuous lines and for low-P suite samples by dashed lines.

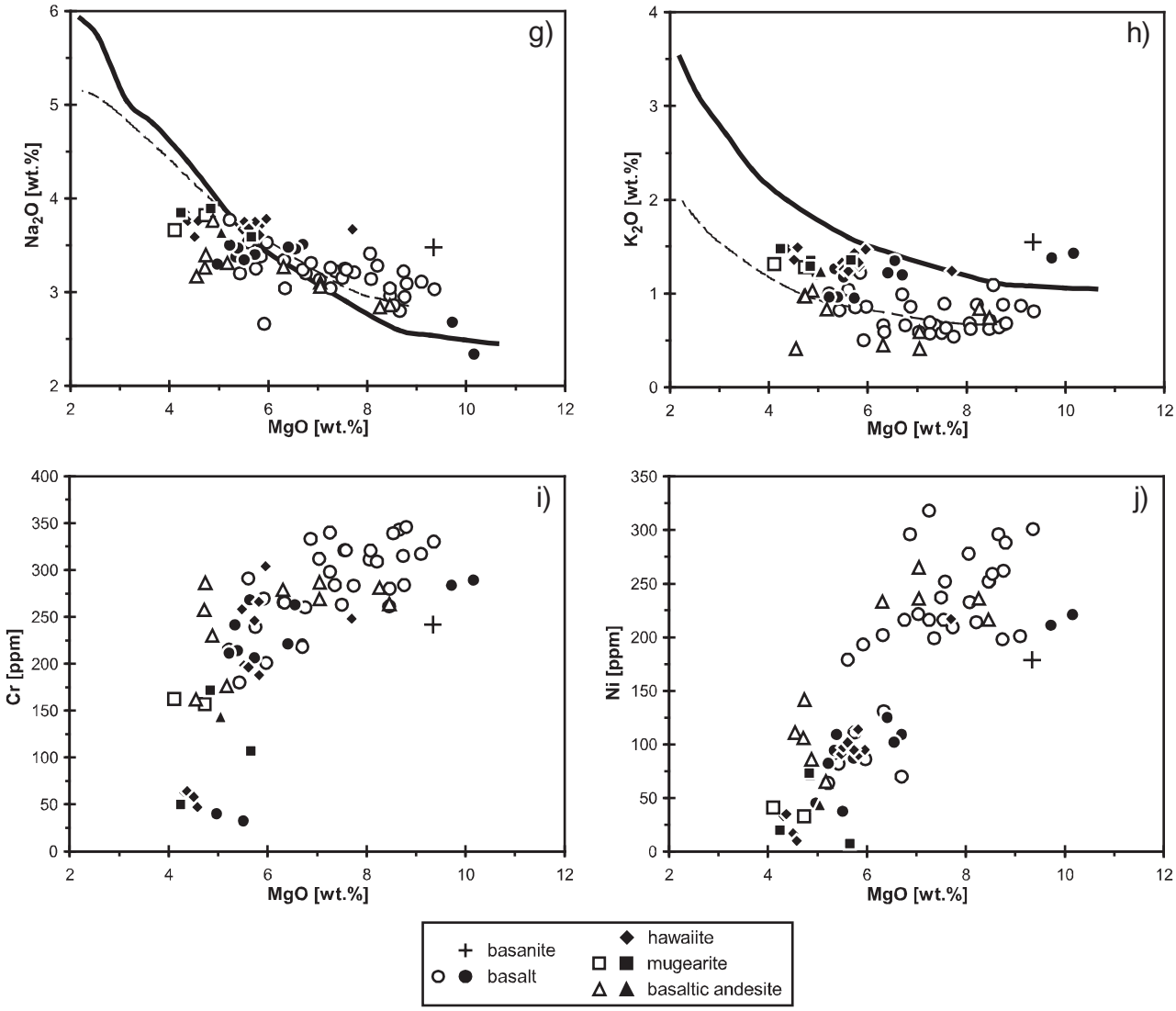

Fig. 1.3. continued

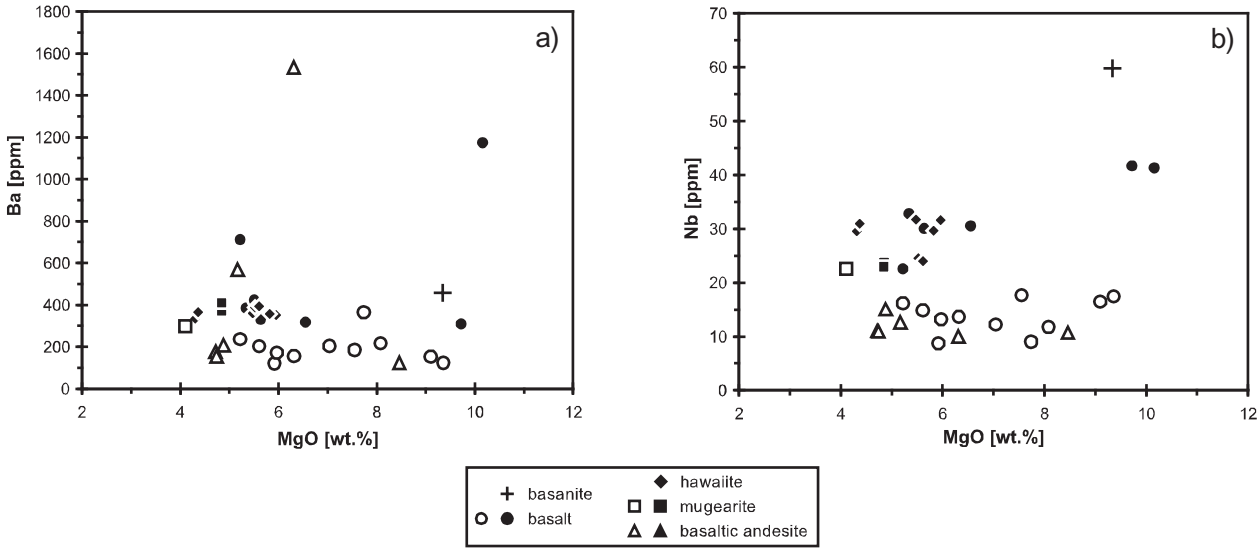

Fig. 1.4. (a – f) Variations in trace element contents and ratios with MgO for the Syrian lavas.

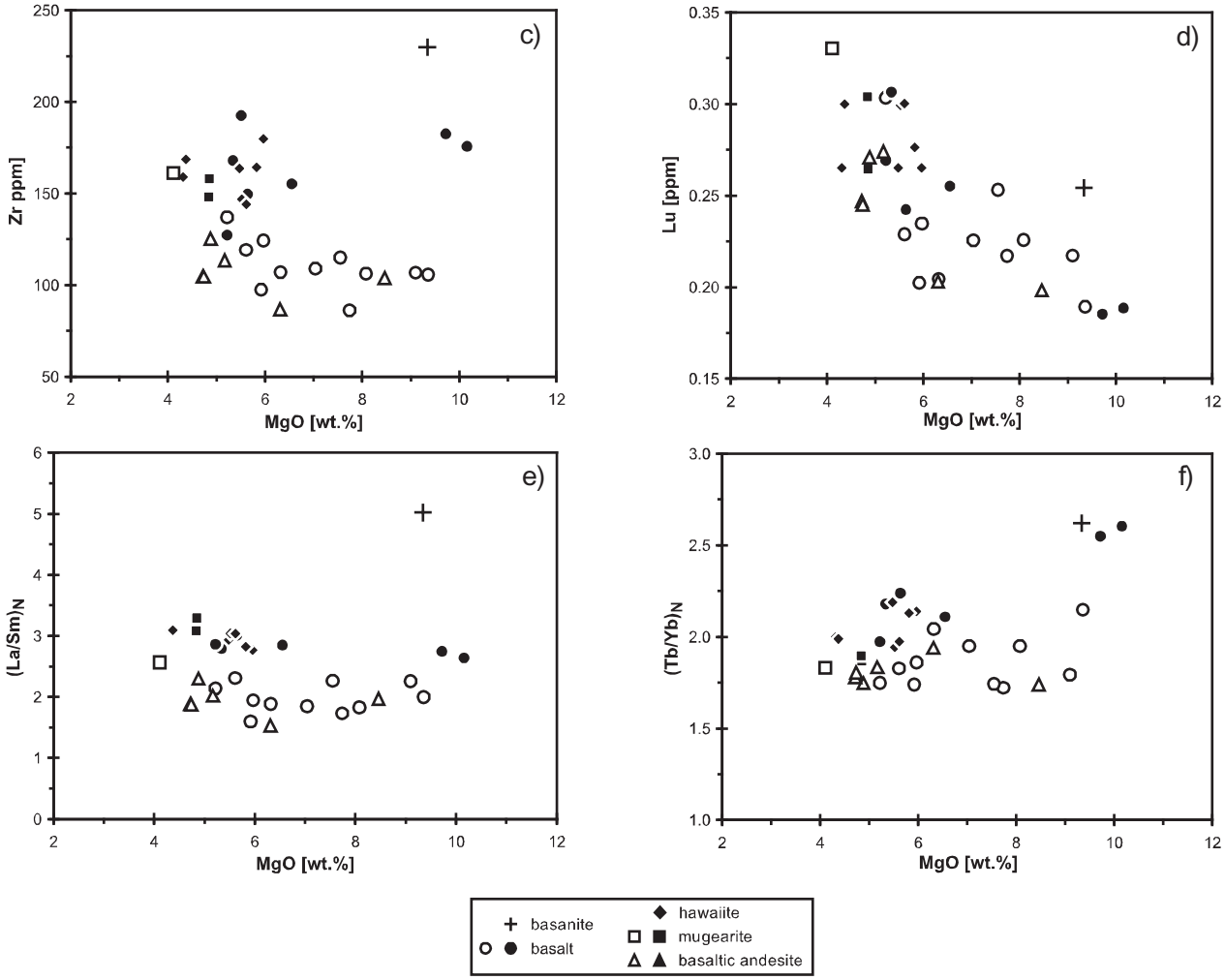

Fig. 1.4 continued

$[(La/Sm)_N]$ ratios between 3.3 and 2.6 (basanite 5.0) and $(Tb/Yb)_N$ ratios from 2.6 - 1.9. In contrast, the low-P suite has $(La/Sm)_N$ between 2.6 and 1.5 and $(Tb/Yb)_N$ ratios in the range of 2.1-1.7 (Figs. 1.4e and f).

Ce/Pb ratios (28-8) of the northwestern Syrian sample suite show a positive correlation with Nb/U (53-16), but are negatively correlated with SiO_2 and $^{87}Sr/^{86}Sr_T$ (Figs. 1.5 and 1.6), whereas Sr isotope ratios become more radiogenic with decreasing MgO contents (Fig. 1.6a). Most of the primitive samples have high Ce/Pb (28-19) and Nb/U (53-22) ratios, have low SiO_2 contents and unradiogenic Sr isotopes similar to compositions of oceanic basalts, whereas basaltic andesites show the lowest incompatible element ratios and high SiO_2 concentrations trending to compositions displayed by average upper and lower continental crust (Figs. 1.5 and 1.6).

1.4.5 Sr-, Nd- and Pb-isotopes

As illustrated in Figure 1.7a the $^{87}Sr/^{86}Sr_T$ (0.7037 - 0.7049) and $^{143}Nd/^{144}Nd_T$ (0.51294 - 0.51269) compositions of the Syrian lavas are negatively correlated, whereby the basaltic samples of the low-P suite have the least radiogenic Sr and the most radiogenic Nd isotope compositions. Mugearites have high $^{87}Sr/^{86}Sr_T$ and show the least radiogenic $^{143}Nd/^{144}Nd_T$. The

array displayed by the northwestern Syrian samples trends towards radiogenic $^{87}Sr/^{86}Sr$ and unradiogenic $^{143}Nd/^{144}Nd$ as observed in crustal samples from Jordan (Jarrar et al., 2003) and Saudi Arabia (Hegner and Pallister, 1989) (Fig. 1.7a). In a plot of $^{206}Pb/^{204}Pb$ versus $^{87}Sr/^{86}Sr$ the array formed by most of the Syrian lavas do overlap with compositions attributed to the Afar plume and trends to compositions characteristically for upper crustal rocks of Saudi Arabia, whereby a few Syrian samples show isotope compositions similar to Syrian lower crust (Fig. 1.

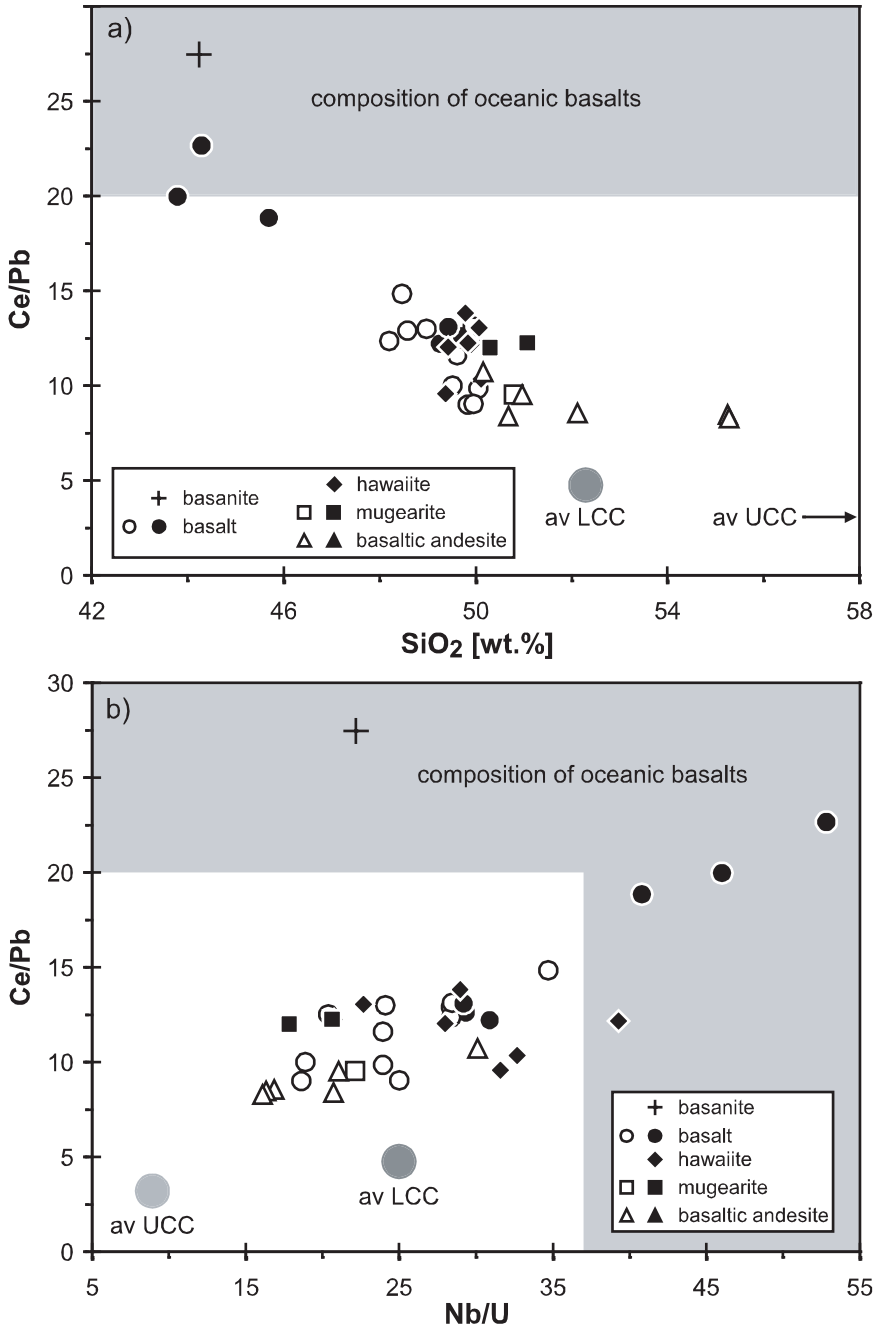

Fig. 1.5. Plots of (a) SiO_2 versus Ce/Pb and (b) Nb/U versus Ce/Pb. Grey fields display Ce/Pb and Nb/U arrays for uncontaminated mantle-derived magmas (Hofmann et al., 1986). Average continental crustal compositions of lower (LCC) and upper crust (UCC) are from Rudnick and Fountain (1995).

7b). The Pb isotopes do not define a trend but rather show significant scatter with $^{206}Pb/^{204}Pb_T$ ranging from 19.0 to 18.6 and $^{207}Pb/^{204}Pb_T$ from 15.7 to 15.6 (Fig. 1.8a). The field of northwestern Syrian lavas as defined by $^{206}Pb/^{204}Pb_T$ and $^{207}Pb/^{204}Pb_T$ ratios overlaps with arrays representative for samples from the Arabian lithospheric mantle and southern Syria, but

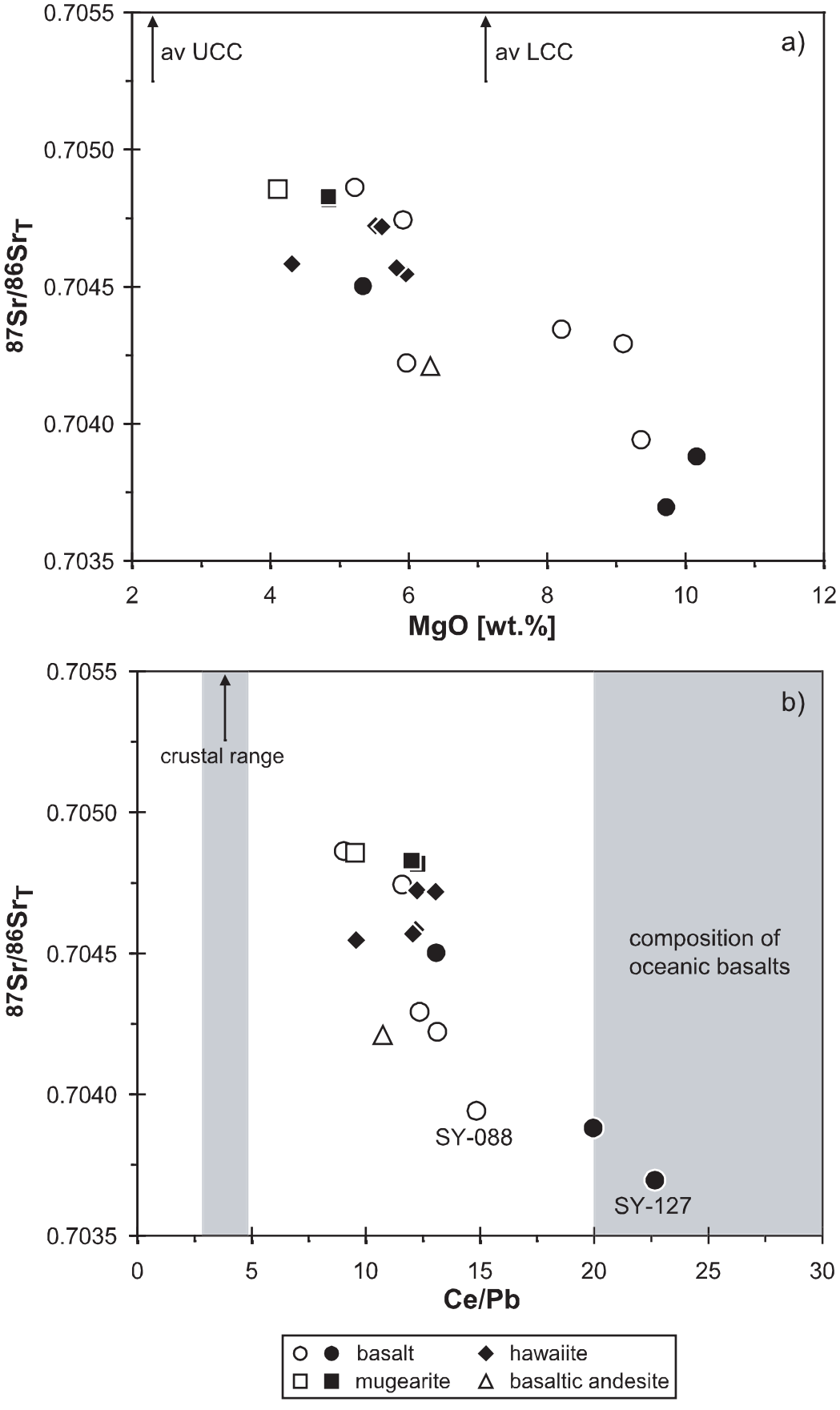

Fig. 1.6. Plots of (a) MgO versus $^{87}Sr/^{86}Sr_T$ and (b) Ce/Pb versus $^{87}Sr/^{86}Sr_T$. Data sources for average lower and upper continental crust and mantle array as in Figure 1.5.

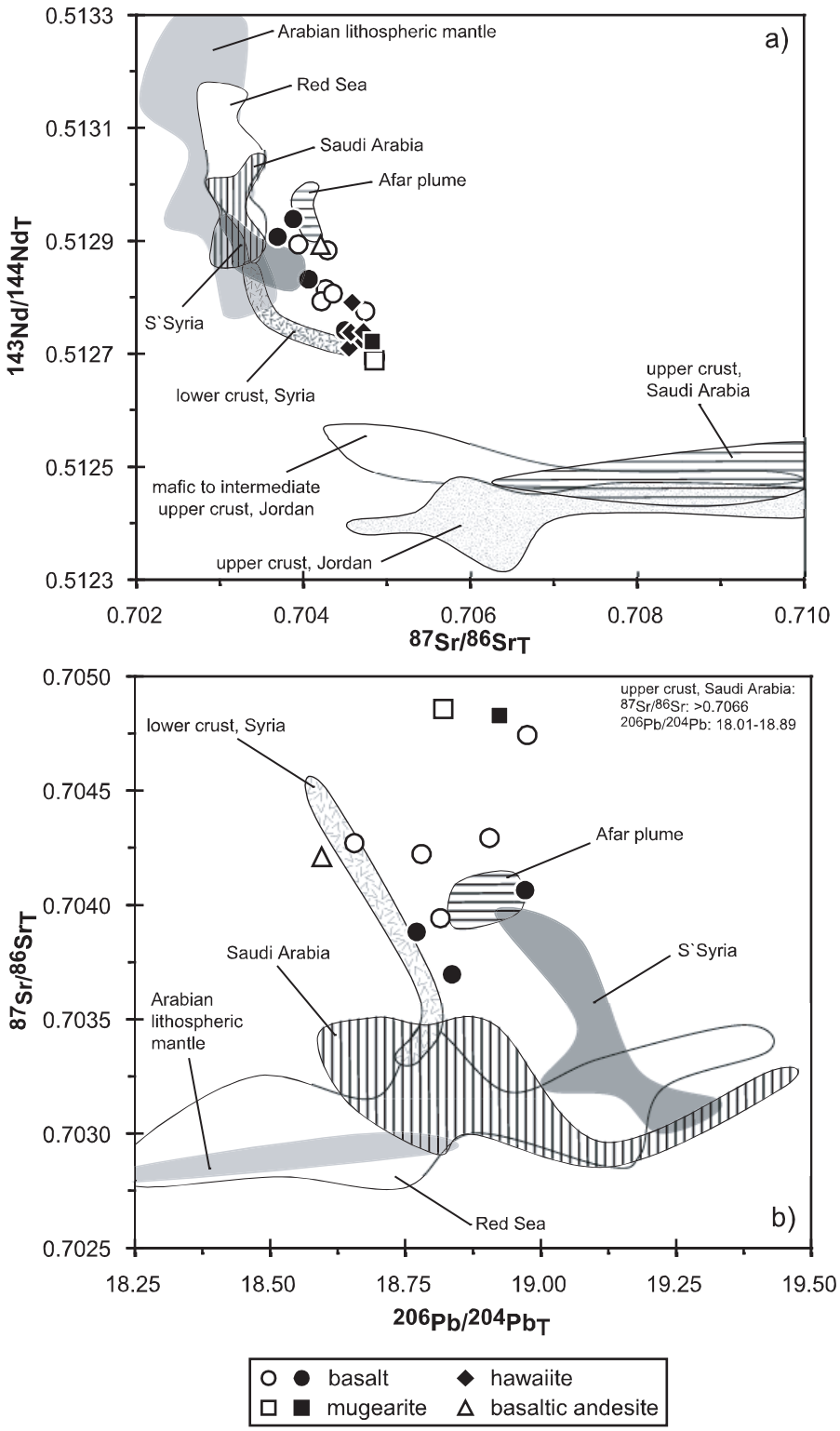

Fig. 1.7. Diagrams of (a) $^{87}Sr/^{86}Sr_T$ versus $^{143}Nd/^{144}Nd_T$ and (b) $^{206}Pb/^{204}Pb_T$ versus $^{87}Sr/^{86}Sr_T$ for Syrian samples analysed in this study compared with Arabian crustal data, clinopyroxene analyses representative of Arabian lithospheric mantle, lavas with high $^{3}He/^{4}He$ ratios, which are influenced by the Afar plume, lavas from the Red Sea region and Saudi Arabia. Data sources: Afar plume (Pik et al., 1999), Arabian lithospheric mantle (Henjes-Kunst et al., 1990; Altherr et al., 1990; Blusztajn et al., 1995), Red Sea (Dupre et al., 1988; Eissen et al., 1989; Schilling et al., 1992; Rogers, 1993), Saudi Arabia and southern Syria (Bertrand et al., 2003), Saudi Arabian upper crust (Hegner and Pallister, 1989), Jordanian upper crust (Jarrar et al., 2003), and Syrian lower crust (this work).

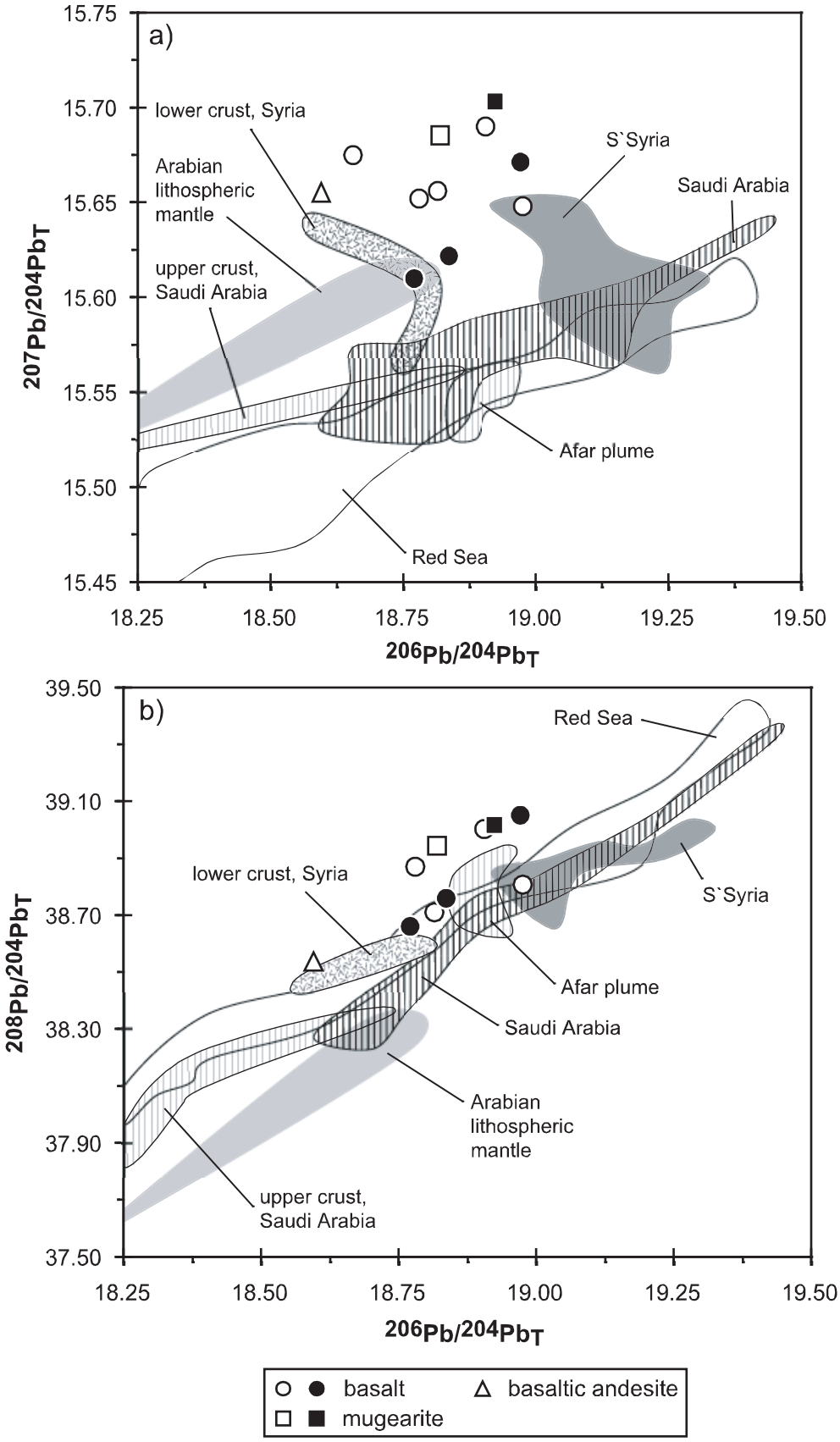

Fig. 1.8. (a) and (b) Pb isotope systematics for investigated Syrian samples (fields and data sources as in Figure 1.7).

has more radiogenic $^{207}Pb/^{204}Pb_T$ ratios compared to lavas influenced by the Afar plume (Fig. 1.8a). $^{206}Pb/^{204}Pb_T$ and $^{208}Pb/^{204}Pb_T$ ratios show a poorly defined positively correlation and similar isotope compositions as the Afar plume and Red Sea samples as well, but lie outside the range representative for the Arabian lithospheric mantle (Fig. 1.8b).

1.5 Discussion

1.5.1 Major and trace element behaviour during fractional crystallisation

Samples of the two different rock suites are most likely related by crystal fractionation processes affecting major and compatible trace element compositions. Primitive, mantle derived magmas in equilibrium with mantle olivine have Mg-numbers of 0.68 - 0.72 and Ni concentrations in the range of 300 - 500 ppm (Frey et al., 1978). Although some tholeiites and alkali basalts have relatively primitive Mg-numbers, ranging from 0.65 to 0.60, and Ni concentrations of about 300 ppm (Fig. 1.3j), most of the rocks show lower values. The decrease of Mg-number in combination with decreasing Ni and Cr content implies olivine, clinopyroxene and spinel fractionation. Clinopyroxene extraction is evident in the increasing Al_2O_3 (Fig. 1.3d) and the positive correlation of CaO/Al_2O_3 ratios with decreasing MgO (not shown). The inflection of Cr at 6 wt.% MgO supports the stronger influence of spinel as fractionating phase. Positive Sr anomalies (average Sr/Sr* = 1.34), the lack of Eu anomalies (average Eu/Eu* = 1.00) and uniformly rising Al_2O_3 concentrations indicate that low pressure plagioclase fractionation did not play a major role throughout the fractionation sequence, but may account for the slight increase of SiO_2 at 5 wt.% MgO displayed by hawaiites, mugearites and basaltic andesites. Although titanomagnetite is observed in samples from both suites, its fractionation is only obvious in the high-P suite, as shown by the positive correlation of TiO_2 with MgO (Fig. 1.3c).

For quantitative modeling of fractionation processes the software MELTS from Ghiorso and Sack (1995) was used (Table 4, Fig. 1.3). As a first approximation the modeling results show that most of the Syrian samples can be related to crystal fractionation, but modeling fails to account for all major element variations even within the single suites. The most evolved lavas from the high-P suite have fractionated about 37% clinopyroxene, 6% olivine, 3% plagioclase, and 7% spinel to evolve from an alkali basalt to a mugearite (Table 4). In contrast, the observed mineral modes of mugearites and basaltic andesites of the low-P suite suggest extraction of olivine, clinopyroxene, spinel, and plagioclase to evolve from a tholeiitic parent. However, quantitative modeling using MELTS indicates 22% clinopyroxene and 8% plagioclase removal (Table 4, Fig. 1.3). The results are consistent with the occurrence of all mineral phases in the rock samples with the exception of olivine. The discrepancy between modeling results and the occurrence of olivine as a major phenocryst phase in primitive samples may be due to high pressure conditions for olivine crystallisation. A loss of olivine even at greater depth may account for the generation of the primitive alkali basalts. Furthermore, the results for high-P lavas are similar to results obtained for Pleistocene volcanic rocks from Israel which have undergone up to 30% of mainly clinopyroxene

Table 4. Fractional crystallisation modelling for lavas of NW Syria using MELTS.

	Input values			Initial values recalculated by MELTS	
	low P-group	high P-group		low P-group	high P-group
T range	1300-850 °C	1300-850 °C	$T_{liquidus}$	1239 °C	1268 °C
P	3 kbar	3 kbar	P	3 kbar	3 kbar
$\log_{(10)} fO_2$	0	0	$\log_{(10)} fO_2$	-6.87	-6.57
QFM	+1	+1	?QFM	+1	+1
	[wt.%]	[wt.%]		[wt.%]	[wt.%]
SiO_2	49.62	43.79	SiO_2	50.57	45.78
TiO_2	1.68	2.50	TiO_2	1.71	2.61
Al_2O_3	13.34	12.30	Al_2O_3	13.59	12.86
FeO^T	10.45	11.50	FeO^T	10.88	12.29
MnO	0.14	0.17	MnO	0.14	0.18
MgO	8.66	10.16	MgO	8.83	10.62
CaO	9.54	10.49	CaO	9.72	10.97
Na_2O	2.80	2.34	Na_2O	2.85	2.45
K_2O	0.64	1.00	K_2O	0.65	1.05
P_2O_5	0.23	0.35	P_2O_5	0.23	0.37
H_2O	0.50	0.50	H_2O	0.51	0.52
CO_2	0.30	0.30	CO_2	0.31	0.31
Total	97.90	95.40	Total	99.99	100.01

low P-group

Fractionated phases at:		Phase	[wt.%]	Composition
T	1119°C	cpx	21.56	**Di 29, En 22, He 22,** Jd 3.0
MgO	3.92 wt.%	plag	8.43	**Ab 38, An 61,** Sa 1.1
		Total	29.99	

high P-group

Fractionated phases at:		Phase	[wt.%]	Composition
T	1108°C	ol	6.28	Fo 79
MgO	3.67 wt.%	cpx	36.96	**Di 36, En 18, He 17,** Jd 3.1
		plag	2.93	**Ab 37, An 61,** Sa 1.7
		spinel	6.86	**Usp 31, Mt 47,** Sp 5.1
		Total	53.03	

and olivine fractionation and only minor amounts of other phases (Weinstein et al., 1994).

Pressure-temperature estimates for northwestern Syrian lavas based on clinopyroxene-melt equilibria using the approach of Putirka et al. (1996) yield a total pressure range of 7 - 2 kb. The pressure estimates for whole rock data of the Syrian lavas correspond to a total depth interval of 23 - 8 km. High-P suite samples indicate pressure conditions between 7 and 4 kb (23 - 13 km), but mostly give crystallisation pressures in the range of 5.5 to 5 kb (18 - 16 km). Assuming a lower limit of the upper crust in depths of about 20 km (Nasir and Safarjalani, 2000) the pressure conditions during crystal fractionation producing high-P suite lavas suggest that the magmas stagnated already in lower crustal levels, whereas the main phase of crystallisation took place in upper crustal depths. In contrast, fractionation resulting in the formation of the low-P suite occurs at shallower depths of about 3 kb (~10 km) suggesting solely an upper crustal level for crystal formation. These calculations are similar to observations made by Baker et al. (1997) for lavas from western Yemen, which have undergone high-pressure (~30 - 8 kb) and/or polybaric fractionation of olivine, clinopyroxene, plagioclase, and Fe-Ti oxides and, at a later stage, apatite. The variable crystallisation depths of the two Syrian suites indicate rather magma stagnation in several small magma chambers than argue for long magma residence times in a single pronounced magma chamber. Even the presence of xenocrysts and cumulates observed in thin sections suggests a fast ascent of magmas.

1.5.2 Crustal contamination

The decrease of incompatible element ratios such as Ce/Pb or Nb/U and variations of isotope compositions during magmatic differentiation, i.e. increasing SiO_2 or decreasing MgO, cannot be achieved by crystal fractionation (Fig. 1.5a). Since the isotope composition of a magma is independent of crystal fractionation processes as well as of the degree of partial melting, increasing Sr isotopic ratios with decreasing MgO (Fig. 1.6a) are the result of crustal contamination. Thus, the observed correlations between incompatible element ratios and isotopic compositions throughout the differentiation trends are due to the combined effects of assimilation and fractionation (AFC). Hofmann et al. (1986) have shown that the Ce/Pb and Nb/U ratios of uncontaminated mantle-derived magmas are 25±5 and 47±10, respectively. These ratios will be significantly lowered as magmas react with continental crust (Fig. 1.5). The assimilation of continental crust during the evolution of the Syrian lavas is also suggested by the isotopic compositions of the sample suite because Sr and Nd isotope compositions of the evolved lavas fall outside the fields for Arabian lithospheric mantle and lavas from the Afar plume and Red Sea, but trend to crustal compositions with the most evolved samples exhibiting the lowest Nd, but the most radiogenic Sr compositions (Fig. 1.7a). These correlations are evidence for contamination of parental lavas with crustal material. In addition to the geochemical evidence for crustal assimilation, the presence of quartz xenocrysts in some samples supports assimilation processes.

Based on Sr and Nd isotope compositions AFC-processes were modeled using the energy-con-

strained assimilation-fractional crystallisation (EC-AFC) model of Spera and Bohrson (2001). Appropriate end-member compositions were defined on the basis of on the primitive samples SY-088 (low-P suite) and SY-127 (high-P suite) respectively (Fig. 1.6b). The low Sr and high Nd isotopic composition as well as the high Ce/Pb and Nb/U ratios of these samples ensure that these lavas are least or even uncontaminated (Figs. 1.5b, 1.6b, and 1.7a). Since the magmas stagnated at lower crustal levels (Figs. 1.7 and 1.8) it is reasonable to choose as a contaminant material with a composition akin to lower crust. Starting values are given in Table 5, assuming compositions of the contaminant similar to mafic lower crustal xenoliths of the Harrat As Shamah volcanic field in southern Syria (Nasir and Safarjalani, 2000) and an average Sr and Nd isotopic composition of lower crust as cited in Bohrson and Spera (2001) for the lower crustal case. Figure 1.9 shows that isotopic and incompatible element variations of the two different Syrian lava suites can be modeled by AFC processes using two different primary magma compositions. These two primary magmas have similar Sr and Nd isotopic compositions but very different Sr and Nd concentrations, i.e. the high-P suite is much more enriched than the low-P suite lavas. Evolved high-P suite lavas have assimilated between 10% and 50% of mafic lower crust and have fractionated between 30% and 55% to produce the isotopic variability observed in the samples. In contrast, only up to 10% assimilation and 5% to 35% fractionation are needed to change the isotopic composition of the low-P suite lavas (Figs. 1.9a and b). With respect to the amount of crystal fractionation the results are in accordance with quantitative modeling of the crystallisation

Table 5. Input parameters for EC-AFC computations*.

Thermal parameters	T [°C]		
Magma liquidus temperature	1320	**Isobaric specific heat of** magma	1484 J/kg K
Magma initial temperature	1320	**Isobaric specific heat of** assimilant	1370 J/kg K
Assimilant liquidus temperature	1150	Crystallization enthalpy	396000 J/kg
Assimilant initial temperature	650	Fusion enthalpy	270000 J/kg
Solidus temperature	900		
Equilibration temperature	1085		

Compositional parameters	Sr	Nd
Magma A		
Magma initial concentration [ppm]	600	22
Magma isotope ratio	0.7037	0.512907
Magma trace element distribution coefficient	0.7	0.25
Magma B		
Magma initial concentration [ppm]	320	10
Magma isotope ratio	0.7037	0.512907
Magma trace element distribution coefficient	0.7	0.25
Assimilant		
Assimilant initial concentration [ppm]	129	12.7
Assimilant isotope ratio	0.7100	0.5122
Assimilant trace element distribution coefficient	0.05	0.25

* computations were performed using the computer program EC-AFC as cited in Spera and Bohrson (2001)

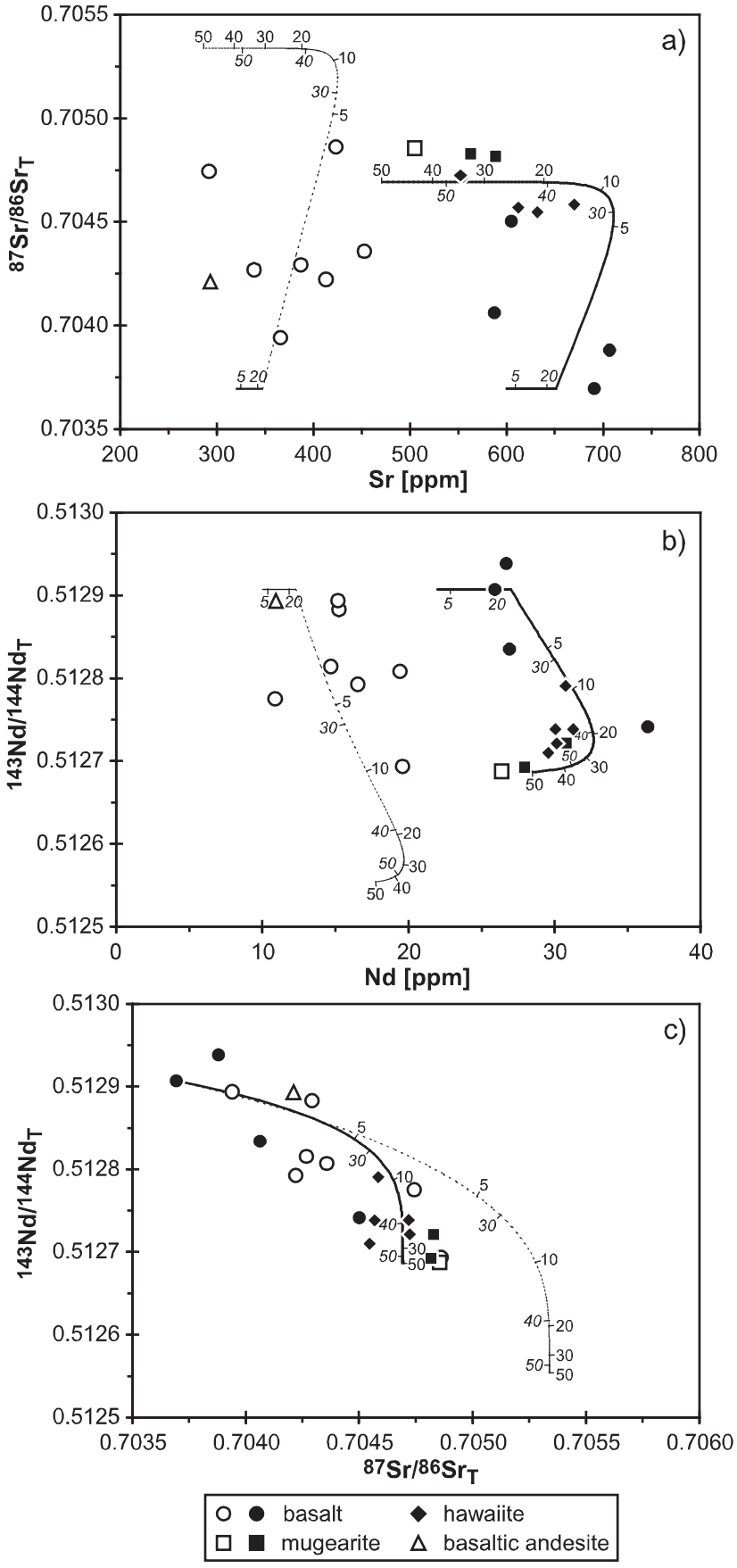

Fig. 1.9. Results for EC-AFC modeling. Continuous lines refer to calculated curves for high-P suite samples (Magma A, Table 5) and dashed lines to low-P suite samples (Magma B, Table 5). Italic numbers give the amount of fractional crystallisation and other numbers the percentage of anatectic melt assimilated.

processes using the MELTS software (Table 4; Fig. 1.3). Exact quantification of AFC processes is limited due to: (1) unknown incompatible element concentrations of the primary magmas, (2) the very heterogeneous geochemical nature of the crust, and (3) uncertainties of the bulk distribution coefficients of Sr during assimilation and fractional crystallisation.

Deep seismic refraction data of El-Isa et al. (1987) and geochemical studies of crustal rocks and xenoliths (Nasir, 1992; Nasir and Safarjalani, 2000; Jarrar et al., 2003) have shown that an upper crustal layer of mafic and intermediate to presumably felsic composition exists in northwestern Arabia followed by a mafic lower crustal layer at a depth of about 20 km. Even though the assimilation of felsic upper crustal rocks (Jarrar et al., 2003) could account for high SiO_2 concentrations in low-P suite lavas, the high K contents of the granitic upper crust (Jarrar et al., 2003) cannot produce the observed differences in K_2O with respect to the two Syrian suites (Fig. 1.3). Additionally, the EC-AFC model in fact leads to realistic results for the assimilation of mafic crustal components, it fails using felsic compositions of even local crust, e.g. Egypt (El-Sayed, 2003), resulting in unrealistically small amounts of assimilated melts (<1%) to produce the observed isotopic variations (Fig. 1.9). Thus, the possibility to generate low-P suite samples by addition of a felsic crustal component to primitive high-P suite magmas can be excluded. The results obtained in our study are different to those for Yemenian flood basalts, that have been shown to have assimilated up to 30% of felsic crust (Baker et al., 1996, Baker et al., 1997). Since the pressure range of crystal fractionation include at least depths below the 20 km boundary indicating magma residence time at lower crustal levels, it is likely that magmas have assimilated

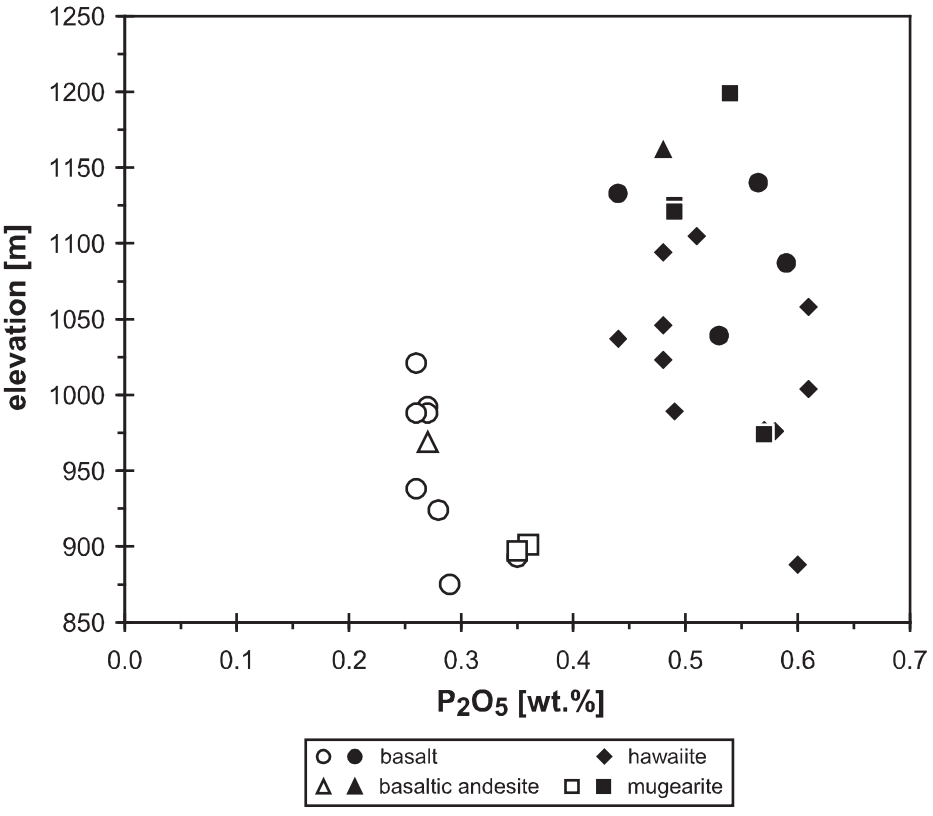

Fig. 1.10. Plot of P_2O_5 versus elevation above sea level for Syrian rocks of known stratigraphic correlation, which were sampled near the town Bulbul (cp. Figure 1.1).

lower crustal melts. But the fact, that most of the high-P lavas as well as the low-P suite yield pressures of fractionation corresponding to upper crustal depths, a contamination with upper crustal material in shallow magma chambers cannot be excluded and it is likely that magmas have assimilated material corresponding to the mafic or intermediate upper crustal sections as found in Jordan (Jarrar et al., 2003).

Another explanation for the development of the low-P and high-P suite lavas could be the melting of an isotopicaly homogeneous mantle source with variable incompatible element compositions (Figs. 1.3 and 1.4). For example, P_2O_5 as well as Ba, Nb, and Zr concentrations are twice as high in the high-P suite compared to low-P lavas (Figs. 1.3 and 1.4), suggesting that low-P lavas may have formed from a depleted mantle source with respect to the high-P. This depletion event must be relatively young because the isotopes are not affected. A source evolution with time should result in a stratigraphic correlation of low and high-P lavas. Re-melting of a source depleted in incompatible elements due to an earlier melting event could explain the observations. However, in the volcanic succession sampled near Bulbul the high-P lavas lie above low-P lavas (Fig. 1.10) implying that increasing depletion of the mantle source with time cannot explain the generation of the magmas. Thus, the temporal distribution of the two lava suites rather indicates that the observed differences are controlled by variable degrees of partial melting. At Bulbul, high degrees of melting have produced lavas of the low-P suite at an early stage, susequently the degree of melting was reduced resulting in the formation of high-P lavas (Fig. 1.10). Because the enrichment of incompatible elements increases by a factor of two the decrease of partial melting must be on the order of 50%.

Given the fact that only primitive samples of the two suites are free of crustal contamination and that all lavas originate from a common source, it seems most likely, that geochemical differences between high-P and low-P lavas were produced by assimilation of variable amounts of lower crust. In addition, differences in major and trace element compositions of primitive, uncontaminated lavas of both the high- and low-P suite are probably caused by variable degrees of partial melting of their source region.

1.5.3 Mantle sources and partial melting

As noted above, Sr, Nd and Pb isotopic compositions of the NW Syrian samples indicate a common mantle source for the two different rock suites and the source may be of lithospheric, asthenospheric, or mantle plume origin (Figs. 1.7 and 1.8). The enriched trace element patterns of even primitive, uncontaminated samples compared to lavas erupted at mid-ocean ridges are a feature typical for continental volcanism and ocean island basalts. Pik et al. (1999) proposed that an ocean island basalt-like mantle component, probably representing the initial material of the Afar plume, accounts for the trace element enrichment of high Ti magmas in the Ethiopian flood basalt province. This component is characterised by $^3He/^4He$ ratios higher than those suggested for upper mantle melts thus indicating its origin in the lower mantle (Marty et al., 1996)

(Figs. 1.7 and 1.8). Unradiogenic $^{87}Sr/^{86}Sr_T$ of primitive Syrian lavas compared to the rather high $^{87}Sr/^{86}Sr$ ratios of lavas affected by the Afar plume exclude an influence of Afar plume material on the mantle source of NW Syria (Baker et al., 1996; Baker et al., 1997; Pik et al., 1999). Thus, the northward channeling of hot asthenospheric material from the Afar region to northwestern Arabia as proposed by Camp and Roobol (1989) is inappropriate to account for the chemical variations observed the Syrian lavas. As suggested in the model of Stein and Hofmann (1992), volcanism in Israel may be the result of lithospheric extension and melting of a fossil plume head beneath the base of the lithosphere. Magmas produced in such a setting should have plume characteristics in the earlier and asthenospheric signatures in the later stages. Samples analysed by Stein and Hofmann (1992), which were proposed to originate from a fossil plume head, that were welded on the continental lithosphere and became a part of it, show lower $^{87}Sr/^{86}Sr$ and more radiogenic $^{206}Pb/^{204}Pb$ ratios compared to northwestern Syrian lavas. Thus, it is unlikely, that such a relic plume material does contribute to the mantle source of Syrian lavas. Primitive lavas from the Red Sea region, probably reflecting the asthenosphere of the Arabian area, might be a possible mantle source component for the NW Syrian lavas. Low $^{87}Sr/^{86}Sr$ and variable but high $^{207}Pb/^{204}Pb$ isotope ratios of Red Sea lavas indicating long time depletion in Rb and U and thus, argue against being a suitable source for the rather enriched mantle source of the NW Syrian lavas (Figs. 1.7 and 1.8).

Since the silica content of a magma is indicative for pressure conditions during partial melting (Hirose and Kushiro, 1993), SiO_2 concentrations of primitive, uncontaminated lavas can be used for pressure estimations. Thus, the SiO_2 content of samples in conjunction with the algorithm developed by Haase (1996) has been used to calculate melting pressures. Melting of primitive Syrian samples occurs at pressures of about 39 kb for high-P lavas and at about 19 kb for low-P lavas, indicating depths of about 120 km and 60 km, respectively. It is notable, that these lavas represent primitive but not primary compositions and have undergone minor extents of olivine fractionation as indicated by Mg-numbers of 0.65 (SY-088) to 0.63 (SY-127) and Ni < 200 ppm. Addition of olivine to primitive lavas generating compositions in equilibrium with mantle melts (i.e. with Mg-numbers of about 0.68 to 0.72; Frey et al., 1978) would lower the SiO_2 content of the lavas. Pressure estimates using such hypothetical parental magmas would therefore result in greater depths for the initiation of the partial melting process. Based on xenolith data McGuire and Bohannon (1989) suggested upwelling asthenospheric material beneath western Arabia and place the lithosphere-asthenosphere boundary at a depth of about 75 km. Assuming similar lithospheric thicknesses for NW Syria, the calculated depths of the Syrian lavas indicate that melting started at the lower boundary of the lithosphere and, with respect to high-P lavas, partial melting occured below lithospheric depths. Given a normal potential mantle temperature of 1280°C, the lithosphere needs to be stretched by a factor of 2-5 to generate partial melts under dry conditions in the mantle region (McKenzie and Bickle, 1988). Due to the fact that there are no indications for extensional processes during the magmatic activity in NW Syria, it appears not

likely that volcanism is a consequence of lithospheric extension. In contrast, the elevated topography of the Aleppo plateau suggests hot material in the mantle region and thus may indicate the presence of an upwelling mantle plume beneath NW Syria. Given the fact, that all lavas were generated from a common source (Figs. 1.7 and 1.8), we conclude, that melting of a plume mantle begun below the lower lithosphere boundary, but incorporation of lithospheric material cannot be excluded.

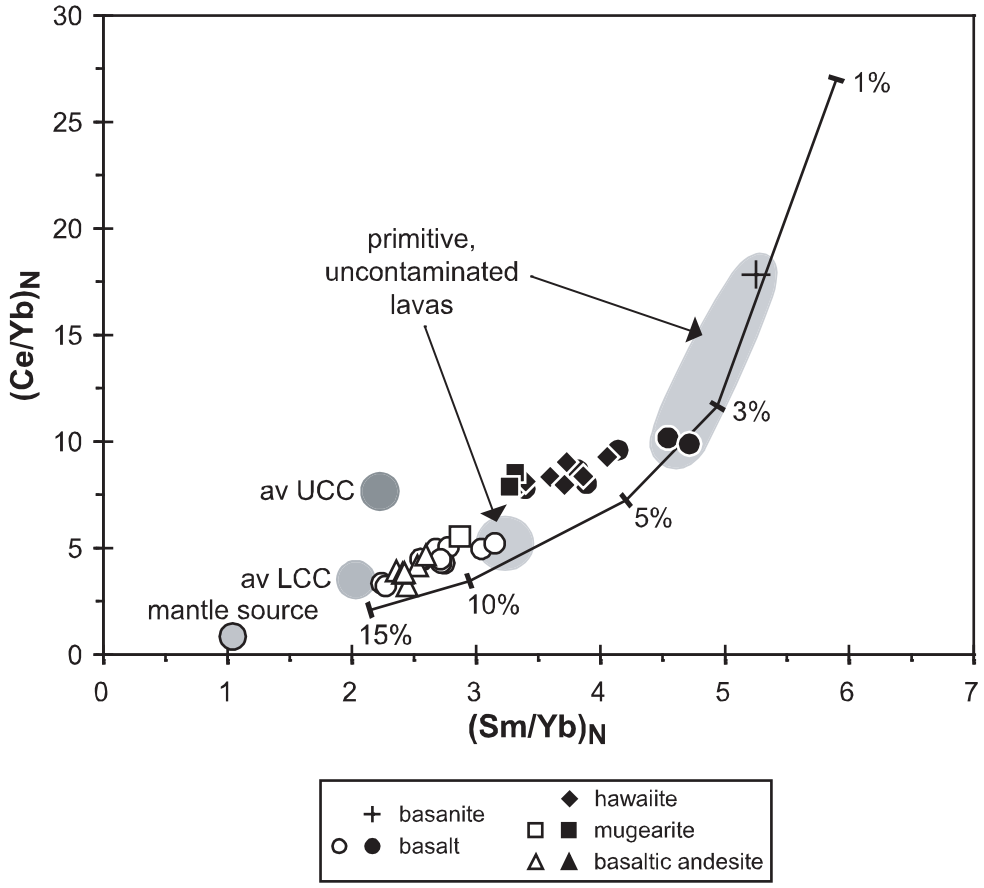

Fig. 1.11. Diagram of chondrite-normalised Sm/Yb and Ce/Yb ratios and a melting curve for non-modal fractional melting of garnet lherzolite. Garnet lherzolite composition: 0.598 olivine, 0.076 clinopyroxene, 0.211 orthopyroxene, 0.115 garnet. Melting proportions: 0.05 olivine, 0.3 clinopyroxene, 0.2 orthopyroxene, 0.45 garnet. Enriched mantle source composition (relative to the mantle source composition of average mid-ocean ridge basalts from Hofmann (1988): Ce 1.56 ppm, Sm 0.39 ppm and Yb 0.41. Distribution coefficients used are from Kelemen et al. (1993) and Johnson (1998). Numbers give the degree of melting and chondrite values are from McDonough and Sun (1995). Average lower (LCC) and upper (UCC) crustal compositions are from Rudnick and Fountain (1995).

The fact that most of the samples are affected by crustal contamination and only primitive lavas of the two Syrian suites are not contaminated, makes an estimation of the degree of partial melting for the whole sample suite difficult. Since garnet has a large distribution coefficient for heavy rare earth elements (HREE), melting of a garnet-bearing mantle source would result in higher LREE/HREE ratios (e. g. Ce/Yb) compared to middle REE/HREE ratios (e. g. Sm/Yb). Therefore, REE ratios shown in Figure 1.11 suggest that melting occured in the garnet stability field. Differences in the REE contents between the uncontaminated lavas of the two Syrian suites

depend either on variable amounts of garnet in the source region or on different degrees of partial melting or both. If the source contains variable amounts of garnet, the mantle residue of the low-P suite should roughly contain half the amount of garnet as it is suggested for high-P samples (Fig. 1.11). But variable contents of garnet cannot explain the observed differences between the high- and low-P suites with respect of their highly incompatible element contents (e. g. P_2O_5, Ba, Nb or Zr; Figs. 1.3 and 1.4). Thus, these differences rather appear to be a feature of variable degrees of partial melting. Melting calculations using the incompatible trace element ratios $(Ce/Yb)_N$ and $(Sm/Yb)_N$ indicate that the mantle source for lavas in NW Syria is garnet-bearing and should be enriched in incompatible elements relative to mantle sources of average mid-ocean ridge basalts (Fig. 1.11). The modeling results indicate that the primitive lavas of the high-P suite are produced by up to 2 - 4% partial melting, whereas primitive low-P samples are generated by 8 - 10% melting of the same mantle source (Fig. 1.11).

1.6 Concluding comments

A detailed geochemical and isotope study of Miocene to Quaternary volcanic rocks erupted in NW Syria indicates that the contamination with substantial amounts of crustal material plays an important role in the magma genesis of continental volcanism. During the plume influenced continental volcanic activity in northwestern Arabia the combination of crystal fractionation, partial melting and crustal assimilation results in the emplacement of two lava types with different geochemical characteristics. As indicated by the petrography and geochemistry and by the quantification of the fractionation processes such differentiated hawaiites and mugearites with high P_2O_5 contents have fractionated up to 6% olivine, 37% clinopyroxene, 3% plagioclase and 7% Fe-Ti oxides, whereas a removal of 22% clinopyroxene and 8% plagioclase produced basaltic andesites and mugearites with relative low P_2O_5 concentrations. From the REE contents in the primitive, uncontaminated basanite and basalts the degree of melting from a common mantle source can be estimated to vary between 2 and 4% for high P_2O_5 lavas and between about 8 and 10% in lavas of the low P_2O_5 suite. As shown by the stratigraphical distribution of the two different lava types the degree of partial melting decreases by about 50% during the period of eruption. Isotopic variations in the samples and AFC modeling suggest that evolved high P_2O_5 lavas assimilated between 10% and 50%, whereas the low P_2O_5 type lavas have assimilated up to 10% of a mafic crustal component. The mantle source of the lavas erupted in NW Syria is garnet-bearing and enriched in incompatible elements relative to mantle sources of mid-ocean ridge basalts, but appears not to be affected by Afar plume material with its characteristically high $^3He/^4He$.

Acknowledgments

This study is part of M.-S.K.´s dissertation and was funded by the Deutsche Forschungsgemeinschaft under grant HA 2568/5. We thank D. Garbe-Schönberg and A. Weinkauf for performing the ICP-MS and XRF analyses and P. Appel and B. Mader for help with

the microprobe. M.-S.K. thanks H. Baier for help with the sample preparation for isotopic measurements and Mr. Zaghier Ali for the excellent “catering service” during field work.

References

Aitcheson, S.J. and Forrest, A.H., 1994. Quantification of crustal contamination in open magmatic systems. Journal of Petrology, 35: 461-488.

Altherr, R., Henjes, K.F. and Baumann, A., 1990. Asthenosphere versus lithosphere as possible sources for basaltic magmas erupted during formation of the Red Sea; constraints from Sr, Pb and Nd isotopes. Earth and Planetary Science Letters, 96: 269-286.

Baker, J.A., Menzies, M.A., Thirlwall, M.F. and Macpherson, C.G., 1997. Petrogenesis of Quaternary intraplate volcanism, Sana’a, Yemen; implications for plume-lithosphere interaction and polybaric melt hybridization. Journal of Petrology, 38: 1359-1390.

Baker, J.A., Thirlwall, M.F. and Menzies, M.A., 1996. Sr-Nd-Pb isotopic and trace element evidence for crustal contamination of plume-derived flood basalts; Oligocene flood volcanism in western Yemen. Geochimica et Cosmochimica Acta, 60: 2559-2581.

Bertrand, H., Chazot, G., Blichert-Toft, J. and Thoral, S., 2003. Implications of widespread high-μ volcanism on the Arabian Plate for Afar mantle plume and lithosphere composition. Chemical Geology, 198: 47-61.

Best, J.A., Barazangi, M., Al, S.D., Sawaf, T. and Gebran, A., 1990. Bouguer gravity trends and crustal structure of the Palmyride mountain belt and surrounding northern Arabian Platform in Syria. Geology, 18: 1235-1239.

Blusztajn, J., Hart, S.R., Shimizu, N. and McGuire, A.V., 1995. Trace-element and isotopic characteristics of spinel peridotite xenoliths from Saudi Arabia. Chemical Geology, 123: 53-65.

Bohannon, R.G., Naeser, C.W., Schmidt, D.L. and Zimmermann, R.A., 1989. The timing of uplift, volcanism, and rifting peripheral to the Red Sea; a case for passive rifting? Journal of Geophysical Research, 94: 1683-1701.

Bohrson, W.A. and Spera, F.J., 2001. Energy-constrained open-system magmatic processes; II, Application of energy-constrained assimilation-fractional crystallization (EC-AFC) model to magmatic systems. Journal of Petrology, 42: 1019-1041.

Camp, V.E. and Roobol, M.J., 1989. The Arabian continental alkali basalt province: Part I, Evolution of Harrat Rahat, Kingdom of Saudi Arabia. Geological Society of America Bulletin, 101: 71-95.

Camp, V.E., Roobol, M.J. and Hooper, P.R., 1991. The Arabian continental alkali basalt province: Part II. Evolution of Harrats Khaybar, Ithnayn, and Kura, Kingdom of Saudi Arabia. Geological Society of America Bulletin, 103: 363-391.

Camp, V.E. and Roobol, M.J., 1992. Upwelling asthenosphere beneath western Arabia and its regional implications. Journal of Geophysical Research, 97: 15,255-15,271.

Coleman, R.G., Gregory, R.T. and Brown, G.F., 1983. Cenozoic volcanic rocks of Saudi Arabia. Open-File Report - U. S. Geological Survey., OF 83-0788: 86.

DePaolo, D.J., 1981. Trace element and isotopic effects of combined wallrock assimilation and fractional crystallization. Earth and Planetary Science Letters, 53: 189-202.

Dupré, B., Blanc, G., Boulegue, J. and Allègre, C.J., 1988. Metal remobilization at a spreading centre studied using lead isotopes. Nature, 333: 165-167.

Eissen, J.P. et al., 1989. Petrology and geochemistry of basalts from the Red Sea axial rift at 18 degrees North. Journal of Petrology, 30: 791-839.

El-Isa, Z.H., Mechie, J., Prodehl, C., Makris, J. and Rihm, R., 1987. A crustal structure study of Jordan derived from seismic refraction data. Tectonophysics, 138: 235-253.

El-Sayed, M.M., 2003. Neoproterozoic magmatism in NW Sinai, Egypt: magma source and evolution of collision-related intracrustal anatectic leucogranite. International Journal of Earth Science, 92: 145-164. DOI 10.1007/s00531-003-0313-3.

Frey, F.A., Green, D.H. and Roy, S.D., 1978. Integrated models of basalt petrogenesis; a study of quartz tholeiites to olivine melilitites from South eastern Australia utilizing geochemical and experimental petrological data. Journal of Petrology, 19: 463-513.

Garbe-Schönberg, C.-D., 1993. Simultaneous determination of thirty-seven trace elements in twenty-eight international rock standards by ICP-MS. Geostandards Newsletter, 17: 81-

97.
Ghiorso, M.S. and Sack, R.O., 1995. Chemical mass transfer in magmatic processes. IV. a revised and internally consistent thermodynamic model for the interpolation and extrapolation of liquid-solid equilibria in magmatic systems at elevated temperatures and pressures. Contributions to Mineralogy and Petrology, 119: 197-212.
Haase, K.M., 1996. The relationship between the age of the lithosphere and the composition of oceanic magmas; constraints on partial melting, mantle sources and the thermal structure of the plates. Earth and Planetary Science Letters, 144: 75-92.
Hegner, E. and Pallister, J.S., 1989. Pb, Sr, and Nd isotopic characteristics of Tertiary Red Sea Rift volcanics from the central Saudi Arabian coastal plain. Journal of Geophysical Research, 94: 7749-7755.
Henjes-Kunst, F., Altherr, R. and Baumann, A., 1990. Evolution and composition of the lithospheric mantle underneath the western Arabian Peninsula; constraints from Sr-Nd isotope systematics of mantle xenoliths. Contributions to Mineralogy and Petrology, 105: 460-472.
Hirose, K. and Kushiro, I., 1993. Partial melting of dry peridotites at high pressures; determination of compositions of melts segregated from peridotite using aggregates of diamond. Earth and Planetary Science Letters, 114: 477-489.
Hofmann, A.W., 1988. Chemical differentiation of the Earth; the relationship between mantle, continental crust, and oceanic crust. Earth and Planetary Science Letters, 90: 297-314.
Hofmann, A.W., Jochum, K.P., Seufert, M. and White, W.M., 1986. Nb and Pb in oceanic basalts; new constraints on mantle evolution. Earth and Planetary Science Letters, 79: 33-45.
Jarrar, G., Stern, R.J., Saffarini, G. and Al-Zubi, H., 2003. Late- and post-orogenic Neoproterozoic intrusions of Jordan: implications for crustal growth in the northernmost segment of the East African Orogen. Precambrian Reseach, 123: 295-319.
Johnson, K.T.M., 1998. Experimental determination of partition coefficients for rare earth and high-field-strength elements between clinopyroxene, garnet, and basaltic melt at high pressure. Contributions to Mineralogy and Petrology, 133: 60-68.
Kelemen, P.B., Shimizu, N. and Dunn, T., 1993. Relative depletion of niobium in some arc magmas and the continental crust; partitioning of K, Nb, La and Ce during melt/rock reaction in the upper mantle. Earth and Planetary Science Letters, 120: 111-133.
Kumar, M.R., Ramesh, D.S., Saul, J., Sarkar, D. and Kind, R., 2002. Crustal structure and upper mantle stratigraphy of the Arabian shield. Geophysical Research Letters, 29: 83/1 - 83/4.
Le Bas, M.J., Le Maitre, R.W., Streckeisen, A. and Zanettin, B.A., 1986. Chemical classification of volcanic rocks based on the total alkali-silica diagram. Journal of Petrology, 27: 745-750.
Le Maitre, R.W. et al., 1989. A classification of igneous rocks and glossary of terms. Blackwell Sci. Publ., Oxford, United Kingdom, 193 pp.
Marty, B., Pik, R. and Gezahegn, Y., 1996. Helium isotopic variations in Ethiopian plume lavas; nature of magmatic sources and limit on lower mantle contribution. Earth and Planetary Science Letters, 144: 223-237.
McBride, J.H. et al., 1990. Seismic reflection structure of intracratonic Palmyride fold-thrust belt and surrounding Arabian Platform, Syria. AAPG Bulletin, 74: 238-259.
McDonough, W.F. and Sun, S.S., 1995. The composition of the Earth. Chemical Geology, 120, 223-253.
McGuire, A.V. and Bohannon, R.G., 1989. Timing of mantle upwelling; evidence for a passive origin for the Red Sea Rift. Journal of Geophysical Research, 94: 1677-1682.
McKenzie, D. and Bickle, M.J., 1988. The volume and composition of melt generated by extension of the lithosphere. Journal of Petrology, 29: 625-679.
Nasir, S., 1992. The lithosphere beneath the northwestern part of the Arabian Plate (Jordan); evidence from xenoliths and geophysics. Tectonophysics, 201: 357-370.
Nasir, S. and Safarjalani, A., 2000. Lithospheric petrology beneath the northern part of the Arabian Plate in Syria: evidence from xenoliths in alkali basalts. Journal of African Earth Sciences, 30: 149-168.
Pik, R., Deniel, C., Coulon, C., Yirgu, G. and Marty, B., 1999. Isotopic and trace element signatures of Ethiopian flood basalts; evidence for plume-lithosphere interactions. Geochimica et Cosmochimica Acta, 63: 2263-2279.

Ponikarov, V.P., Protasevich, L., Maximov, A. and Tkachev, G., 1963. Geological map of Syria 1:200 000. V.O. Technoexport, Russian Federation, Moscow.
Putirka, K., Johnson, M., Kinzler, R., Longhi, R. and Walker, D., 1996. Thermobarometry of mafic igneous rocks based on clinopyroxene-liquid equilibria, 0-30 kbar. Contributions to Mineralogy and Petrology, 123: 92-108.
Rogers, N.W., 1993. The isotope and trace element geochemistry of basalts from the volcanic islands of the southern Red Sea. Geological Society of London, 76, 455-467.
Rudnick, R.L. and Fountain, D.M., 1995. Nature and composition of the continental crust; a lower crustal perspective. Reviews of Geophysics, 33: 267-309.
Sandvol, E. et al., 1998. Lithospheric seismic velocity discontinuities beneath the Arabian Shield. Geophysical Research Letters, 25: 2873-2876.
Schilling, J.G., Kingsley, R.H., Hanan, B.B. and McCully, B.L., 1992. Nd-Sr-Pb isotopic variations along the Gulf of Aden; evidence for Afar mantle plume-continental lithosphere interaction. Journal of Geophysical Research, 97: 10,927-10,966.
Searle, M.P., 1994. Structure of the intraplate eastern Palmyride fold belt, Syria. Geological Society of America Bulletin, 106: 1332-1350.
Sengor, A.M.C. and Burke, K., 1978. Relative timing of rifting and volcanism on Earth and its tectonic implications. Geophysical Research Letters, 5: 419-421.
Sharkov, Y.V. et al., 1994. Geokhronologiya pozdnekaynozoyskikh bazal'tov Zapadnoy Sirii Translated Title: Geochronology of late Cenozoic basalts in western Syria. Petrologiya, 2: 385-394.
Spera, F.J. and Bohrson, W.A., 2001. Energy-constrained open-system magmatic processes; I, General model and energy-constrained assimilation and fractional crystallization (EC-AFC) formulation. Journal of Petrology, 42: 999-1018.
Stein, M. and Hofmann, A.W., 1992. Fossil plume head beneath the Arabian lithosphere? Earth and Planetary Science Letters, 114: 193-209.
Walley, C.D., 1998. Some outstanding issues in the geology of Lebanon and their importance in the tectonic evolution of the Levantine region. Tectonophysics, 298: 37-62.
Weinstein, Y., Navon, O. and Lang, B., 1994. Fractionation of Pleistocene alkali-basalts from the northern Golan Heights, Israel. Israel Journal of Earth-Sciences, 43: 63-79.

CHAPTER TWO

The Harrat Ash Shamah Volcanic Field in Southern Syria: Magmatic Sources, Magma Genesis and Indications for Plume-Asthenosphere Interaction

M.-S. Krienitz[1*], K.M. Haase[1], K. Mezger[2], and M.A. Shaikh-Mashail[3]

[1] Institut für Geowissenschaften der Universität Kiel, Olshausenstr. 40, 24118 Kiel, Germany
[2] Institut für Mineralogie der Universität Münster, Corrensstr. 24, 48149 Münster, Germany
[3] Faculty of Civil Engineering, University of Aleppo, PO-Box 5427, Aleppo, Syria
[*] Corresponding author. Telephone +49 (0) 431 880 3694. Fax +49 (0) 431 880 4376. E-mail: mk@gpi.uni-kiel.de

Abstract

The geochemical and isotope composition of Miocene to recent lavas of the Harrat Ash Shamah volcanic field in southern Syria provide important constraints on their source characteristics and magma genesis. The lava suite comprises alkali basalts, basanites, hawaiites and mugearites as well as trachytes and phonolites. The lavas have undergone fractional crystallisation of olivine, clinopyroxene, ±plagioclase, and ±Fe-Ti oxides, the most differentiated lavas have also fractionated alkalifeldspar and apatite. The low Ce/Pb and Nb/U ratios in conjunction with high $^{87}Sr/^{86}Sr$ and low $^{143}Nd/^{144}Nd$ ratios of some lavas are characteristic for the assimilation of variable amounts of continental crust. Major element variations and variable fractionated heavy rare earth elements of crustaly uncontaminated primitive lavas indicate that they formed by variable degrees of melting of a garnet peridotite at different depths. The large range of isotopic compositions and the variable trace element enrichment of the lavas imply that the magmas were generated in both a volatile- and incompatible element-enriched lithospheric or asthenospheric mantle and in a mantle plume as indicated by a maximum excess temperature of about 180°C. The discontinuous volcanic activity, the temporal changes in the partial melting process as well as in the chemical and isotopic compositions of the Syrian lavas suggest that volcanism was triggered by a pulsing mantle plume situated underneath northwestern Arabia.

2.1 Introduction

Continental volcanic rocks exhibit large variations in chemical and isotopic compositions and their geochemical signatures can be used to constrain the dynamic processes of the Earth´s interior and its continental crust. Magmatism in continental regions is often accompanied by thinning and rifting of the continental lithosphere resulting in upwelling of the underlying mantle. Thus, decompressional melting of the rising mantle and the volume of melt produced depends on the stretching factor of the lithosphere as well as on the temperature and composition of the mantle (McKenzie and Bickle, 1988). The cause of lithospheric thinning often remains unclear but magmatism may be initiated by a mantle plume resulting in regional doming of the asthenosphere followed by volcanism and rifting (active rift hypothesis). In contrast, plate boundary forces may lead to breaking and rifting of the lithosphere due to transtensional stresses resulting in regional uplift and finally in volcanism (passive rift hypothesis; Sengör and Burke, 1978). In this context White and McKenzie (1989) suggest that lithospheric stretching without any influence of a hot mantle (i.e. a mantle plume) cannot account for extensive magma generation. In their model continental flood volcanism is restricted to the development of extreme lithospheric thinning coinciding with the arrival of the head of a mantle plume and an onset of volcanism by passive upwelling of the mantle as the lithosphere thins. In contrast, Campbell and Griffiths (1990) consider that extensive volcanism results from a starting mantle plume, but that both continental rifting and an ascending mantle plume are not necessarily required to generate large igneous provinces. The model developed by Campbell and Griffiths (1990) predicts first uplift of the affected regions followed by subsidence prior to volcanism as the new mantle plume rises and spreads out laterally on the base of the lithosphere. During volcanism a period of enhanced subsidence is predicted in response to the escape of magma from the mantle and to the volcanic load on the Earth`s surface. As the thermal plume anomaly gradually decays with time, ongoing but slow subsidence of the region may occur (Campbell and Griffiths, 1990). Subcontinental lithospheric as well as asthenospheric and plume mantle may all contribute to magma genesis during rifting processes.

This study investigates the geochemistry and isotopic signature of lavas from the largest Cenozoic intraplate volcanic field of western Arabia, the Harrat Ash Shamah in Syria, with the following objectives: (1) to determine the processes controlling the major and trace element chemistry as well as the isotopic composition of the volcanic rocks, (2) to determine the geochemical characteristics of the magmatic sources, and (3) to constrain the temporal evolution of lavas and their mantle sources during at least 24 million years of magmatic activity.

2.2 Geological setting

Voluminous Cenozoic alkali basaltic volcanism occurs in western Arabia, extending from Yemen over a distance of 2,500 km to southeastern Turkey (Fig. 2.1a). These volcanic fields, the so-

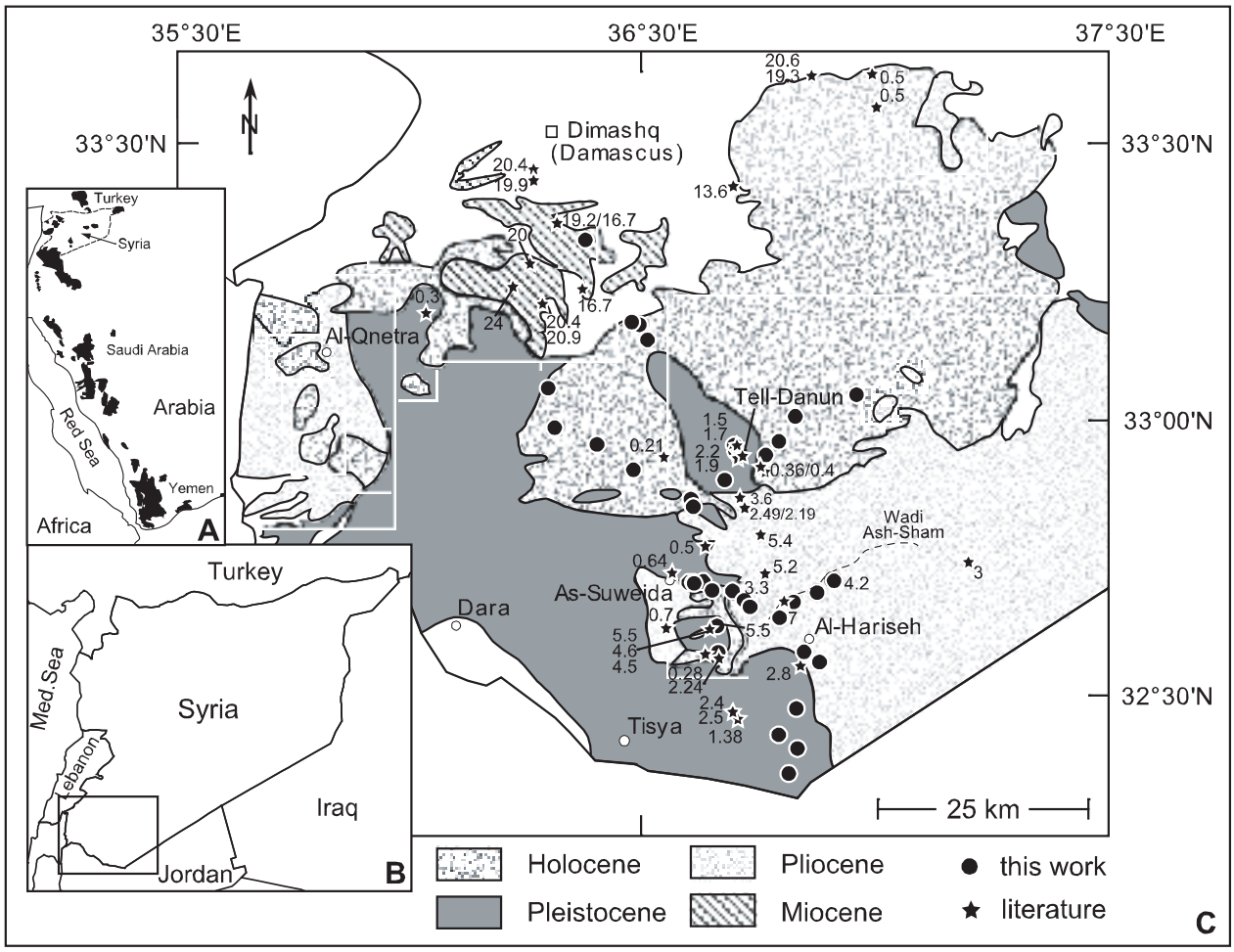

Fig. 2.1. (A) Distribution of volcanic fields along western Arabia. (B) The study area in relation to adjacent countries (C) Generalised geological map of the Syrian part of the Harrat Ash Shamah volcanic field based on geological maps of Ponikarov et al. (1963) showing the distribution of Miocene to Holocene volcanic rocks and sample locations (cycles – own work; stars – data taken from literature. The numbers give K-Ar and Ar-Ar ages in million years. Data sources from Giannerini et al. (1988), Mouty et al. (1992), Sharkov et al. (1994) and Krienitz et al. (Chapter III).

called Harrats, cover an area of approximately 200,000 km^2 and exhibit an average thickness of about 100 m (Coleman et al., 1983; Nasir, 1994; Tarawneh et al., 2000). The tectonomagmatic history of the Harrat volcanism has been discussed by several authors (e.g. Pallister, 1987; Bohannon et al., 1989; Camp and Robool, 1989; Camp and Roobol, 1992; Nasir, 1994). Rifting, faulting and volcanism in Arabia is generally linked to the two-stage evolution of the Red Sea and the Dead Sea rift systems in Miocene and Pliocene times. In addition, volcanism in southwestern Arabia is associated with the activity of the Afar mantle plume with a well-defined centre in the vicinity of the Afro-Arabian triple junction (Schilling, 1973; Baker et al., 1997; Debayle et al., 2001). The composition of the Afar plume magmas is characterised by relatively high $^{206}Pb/^{204}Pb$ (Schilling et al., 1992) and high $^3He/^4He$ ratios (Marty et al., 1996). Whereas the magma genesis and the magma sources (i.e. crust, lithospheric mantle, asthenosphere and plume mantle) in southwestern Arabia are well characterised, the causes and sources of volcanism in northern Arabia are less clear. The following models have been proposed to explain this

volcanic activity: (1) lithospheric rifting mobilising old fossile plume head material beneath the subcontinental lithosphere (Stein and Hofmann, 1992), (2) a separate mantle plume existing underneath northern Arabia (Camp and Roobol, 1992), (3) progressive lithospheric thinning tapping lithospheric (fossil-plume material) to asthenospheric sources (Bertrand et al., 2003; Shaw et al., 2003), or (4) northwestward channelling of hot Afar plume material (Camp and Roobol, 1992).

The Harrat Ash Shamah (or Harrat Ash-Shaam: HAS) is the largest volcanic field (Fig. 2.1) and lies at the northwestern margin of the Afro-Arabian dome as outlined by Camp and Roobol (1992). The Harrat strikes parallel to the Red Sea and extends some 500 km from northeast Israel through southern Syria, Jordan to Saudi Arabia covering more than 50,000 km^2 (Ilani et al., 2001). The volcanic field varies in width between 200 and 300 km (Tarawneh et al., 2000) and the lava pile reaches a maximum thickness of 1.5 km and an altitude of approximately 1800 m in Syria (Guba and Mustafa, 1988). Two NE-SW striking late Cretaceous rifts, the Wadi Sirhan and the Khor Umm Wial grabens lie south and north of the HAS, respectively (Almond, 1986). The main types of volcanic rocks and volcanic structures found in this area are massive lava flows, which are often separated by sedimentary layers and red lateritic weathering crust (Sharkov et al., 1994; Snyder et al., 1993), feeder dikes, strato and shield volcanoes as well as cinder cones. The cinder cones are the youngest eruption type and are situated on top of older flow units. The northern part of the HAS field, also known as the Hauran-Druze Plateau in Syria (Ponikarov, 1969), lies on the so-called Rutbah uplifted region (Best et al., 1990; McBride et al., 1990) and can be divided into four major areas ranging in age from Miocene to historical times (Fig. 2.1). K-Ar ages of volcanic rocks range from 24 Ma to subrecent, with a volcanic hiatus between 13 Ma and 7 Ma (Mouty et al., 1992; Sharkov et al., 1994). The oldest flow units are of early Miocene age (24-16 Ma) and cover an area of about 200 km^2 in the northwestern part of the HAS plateau (Fig. 2.1). This volcanic sequence is composed of 20 to 22 lava flows and is up to 400 m thick (Snyder et al., 1993). The lavas unconformably overlie Cretaceous and Paleogene sediments and are overlain by younger Pliocene to Quaternary lavas (Tarawneh et al., 2000). Mostly Pliocene (7-3.5 Ma) volcanic rocks are concentrated in the southeast, whereas the southwestern area, near the Jordan border, is covered by Quaternary units (Fig. 2.1). The youngest lavas of Holocene age form the northeastern part of the HAS. Volcanic cones up to 100 m high are the products of the youngest volcanic activity of each period and cover the surfaces of the lava plateaus. These cones often form chains trending in NW-SE direction and seem to trace faults that probably provided conduits for the magmas (Giannerini et al., 1988). Crustal as well as mantle xenoliths occur in several young cones (Sharkov et al., 1989; Nasir, 1992), but Precambrian crystalline basement of the Arabian-Nubian shield crops out only in southern Jordan and dips to the northeast. The basement in Syria is overlain by predominantly flat lying Phanerozoic marine and continental sediments (Sharkov et al., 1994). Seismic reflection data as well as refraction profiling have shown that the metamorphic basement lies generally deeper than 6 km (Seber et al., 1993; Brew et al., 1997; Brew et al., 2001a) and varies beneath the

Rutbah uplifted region between 6 km and >8 km (McBride et al., 1990; Searle, 1994). Gravity models of the crust in southern Syria suggest a thickness of 40±4 km similar to crustal thicknesses interpreted from seismic refraction data in Jordan and Saudi Arabia (El-Isa et al., 1987; Best et al., 1990; McBride et al., 1990).

2.3 Sample preparation and analytical methods

During a field trip in the year 2000 large parts of the Syrian Harrat Ash Shamah volcanic field were sampled and lavas of each volcanic period were obtained (Fig. 2.1). Hand specimens were sawn into pieces and weathered surfaces and cracks were removed. After washing with deionised water in an ultrasonic bath the samples were crushed with a screw press and washed again. The crushed material was powdered in an agate ball mill for major, trace and isotope analyses. Four samples contain fresh glass, which was handpicked under a binocular for chemical analysis.

Mineral phases and the glassy samples were analysed with a JEOL Superprobe 8900 electron microprobe (EMP) at the Institut für Geowissenschaften, Universität Kiel, using standard wavelength dispersive techniques. The instrument was operated at an accelerating voltage of 15 kV and a beam current of 15 nA. The beam diameter during calibration and measurement was set at 5 µm for feldspars and glasses and at 1 µm for the remaining phases. Counting times on peaks were set at 15 s, whereas background counting times were always set to half of peak counting times. The quality of the data was checked by repeated measurement of a set of mineral standards. The results of representative mineral analyses are presented in Table 1 and of glass analyses in Table 2.

Major and selected trace (Cr, Ni, Zn, Rb, Sr, Zr) element analyses of whole rock samples were performed at the Universität Kiel with a Philips PW 1400 XRF using international rock standards for calibration and data quality control. Sample powders (0.6 g) were mixed with lithiumtetraborate (3.6 g) serving as flux and fused to glass tablets. Replicate measurements of the BHVO-1 standard gave a precision better than 0.30% (SD) for all major elements and generally better than 8% (SD) for trace elements. The accuracy of standard analyses relative to reference values is generally better than 4% for most of the major and trace elements and only Na_2O, P_2O_5 and Ni (<7%) show higher deviations (Table 2).

Trace and rare earth element analyses were carried out at the Universität Kiel with an upgraded PlasmaQuad PQ1 ICP-MS using 100 mg of sample material. Sample preparation was performed following the method of Garbe-Schönberg (1993). Comparison of duplicate analyses of sample SY-234 gave a precision generally better than 1% (SD) except for V, Zr (<2% SD), Sr and Ba (<4% SD). The accuracy of the data based on the international rock standard BR is better than 9% except for Cs, Nb (<10%) and Li (14%; Table 2).

Table 1. Representative microprobe analyses of Syrian Harrat Ash Shamah lavas.

Phase	plagioclase	alkali feldspar			clinopyroxene			olivine							magnetite	
Sample	SY-256	SY-267			SY-256	SY-223	SY-229	SY-272			SY-218			SY-267	SY-256	SY-180
Host rock	basanite	trachyte			basanite	hawaiite	phonolite	basanite			alk. basalt			trachyte	basanite	alk. basalt
	matrix	core	rim	matrix	matrix	matrix	matrix	core	rim	xeno*	core	rim	matrix	matrix	matrix	matrix
SiO_2	52.48	63.73	66.81	66.23	46.97	48.73	51.42	39.73	38.46	40.02	39.21	38.90	37.33	30.51	0.10	0.05
TiO_2	-	-	-	-	3.12	2.30	0.23	-	0.02	0.01	0.05	0.02	0.01	0.03	22.95	23.13
Al_2O_3	30.32	21.96	18.94	20.30	5.96	4.58	0.80	0.02	0.03	0.04	0.05	0.06	0.06	0.04	1.31	1.90
FeO^T	0.48	0.18	0.44	0.35	8.01	7.27	15.42	15.58	20.03	13.53	17.84	20.39	27.62	64.05	69.09	69.20
MnO	-	-	-	-	0.20	0.11	0.49	0.22	0.38	0.22	0.22	0.33	0.37	3.48	0.77	0.64
MgO	-	-	-	-	12.88	13.66	8.85	44.02	39.95	45.53	41.81	39.46	34.07	1.50	2.14	2.64
CaO	12.13	2.89	0.06	0.92	21.98	22.07	20.83	0.04	0.13	0.10	0.27	0.29	0.40	1.18	0.11	0.05
Na_2O	4.20	8.03	6.53	8.40	0.50	0.53	1.22	0.03	0.04	0.03	-	-	-	-	0.02	0.04
K_2O	0.24	2.40	7.36	3.53	-	0.01	-	-	-	-	-	-	-	-	0.03	0.00
P_2O_5	-	-	-	-	-	-	-	-	-	-	-	-	-	-	-	-
Cr_2O_3	-	-	-	-	0.02	0.03	-	0.02	-	-	0.07	0.02	-	-	0.11	0.20
NiO	-	-	-	-	-	-	-	-	-	-	-	-	-	-	-	-
Total	99.85	99.19	100.14	99.72	99.64	99.29	99.26	99.66	99.04	99.48	99.50	99.46	99.88	100.79	96.62	97.85
Ab	38.0	71.8	57.7	75.1												
An	1.4	13.9	42.0	20.4												
Or	60.6	14.3	0.3	4.5												
En					38.8	40.7	27.3									
Fs					47.6	47.2	46.1									
Wo					13.5	12.1	26.6									
Fo								83	78	86	81	78	69	4		
Usp															64.8	67.1

* xenolith

Table 2. Coordinates, rock type, major (XRF) and trace element (XRF, ICP-MS) analyses of the Syrian samples. Averages of analyses of the standard BHVO-1 (XRF n = 9) and BR (ICP-MS n = 3) are also given.

Sample	SY-175	SY-177	SY-179	SY-180	SY-184	SY-186	SY-189	SY-190	SY-191	SY-192gl	SY-193	SY-194
Lat. [°N]	33°19`37``	33°10`47``	33°10`16``	33°08`54``	32°42`13``	32°42`13``	32°42`14``	32°42`07``	32°42`07``	32°42`07``	32°42`07``	32°42`28``
Long. [°E]	36°23`05``	36°29`04``	36°30`00``	36°31`08``	36°36`44``	36°36`44``	36°37`03``	36°37`13``	36°37`13``	36°37`13``	36°37`13``	36°38`31``
Elevation [m]	-	-	637	661	1324	1314	1296	1306	1306	1306	1306	1450
Rock type	alk. basalt	alk. basalt	alk. basalt	alk. basalt	basanite	basanite	mugearite	basanite	basanite	basanite	mugearite	alk. basalt
SiO_2	46.15	46.03	46.26	45.37	43.63	43.92	49.28	43.00	43.44	46.16	49.39	46.75
TiO_2	2.75	2.43	2.35	2.55	3.35	3.32	2.14	3.51	3.21	3.53	2.13	2.59
Al_2O_3	14.61	14.89	14.75	15.43	15.18	15.05	17.82	14.77	14.74	17.47	17.46	16.29
$Fe_2O_3^T$	13.13	13.61	13.69	13.08	14.30	14.08	12.50	13.62	13.69	10.37	12.22	12.69
MnO	0.13	0.17	0.17	0.16	0.17	0.18	0.17	0.17	0.18	0.15	0.18	0.17
MgO	5.90	9.07	9.69	6.98	6.78	7.22	2.60	8.40	9.06	3.84	3.24	5.80
CaO	8.43	9.06	8.95	10.37	7.89	8.02	5.68	8.79	9.02	10.40	5.89	10.41
Na_2O	3.08	3.55	3.40	3.06	4.71	4.40	4.11	4.00	3.86	5.07	5.34	3.59
K_2O	1.59	0.79	0.80	0.42	1.31	1.92	2.10	1.79	1.86	2.42	2.17	1.01
P_2O_5	0.70	0.45	0.45	0.45	0.79	0.74	1.02	0.61	0.64	0.89	1.00	0.45
L.O.I.	3.72	0.00	0.00	1.89	1.05	0.93	1.99	0.31	0.58	-	0.28	0.00
Total	100.19	100.05	100.51	99.76	99.16	99.78	99.41	98.97	100.28	100.47	99.30	99.75
Mg-no.	0.51	0.61	0.62	0.55	0.52	0.54	0.33	0.59	0.61	0.44	0.38	0.52
Li	-	-	4.81	-	2.97	-	-	-	-	7.62	-	3.59
Sc	-	-	15.6	-	10.1	-	-	-	-	18.7	-	25.5
V	-	-	-	-	122	-	-	-	-	-	-	255
Cr	167	253	253	172	68.9	107	-	130	155	131	-	106
Co	-	-	55.4	-	38.4	-	-	-	-	54.8	-	44.1
Ni	169	199	209	61	78.7	118	9	161	170	170	2	44.7
Cu	-	-	59.0	-	29.1	-	-	-	-	55.4	-	67.5
Zn	146	113	112	100	106	122	97	97	103	110	95	105
Ga	-	-	21.3	-	33.4	-	-	-	-	-	-	24.3
Rb	18	9	9.79	3	22.3	32	22	34	31	38.9	31	12.5
Y	-	-	21.0	-	22.3	-	-	-	-	22.0	-	24.9
Cs	-	-	0.079	-	0.469	-	-	-	-	0.385	-	0.079
Sr	258	539	530	560	1016	977	945	802	861	812	943	641
Ba	-	-	198	-	401	-	-	-	-	396	-	263
Zr	444	186	152	192	312	359	355	269	387	248	3	172
Hf	-	-	3.70	-	8.16	-	-	-	-	5.89	-	3.43
Nb	-	-	24.1	-	48.0	-	-	-	-	50.8	-	30.6
Ta	-	-	1.47	-	3.11	-	-	-	-	1.58	-	1.64
Pb	-	-	1.55	-	2.85	-	-	-	-	2.82	-	1.77
Th	-	-	1.83	-	4.13	-	-	-	-	4.41	-	1.66
U	-	-	0.413	-	1.15	-	-	-	-	1.27	-	0.464
La	-	-	20.2	-	41.8	-	-	-	-	36.2	-	20.1
Ce	-	-	44.0	-	88.1	-	-	-	-	73.9	-	44.5
Pr	-	-	5.54	-	11.2	-	-	-	-	8.83	-	5.53
Nd	-	-	23.7	-	45.5	-	-	-	-	35.4	-	23.6
Sm	-	-	5.40	-	9.52	-	-	-	-	7.35	-	5.53
Eu	-	-	1.85	-	3.06	-	-	-	-	2.35	-	2.01
Gd	-	-	5.28	-	8.40	-	-	-	-	6.85	-	5.27
Tb	-	-	0.755	-	1.193	-	-	-	-	0.938	-	0.777
Dy	-	-	4.19	-	5.99	-	-	-	-	4.92	-	4.29
Ho	-	-	0.763	-	0.995	-	-	-	-	0.861	-	0.807
Er	-	-	1.90	-	2.38	-	-	-	-	2.11	-	2.10
Tm	-	-	0.248	-	0.290	-	-	-	-	0.276	-	0.313
Yb	-	-	1.53	-	1.74	-	-	-	-	1.66	-	1.82
Lu	-	-	0.210	-	0.244	-	-	-	-	0.235	-	0.242

Major elements in wt.%, trace elements in ppm.

gl - glass analyses (EMP)

n.d. - not detected

Mg-no. = Mg/(Mg + Fe^{2+}), assuming FeO = 0.85Fe^T.

Table 2. (continued)

Sample	SY-196	SY-197	SY-198	SY-199	SY-200	SY-201	SY-202	SY-203	SY-205	SY-206	SY-210	SY-211
Lat. [°N]	32°41`29``	32°41`29``	32°41`29``	32°41`20``	32°41`20``	32°41`20``	32°41`25``	32°40`20``	32°39`52``	32°38`34``	32°40`04``	32°40`04``
Long. [°E]	36°39`43``	36°39`43``	36°39`43``	36°42`14``	36°42`14``	36°42`14``	36°42`12``	36°43`59``	36°44`35``	36°48`19``	36°50`00``	36°50`00``
Elevation [m]	1603	1603	1603	1741	1741	1741	1660	1763	1797	1555	1445	1447
Rock type	**alk.** basalt	**alk.** basalt	**alk.** basalt	basanite	basanite	basanite	basanite	hawaiite	hawaiite	hawaiite	**alk.** basalt	**alk.** basalt
SiO_2	46.01	46.47	45.88	44.17	44.95	44.77	44.30	45.12	45.10	46.96	46.10	46.16
TiO_2	2.60	2.53	2.65	2.78	2.83	2.84	2.85	3.04	3.13	2.83	2.25	2.23
Al_2O_3	16.17	16.55	16.76	15.23	15.81	15.64	15.31	14.75	15.16	17.31	15.45	15.48
$Fe_2O_3^T$	12.58	12.52	13.05	12.77	12.93	13.00	12.83	12.06	12.09	11.91	13.25	12.96
MnO	0.17	0.17	0.17	0.18	0.18	0.18	0.18	0.16	0.16	0.16	0.16	0.17
MgO	5.62	5.80	5.95	7.69	7.69	7.51	7.47	6.56	5.82	4.12	7.63	7.69
CaO	10.17	10.25	10.08	8.46	8.53	8.43	8.39	10.27	10.10	9.10	9.48	9.79
Na_2O	3.56	3.70	2.95	4.91	4.63	3.50	4.49	3.77	3.65	4.23	2.72	3.11
K_2O	1.07	1.01	0.80	1.05	1.28	2.04	0.86	1.46	1.51	1.50	0.76	0.73
P_2O_5	0.51	0.49	0.45	0.77	0.76	0.77	0.75	1.10	1.19	0.53	0.38	0.37
L.O.I.	0.00	0.00	1.20	0.36	0.51	0.10	0.77	0.68	0.52	0.39	1.18	0.25
Total	98.46	99.49	99.94	98.37	100.10	98.78	98.20	98.97	98.43	99.04	99.36	98.94
Mg-no.	0.51	0.52	0.52	0.58	0.58	0.57	0.58	0.56	0.53	0.45	0.57	0.58
Li	-	-	-	-	2.03	-	2.23	-	5.04	8.95	3.82	-
Sc	-	-	-	-	14.7	-	14.6	-	18.1	14.3	23.1	-
V	-	-	-	-	134	-	130	-	-	-	237	-
Cr	106	101	100	134	93.3	143	83.7	157	119	39.0	281	279
Co	-	-	-	-	35.0	-	34.4	-	42.1	31.9	47.0	-
Ni	42	46	52	139	92.6	126	79.3	83	61.0	34.0	120	126
Cu	-	-	-	-	30.8	-	26.3	-	49.2	33.0	52.0	-
Zn	97	103	106	89	77.4	86	76.7	116	111	103	100	104
Ga	-	-	-	-	29.0	-	28.4	-	26.6	25.4	21.3	-
Rb	15	15	8	36	39.5	28	27.2	20	17.6	25.0	8.41	6
Y	-	-	-	-	25.4	-	25.3	-	25.7	26.7	19.2	-
Cs	-	-	-	-	0.354	-	0.343	-	0.148	0.418	0.046	-
Sr	586	613	638	833	883	884	858	1634	1711	733	530	577
Ba	-	-	-	-	375	-	362	-	662	276	217	-
Zr	195	185	196	329	289	339	287	330	257	216	130	161
Hf	-	-	-	-	7.48	-	7.30	-	5.82	5.14	3.16	-
Nb	-	-	-	-	53.0	-	51.4	-	52.8	41.9	23.6	-
Ta	-	-	-	-	3.77	-	3.62	-	3.06	2.73	1.46	-
Pb	-	-	-	-	2.70	-	3.02	-	2.79	2.79	1.62	-
Th	-	-	-	-	4.02	-	4.01	-	2.91	3.31	1.89	-
U	-	-	-	-	1.23	-	1.24	-	0.882	1.13	0.531	-
La	-	-	-	-	40.1	-	38.9	-	51.2	27.8	18.9	-
Ce	-	-	-	-	83.2	-	80.9	-	107	58.7	39.6	-
Pr	-	-	-	-	10.3	-	10.0	-	13.2	7.25	4.92	-
Nd	-	-	-	-	40.8	-	40.0	-	54.1	29.8	20.4	-
Sm	-	-	-	-	8.49	-	8.29	-	10.6	6.57	4.68	-
Eu	-	-	-	-	2.75	-	2.67	-	3.54	2.13	1.67	-
Gd	-	-	-	-	7.63	-	7.47	-	8.86	6.36	4.67	-
Tb	-	-	-	-	1.142	-	1.120	-	1.117	0.926	0.695	-
Dy	-	-	-	-	6.18	-	6.11	-	5.61	5.26	3.94	-
Ho	-	-	-	-	1.12	-	1.11	-	0.948	0.976	0.734	-
Er	-	-	-	-	2.87	-	2.85	-	2.25	2.51	1.87	-
Tm	-	-	-	-	0.387	-	0.379	-	0.280	0.341	0.249	-
Yb	-	-	-	-	2.39	-	2.41	-	1.67	2.14	1.52	-
Lu	-	-	-	-	0.345	-	0.342	-	0.225	0.298	0.213	-

Table 2. (continued)

Sample	SY-212	SY-213	SY-214	SY-215	SY-216	SY-217	SY-218	SY-220	SY-221	SY-223	SY-224	SY-226
Lat. [°N]	32°40`04``	32°40`04``	32°40`04``	32°40`04``	32°41`04``	32°41`04``	32°41`04``	32°41`04``	32°41`04``	32°42`40``	32°42`40``	32°42`41``
Long. [°E]	36°50`00``	36°50`00``	36°50`00``	36°50`00``	36°53`05``	36°53`05``	36°53`05``	36°53`05``	36°53`05``	36°55`18``	36°55`18``	36°55`14``
Elevation [m]	1449	1451	1453	1460	1286	-	-	-	1320	-	-	1068
Rock type	**alk.** basalt	**alk.** basalt	**alk.** basalt	**alk.** basalt	basanite	**alk.** basalt	**alk.** basalt	**alk.** basalt	**alk.** basalt	hawaiite	**alk.** basalt	**alk.** basalt
SiO_2	46.48	45.99	46.25	46.27	42.74	46.95	46.94	46.90	46.95	44.26	43.51	46.40
TiO_2	2.20	2.17	2.13	2.35	3.36	1.99	2.01	2.01	2.02	3.11	2.99	2.55
Al_2O_3	15.75	15.58	15.45	15.56	16.15	14.91	15.08	14.92	15.00	14.34	14.17	15.90
$Fe_2O_3^T$	13.02	12.76	12.52	12.41	14.28	12.12	12.04	12.10	12.05	12.31	12.20	12.45
MnO	0.17	0.16	0.15	0.16	0.20	0.16	0.16	0.17	0.17	0.16	0.16	0.17
MgO	7.40	7.35	7.55	7.48	4.97	9.15	8.62	9.03	8.74	7.91	8.15	6.12
CaO	9.73	9.64	10.03	10.62	8.68	9.36	9.55	9.61	9.62	10.17	10.40	10.97
Na_2O	3.08	2.64	2.69	3.18	3.65	3.02	3.07	3.15	3.18	3.20	2.80	3.86
K_2O	0.76	0.80	0.78	0.82	1.42	0.97	1.02	0.98	0.99	1.67	1.81	0.69
P_2O_5	0.39	0.39	0.37	0.44	1.30	0.30	0.31	0.30	0.31	1.03	0.99	0.41
L.O.I.	0.86	0.92	1.17	0.17	1.61	0.00	0.11	0.02	0.06	1.42	1.85	0.09
Total	99.84	98.40	99.09	99.46	98.36	98.93	98.91	99.19	99.09	99.58	99.03	99.61
Mg-no.	0.57	0.57	0.58	0.58	0.45	0.64	0.63	0.63	0.63	0.60	0.61	0.53
Li	5.21	5.37	-	4.07	8.72	-	-	-	7.67	-	6.92	1.93
Sc	18.4	18.9	-	24.7	11.6	-	-	-	20.6	-	16.8	18.1
V	-	-	-	248	-	-	-	-	-	-	-	163
Cr	285	263	274	227	18.0	364	335	363	332	192	209	101
Co	45.8	46.6	-	51.2	37.0	-	-	-	49.4	-	43.9	33.2
Ni	129	116	107	95.5	17.0	195	173	181	168	131	143	36.5
Cu	52.5	53.8	-	54.5	27.2	-	-	-	59.4	-	51.6	41.6
Zn	99.0	106	97	99.3	104	96	95	93	92.0	118	115	87.5
Ga	20.8	21.6	-	22.3	22.3	-	-	-	21.4	-	22.7	28.5
Rb	9.30	10.1	11	10.8	19.6	21	25	23	21.6	27	19.6	6.95
Y	19.8	20.8	-	20.1	29.7	-	-	-	23.9	-	23.2	20.6
Cs	0.072	0.072	-	0.106	0.454	-	-	-	0.358	-	0.178	0.080
Sr	576	582	587	665	1411	478	493	486	494	1519	1536	517
Ba	209	233	-	240	-	-	-	-	197	-	588	333
Zr	126	134	164	160	324	168	170	168	147	364	272	142
Hf	3.17	3.47	-	3.40	6.32	-	-	-	3.82	-	5.83	4.08
Nb	22.5	24.3	-	30.3	89.3	-	-	-	23.3	-	55.6	19.3
Ta	1.35	1.45	-	1.66	4.96	-	-	-	1.58	-	3.32	1.34
Pb	6.43	1.62	-	1.68	3.08	-	-	-	2.55	-	3.07	1.40
Th	1.84	2.04	-	2.06	4.74	-	-	-	2.46	-	3.49	1.30
U	0.497	0.529	-	0.555	1.32	-	-	-	0.831	-	0.806	0.341
La	18.4	20.0	-	21.7	58.5	-	-	-	17.3	-	49.9	16.4
Ce	38.5	41.7	-	46.4	118	-	-	-	38.1	-	102	38.2
Pr	4.74	5.12	-	5.52	13.8	-	-	-	4.85	-	12.2	5.27
Nd	20.0	21.6	-	22.7	53.7	-	-	-	20.3	-	49.4	23.2
Sm	4.63	4.91	-	5.03	10.0	-	-	-	4.95	-	9.47	5.76
Eu	1.61	1.68	-	1.84	3.16	-	-	-	1.54	-	3.06	2.03
Gd	4.57	4.85	-	4.86	8.66	-	-	-	4.97	-	7.99	5.75
Tb	0.688	0.717	-	0.696	1.137	-	-	-	0.762	-	1.010	0.883
Dy	3.87	4.06	-	3.81	6.02	-	-	-	4.52	-	5.12	5.03
Ho	0.716	0.753	-	0.707	1.07	-	-	-	0.843	-	0.863	0.932
Er	1.83	1.92	-	1.80	2.68	-	-	-	2.24	-	2.07	2.35
Tm	0.244	0.254	-	0.254	0.351	-	-	-	0.307	-	0.260	0.311
Yb	1.48	1.54	-	1.54	2.14	-	-	-	1.97	-	1.53	1.93
Lu	0.207	0.223	-	0.209	0.303	-	-	-	0.276	-	0.209	0.275

Table 2. (continued)

Sample	SY-227	SY-228	SY-229	SY-230	SY-234	SY-236	SY-238	SY-241gl	SY-243	SY-245	SY-253	SY-256
Lat. [°N]	32°42`34``	32°34`58``	32°33`50``	32°28`43``	32°25`53``	32°50`43``	32°50`43``	32°51`40``	32°53`46``	32°57`11``	32°56`02``	32°57`51``
Long. [°E]	36°55`25``	36°51`38``	36°53`39``	36°50`36``	36°48`07``	36°37`01``	36°37`01``	36°37`00``	36°41`12``	36°42`33``	36°46`39``	36°48`09``
Elevation [m]	1052	1436	-	1374	-	-	-	-	-	1050	1050	954
Rock type	**alk.** basalt	mugearite	phonolite	**alk.** basalt	basanite	hawaiite	hawaiite	basanite	basanite	basanite	basanite	basanite
SiO_2	47.12	49.36	55.80	47.89	44.55	46.46	46.17	46.17	45.49	43.52	42.12	43.66
TiO_2	2.07	2.37	0.41	2.04	2.33	3.21	3.18	3.25	2.45	2.87	2.73	3.18
Al_2O_3	14.86	17.05	19.33	16.34	14.76	16.42	16.31	17.16	14.71	15.13	13.74	14.47
$Fe_2O_3^T$	12.11	11.08	6.64	11.75	13.88	12.15	12.09	11.18	12.78	12.67	12.78	13.37
MnO	0.16	0.18	0.12	0.16	0.21	0.16	0.16	0.18	0.17	0.17	0.18	0.18
MgO	8.75	2.92	0.88	6.61	6.73	5.05	4.98	3.76	8.66	7.27	9.82	8.10
CaO	9.59	7.18	2.05	9.69	8.06	9.67	9.60	9.20	7.99	9.59	10.46	8.62
Na_2O	3.13	5.16	8.84	3.24	4.86	4.31	4.44	5.24	4.70	4.87	3.86	4.45
K_2O	1.02	2.18	3.44	0.84	2.10	1.52	1.54	2.24	1.72	0.93	0.73	1.45
P_2O_5	0.31	0.90	0.35	0.33	0.91	0.67	0.68	1.02	0.70	0.90	0.74	0.84
L.O.I.	0.03	0.58	1.38	0.14	0.83	0.14	0.35	-	0.00	1.43	1.73	1.81
Total	99.15	98.96	99.24	99.03	99.22	99.76	99.50	99.60	99.37	99.35	98.89	100.13
Mg-no.	0.63	0.38	0.24	0.57	0.53	0.49	0.49	0.41	0.61	0.57	0.64	0.59
Li	8.51	-	-	-	3.22	4.58	-	8.80	-	-	-	-
Sc	20.6	-	-	-	12.0	21.8	-	17.5	-	-	-	-
V	-	-	-	-	149	255	-	-	-	-	-	-
Cr	323	1	n.d.	170	124	55.2	55	107	245	185	267	205
Co	47.8	-	-	-	43.6	40.3	-	55.6	-	-	-	-
Ni	175	n.d.	n.d.	74	126	31.6	26	148	205	117	200	163
Cu	62.7	-	-	-	38.3	54.4	-	47.1	-	-	-	-
Zn	93.0	114	154	98	125	117	105	118	105	99	103	115
Ga	21.1	-	-	-	24.3	26.0	-	-	-	-	-	-
Rb	22.4	39	42	9	26.6	20.8	26	38.9	24	8	7	16
Y	24.2	-	-	-	26.3	25.1	-	23.9	-	-	-	-
Cs	0.443	-	-	-	0.477	0.174	-	0.375	-	-	-	-
Sr	483	698	846	496	1288	902	815	850	798	963	917	1133
Ba	189	-	-	-	459	386	-	391	-	-	-	
Zr	150	328	574	160	384	251	270	279	308	320	300	378
Hf	3.70	-	-	-	6.67	4.69	-	6.44	-	-	-	-
Nb	23.9	-	-	-	70.2	52.5	-	46.7	-	-	-	-
Ta	1.61	-	-	-	3.90	2.77	-	2.43	-	-	-	-
Pb	2.41	-	-	-	4.70	2.48	-	2.52	-	-	-	-
Th	2.50	-	-	-	6.01	2.56	-	4.00	-	-	-	-
U	0.891	-	-	-	1.72	0.669	-	1.18	-	-	-	-
La	17.7	-	-	-	60.8	31.9	-	37.7	-	-	-	-
Ce	38.3	-	-	-	121	68.8	-	79.2	-	-	-	-
Pr	4.85	-	-	-	13.3	8.29	-	9.59	-	-	-	-
Nd	20.6	-	-	-	49.6	34.1	-	38.2	-	-	-	-
Sm	4.93	-	-	-	9.47	7.30	-	7.93	-	-	-	-
Eu	1.57	-	-	-	3.28	2.72	-	2.53	-	-	-	-
Gd	4.98	-	-	-	8.02	6.54	-	7.33	-	-	-	-
Tb	0.766	-	-	-	1.074	0.890	-	0.998	-	-	-	-
Dy	4.49	-	-	-	5.19	4.60	-	5.26	-	-	-	-
Ho	0.857	-	-	-	0.862	0.816	-	0.935	-	-	-	-
Er	2.27	-	-	-	2.02	2.04	-	2.34	-	-	-	-
Tm	0.312	-	-	-	0.265	0.291	-	0.302	-	-	-	-
Yb	1.95	-	-	-	1.45	1.71	-	1.83	-	-	-	-
Lu	0.278	-	-	-	0.177	0.222	-	0.263	-	-	-	-

Table 2. (continued)

Sample	SY-258	SY-261	SY-267	SY-269	SY-271	SY-272	SY-273gl	SY-274	SY-278	SY-279	SY-280	SY-281
Lat. [°N]	33°00`25``	33°02`59``	32°37`41``	32°37`41``	32°34`53``	32°21`28``	32°21`28``	32°24`03``	32°54`42``	32°57`19``	32°59`00``	33°03`30``
Long. [°E]	36°50`20``	36°58`16``	36°40`08``	36°40`08``	36°40`25``	36°49`38``	36°49`38``	36°50`52``	36°29`25``	36°24`53``	36°19`07``	36°18`24``
Elevation [m]	912	641	1143	1448	1375	1260	1260	1278	905	731	648	651
Rock type	**alk.** basalt	**alk.** basalt	trachyte	trachyte	**alk.** basalt	basanite	**alk.** basalt	basanite	**alk.** basalt	**alk.** basalt	**alk.** basalt	**alk.** basalt
SiO_2	45.35	46.43	60.22	59.48	47.60	42.53	46.57	43.29	47.08	47.02	44.99	45.92
TiO_2	2.05	2.04	0.30	0.29	2.47	2.56	3.26	3.24	2.26	2.31	2.45	2.60
Al_2O_3	14.40	15.95	18.02	17.70	16.35	13.05	16.95	14.98	15.86	16.16	14.09	14.51
$Fe_2O_3^T$	12.48	12.20	5.24	5.43	12.09	13.19	11.58	13.11	12.20	12.21	13.66	13.76
MnO	0.16	0.17	0.14	0.18	0.16	0.18	0.14	0.17	0.16	0.16	0.17	0.18
MgO	8.99	7.22	0.23	0.25	6.19	11.40	5.06	8.70	6.43	6.37	9.26	9.39
CaO	10.42	10.05	1.54	1.64	9.34	9.17	10.77	8.95	9.77	9.94	9.41	9.44
Na_2O	3.08	3.15	7.37	7.17	3.62	3.64	2.57	4.14	3.33	3.49	3.28	3.13
K_2O	0.75	0.72	4.93	4.84	1.10	0.65	2.29	1.99	1.00	0.88	0.87	0.83
P_2O_5	0.32	0.37	0.12	0.14	0.42	0.77	0.99	0.67	0.45	0.39	0.48	0.48
L.O.I.	0.69	2.68	0.41	0.74	0.26	1.84	-	0.03	0.03	0.00	0.00	0.00
Total	98.69	100.98	98.52	102.69	99.60	98.98	100.33	99.27	98.57	98.93	98.66	100.24
Mg-no.	0.63	0.58	0.09	0.10	0.54	0.67	0.48	0.61	0.55	0.55	0.61	0.61
Li	1.72	5.01	24.6	19.9	-	-	1.91	-	1.95	1.96	1.63	-
Sc	16.4	20.4	2.32	2.32	-	-	24.3	-	15.7	16.1	14.8	-
V	139	-	-	-	-	-	-	-	148	145	138	-
Cr	254	185	> 1	> 1	113	363	307	164	109	119	189	246
Co	42.4	45.2	1.26	1.22	-	-	52.9	-	33.7	33.5	44.5	-
Ni	145	86.0	> 1	> 1	67	387	183	161	53.7	53.9	154	210
Cu	36.9	55.5	8.27	8.74	-	-	5.41	-	38.0	38.5	48.0	-
Zn	81.0	98.0	110	110	97	97	99.1	93	84.8	85.4	93.7	119
Ga	30.3	22.1	-	-	-	-	-	-	25.3	25.7	24.5	-
Rb	10.6	8.42	59.7	52.5	17	7	29.6	22	16.0	11.4	11.4	15
Y	17.2	24.3	32.4	32.5	-	-	22.7	-	22.0	22.1	20.6	-
Cs	0.059	0.066	0.877	0.637	-	-	0.431	-	0.188	0.106	0.106	-
Sr	561	463	109	240	692	944	739	881	545	563	559	549
Ba	473	204	765	757	-	-	351	-	232	232	235	-
Zr	122	159	848	866	205	281	234	302	187	185	165	192
Hf	3.60	3.86	19.5	19.8	-	-	5.60	-	5.25	5.15	4.69	-
Nb	20.2	22.0	93.3	94.0	-	-	46.1	-	27.0	27.0	26.4	-
Ta	1.37	1.35	7.09	7.13	-	-	2.91	-	1.82	1.82	1.77	-
Pb	1.52	1.54	11.8	11.6	-	-	2.46	-	1.98	1.91	1.93	-
Th	1.40	1.33	13.0	13.3	-	-	3.73	-	2.13	2.01	2.24	-
U	0.381	0.301	3.58	2.72	-	-	1.19	-	1.23	0.557	0.615	-
La	17.7	18.3	69.5	67.8	-	-	36.1	-	26.6	25.7	24.5	-
Ce	38.6	40.6	129	126	-	-	75.0	-	56.9	55.2	53.6	-
Pr	5.06	5.16	13.7	13.4	-	-	9.00	-	7.30	7.14	7.04	-
Nd	21.5	22.1	46.1	45.3	-	-	36.3	-	30.2	29.9	29.8	-
Sm	5.02	5.07	7.96	7.90	-	-	7.50	-	6.71	6.70	6.82	-
Eu	1.78	1.72	1.69	1.65	-	-	2.35	-	2.19	2.25	2.31	-
Gd	4.90	5.13	7.28	7.26	-	-	6.99	-	6.35	6.41	6.44	-
Tb	0.753	0.775	1.107	1.097	-	-	0.961	-	0.972	0.973	0.955	-
Dy	4.24	4.60	6.68	6.61	-	-	5.10	-	5.41	5.40	5.14	-
Ho	0.782	0.891	1.36	1.36	-	-	0.911	-	0.995	0.987	0.927	-
Er	1.96	2.34	3.99	4.01	-	-	2.27	-	2.52	2.51	2.28	-
Tm	0.262	0.321	0.630	0.628	-	-	0.295	-	0.337	0.337	0.301	-
Yb	1.61	2.01	4.46	4.49	-	-	1.82	-	2.12	2.10	1.83	-
Lu	0.232	0.289	0.703	0.701	-	-	0.254	-	0.301	0.303	0.262	-

Table 2. (continued)

Sample	**BHVO-1** (XRF)	**BR** (ICP-MS)
Lat. [°N]		
Long. [°E]		
Elevation [m]		
Rock type	standard	standard
SiO_2	49.68	-
TiO_2	2.74	-
Al_2O_3	13.72	-
$Fe_2O_3^T$	12.03	-
MnO	0.17	-
MgO	7.26	-
CaO	11.34	-
Na_2O	2.37	-
K_2O	0.53	-
P_2O_5	0.28	-
L.O.I.	-	-
Total	100.13	-
Mg-no.		
Li	-	11.4
Sc	-	19.9
V	-	217
Cr	286	353
Co	-	54.6
Ni	108	249
Cu	-	65.9
Zn	102	149
Ga	-	18.1
Rb	11	27.4
Y	-	45.6
Cs	-	0.743
Sr	396	1365
Ba	-	1058
Zr	184	267
Hf	-	5.90
Nb	-	105
	-	5.58
Pb	-	4.42
Th	-	10.6
U	-	2.48
La	-	79.8
Ce	-	151
Pr	-	16.8
Nd	-	64.3
Sm	-	12.0
Eu	-	3.55
Gd	-	9.94
Tb	-	1.29
Dy	-	6.37
Ho	-	1.07
Er	-	2.53
Tm	-	0.307
Yb	-	1.80
Lu	-	0.241

Table 3. Sr, Nd and Pb isotopic compositions of selected Syrian lavas.

	Isotopic compositions						age corrected Isotopic compositions					
Sample	$^{87}Sr/^{86}Sr$ (2s)	$^{143}Nd/^{144}Nd$ (2s)	$^{206}Pb/^{204}Pb$	$^{207}Pb/^{204}Pb$	$^{208}Pb/^{204}Pb$	Age* [m.y.]	$^{87}Sr/^{86}Sr_T$	$^{143}Nd/^{144}Nd_T$	$^{206}Pb/^{204}Pb_T$	$^{207}Pb/^{204}Pb_T$	$^{208}Pb/^{204}Pb_T$
SY-179	0.703314 (9)	0.512837 (13)	19.122	15.634	39.020	0.5	0.70331	0.512837	19.12	15.63	39.02
SY-184	0.703259 (2)	0.512934 (2)				2.0	0.70326	0.512932			
SY-200	0.703094 (3)	0.512940 (2)				2.0	0.70309	0.512938			
SY-202	0.703048 (3)	0.512944 (2)				2.0	0.70305	0.512942			
SY-213	0.703413 (11)	0.512910 (12)	19.102	15.622	38.996	4.0	0.70341	0.512906	19.09	15.62	38.98
SY-216	0.703298 (13)	0.512913 (12)	19.107	15.627	38.938	4.0	0.70330	0.512910	19.09	15.63	38.92
SY-221	0.703859 (14)	0.512887 (10)	19.443	15.649	38.829	4.0	0.70385	0.512883	19.43	15.65	38.82
SY-224	0.703425 (10)	0.512895 (10)	19.046	15.615	38.839	4.2	0.70342	0.512892	19.04	15.61	38.82
SY-227	0.703962 (11)	0.512861 (14)	19.276	15.646	38.729	4.2	0.70395	0.512857	19.26	15.64	38.72
SY-234	0.703118 (10)	0.512989 (7)	19.046	15.586	38.778	2.0	0.70312	0.512987	19.04	15.59	38.77
SY-261	0.703318 (9)	0.512840 (12)	18.854	15.613	38.687	0.5	0.70332	0.512840	18.85	15.61	38.69
SY-279	0.703313 (3)					0.5	0.70331				
SY-280	0.703301 (3)	0.512843 (3)				0.5	0.70330	0.512843			

*correction age depends on geological map of Ponikarov et al. (1963) and K-Ar ages of Sharkov et al. (1994), Mouty et al. (1992) and Giannerini et al. (1988) and Ar-Ar data of Krienitz et al. (in preparation)

Most of the Sr, Nd, and Pb isotopic analyses were performed at the Zentrallaboratorium für Geochronologie in Münster using a VG Sector 54 multicollector mass spectrometer. A few Sr and Nd isotope analyses were made at the Leibnitz Institut für Meereswissenschaften in Kiel on a Finnigan Triton mass spectrometer. Isotopic analyses were carried out with 100 mg of powdered sample material and standard ion exchange techniques were used to produce clean Sr, Nd, and Pb separates. Isotope fractionation was corrected using $^{86}Sr/^{88}Sr = 0.1194$ and $^{146}Nd/^{144}Nd = 0.7219$. In Münster, standard runs for Sr isotopes gave NBS987 (n = 16): 0.710299 (2SD = 0.000026) and all Sr isotope analyses were normalised to NBS987 = 0.710250. Standard runs for $^{143}Nd/^{144}Nd$ gave La Jolla (n = 14): 0.511862 (2SD = 0.000024). In Kiel, the NBS 987 (n=4) gave 0.710252 (2SD = 0.000002) and all Sr isotope analyses were normalised to NBS 987 = 0.710250. Standard runs for $^{143}Nd/^{144}Nd$ gave 0.511711 (2SD = 0.000012) for the Nd Spex standard (n=7) corresponding to a La Jolla value of 0.511855. All Nd isotope analyses were corrected to the La Jolla standard measured in Münster. The NBS982 standard was used to correct Pb isotopic ratios for mass fractionation. Correction factors are $^{206}Pb/^{204}Pb = 0.002$, $^{207}Pb/^{204}Pb = 0.003$ and $^{208}Pb/^{204}Pb = 0.004$ and standard runs (n = 10) gave $^{206}Pb/^{204}Pb = 36.646$, $^{207}Pb/^{204}Pb = 17.101$ and $^{208}Pb/^{204}Pb = 36.593$ with a precision of ±0.022, ±0.014 and ±0.038 (2SD), respectively. Procedural blanks at this time were generally better than 0.2 ng, 0.1 ng and 0.04 ng for Sr, Nd and Pb. All isotopic data were age-corrected using the ages from the geological maps of Ponikarov et al. (1963) and on K-Ar and Ar-Ar data of Giannerini et al. (1988), Mouty et al. (1992), Sharkov et al. (1994), and Krienitz et al. (CHAPTER III) (Table 3). The age-corrected isotopic data were used in the figures.

2.4 Classification

In the total alkali versus silica diagram the HAS samples show a bimodal distribution, but evolved lavas are rare. All basaltic rocks fall into the alkaline field using the division line of MacDonald (1968) and, except for four samples all basalts are nepheline-normative and thus can be classified as alkali basalts. The entire dataset is grouped into four different series on the basis of their stratigraphic occurrence and age (Figs. 2.1 and 2.2). The oldest lavas (>13 Ma, series IV) in the NW of the HAS have been previously dated and sampled by Mouty et al. (1992) and we use these published data to determine the composition of the parental series IV magma. Whereas series I comprises lavas younger than <1 Ma, volcanic rocks of series II erupted between 1 and 3.5 Ma and lavas of series III between 3.5 and 7 Ma. Series IV comprises lavas yielding ages older than 13 Ma. Generally, the oldest lavas of series IV are alkali basalts, series III ranges from alkali basalts to basanites and evolved lavas, most series II lavas are basanitic and tephritic while the youngest series I lavas are alkali basalts (Fig. 2.2). The major element composition of the series IV lavas generally resembles that of series III alkali basalts (Figs. 2.2 and 2.3).

2.5 Petrographic and geochemical results

2.5.1 Petrography

Hand specimen of the investigated volcanic rocks are generally fresh with only a few samples showing evidence of alteration. Almost all samples have porphyritic textures and contain variable amounts of phenocrysts with olivine and clinopyroxene being most abundant, feldspars are rare. Most olivines show iddingsite rims and some are completely altered. The predominant feldspar is plagioclase but in trachytic and phonolitic lavas mainly alkalifeldspars occur (Table 1). The mostly fine-grained groundmass consists of olivine, clinopyroxene, plagioclase, and Fe-Ti oxides. Rare calcite-filled vesicles are visible in hand specimen. Some lavas contain agglomerates of clinopyroxene and olivine. Sample SY-272 contains a cumulate composed of olivine and orthopyroxene with strong resorbed rims and thus these phases are interpreted as xenocrysts (Table 1).

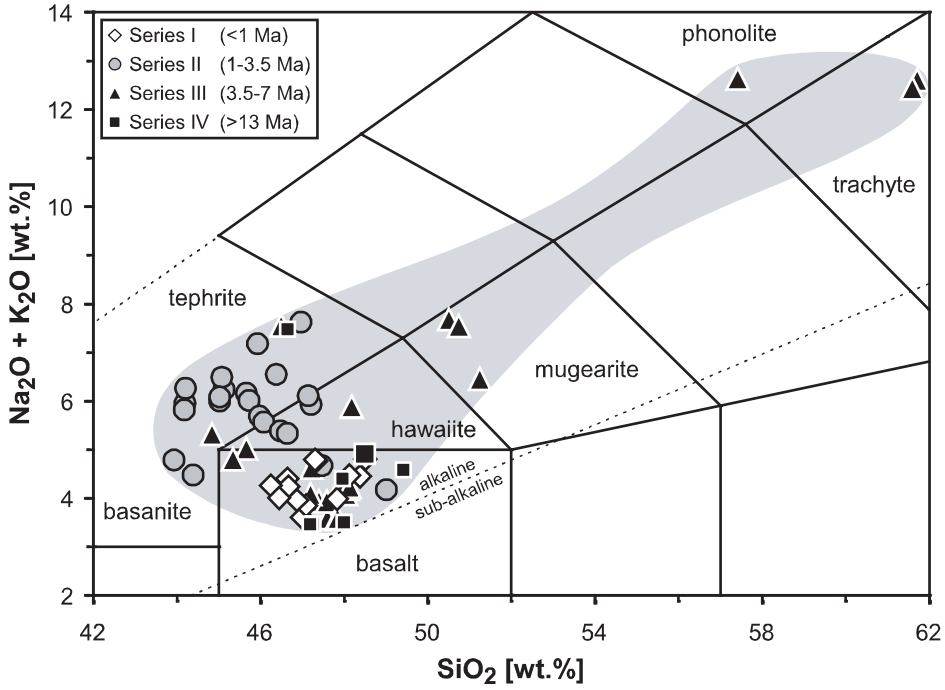

Fig. 2.2. Classification of the lava samples in the TAS diagram after Le Bas et al. (1986) with rock type discrimination after Le Maitre et al. (1989). Division into alkaline and sub-alkaline rocks is from MacDonald (1968). The sample set of series IV lavas is supplemented with data from Mouty et al. (1992) (small black squares).

2.5.2 Major and trace element content

The lavas span a range of MgO concentrations between 11.4 and 0.2 wt.% with Mg-numbers varying from 0.67 to 0.09. Lavas with MgO contents below 4 wt.% are restricted to the series III lavas (Fig. 2.3). Relatively primitive lavas show slight increases in SiO_2, Na_2O and K_2O concentrations with decreasing MgO, but these elements strongly increase in lavas with MgO contents <5 wt.%. Whilst TiO_2, FeO^T, CaO and P_2O_5 concentrations are relatively constant or increase slightly down to a MgO content of 5 wt.%, they sharply decrease below 5 wt.% MgO. Al_2O_3 increases throughout the whole differentiation sequence. The series II lavas with MgO >6 wt.%

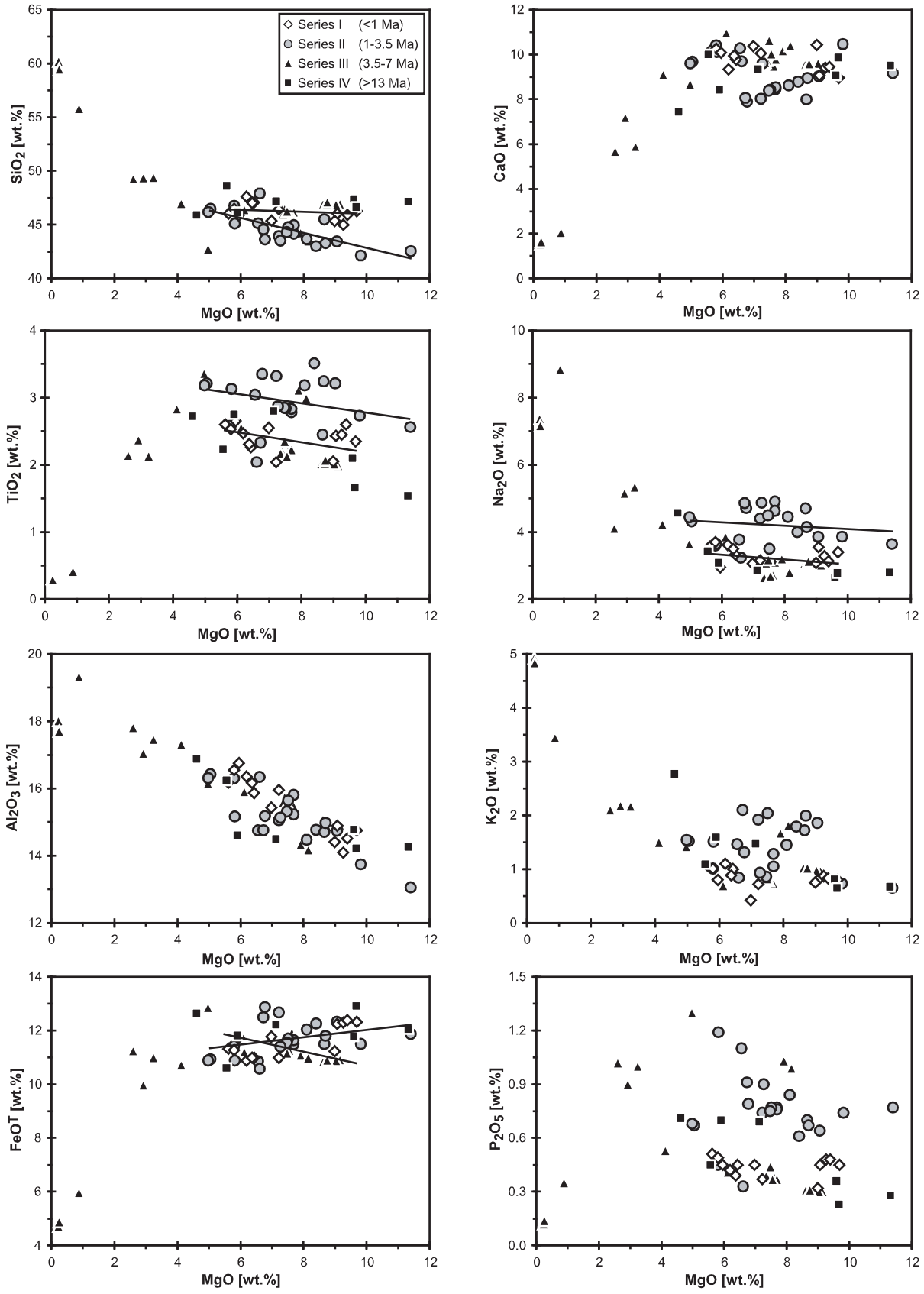

Fig. 2.3. Diagrams of major elements versus MgO for the Syrian sample suites. For a better comparison of the single HAS groups series IV lavas were completed with data taken from Mouty et al. (1992). Additionally shown are regression lines for SiO_2, TiO_2, FeO^T and Na_2O which were used to correct for fractionation (cp. Fig. 2.7).

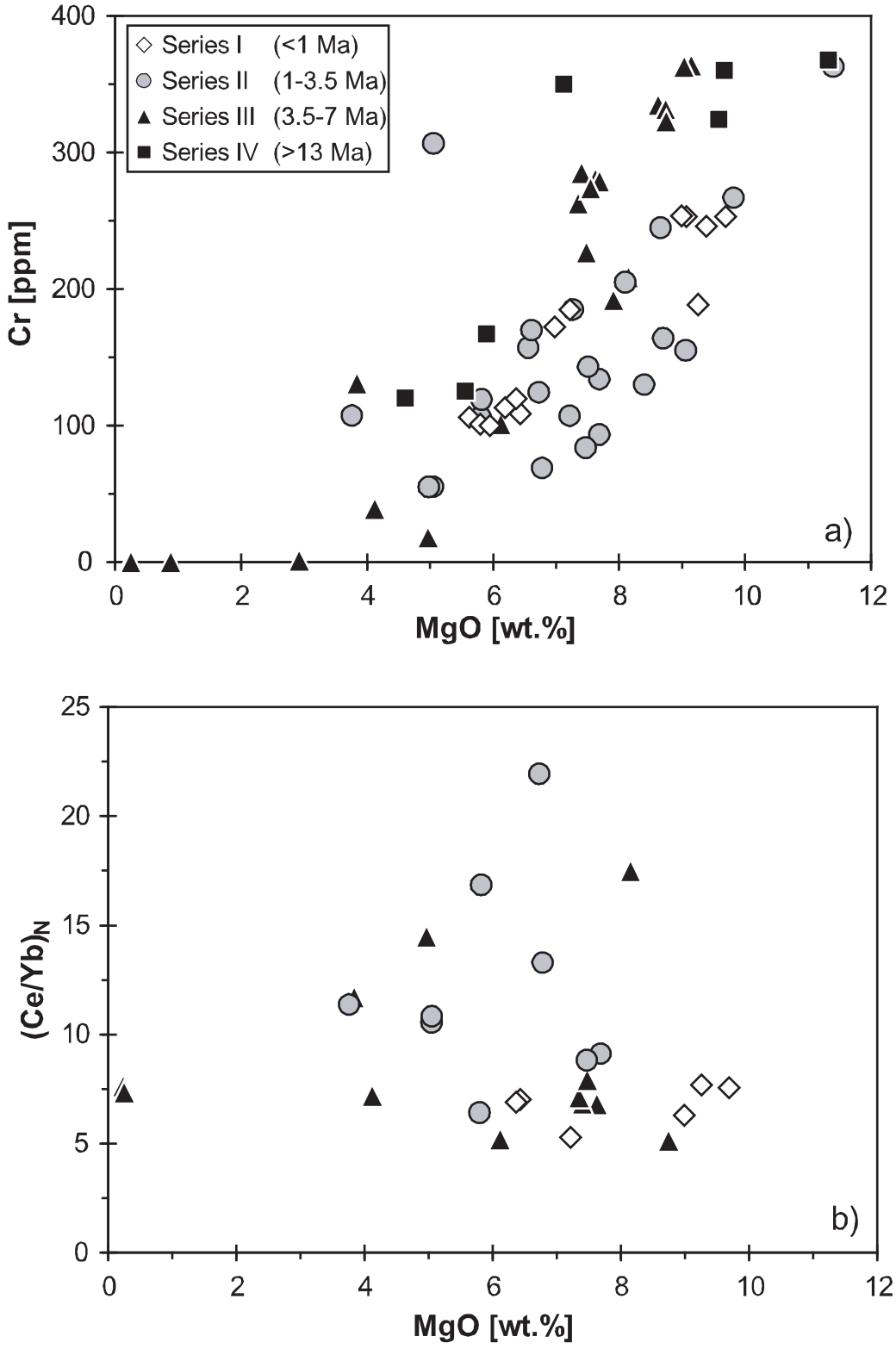

Fig. 2.4. (a) Plot of Cr concentrations versus MgO content of the Syrian lavas. (b) Chondrite-normalised Ce/Yb ratios of the HAS lavas versus MgO. Chondrite values are taken from McDonough and Sun (1995).

generally have much lower SiO_2 and higher TiO_2, Na_2O, K_2O as well as high P_2O_5 contents compared to the other Syrian lava series (Fig. 2.3). Series IV basalts form a relatively consistent group and resemble most mafic series III samples. However, series III is heterogeneous with several samples resembling the basanitic/tephritic series II. Series I is slightly more alkaline than series IV having higher Na_2O and TiO_2 and lower SiO_2 contents at a given MgO concentration. These striking chemical difference indicate that the petrogenesis of the Syrian HAS lavas changed with time.

Compatible trace elements, such as Cr are positively correlated with MgO (Fig. 2.4a). Series II lavas exhibit the lowest Cr concentrations at a given MgO content compared to the other groups (Figs. 2.4a). The HAS lavas show a large variation in $(Ce/Yb)_N$ which do not correlate with MgO contents (Fig. 2.4b). Lavas from series I are relatively homogeneous and have consistently low $(Ce/Yb)_N$ of 5 to 8 while series II and III lavas are highly variable ranging from 5 to 24 pointing to variable melting conditions during magma genesis. The samples show a rough positive correlation between Ce/Pb and Nb/U ratios and most samples have compositions similar to oceanic basalts but a few lavas tend to lower values resembling average continental crust (Fig. 2.5a). At constant $(Ce/Yb)_N$ of ~7 we find a significant variation of Nb/La ratios with series I lavas having the lowest Nb/La ratios at relatively low $(Ce/Yb)_N$, which could be caused by variable compositions of the mantle source(s) at similar degrees of partial melting. At $(Ce/Yb)_N$ higher than 8 several series III and most series II samples form a negative trend (Fig. 2.5b). Except for the trachytes all Syrian volcanic rocks lie on a negative correlation trend of Nb and K/Nb ratios probably indicating heterogeneities of the mantle source(s) of the lavas (Fig. 2.5c). Whereas series II lavas have the highest and series I have consistently low Nb contents, the Nb concentrations of series III samples are variable and lie between the other two series.

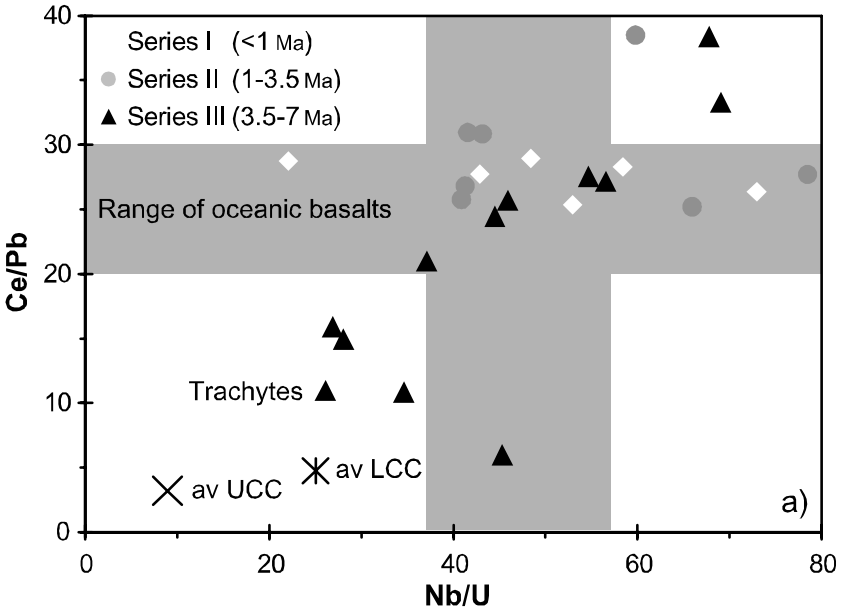

Fig. 2.5. (a) Diagram of Nb/U versus Ce/Pb ratios. Average compositions of upper (UCC) and lower (LCC) continental crust are from Rudnick and Fountain (1995). Grey fields are defined by mantle-like compositions of oceanic basalts (Hofmann et al., 1986). (b) $(Ce/Yb)_N$ versus Nb/La and (c) Nb versus K/Nb of the Syrian lavas. Chondrite values are from McDonough and Sun (1995).

2.5.3 Isotopic correlations

The Syrian HAS volcanic rocks show a negative correlation between Sr and Nd isotope ratios. The one series II sample has the highest $^{143}Nd/^{144}Nd$ ratio, while the series I samples have

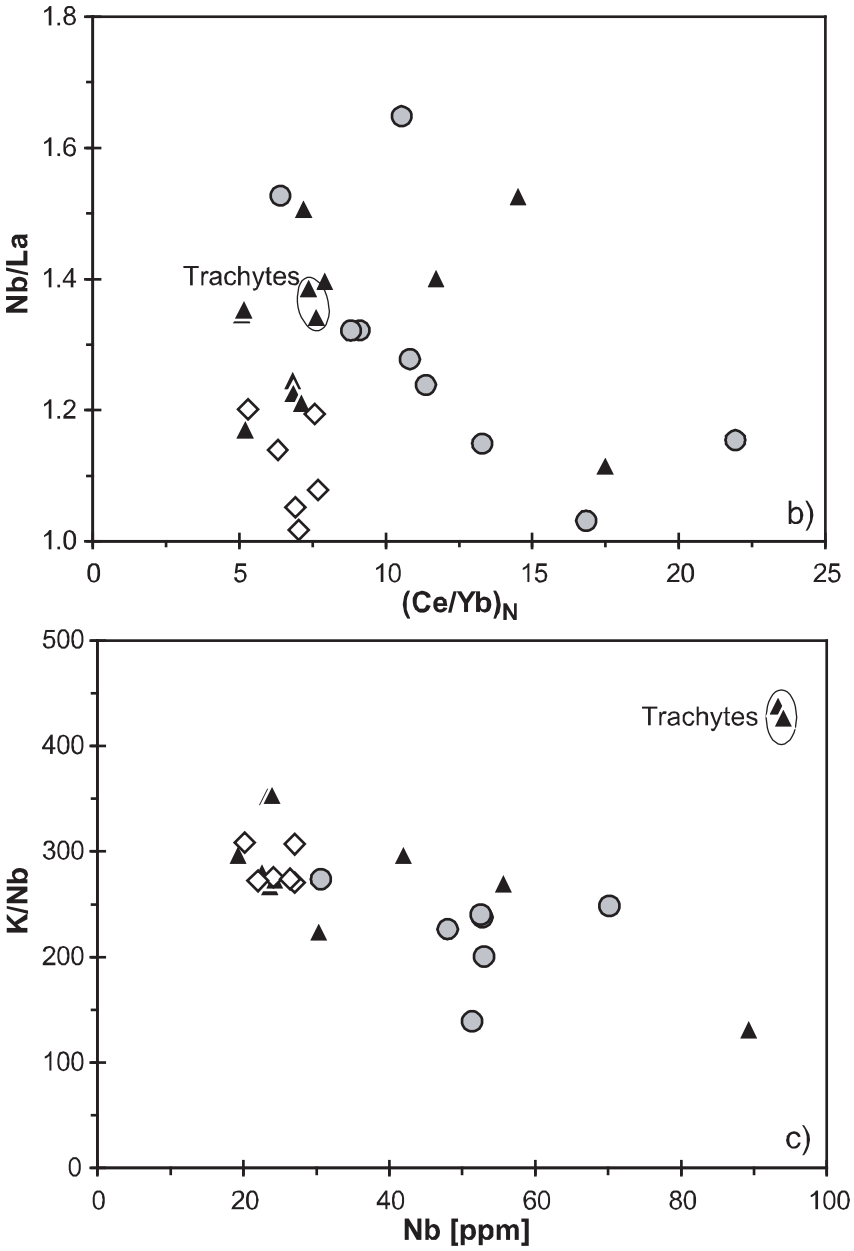

Fig. 2.5. continued

the lowest ratios (Fig. 2.6a). Series III samples have intermediate Nd isotope ratios and define a shallow negative trend towards high $^{87}Sr/^{86}Sr$. The isotopic compositions of the Syrian HAS lavas largely overlap with the volcanic rocks of the Jordanian HAS part with the exception of the series III lavas with the highest $^{87}Sr/^{86}Sr$, that also show the highest Pb isotope ratios. In terms of Sr and Nd isotope ratios the Syrian HAS lavas also overlap with the field of enriched Arabian lithospheric mantle peridotites and the series II sample resembles the Red Sea lavas in terms of Pb isotopes. However, most Syrian HAS lavas show higher $^{207}Pb/^{204}Pb$ ratios than the Red Sea lavas and they also have lower $^{87}Sr/^{86}Sr$ ratios for a given $^{143}Nd/^{144}Nd$ ratio than the Afar plume lavas with high $^{3}He/^{4}He$ (Fig. 2.6a). $^{206}Pb/^{204}Pb$ is generally positively correlated with

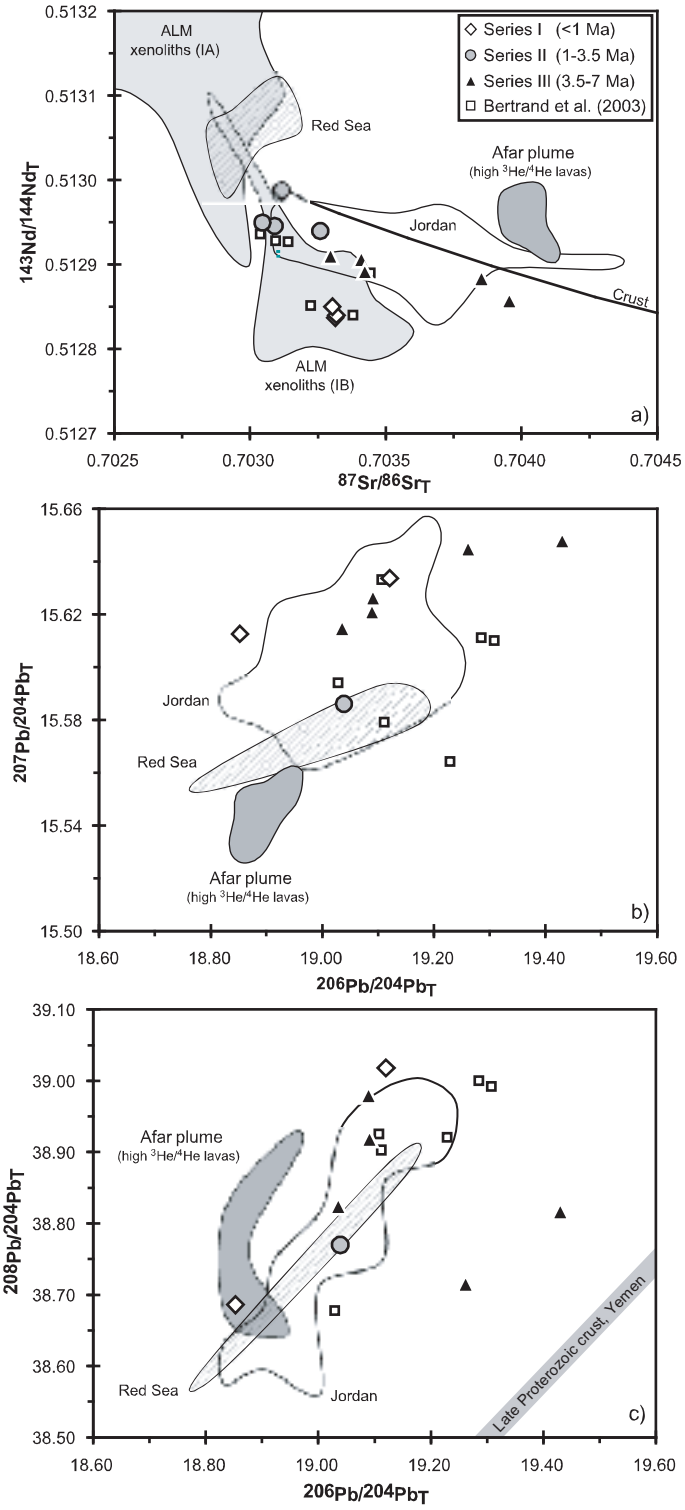

Fig. 2.6. (a) Age-corrected Sr versus Nd isotopic compositions of the HAS lavas. Fields are representative of Jordan volcanic rocks (Bertrand et al., 2003; Shaw et al., 2003), for Red Sea lavas (Eissen et al., 1989; Haase et al., 2000), and for Afar plume lavas yielding high $^{3}He/^{4}He$ ratios (Pik et al., 1999) as well as for cpx analyses representing Arabian lithospheric mantle (ALM; Henjes-Kunst et al., 1990; Blusztajn et al., 1995). Additional data of the Syrian HAS field are taken from Bertrand et al. (2003). The line represents a bulk mixing curve between sample "SY-234" and average Proterozoic crust (data from Hegner and Pallister, 1989). (b and c) $^{206}Pb/^{204}Pb_T$ versus $^{207}Pb/^{204}Pb_T$ and $^{208}Pb/^{204}Pb_T$ ratios of the HAS lavas. Compositions of Late Proterozoic crustal rocks are taken from Baker et al. (2000).

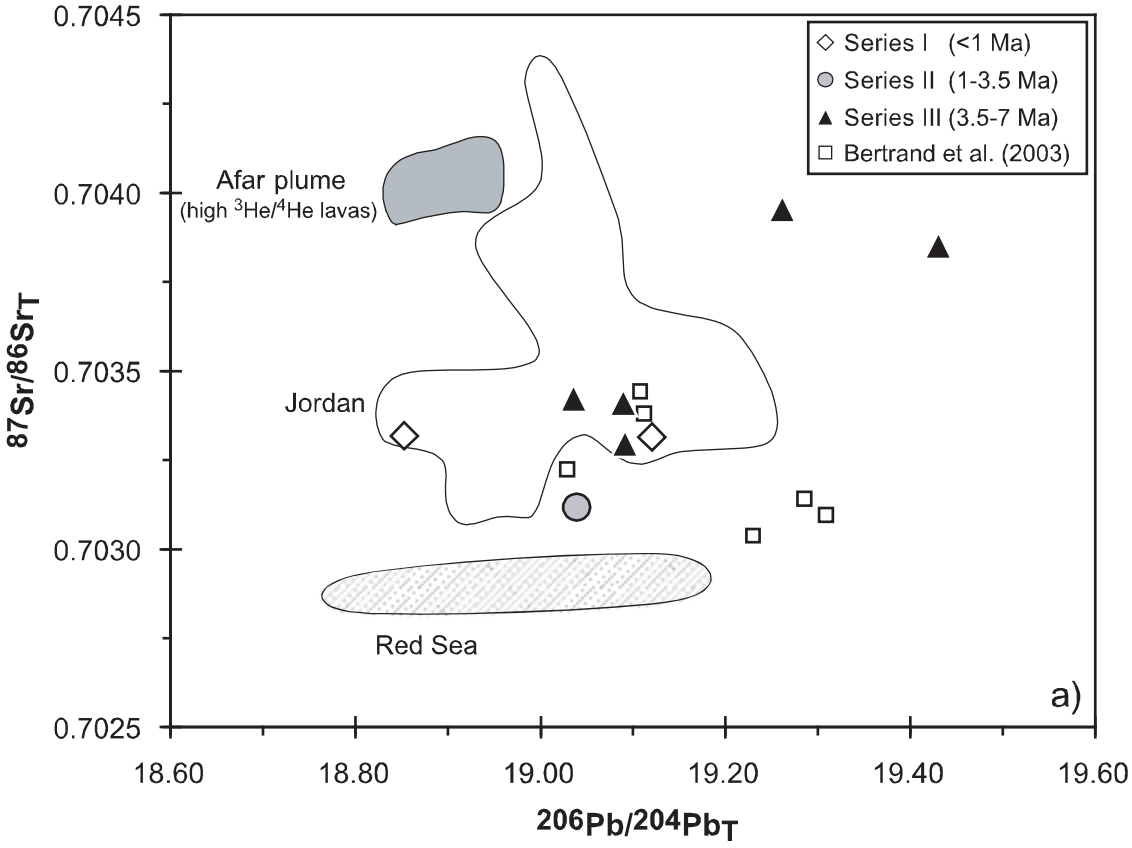

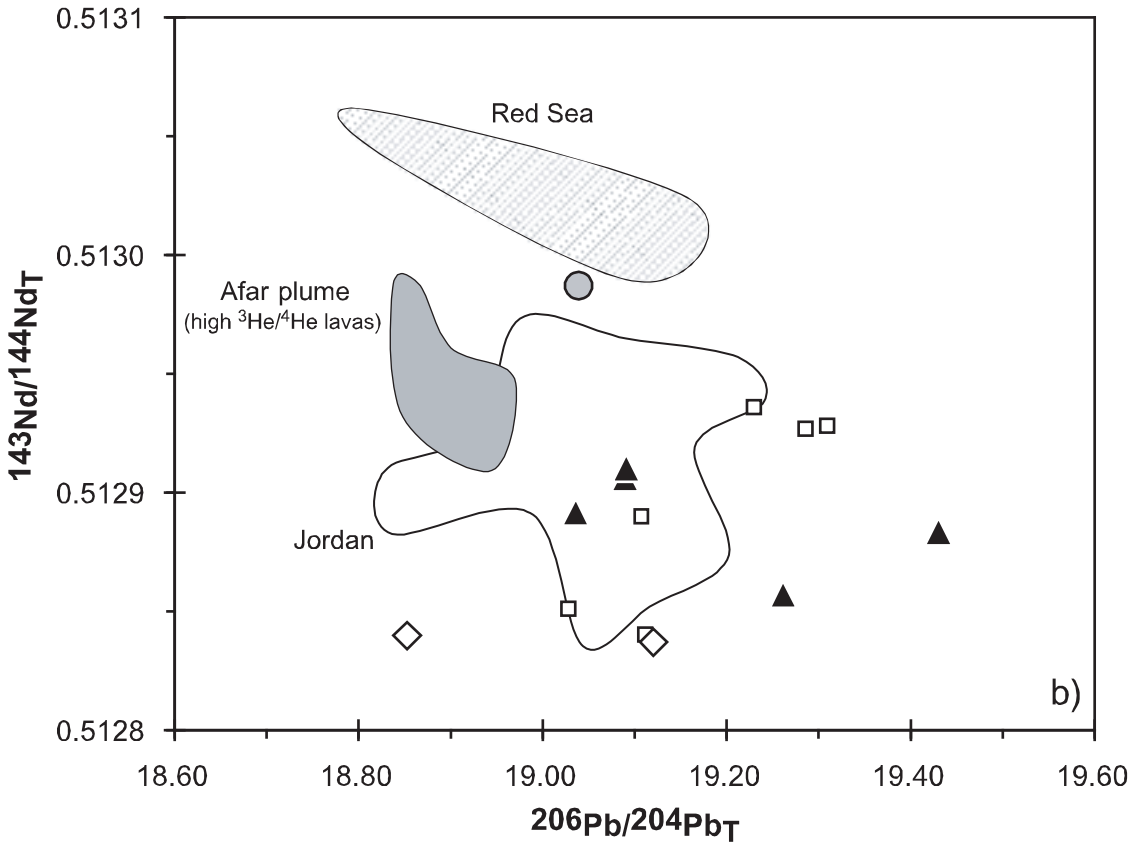

Fig. 2.7. (a) Age-corrected $^{206}Pb/^{204}Pb$ versus Sr isotopic composition of the Syrian HAS lavas and (b) versus $^{143}Nd/^{144}Nd_T$. Data sources as in Figure 2.6.

$^{87}Sr/^{86}Sr$ in the Syrian HAS lavas and they lie between the fields representative for Afar plume material and Red Sea lavas (Fig. 2.7a). As shown in Figure 2.7b the Syrian volcanic rocks also display higher $^{206}Pb/^{204}Pb$ for a given $^{143}Nd/^{144}Nd$ ratio to the Afar lower mantle plume material with high $^{3}He/^{4}He$. In Figure 2.8a the Ba/Nb ratios and $^{87}Sr/^{86}Sr$ isotopic composition of the Syrian HAS series form a triangular array similar to lavas from the Jordanian part of the HAS field. In lavas with $^{87}Sr/^{86}Sr < 0.7035$ a positive correlation between Ba/Nb and $^{87}Sr/^{86}Sr$ is observed. Series II lavas exhibit low incompatible element ratios with respect to series I lavas, Ba/Nb of series III lavas is highly variable comprising the highest and the lowest values of the whole Syrian data set (Fig. 2.8a). Series III lavas with the most radiogenic $^{87}Sr/^{86}Sr$ show intermediate compositions in terms of Ba/Nb. In Figure 2.8b the Nd isotopic compositions of the HAS lavas are plotted against the $(Ce/Yb)_N$ ratios. Compared to Red Sea lavas and Arabian lithospheric mantle xenoliths (IA) the investigated samples have generally higher $(Ce/Yb)_N$, but are similar to the Jordanian HAS lavas. Whereas series I and III lavas overlap with the arrays

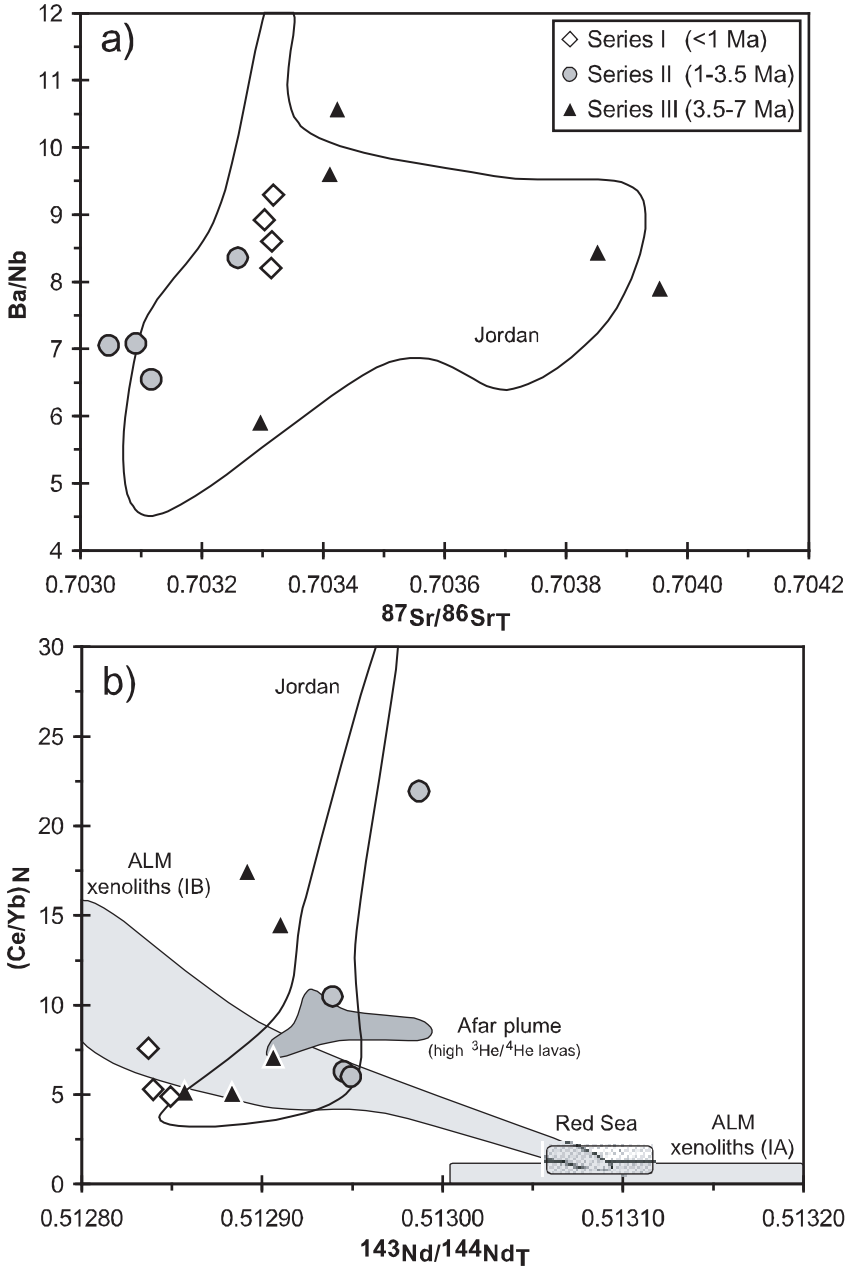

Fig. 2.8. (a) $^{87}Sr/^{86}Sr$ versus Ba/Nb ratios. (b) $^{143}Nd/^{144}Nd$ versus chondrite-normalised Ce/Yb ratios of the Syrian lavas and of two groups of xenoliths analyses representative for Arabian lithospheric mantle (Blusztajn et al., 1995). Chondrite composition is taken from McDonough and Sun (1995). Data sources for additional fields as in Figure 2.6.

spanned by the ALM xenoliths (IB) and by the Afar plume, lavas of series II show significantly higher $(Ce/Yb)_N$.

2.6 Discussion

2.6.1 Effects of alteration

During weathering of rocks a negative correlation between LOI (loss on ignition) and mobile elements such as K, Rb, Cs or U is expected because alteration results in a loss of these elements and in increasing H_2O and/or CO_2 contents as it is expressed by elevated LOI values. Despite the fact that some HAS lavas contain minor amounts of calcite and that the olivines are often partially or completely altered to iddingsite the investigated lavas generally appear fresh and no correlation is observed between mobile elements and LOI values. Except for two samples with high LOI values (2.7 and 3.7 wt.%) the LOI content generally lies below 2 wt.% which is typical for alkaline lavas (Table 2). The majority of the lavas have Nb/U ratios similar to or lower than oceanic basalts (Fig. 2.5a) thus they have not been affect by alteration because U is usually quite mobile during alteration compared to Nb, resulting in elevated Nb/U ratios. Thus, alteration processes have a minimal effect even on mobile element contents and did not affect the geochemistry of the HAS lavas significantly.

2.6.2 Control of fractional crystallisation and crystal accumulation on HAS lavas

Differences in the major and compatible trace element contents in particular between the primitive lavas of the HAS series can be caused by different source compositions, variable degrees of partial melting or by contamination processes, whereby variations within each of the Syrian HAS series are probably due to fractionational crystallisation of different mineral phases. The abundance of phenocryst phases as well as the wide range of MgO contents and Mg-numbers of the samples imply crystal fractionation during magmatic ascent (Figs. 2.3 and 2.4). Throughout the differentiation sequence the volcanic series is influenced by crystallisation of olivine, clinopyroxene, and spinel and, at later stages, feldspar and apatite. Olivine is one of the major fractionating phases and its extraction is indicated by decreasing Ni and MgO contents. On the other hand, the most primitive sample SY-272, with a Mg-number of 0.67, has a high Ni content and a high Ni/Cr ratio, but shows compatible and major element concentrations similar to other lavas (Table 2), suggesting olivine accumulation. This assumption is also confirmed by the occurrence of olivine xenocrysts in thin section. Decreasing Cr contents at a MgO of about 9 wt.% indicate the begin of clinopyroxene fractionation and the removal of spinel. The combination of olivine, clinopyroxene and spinel fractionation accounts for the constant CaO contents (Figs. 2.3 and 2.4a). The increasing Al_2O_3 and Sr concentrations show that plagioclase fractionation has played no major role in the early stages of differentiation. Feldspar removal in the differentiated rocks is indicated by inflections of Sr and SiO_2 and decreasing CaO between 6 and 5 wt.% MgO. The crystallisation of titanomagnetite is responsible for the lower FeO^T and TiO_2

contents in samples with MgO concentrations below 5 wt.%. The P_2O_5 decrease starting at 5 wt.% MgO is caused by apatite fractionation and is restricted to the evolved lavas belonging to series III (Fig. 2.3).

2.6.3 Crustal contamination of the HAS magmas

Magmas rising through the continental lithosphere often stagnate at crustal levels and assimilate crustal material. Mid-ocean ridge and ocean island basalts have average Nb/U ratios of 47±10 and average Ce/Pb ratios of 25±5 reflecting the composition of the Earth's mantle, while the continental crust has characteristically low Ce/Pb and Nb/U ratios (Hofmann et al., 1986). Most HAS lavas have high Nb/U and Ce/Pb implying negligible crustal contamination, but the low Ce/Pb and Nb/U ratios of several lavas from series III imply crustal contamination (Fig. 2.5a). The trachytes show the most significant contamination suggesting that assimilation-fractional crystallization processes affected the ascending magmas. Isotopic compositions are neither influenced by crystal fractionation nor by the degree of partial melting and the isotopic array of the HAS lavas in the Sr versus Nd isotope diagram implies that at least three isotopically distinct end members are involved in their magma genesis (Fig. 2.6a). Shaw et al. (2003) postulated that lavas of the Jordan HAS part have assimilated up to 20% of Late Proterozoic crust during their ascent to the surface. These crustal basement rocks are highly variable in their $^{206}Pb/^{204}Pb$ and $^{207}Pb/^{204}Pb$ compositions but have comparatively low $^{208}Pb/^{204}Pb$ ratios for a given $^{206}Pb/^{204}Pb$ when compared with the Syrian lavas (Fig. 2.6c). The Syrian HAS lavas display a similar isotopic trend to the Jordan HAS lavas suggesting crustal assimilation. Bulk mixing calculations of Syrian lavas with average Proterozoic crust confirm this assumption (continuous line, Fig. 2.6a) and the lavas with the highest $^{87}Sr/^{86}Sr$ have crust-like Ce/Pb and Nb/U ratios and trend to $^{208}Pb/^{204}Pb$ compositions observed in crustal rocks from Yemen (Figs. 2.5 and 6). Thus, akin to the Jordan HAS lavas, some of the Syrian lava series III rocks have assimilated crustal material leading to high $^{87}Sr/^{86}Sr$ and $^{206}Pb/^{204}Pb$ isotope ratios and to low $^{208}Pb/^{204}Pb$ (Figs. 2.6 and 2.7).

2.6.4 Parental magma composition

The combined processes of crustal assimilation and crystal fractionation modified the Syrian lavas and thus no primary magmas from the mantle have been sampled. In order to determine the mantle melting processes and the mantle sources involved in the formation of the HAS volcanic rocks we compare fractionation-corrected compositions of uncontaminated lavas, i.e. those within the range of mantle compositions in terms of Nb/U and Ce/Pb (Fig. 2.5a). Lavas with MgO concentrations below 5 wt.% are not included in the fractionation correction because they do not lie on linear trends (olivine control lines) thus indicating a complex crystallisation history. First, the effects of fractional crystallisation on the major elements SiO_2, FeO^T, Na_2O, and TiO_2 have been corrected to MgO contents of 9 wt.% (Fig. 2.9) similar to the approach of Klein and Langmuir (1987). While Si, Na and Ti show relatively clear fractionation trends for each series, Fe is highly variable (Fig. 2.3). The fractionation-corrected lava compositions do not represent

primary magma compositions because they have average Mg# of 0.62 compared to Mg# of 0.68-0.72 of mantle melts (Frey et al., 1978). To determine the primary magma compositions of the HAS lavas, the fractionation-corrected FeO^T data were recalculated to compositions having a Mg# of 0.72, which is characteristic for a melt that is in equilibrium with mantle olivine having Fo_{89}, by adding olivine with Fo_{88} found in sample SY-272 (Table 1, Fig. 2.9). The variable FeO^T contents in the HAS lavas suggest a significant range of primary magma compositions with MgO contents of 13 to 15 wt.% MgO (Fig. 2.9). Hypothetical parental liquid concentrations of the different series of HAS lavas are listed in Table 4 and it appears that the lavas series I, II, and IV have higher FeO^T contents than the series III samples. These differences in primary magma compositions suggest significant changes in the processes of magma genesis in the last 24 Ma

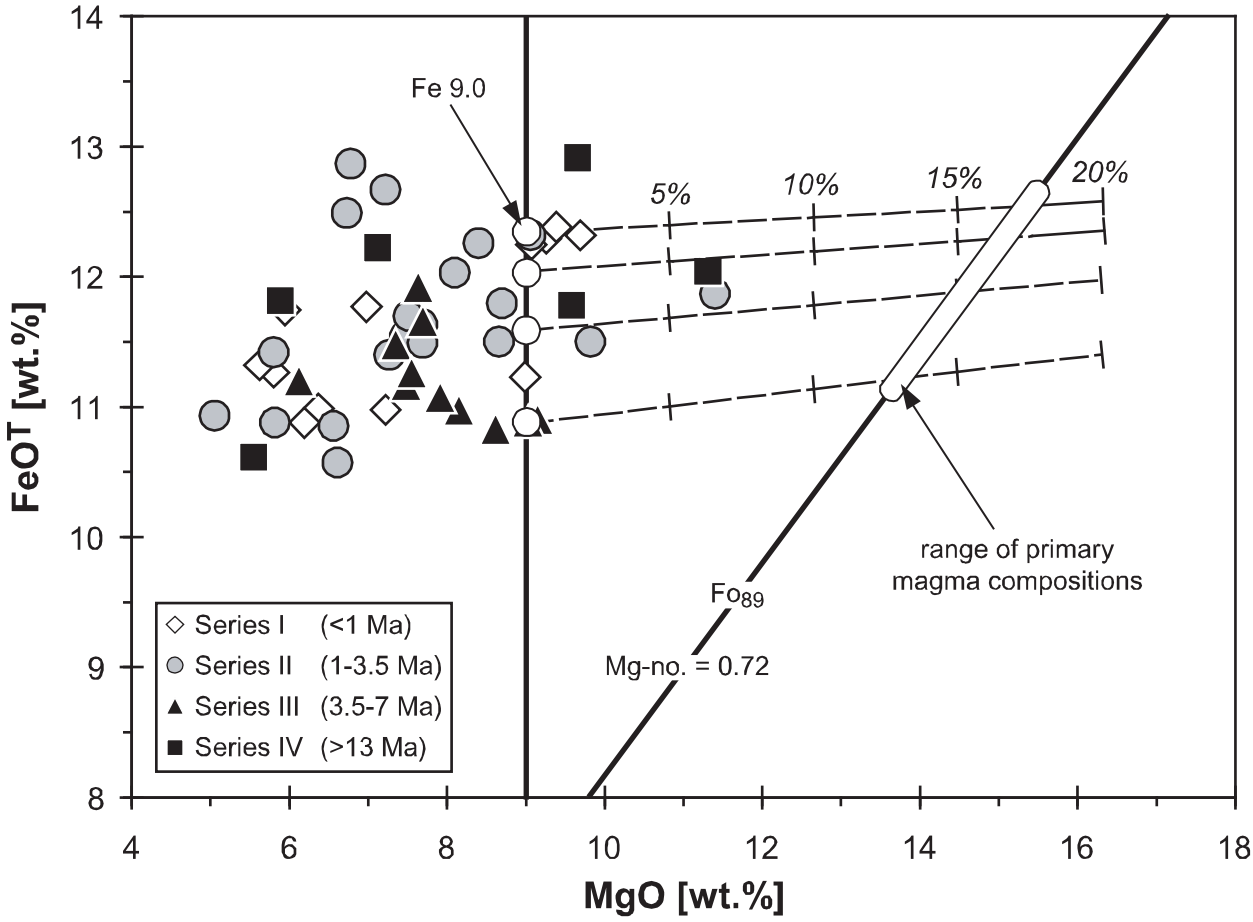

Fig. 2.9. Plot of MgO versus FeO^T concentrations showing the fractionation-correction scheme for the Syrian lavas. Samples with MgO concentrations below 5 wt.% and crustaly contaminated samples were rejected from regression (see text for discussion). Open circles give FeO^T concentrations at 9 wt.% MgO ($Fe_{9.0}$) for representative lavas of the single volcanic suites. Dashed lines refer to addition of Fo_{88} olivine (olivine control lines) as found in the most primitive sample "SY-272" and numbers give the amount of olivine added. Left tilted line shows composition of constant Mg-number of 0.72 which is in equilibrium with Fo_{89} olivine, assuming $K_d^{Fe\text{-}Mg} = 0.3$. Hypothetical representative primary magma compositions for the single HAS series are listed in Table 4. Data for series IV are from Mouty et al. (1992).

since the eruption of series IV lavas.

2.6.5 Partial melting processes beneath the HAS

As apparent from Figure 2.10 the $Ti_{9.0}$ and $Na_{9.0}$ contents in the HAS lavas are positively correlated, whereby negative correlations can be observed when $Si_{9.0}$ contents of lavas are plotted versus $Na_{9.0}$, and $(Tb/Yb)_N$. Thus the lavas with high $Si_{9.0}$ contents (>45 wt.%) have lower $Ti_{9.0}$ and $Na_{9.0}$ concentrations compared to lavas yielding relatively low $Si_{9.0}$ contents in the range between 45 and 42 wt.%. Such differences can be generated by variable mantle source compositions or could reflect variations in the pressure-temperature regime as well as in the extent of partial melting. Thus, the variation in $Ti_{9.0}$ and $Na_{9.0}$ suggests that the HAS magmas formed by 4 to 11 % of partial melting of a slightly enriched garnet peridotite source (Fig. 2.10a). The series II lavas formed by the lowest degrees of melting while the oldest series III and IV magmas represent the highest degree melts. The youngest lavas of series I indicate an increasing degree of melting during the past 1 Ma. Since garnet possesses significantly higher distribution coefficients for heavy rare earth elements (REE) than for the middle and light REEs, melting in the presence of residual garnet retains the HREE over the middle and light ones. The REE ratios

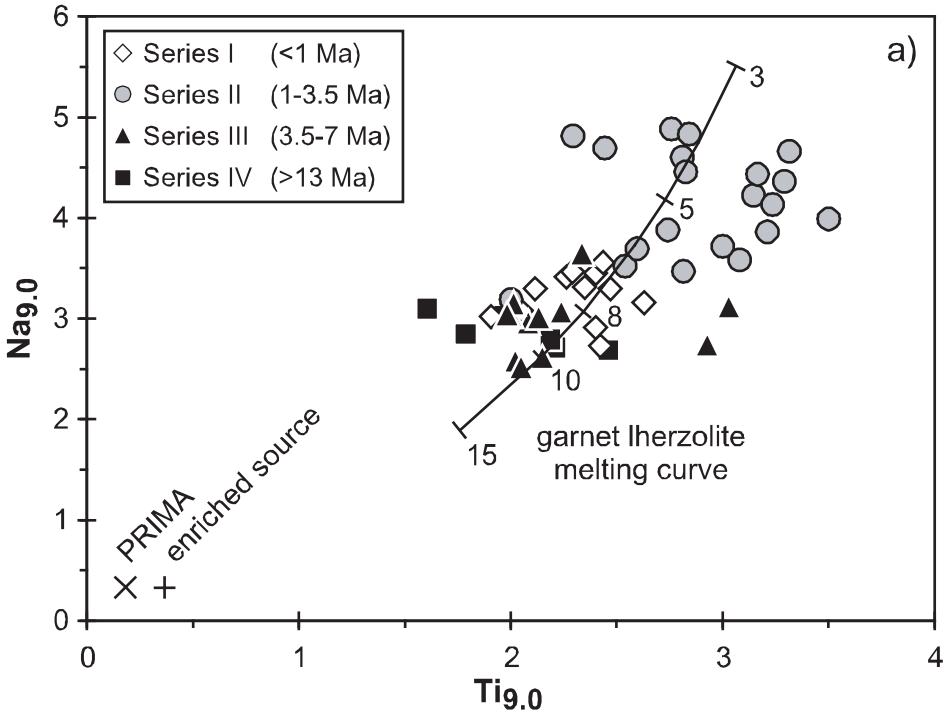

Fig. 2.10. (a) Fractionation compensated Ti and Na concentrations of the Syrian lavas. Shown also is the melting curve for non-modal batch melting of a garnet lherzolite, whereby the numbers give the degree of melting (F). Garnet lherzolite composition: 0.598 olivine, 0.076 clinopyroxene, 0.211 orthopyroxene, 0.115 garnet. Assumed mantle source concentrations: Ti 0.37 wt.%, Na 0.33 wt.%. Distribution coefficients used are from, Onuma et al. (1968), Hart and Dunn (1993), Leeman and Scheidegger (1977) and Suzuki et al. (2000). PRIMA and chondrite values are from McDonough and Sun (1995). (b) Plot of $Si_{9.0}$ vs $Na_{9.0}$. Grey fields with numbers correspond to the amount of melting (F) calculated on the basis of Na concentrations using experimental data from peridotite KLB-1 conducted by Hirose and Kushiro (1993). A regression through the data from their experimental study gives the relationship: F [%] = -0.1568*ln(Na_2O) + 0.2818 with a correlation factor R^2 = 0.9180. This algorithm was used to calculate the extent of melting of the HAS lavas. (c) $Si_{9.0}$ versus chondrite-normalised Tb/Yb ratios for the HAS lava series.

Table 4. Hypothetical compositions of primary liquids

		Series I	Series II	Series III	Series IV
Sample		**I (SY-197)**	**II (SY-190)**	**III (SY-218)**	**IV (SY-175)**
SiO_2	[wt.%]	45.25	42.13	46.01	44.87
TiO_2	[wt.%]	2.42	2.89	1.78	1.80
Al_2O_3	[wt.%]	12.61	11.97	12.95	11.51
FeO^T	[wt.%]	11.88	12.55	11.22	12.59
MnO	[wt.%]	0.18	0.18	0.17	0.16
MgO	[wt.%]	14.59	15.39	13.75	15.45
CaO	[wt.%]	8.10	7.22	8.25	7.08
Na_2O	[wt.%]	2.94	3.30	2.65	2.30
K_2O	[wt.%]	0.90	1.45	0.89	0.94
P_2O_5	[wt.%]	0.37	0.50	0.26	0.41
Mg-no.		0.72	0.72	0.72	0.72

Table 5. Calculated pressures and depths for fractionation-corrected HAS lava series and parental compositions during partial melting.

	P_{range} [kbar]	$P_{parental}$ [kbar]	$Depth_{range}$ [km]	$Depth_{parental}$ [km]
Series I	35 - 25	34	111 - 80	107
Series II	48 - 30	48	150 - 95	149
Series III	46 - 26	31	145 - 83	97
Series IV	31 - 20	36	101 - 66	112

displayed in Figures 2.10c and 2.12 therefore suggest that partial melting occurs in depths where garnet is present. This is consistent with our depth estimates placing the melting process within the garnet lherzolite stability field (Table 5, Fig. 2.11). The calculations assume a mantle source enriched relative to a primitive mantle (PRIMA) composition (McDonough and Sun ,1995). The range of REE ratios described by the uncontaminated HAS lavas indicates that the most primitive lavas of series II were formed by about 3-5% melting of a garnet lherzolite, whereas most of the primitive lavas of series I and III were generated by larger degrees of partial melting of about 8-10% (Fig. 2.12). Differences within the HAS series may be either due to variable amounts of garnet in the source or to different degrees of partial melting or both. If the source region contains variable amounts of garnet, the mantle source of series I and III lavas must contain less garnet than the source of series II magmas (Fig. 2.12). However, results of the two approaches used in this study (based on Na contents and REE calculations) are similar within the errors of

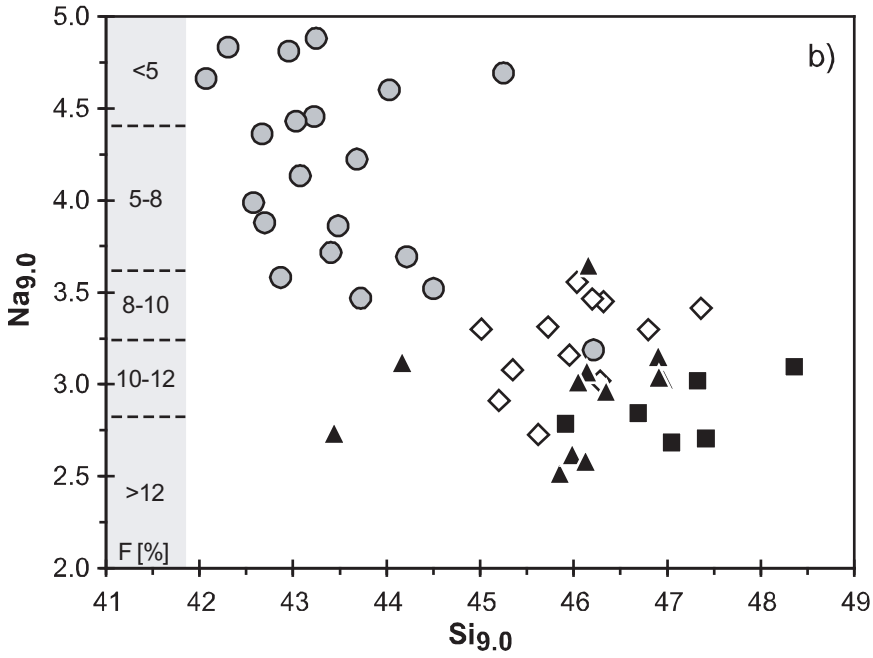

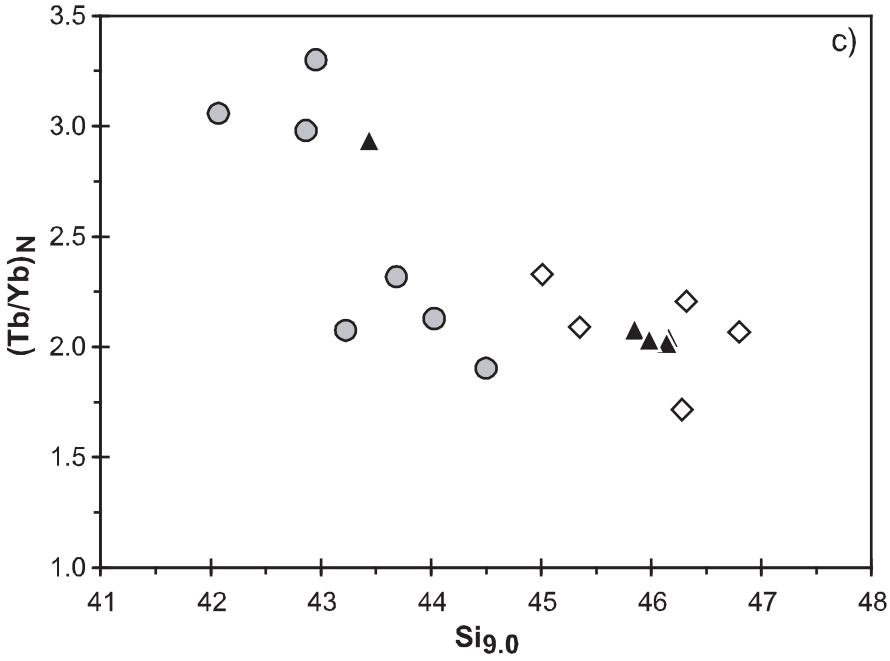

Fig. 2.10. continued

the methods. Nonetheless, differences in the degree of melting at different depths can account for variable incompatible element concentrations of primitive and fractionation-corrected samples (e.g. Ti, P; Figs. 2.3 and 2.10).

Melting experiments with natural dry lherzolites have shown that the SiO_2 contents of primary melts mainly reflect the pressure of melt formation rather than the degree of partial melting and increasing pressures lead to decreasing SiO_2 in the melt (Hirose and Kushiro, 1993). Consequently, if the mantle source of the HAS magmas is dry then the large variability in $Si_{9.0}$ may suggest different melting depths throughout the period of magmatic activity (Fig. 2.11, Table

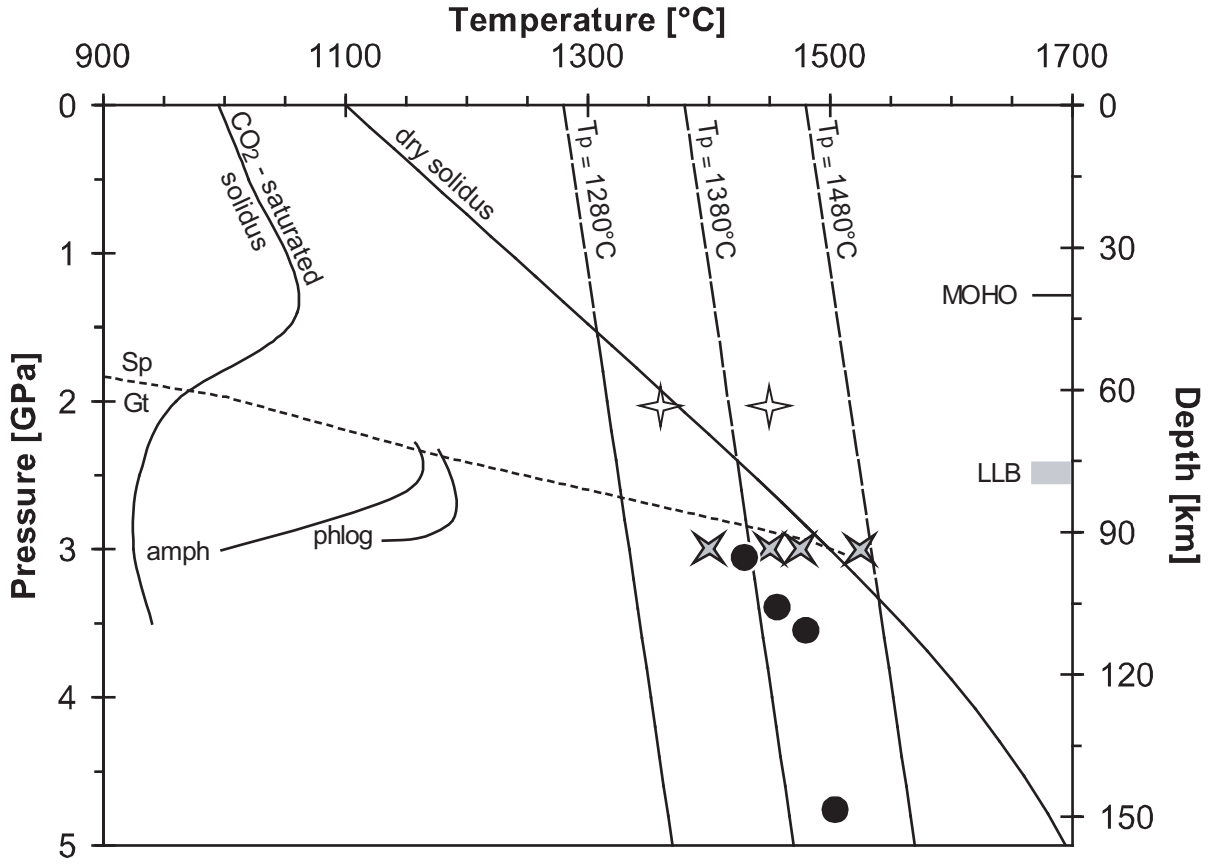

Fig. 2.11. Pressure-temperature (p-T) diagram. p-T estimates depend on primary liquid compositions (black circles) of the single HAS series. Additionally illustrated are the solidi for CO_2-saturated mantle peridotite (Falloon and Green, 1990) and dry mantle (McKenzie and Bickle, 1988) as well as an asthenospheric mantle adiabat (McKenzie and Bickle, 1988) and different potential mantle temperatures. Open stars are melting experiments of peridotite + CO_2 from Mysen and Kushiro (1977) and filled stars from Hirose (1997). The spinel to garnet transition is shown as dotted line and amphibole (amph), and phlogopite (phlog) stability boundaries as continuous curved lines based on experimental data (Mengel and Green, 1989; Wallace and Green, 1991; Robinson and Wood, 1998). Temperature estimates are based on the empirical relation: T [°C] =2000*(MgO/SiO_2*MgO) + 969 (Albarède, 1992) and pressure calculations based on melting experiments using the equation P [GPa] = 23.217-0.4381*SiO_2 with a correlation factor R = 0.878 as cited in Haase (1996). Pressure-depth conversion is made by the relationship: Depth [km] = 3.02*P [kbar] + 5. Crustal thickness is based on geophysical data of Best et al. (1990) and McBride et al. (1990) and the lower lithosphere boundary (LLB, grey field) is adopted from McGuire and Bohannon (1989).

4) and the correlation between Na and Si could imply a link between the degree and depth of melting. In this case, the relatively low degree series II magmas were generated at high pressures whereas the rest of the investigated lavas probably are the result of larger melting proportions at shallower depth (Fig. 2.11). Applying the algorithm developed by Haase (1996) to calculate the average pressures of melting of the HAS magmas that series I, III, and IV are derived from similar depths of about 110-100 km (Fig. 2.11) while the low SiO_2 contents of the series II lavas implies a deeper region (~150 km) of melting (Table 5). On the basis of a dry peridotite solidus McKenzie and Bickle (1988) and White and McKenzie (1989) pointed out that decompressional melting of the asthenosphere with a potential temperature of 1280°C requires a stretching factor (i.e. the ratio of initial to thinned lithospheric thicknesses) of the lithosphere in the range of 2 to 5. Assuming an initial lithospheric thickness of about 100-120 km underneath northwestern Arabia (Mooney et al., 1985; Shaw et al., 2003) and a thinned lithospheric thick-

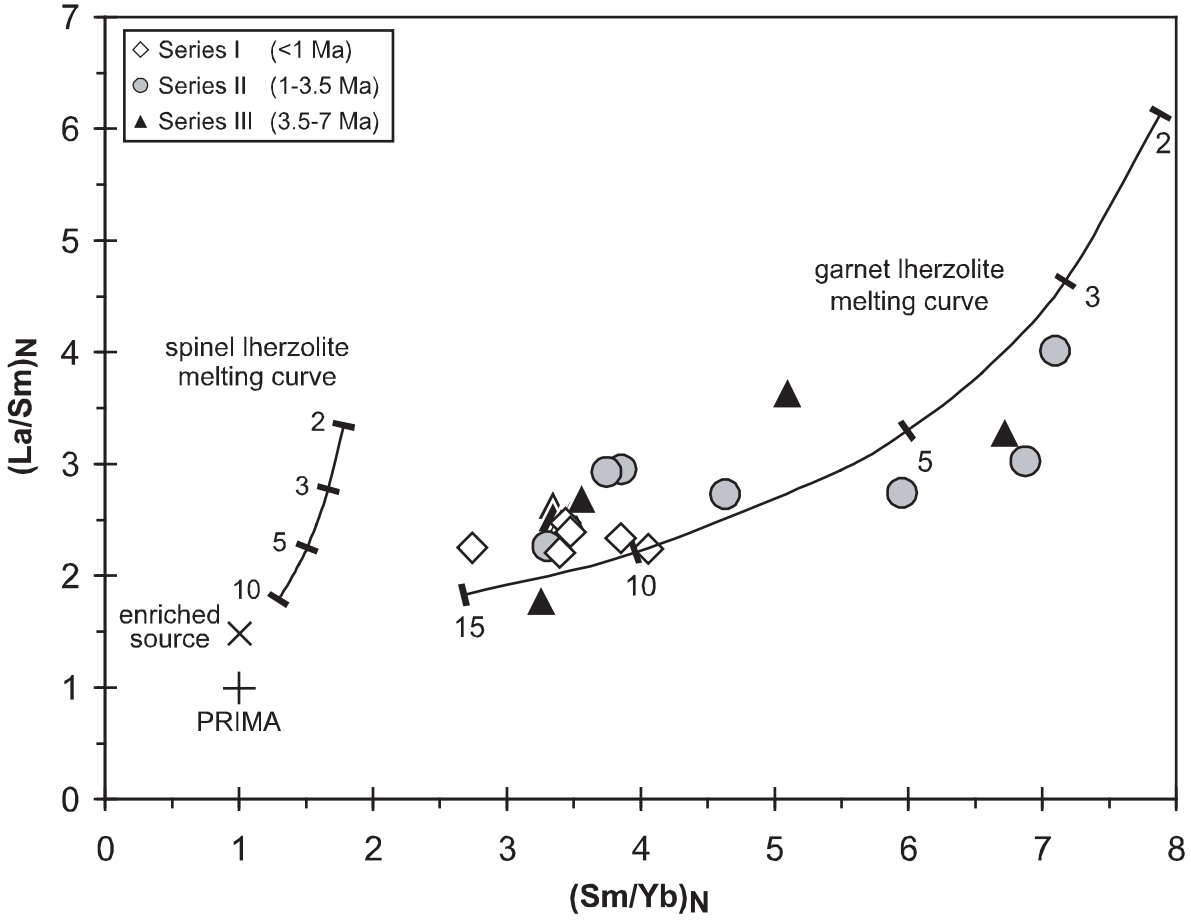

Fig. 2.12. Diagram of chondrite-normalised La/Sm and Sm/Yb ratios for uncontaminated HAS lavas. Additionally shown are melting curves for non-modal batch melting of garnet and spinel lherzolites. Garnet lherzolite composition: 0.598 olivine, 0.076 clinopyroxene, 0.211 orthopyroxene, 0.115 garnet. Melting proportions of garnet lherzolite: 0.05 olivine, 0.3 clinopyroxene, 0.2 orthopyroxene, 0.45 garnet. Spinel lherzolite composition: 0.578 olivine, 0.119 clinopyroxene, 0.27 orthopyroxene, 0.033 spinel. Melting proportions of spinel lherzolite: 0.10 olivine, 0.50 clinopyroxene, 0.27 orthopyroxene, 0.13 spinel. Assumed mantle source concentrations: La 0.95ppm, Sm 0.41ppm and Yb 0.44ppm. Distribution coefficients used are from Kelemen et al. (1993) and Johnson (1998). Numbers give the degree of melting (F). PRIMA and chondrite values are from McDonough and Sun (1995).

ness of <80 km beneath Syria (Nasir and Safarjalani, 2000), which is similar to the thickness proposed by McGuire and Bohannon (1989) for Saudi Arabia (~75-80 km), a stretching factor of about 1.3 to 1.6 can be calculated. This calculated stretching factor is too low to explain the voluminous magma formation in southern Syria suggesting that the mantle must be hotter beneath the HAS to allow significant partial melting at great depth. We conclude that the series IV, III and I magmas most likely formed in a relatively dry mantle with significant excess temperature, i.e. a mantle plume. Following the empirical algorithm cited by Albarède (1992) formation temperatures of the hypothetical parental magmas are calculated to be 1457°C, 1504°C, 1429°C, and 1484°C (Fig. 2.11). These temperatures are approximately 130-200°C higher than average potential mantle temperature of 1300°C (McKenzie and Bickle, 1988) and fall into the range of excess temperatures thought to be characteristic for the presence of mantle plumes (e.g. White and McKenzie, 1989).

However, magmas with SiO_2 <45 wt.% may form in the presence of CO_2 (e.g. Eggler, 1978; Wyllie, 1978) requiring relatively high CO_2 contents in the mantle source of the series II magmas. For example, Hirose (1997) concluded on the basis of diamond aggregate melting experiments that nephelinitic to basanitic magmas form at 3 GPa and >1475°C in the presence of CO_2 rather than being the product of high temperature melting above 3 GPa (Fig. 2.11). Thus, the pressure estimates for the HAS series II could be lower if minor amounts of volatiles occur in the source (Fig. 2.11). Volatiles are stored in either amphibole or phlogopite in the upper mantle and thus melting may occur at lower pressures when these phases were involved in the melting process. On the other hand, those minerals, if they occur as residual phases, may leave a characteristic chemical signature in melts. High Nb/La ratios accompanied by low K/Nb ratios of uncontaminated series II lavas imply a mantle component relatively enriched in Nb compared to the rather depleted samples of series I and III (Figs. 2.5b and c). One could assume that the negative trend in Figure 2.5c is due to residual amphibole in the source region of the HAS lavas. Because amphibole has a high distribution coefficient for K, melting in the presence of residual amphibole in the mantle would retain K over Nb. Thus, the comparatively low K/Nb ratios of series II lavas suggest that amphibole might be present in the melting region. However, this argument is contrary to the depth estimates for series II lavas, which were formed deep in the mantle at temperatures, where amphibole is not stable (Fig. 2.11). In this context Le Roex et al. (2001) and Class and Goldstein (1997) note that amphibole is neither a stable phase under asthenospheric mantle nor under mantle plume conditions. Also the isotopic variability of the HAS series cannot be explained by variable amounts of amphibole in the source (Figs. 2.6 and 2.7). Instead, the negative correlation between Nb contents and K/Nb ratios (Fig. 2.5c) can be explained by the mixing of two, variably highly incompatible element enriched and isotopicaly distinct mantle sources that were melted at variable degrees (Fig. 2.12).

The discrepancy of projected surface heat flow measurements conducted by Gettings et al. (1981) and Gettings et al. (1986) and temperatures calculated based on xenolith data from Saudi

Arabia (McGuire and Bohannon, 1989) has been interpreted as evidence for hot upwelling asthenosphere beneath western Arabia (McGuire and Bohannon, 1989). Snyder et al. (1993) come to similar conclusions in their interpretion of HAS mantle xenoliths. Nasir (1992) and Nasir and Safarjalani (2000) note that the elevated geotherms below the Cenozoic basalt fields are a widespread phenomenon on the Arabian peninsula. Hot upwelling material beneath the lithosphere would result in regional doming as suggested in the active rift hypothesis of Sengör and Burke (1978). The Rutbah uplifted region beneath the HAS volcanic field is elevated by approximately 2000 m and supports hot upwelling material underneath the lithosphere. Paleogene sediments are unconformably overlain by the HAS lavas suggesting that the process of mantle upwelling is probably young, starting in Miocene times, similar to or sometime before the onset of volcanic activity. Moreover, seismic tomography studies show a region with diminished shear-wave velocities due to a roughly horizontal layer of hot material at upper mantle depths of 100 km beneath northwestern Arabia (Daradich et al., 2003; Debayle et al., 2001). We conclude that the youngest lavas of series I as well as the lavas older than 3.5 Ma from series III and IV are derived by relative large degrees of melting from deep mantle plume material with a significant excess temperature. In contrast, the series II lavas with ages between 3.5 and 1 Ma probably formed by relative low degrees melting from a volatile- and incompatible element-enriched asthenospheric or lithospheric mantle source.

2.6.6 Mantle sources of the Syrian HAS magmas

Although the HAS lavas show a large range of isotopic compositions and highly ratios of incompatible elements it is possible to define three distinct mantle end members and one crustal contaminant (Figs. 2.5 to 2.7). The crustal contaminant was discussed above and has high Sr and Pb isotope ratios together with low Ce/Pb and probably represents Proterozoic upper crustal rocks. One mantle end member is represented by series II lavas and has a high $^{143}Nd/^{144}Nd$ of 0.5130, $^{87}Sr/^{86}Sr$ of 0.7031 and relatively unradiogenic Pb isotope ratios (Figs. 2.6 and 7). The second mantle end member has low $^{143}Nd/^{144}Nd$ at relatively low Sr isotope ratios similar to series I lavas. However, this end member has very variable Pb isotope ratios ranging from $^{206}Pb/^{204}Pb$ of about 19.1 to the lowest $^{206}Pb/^{204}Pb$ observed in the lavas and thus this mantle end member could also could reflect a mixture of different mantle sources. Nonetheless, in terms of their Sr and Nd isotopic compositions crustaly uncontaminated series III lavas could represent a mixture between the two mantle end member compositions, but they have slightly higher $^{87}Sr/^{86}Sr$ and Ba/Nb than the series I lavas (Fig. 2.8a). Consequently, either all series III samples are crustally contaminated or they formed from a third mantle source. The similar Sr, Nd, and Pb isotopic compositions of the HAS series II and the Red Sea lavas suggest that the series II lavas formed from an asthenospheric source (Figs. 2.6 and 2.7). However, the mantle source of series II lavas is much more enriched in incompatible elements and has slightly higher Sr isotope ratios implying a higher Rb/Sr compared to the Red Sea mantle source. Because the Nd and Pb isotopic ratios of the HAS series II lavas are similar to Red Sea basalts this enrichment must have occurred recently probably shortly before or during the eruption of series III lavas. In

agreement with the melting model described above we suggest that the source of the series II lavas resides largely in the asthenosphere but may have been enriched either by mixing with plume material or by metasomatic processes at the base of the thermal boundary layer.

The Afro-Arabian dome may have formed by northward flow of material from the Afar plume which is supported by the low shear wave velocities beneath western and northern Arabia (Debayle et al., 2001). It has been proposed that composition of the Afar mantle plume is reflected in Ethiopian lavas with high $^{3}He/^{4}He$ ratios (Marty et al., 1996). Even though the HAS lavas have enriched trace element compositions an influence of Afar plume material from the lower undegassed mantle can be eliminated because of the higher $^{87}Sr/^{86}Sr$ for a given $^{143}Nd/^{144}Nd$ and $^{206}Pb/^{204}Pb$ of this Afar plume material (Figs. 2.6 and 2.7). Furthermore, the Ethiopian lavas have lower $^{206}Pb/^{204}Pb$ but a similar range of $^{208}Pb/^{204}Pb$ compared to the HAS lavas, additionally supporting the fact that the Afar plume source with high $^{3}He/^{4}He$ does not play a role in Syrian HAS volcanism, in agreement with the conclusions of Shaw et al. (2003). However, a component with radiogenic Pb isotopic compositions occurs in lavas from Afar, southwestern Arabia and, most importantly, from the Gulf of Aden, i.e. from oceanic crust (e.g. Schilling et al., 1992; Baker et al., 1996; Stewart and Rogers, 1996). The presence of this component beneath the HAS can explain the generation of the series I and III magmas and it has been suggested to reside either in the Afar plume or in the Arabian subcontinental lithosphere (Vidal et al., 1991; Deniel et al., 1994; Bertrand et al., 2003). However, we propose that this component must have relatively high excess temperatures to explain the increased degree of melting at great pressure of the series III and I magmas and thus represents material from a deep mantle plume. Furthermore, the fact that this component occurs in oceanic lithosphere also rules out a continental lithospheric origin. Finally, the presence of relatively hot mantle material beneath large parts of Arabia is known from the seismic tomography (Daradich et al., 2003) and it appears likely that this abundant material is represented by the component with high Pb isotope ratios.

2.6.7 Temporal variations in the melting regime

The variable rare earth element ratios and the fractionation corrected major element contents in relation with the different ages of the HAS series indicate that the melting processes varied considerably with time underneath the HAS region (Figs. 2.10 and 2.12). These variations could be caused by variations in lithospheric thickness or by variations of the temperature or composition of the mantle source. Initially, relatively large degrees of melting produced the series IV and III magmas, then melting decreased between 3.5 to 1 Ma ago and then increased again producing the series I magmas. Continued lithospheric thinning can be ruled out as cause for the observed variations because this should lead to increasingly shallower melt generation in the mantle as it is observed in the Basin and Range province (DePaolo and Daley, 2000). The variable degrees of melting observed in the HAS lavas could be due to a pulsing mantle plume that is rising further in the south. Lateral plume flux is well known in the ocean basins and the occurrence of V-

shaped ridges along the Reykjanes spreading axis south of Iceland has been interpreted to reflect the pulsing of the Iceland plume influence (White et al., 1995). Consequently, the inflowing plume material beneath the HAS may have been pulsing during the last 13 Ma with a decreasing influx between 3.5 and 1 Ma when apparently mainly asthenospheric material was molten at lower degrees of partial melting. A first period of volcanic activity occurred during the eruption of the series IV lavas between 25 and 19 Ma and this may also point to long-term pulsing with a major break in plume influx between 19 and 13 Ma, when no volcanic activity occurred in the HAS.

A variation in magma genesis is also observed on a shorter time period in a stratigraphic section of lava flows sampled along the Wadi Ash-Sham (Fig. 2.1). These lava flows represent a temporal sequence where the heights of the lavas correlate with age. Two Ar-Ar ages of the lowermost and uppermost section yield ages of 4.2 Ma and 3.3 Ma, respectively (Krienitz et al., Chapter III)

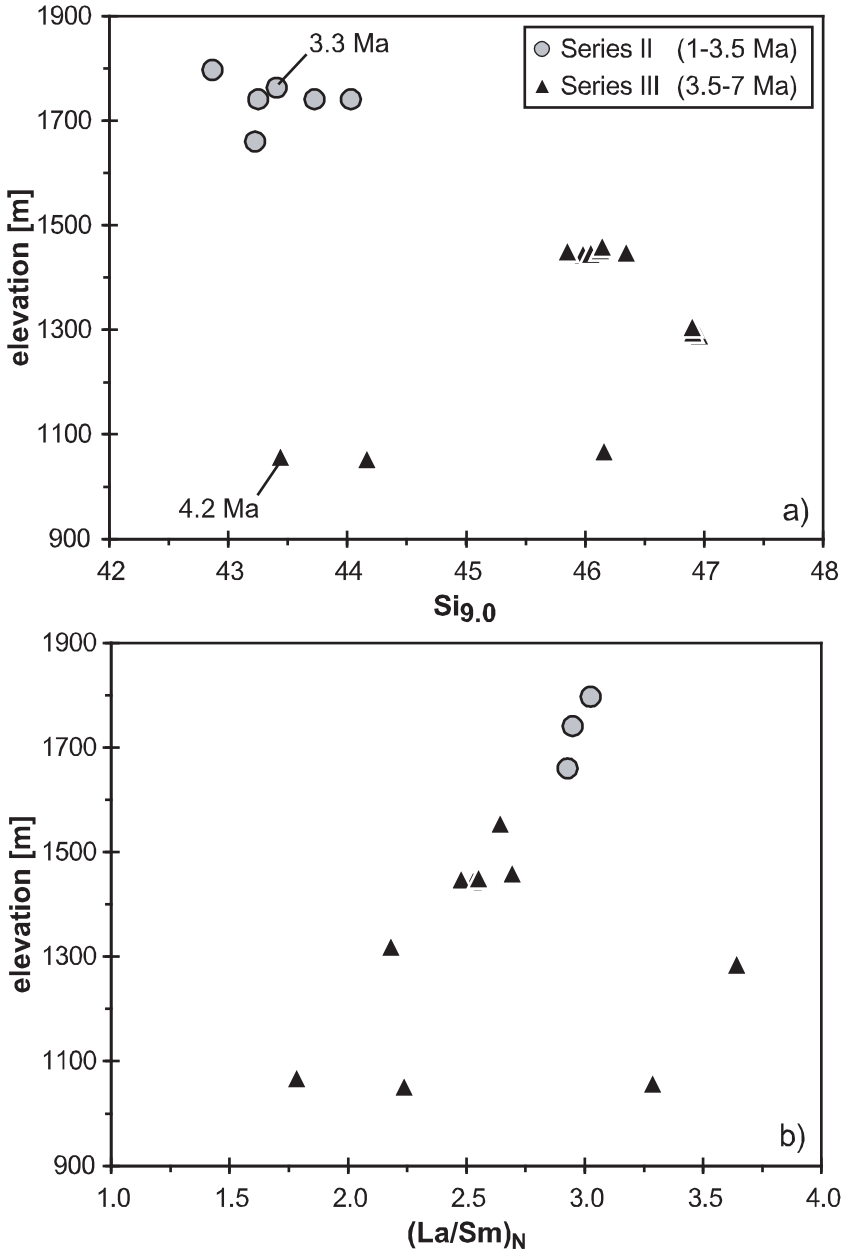

Fig. 2.13. Diagrams of lavas of known stratigraphic correlation sampled in the region of Wadi Ash-Sham (Figure 2.1). Elevation of lavas is plotted versus (a) $Si_{9.0}$ and (b) chondrite-normalised La/Sm ratios. Ar-Ar ages of the samples are from Krienitz et al. (Chapter III).

suggesting that about 800 m of lavas erupted within about 900,000 years. Except two samples that have low $Si_{9.0}$ and variable $(La/Sm)_N$ generally suggesting low degrees of partial melting, the series III lavas of the lower section show high silica contents accompanied by relatively low $(La/Sm)_N$ thus reflecting high degrees of partial melting (Fig. 2.13). Because most of the lavas show no evidence for crustal contamination the increasing $(La/Sm)_N$ and decreasing $Si_{9.0}$ towards the top of the sequence indicate a decreasing degree of partial melting from series III to series II. This rapidly changing degree of melting cannot be due to lithospheric dynamics, but must be due to the variable influx of mantle with different temperatures and compositions as indicated by the distinct isotope compositions of the two series. No extensional tectonic features (e.g. the formation of graben structures) can be related to the volcanism in this time interval and tectonic movements are limited to the Dead Sea fault system (e.g. Heimann and Ron, 1993; Brew et al., 2001b) supporting our model of magma genesis by mantle plume activity. This assumption is further supported by the interpretation of seismic data suggesting a layer of hot material at a depth of about 100 km (Debayle et al., 2001) and by elevated geotherms underneath southern Syria as indicated by xenolith data (Nasir, 1992) and heat flow measurements (McGuire and Bohannon, 1989).

2.7 Conclusions

1. The investigated lava set of the Harrat Ash Shamah volcanic field in southern Syria comprises alkali basalts, basanites, tehprites, hawaiites, mugearites, and rare trachytes and phonolites.
2. The major and compatible trace element geochemistry indicates that the lavas have undergone fractional crystallisation of olivine, clinopyroxene, plagioclase and Fe-Ti oxides. The highly differentiated lavas show evidence for the fractionation of alka lifeldspar and apatite.
3. Low Ce/Pb and Nb/U ratios as well as high $^{87}Sr/^{86}Sr$ ratios in some lavas indicate the assimilation of continental crustal material.
4. The variable range of fractionation-corrected compositions and REE ratios of crustaly uncontaminated primitive Syrian lavas are the result of different degrees of partial melt ing of garnet peridotites at variable depths, i.e. ~8-10% melting at depths of about 100-110 km for series I, III, and IV lavas and 3-5% melting at 150 km for series II lavas.
5. Isotopic and incompatible trace element ratios imply that lavas of series I, III, and IV are derived from a mantle plume source yielding significant excess temperatures, whereas series II lavas, which were erupted between 3.5 and 1 Ma, probably were generated in a volatile- and incompatible element-enriched lithospheric or asthenos pheric mantle.
6. The discontinuous volcanism found throughout the HAS volcanic field, the temporal variations in the melting regime and in the compositions of the lavas are consistent with a model of a pulsing mantle plume underneath southern Syria.

Acknowledgements

This study was funded by the Deutsche Forschungsgemeinschaft (grant HA 2568/5) and is part of M.-S.K.´s dissertation. The “field team” is deeply indebted to the University of Aleppo for the support in Syria. H. Blaschek, D. Garbe-Schönberg, and K. Kißling be thanked for help with the ICP-MS analyses. P. Appel, H. Baier, B. Mader, P. Rengers and A. Weinkauf are acknowledged for their help during analytical work. M.-S.K. would like to thank N. A. Stroncik for helpful comments on the paper.

References

Albarede, F., 1992. How deep do common basaltic magmas form and differentiate? Journal of Geophysical Research, 97: 10,997-11,009.

Almond, D.C., 1986. Geological evolution of the Afro-Arabian Dome. Tectonophysics, 131: 301-332.

Baker, J.A., Menzies, M.A., Thirlwall, M.F. and Macpherson, C.G., 1997. Petrogenesis of Quaternary intraplate volcanism, Sana’a, Yemen; implications for plume-lithosphere interaction and polybaric melt hybridization. Journal of Petrology, 38: 1359-1390.

Baker, J.A., Thirlwall, M.F. and Menzies, M.A., 1996. Sr-Nd-Pb isotopic and trace element evidence for crustal contamination of plume-derived flood basalts; Oligocene flood volcanism in western Yemen. Geochimica et Cosmochimica Acta, 60: 2559-2581.

Baker, J.A. et al., 2000. Resolving crustal and mantle contributions to continental flood volcanism, Yemen; constraints from mineral oxygen isotope data. Journal of Petrology, 41: 1805-1820.

Bertrand, H., Chazot, G., Blichert-Toft, J. and Thoral, S., 2003. Implications of widespread high-μ volcanism on the Arabian Plate for Afar mantle plume and lithosphere composition. Chemical Geology, 198: 47-61.

Best, J.A., Barazangi, M., Al, S.D., Sawaf, T. and Gebran, A., 1990. Bouguer gravity trends and crustal structure of the Palmyride mountain belt and surrounding northern Arabian Platform in Syria. Geology, 18: 1235-1239.

Blusztajn, J., Hart, S.R., Shimizu, N. and McGuire, A.V., 1995. Trace-element and isotopic characteristics of spinel peridotite xenoliths from Saudi Arabia. Chemical Geology, 123: 53-65.

Bohannon, R.G., Naeser, C.W., Schmidt, D.L. and Zimmermann, R.A., 1989. The timing of uplift, volcanism, and rifting peripheral to the Red Sea; a case for passive rifting? Journal of Geophysical Research, 94: 1683-1701.

Brew, G., Barazangi, M., Al-Maleh, A.K. and Sawaf, T., 2001a. Tectonic and Geologic Evolution of Syria. GeoArabia, 6: 573-616.

Brew, G. et al., 1997. Basement depth and sedimentary velocity structure in the northern Arabian platform, eastern Syria. Geophysical Journal International, 128: 617-631.

Brew, G. et al., 2001b. Structure and tectonic development of the Ghab basin and the Dead Sea fault system, Syria. Journal of the Geological Society of London, 158: 665-674.

Camp, V.E. and Roobol, M.J., 1989. The Arabian continental alkali basalt province; Part I, Evolution of Harrat Rahat, Kingdom of Saudi Arabia. Geological Society of America Bulletin, 101: 71-95.

Camp, V.E. and Roobol, M.J., 1992. Upwelling asthenosphere beneath western Arabia and its regional implications. Journal of Geophysical Research, 97: 15,255-15,271.

Campbell, I.H. and Griffiths, R.W., 1990. Implications of mantle plume structure for the evolution of flood basalts. Earth and Planetary Science Letters, 99: 79-93.

Class, C. and Goldstein, S.L., 1997. Plume-lithosphere interactions in the ocean basins; constraints from the source mineralogy. Earth and Planetary Science Letters, 150: 245-260.

Coleman, R.G., Gregory, R.T. and Brown, G.F., 1983. Cenozoic volcanic rocks of Saudi Arabia. Open File Report - U. S. Geological Survey, p. 86

Daradich, A., Mitrovica, J.X., Pysklywec, R.N., Willett, S.D. and Forte, A., M, 2003. Mantle flow, dynamic topography, and rift-flank uplift of Arabia. Geology, 31: 901-904.

Debayle, E., Leveque, J.J. and Cara, M., 2001. Seismic evidence for a deeply rooted low-velocity anomaly in the upper mantle beneath the northeastern Afro/Arabian continent. Earth and Planetary Science Letters, 193: 423-436.

Deniel, C., Vidal, P., Coulon, C., Vellutini, P.-J. and Piguet, P., 1994. Temporal evolution of mantle sources during continental rifting: The volcanism of Djibouti (Afar). Journal of Geophysical Research, 99: 2853-2869.

DePaolo, D.J. and Daley, E.E., 2000. Neodymium isotopes in basalts of the southwest basin and range and lithospheric thinning during continental extension. Chemical Geology, 169: 157-185.

Eggler, D.H., 1978. The effect of CO_2 upon partial melting of peridotite in the system Na_2O-CaO-Al_2O_3-MgO-SiO_2-CO_2 to 35 kb, with an analysis of melting in a peridotite-H_2O-CO_2 system. American Journal of Science, 278: 305-343.

Eissen, J.P. et al., 1989. Petrology and geochemistry of basalts from the Red Sea axial rift at 18 degrees North. Journal of Petrology, 30: 791-839.

El-Isa, Z.H., Mechie, J., Prodehl, C., Makris, J. and Rihm, R., 1987. A crustal structure study of Jordan derived from seismic refraction data. Tectonophysics, 138: 235-253.

Falloon, T.J. and Green, D.H., 1990. Solidus of carbonated fertile peridotite under fluid-saturated conditions. Geology, 18: 195-199.

Frey, F.A., Green, D.H. and Roy, S.D., 1978. Integrated models of basalt petrogenesis; a study of quartz tholeiites to olivine melilitites from South eastern Australia utilizing geochemical and experimental petrological data. Journal of Petrology, 19: 463-513.

Garbe-Schönberg, C.-D., 1993. Simultaneous determination of thirty-seven trace elements in twenty-eight international rock standards by ICP-MS. Geostandards Newsletter, 17: 81-97.

Gettings, M.E., 1981. A heat flow profile across the Arabian Shield and Red Sea. Eos, Transactions, 62: 407.

Gettings, M.E., Blank, H.R., Jr., Mooney, W.D. and Healy, J.H., 1986. Crustal structure of southwestern Saudi Arabia. Journal of Geophysical Research, 91: 6491-6512.

Giannerini, G., Campredon, R., Feraud, G. and Abou, Z.B., 1988. Deformations intraplaques et volcanisme associe; exemple de la bordure NW de la plaque Arabique au Cenozoique Bulletin de la Societe Geologique de France, Huitieme Serie, 4: 937-947.

Guba, I. and Mustafa, H., 1988. Structural control of Young basaltic fissure eruptions in the plateau basalt area of the Arabian Plate, northeastern Jordan. Journal of Volcanology and Geothermal Research, 35: 319-334.

Haase, K.M., 1996. The relationship between the age of the lithosphere and the composition of oceanic magmas; constraints on partial melting, mantle sources and the thermal structure of the plates. Earth and Planetary Science Letters, 144: 75-92.

Haase, K.M., Muehe, R. and Stoffers, P., 2000. Magmatism during extension of the lithosphere; geochemical constraints from lavas of the Shaban Deep, northern Red Sea. Chemical Geology, 166: 225-239.

Hart, S.R. and Dunn, T., 1993. Experimental cpx/melt partitioning of 24 trace elements. Contributions to Mineralogy and Petrology, 113: 1-8.

Hegner, E. and Pallister, J.S., 1989. Pb, Sr, and Nd isotopic characteristics of Tertiary Red Sea Rift volcanics from the central Saudi Arabian coastal plain. Journal of Geophysical Research, 94: 7749-7755.

Heimann, A. and Ron, H., 1993. Geometric changes of plate boundaries along part of the northern Dead Sea Transform; geochronologic and paleomagnetic evidence. Tectonics, 12: 477-491.

Henjes-Kunst, F., Altherr, R. and Baumann, A., 1990. Evolution and composition of the lithospheric mantle underneath the western Arabian Peninsula; constraints from Sr-Nd isotope systematics of mantle xenoliths. Contributions to Mineralogy and Petrology, 105: 460-472.

Hirose, K., 1997. Partial melt compositions of carbonated peridotite at 3 GPa and role of CO2 in alkali-basalt magma generation. Geophysical Research Letters, 24: 2837-2840.

Hirose, K. and Kushiro, I., 1993. Partial melting of dry peridotites at high pressures; determination of compositions of melts segregated from peridotite using aggregates of diamond. Earth and Planetary Science Letters, 114: 477-489.

Hofmann, A.W., Jochum, K.P., Seufert, M. and White, W.M., 1986. Nb and Pb in oceanic basalts; new constraints on mantle evolution. Earth and Planetary Science Letters, 79:

33-45.
Ilani, S. et al., 2001. New K-Ar ages of basalts from the Harrat Ash Shaam volcanic field in Jordan: Implications for the span and duration of the upper-mantle upwelling beneath the western Arabian plate. Geology, 29: 171-174.
Johnson, K.T.M., 1998. Experimental determination of partition coefficients for rare earth and high-field-strength elements between clinopyroxene, garnet, and basaltic melt at high pressure. Contributions to Mineralogy and Petrology, 133: 60-68.
Keen, C.E., 1985. The dynamics of rifting; deformation of the lithosphere by active and passive driving forces. Geophysical Journal of the Royal Astronomical Society, 80: 95-120.
Kelemen, P.B., Shimizu, N. and Dunn, T., 1993. Relative depletion of niobium in some arc magmas and the continental crust; partitioning of K, Nb, La and Ce during melt/ rock reaction in the upper mantle. Earth and Planetary Science Letters, 120: 111-133.
Klein, E.M. and Langmuir, C.H., 1987. Global correlations of ocean ridge basalt chemistry with axial depth and crustal thickness. Journal of Geophysical Research, 92: 8089-8115.
Le Bas, M.J., Le Maitre, R.W., Streckeisen, A. and Zanettin, B.A., 1986. Chemical classification of volcanic rocks based on the total alkali-silica diagram. Journal of Petrology, 27: 745-750.
Le Maitre, R.W. et al., 1989. A classification of igneous rocks and glossary of terms. Blackwell Sci. Publ., Oxford, United Kingdom, 193 pp.
Le Roex, A.P., Spath, A. and Zartmann, R.E., 2001. Lithospheric thickness beneath the southern Kenya Rift: implications from basalt geochemistry. Contributions to Mineralogy and Petrology, 142: 89-106.
Leeman, W.P. and Scheidegger, K.F., 1977. Olivine/ liquid distribution coefficients and a test for crystal-liquid equilibrium. Earth and Planetary Science Letters, 35: 247-257.
MacDonald, G.A., 1968. Composition and origin of Hawaiian lavas. Geological Society of America – Memoir, 116: 477-522.
Marty, B., Pik, R. and Gezahegn, Y., 1996. Helium isotopic variations in Ethiopian plume lavas; nature of magmatic sources and limit on lower mantle contribution. Earth and Planetary Science Letters, 144: 223-237.
McBride, J.H. et al., 1990. Seismic reflection structure of intracratonic Palmyride fold-thrust belt and surrounding Arabian Platform, Syria. AAPG Bulletin, 74: 238-259.
McDonough, W.F. and Sun, S.S., 1995. The composition of the Earth. Chemical Geology, 120: 223-253.
McGuire, A.V. and Bohannon, R.G., 1989. Timing of mantle upwelling; evidence for a passive origin for the Red Sea Rift. Journal of Geophysical Research, 94: 1677-1682.
McKenzie, D. and Bickle, M.J., 1988. The volume and composition of melt generated by extension of the lithosphere. Journal of Petrology, 29: 625-679.
Mengel, K. and Green, D.H., 1989. Stability of amphibole and phlogopite in metasomatized peridotite under water-saturated and water-undersaturated conditions. IV International Kimberlite Conference; 571-581.
Mooney, W.D., Gettings, M.E., Blank, H.R. and Healy, J.H., 1985. Saudi Arabian seismic-refraction profile: a traveltime interpretation of crustal and upper mantle structure. Tectonophysics, 111: 173-246.
Mouty, M., Delaloye, M., Fontignie, D., Piskin, O. and Wagner, J.J., 1992. The volcanic activity in Syria and Lebanon between Jurassic and Actual. Schweizerische Mineralogische und Petrographische Mitteilungen = Bulletin Suisse de Mineralogie et Petrographie, 72: 91-105.
Mysen, B.O. and Kushiro, I., 1977. Compositional variations of coexisting phases with degree of melting of peridotite in the upper mantle. American Mineralogist, 62: 843-865.
Nasir, S., 1992. The lithosphere beneath the northwestern part of the Arabian Plate (Jordan); evidence from xenoliths and geophysics. Tectonophysics, 201: 357-370.
Nasir, S., 1994. Geochemistry and petrogenesis of Cenozoic volcanic rocks from the northwestern part of the Arabian continental alkali basalt province, Jordan. Africa Geoscience Review, 1: 455-467.
Nasir, S. and Safarjalani, A., 2000. Lithospheric petrology beneath the northern part of the Arabian Plate in Syria: evidence from xenoliths in alkali basalts. Journal of African Earth Sciences, 30: 149-168.
Onuma, N., Higuchi, H., Wakita, H. and Nagasawa, H., 1968. Trace element partition between two pyroxenes and the host lava. Earth and Planetary Science Letters, 5: 47-51.

Pallister, J.S., 1987. Magmatic history of Red Sea rifting; perspective from the central Saudi Arabian coastal plain. Geological Society of America Bulletin, 98: 400-417.
Pik, R., Deniel, C., Coulon, C., Yirgu, G. and Marty, B., 1999. Isotopic and trace element signatures of Ethiopian flood basalts; evidence for plume-lithosphere interactions. Geochimica et Cosmochimica Acta, 63: 2263-2279.
Ponikarov, V.P., 1969. Syria (in Russian). Nedra Press, Moscow, 216 pp.
Ponikarov, V.P., Protasevich, L., Maximov, A. and Tkachev, G., 1963. Geological map of Syria 1:200 000. V.O. Technoexport, Russian Federation, Moscow.
Robinson, J.A.C. and Wood, B.J., 1998. The depth of the spinel to garnet transition at the peridotite solidus. Earth and Planetary Science Letters, 164: 277-284.
Rudnick, R.L. and Fountain, D.M., 1995. Nature and composition of the continental crust; a lower crustal perspective. Reviews of Geophysics, 33: 267-309.
Schilling, J.G., 1973. Afar mantle plume: Rare earth evidence. Nature, 242: 2-5.
Schilling, J.G., Kingsley, R.H., Hanan, B.B. and McCully, B.L., 1992. Nd-Sr-Pb isotopic variations along the Gulf of Aden; evidence for Afar mantle plume-continental lithosphere interaction. Journal of Geophysical Research, 97: 10,927-10,966.
Searle, M.P., 1994. Structure of the intraplate eastern Palmyride fold belt, Syria. Geological Society of America Bulletin, 106: 1332-1350.
Seber, D. et al., 1993. Upper crustal velocity structure and basement morphology beneath the intracontinental Palmyride fold-thrust belt and north Arabian platform in Syria. Geophysical Journal International, 113: 752-766.
Sengor, A.M.C. and Burke, K., 1978. Relative timing of rifting and volcanism on Earth and its tectonic implications. Geophysical Research Letters, 5: 419-421.
Sharkov, Y.V. et al., 1994. Geokhronologiya pozdnekaynozoyskikh bazal'tov Zapadnoy Sirii Translated Title: Geochronology of late Cenozoic basalts in western Syria. Petrologiya, 2: 385-394.
Sharkov, Y.V., Laz, k.Y.Y., Fedosova, S.P. and Khanna, S., 1989. Glubinnyye vklyucheniya chetvertichnogo vulkana Tel'-Danun (Yuzhnaya Siriya) v svyazi s problemoy vnutriplitnogo bazal'tovogo magmatizma Translated Title: Depth-derived inclusions of the Quaternary volcano Tel-Danun, southern Syria, in relation to the problem of intraplate basaltic magmatism. Geokhimiya, 1989: 1609-1623.
Shaw, J.E., Baker, J.A., Menzies, M.A., Thirlwall, M.F. and Ibrahim, K.M., 2003. Petrogenesis of the Largest Intraplate Volcanic Field on the Arabian Plate (Jordan): a Mixed Lithosphere-Asthenosphere Source Activated by Lithospheric Extension. Journal of Petrology, 44: 1657-1679.
Snyder, G.A. et al., 1993. Petrogenesis of garnet pyroxenite and spinel peridotite xenoliths of the Tell-Danun alkali basalt volcano, Harrat as Shamah, Syria. International Geology Review, 35: 1104-1120.
Stein, M. and Hofmann, A.W., 1992. Fossil plume head beneath the Arabian lithosphere? Earth and Planetary Science Letters, 114: 193-209.
Stewart, K. and Rogers, N., 1996. Mantle plume and lithosphere contributions to basalts from southern Ethiopia. Earth and Planetary Science Letters, 139: 195-211.
Suzuki, T., Akaogi, M. and Nakamura, E., 2000. Partitioning of major elements between garnet-structured minerals and silicate melt at pressure of 3-15 GPa. Physics of the Earth and Planetary Interiors, 120: 79-92.
Tarawneh, K. et al., 2000. Dating of the Harrat Ash Shaam Basalts Northeast Jordan (Phase 1). Hashemite Kingdom of Jordan, Natural Resources Authority; Geol. Surv. Isr. Rep. GSI/2/2000: 59.
Vidal, P. et al., 1991. Changes of mantle sources in the course of a rift evolution: The Afar case. Geophysical Research Letters, 18: 1913-1916.
Wallace, M.E. and Green, D.H., 1991. The Effect of Bulk Rock Composition on the Stability of Amphibole in the Upper Mantle: Implications for Solidus Positions and Mantle Metasomatism. Mineralogy and Petrology, 44: 1-19.
White, R. and McKenzie, D., 1989. Magmatism at rift zones; the generation of volcanic continental margins and flood basalts. In: W.P. Leeman and J.G. Fitton (Editors), Special section on Magmatism associated with lithospheric extension. Journal of Geophysical Research, 7685-7729.
White, R.S., Bown, J.W. and Smallwood, J.R., 1995. The temperature of the Iceland plume and origin of outward-propagating V-shaped ridges. Journal of the Geological Society of

London, 152: 1039-1045.
Wyllie, P.J., 1978. Mantle fluid compositions buffered in peridotite-CO_2-H_2O by carbonates, amphibole, and phlogopite. Journal of Geology, 86: 687-713.

CHAPTER THREE

The Afro-Arabian Connection: Volcanism in Syria and the Role of the Afar Plume

M.-S. Krienitz[1*], K.M. Haase[1], K. Mezger[2], M.A. Shaikh-Mashail[3], P. van den Bogaard[4] and V. Thiemann[2]

[1] Institut für Geowissenschaften der Universität Kiel, Olshausenstr. 40, 24118 Kiel, Germany
[2] Institut für Mineralogie der Universität Münster, Corrensstr. 24, 48149 Münster, Germany
[3] Faculty of Civil Engineering, University of Aleppo, PO-Box 5427, Aleppo, Syria
[4] Leibniz-Institut für Meereswissenschaften, Wischhofstr. 1-3, 24148 Kiel, Germany
[*] Corresponding author. Telephone +49 (0) 431 880 3694. Fax +49 (0) 431 880 4376. E-mail: mk@gpi.uni-kiel.de

Abstract

New geochemical and isotope data as well as radiometric age data of the continental intraplate lavas from Syria provide important constraints on large scale mantle dynamics beneath western Arabia. $^{40}Ar/^{39}Ar$ dating of mineral separates and whole rock samples establish Miocene to recent volcanic activity in Syria. These age data in conjunction with radiometric ages of lavas from the Afro-Arabian region suggest a northward progression of volcanism since the arrival of the Afar plume beneath Ethiopia/Djibouti some 30 Ma ago. The compositions of lavas from western Arabia and the Afar region indicate significant variations in both the depth and the extent of partial melting, varying from relatively shallow but high degree melting in the south to increasingly deeper regions and lower extents of partial melting in the north. Sr, Nd, and Pb isotope characteristics of the Syrian volcanic rocks indicate that crustal assimilation is involved in their magma genesis, but also that different mantle sources, a relatively depleted asthenospheric mantle source, a lithospheric source, and a mantle plume, have been involved in their formation. Whereas an influence of the undegassed Afar mantle plume source can be ruled out, the plume end member contributing to Syrian volcanism may represent an entrained upper mantle component related to the Afar plume. Increasing $^{206}Pb/^{204}Pb$ ratios observed in the last 13 Ma in Syrian lavas imply an increasing influence of this plume component with time. The distribution of the high $^{206}Pb/^{204}Pb$ lavas in Arabia indicates a spatial influence of the Afar plume of about 2,500 km in northward direction, significantly exceeding previous predictions.

3.1 Introduction

The emplacement of continental flood basalts is generally explained by the arrival of new mantle plumes which provide the most likely source of required heat to induce such massive melting events (White and McKenzie, 1989; Campbell and Griffiths, 1990; Griffiths and Campbell, 1990). According to the active rift hypothesis of Sengör and Burke (1978) the impinging plume on the base of the lithosphere leads to thermal erosion, thinning, rifting, and continental breakup, finally resulting in the formation of new ocean basins. Rifting of the lithosphere may be accompanied by decompression allowing extensive melting to occur (passive rifting). The wide compositional range in terms of trace element and isotope compositions of flood basalts suggest that not only plume-type mantle sources are involved but indicate that different crustal and mantle components contribute to the magma genesis. The identification of magma sources and melting processes as well as their spatial and temporal distribution provide important constraints on magmatic processes and mantle dynamics during flood basalt volcanism and evolution of continental rift systems.

The Red Sea area is the best example of the development of a continental rift system into a young ocean basin being accompanied by extensive magmatism (Fig. 3.1a). Large alkali basaltic provinces cover the western edge of Arabia extending from Turkey in the north over a distance of 2,500 km to Yemen in the south, whereby in eastern Africa large parts of Eritrea, Ethiopia, and Djibouti are covered by the Ethiopian flood basalt province (Fig. 3.1a). One model suggests that the widespread volcanism on the Arabian plate since the Miocene has been linked to the formation of the Red Sea and to movements along the Dead Sea fault system (Bohannon et al., 1989; Nasir and Safarjalani, 2000). On the other hand the extensive volcanism has also been linked to the impact of the Afar plume beneath the lithosphere about 30 Ma ago (Hofmann et al., 1997). Several authors (e.g. Vidal et al., 1991; Schilling et al., 1992; Deniel et al., 1994; Baker et al., 1996a) proposed that the arrival of the Afar plume caused the late Oligocene to early Miocene volcanism in Ethiopia and Djibuti and contributed to volcanism in Yemen, the Gulf of Aden and the southern Red Sea area (Fig. 3.1a). Nonetheless, the cause for the volcanic activity in the northern part of the Arabian peninsula, far-off the Afar region, is not well understood and existing models are contradictive. Stein and Hofmann (1992) introduced the model of a fossil plume head below the sub-continental lithosphere and argued that magmas were generated in times of lithospheric thinning by tapping this reservoir. In contrast, Camp and Robool (1992) speculated about the existence of a separate mantle plume underneath northern Arabia or whether asthenospheric material was channeled from the Afar region in a northwestward direction accounting for the volcanism in northern Arabia. In the view of Bertrand et al. (2003) and Shaw et al. (2003) volcanism has been triggered by ongoing extension of the lithosphere leading to the involvement of lithospheric (fossil plume material) to asthenospheric sources in volcanism.

Here we present new $^{40}Ar/^{39}Ar$ data and geochemical as well as Sr, Nd, and Pb isotope data

of Syrian volcanic rocks in order to relate the volcanic activity of northwestern Arabia to the widespread volcanism along the western Arabian edge and to the magmatic activity in the Afar region (i. e. in Ethiopia and Djibouti). We will discuss the compositional characteristics of the magmatic sources contributing to the magmas and focus on the melting regime in order to evaluate the spatial, temporal and dynamic implications for magmatism in the Afro-Arabian region.

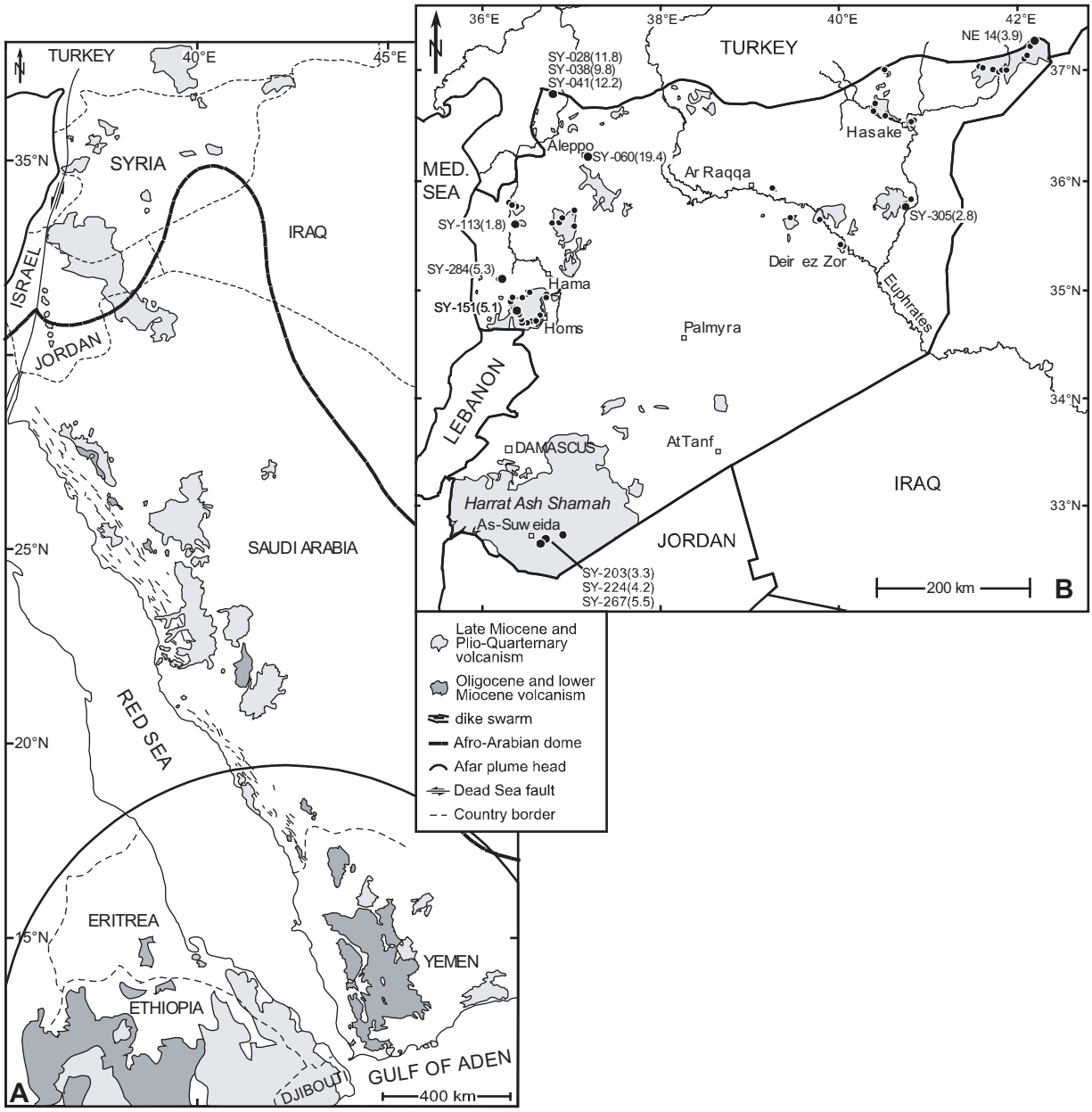

Fig. 3.1. (a) Distribution of volcanic fields along western Arabia and the Gulf of Aden region modified after Bertrand et al. (2003) and Pik et al. (1998). The presumed area of the flattened Afar plume head is after Schilling et al. (1992) and the dimension of the Afro-Arabian dome after Camp and Roobol (1992). (b) Generalised map of Syria and surrounding countries showing the distribution of Miocene to recent volcanism in Syria modified after geological maps of Ponikarov (1963). Small black circles denote locations of which samples were collected. Location of volcanic rocks used for Ar-Ar dating are shown by large black circles together with sample names. Numbers in brackets give Ar-Ar ages of the volcanic rocks in Ma. Complete lists of available chemical data for the samples SY-028, SY-038, SY-041, and SY-060 are given in Krienitz et al. (Chapter I) and for the samples SY-203, SY-224, and SY-267 in Krienitz et al. (Chapter II).

3.2 Geological setting

Syria is located at the northwestern end of the Arabian peninsula close to the continent-continent collision zone where Arabia is converging on Eurasia (Fig. 3.1b). On the basis of Bouguer gravity anomalies Syria can be divided into the SW-NE striking mountain range of the Palmyride Fold Zone, which is bounded in the north by the Aleppo plateau and by the Rutbah uplifted region in the south (Best et al., 1990; McBride et al., 1990; Searle, 1994). The main “tectonic zones” in the eastern parts of the country are the Abd el Aziz-Sinjar uplifted area and the Euphrates Fault system (Brew et al., 2001). Refraction profiling, seismic reflection data, and gravity models of the crust of the uplifted regions of Syria indicate that the metamorphic basement generally lies more than 6 km deep and that the crustal thickness is about 40 km, i.e. similar to crustal thicknesses in Jordan and Saudi Arabia (El-Isa et al., 1987; Best et al., 1990; McBride et al., 1990; Seber et al., 1993; Brew et al., 1997; Sandvol et al., 1998; Walley, 1998; Brew et al., 2001; Kumar et al., 2002;).

Syria is covered by numerous volcanic centres with a concentration of the volcanism in western Syria close to the Dead Sea transform fault (Figs. 3.1a and b). However, the most prominent volcanic field, the Harrat Ash Shamah (HAS), covers large parts of southern Syria extending about 500 km from Israel through Syria and Jordan to Saudi Arabia reaching a maximum thickness of 1,500 m (Guba and Mustafa, 1988; Ilani et al., 2001). Whereas a few K-Ar ages of volcanic rocks suggest an Cretaceous phase of magmatic activity, ranging from 130 Ma to 90 Ma (Mouty et al., 1992), most of the age data show that volcanism is younger, starting at about 26 Ma and probably lasting to the Holocene (Giannerini et al., 1988; Mouty et al., 1992; Sharkov et al., 1994; Sharkov et al., 1998).

3.3 Analytical procedures

The sample material was recovered during a field trip in the year 2000 (Fig. 3.1b). Weathered surfaces of lavas were cut off and hand specimens were cut into pieces for analyses and thin section preparation. After washing with deionised water in an ultrasonic bath lavas were crushed with a screw press and washed again. The crushed material was powdered in an agate ball mill for major, trace and isotope analyses.

Major and selected trace element analyses of whole rock samples were obtained with a Philips PW 1400 XRF at the Universität Kiel, Germany, using international rock standards for calibration and data quality control. The accuracy of standard analyses relative to reference values is better than 4% for most of the major and trace elements and can be estimated from average values of the BHVO-1 standard listed in Table 1. Except for SiO_2 (0.25%) the replicate measurements of the BHVO-1 standard gave a precision better than 0.20% (SD) for major elements and generally better than 8% (SD) for trace elements.

Trace and rare earth elements were determined at the Universität Kiel with an upgraded PlasmaQuad PQ1 ICP-MS. Details of the analytical procedure have been described by Garbe-Schönberg (1993). Duplicate analyses gave a precision generally better than 1% (SD) except for V, Zr (<2% SD), Sr and Ba (<4% SD; Table 1). The accuracy of the data based on the international rock standard BR is better than 9% except for Cs, Nb (<10%) and Li (14%).

Isotope analyses were performed at the Zentrallaboratorium für Geochronologie in Münster, Germany, using a VG Sector 54 multicollector mass spectrometer and Standard ion exchange techniques to produce Sr, Nd and Pb separates. Pb isotopes were measured in static mode and the NBS982 standard was used to correct Pb isotope ratios for mass fractionation. Correction factors are $^{206}Pb/^{204}Pb$ = 0.02%, $^{207}Pb/^{204}Pb$ = 0.03% and $^{208}Pb/^{204}Pb$ = 0.04% and standard runs (n = 10) gave $^{206}Pb/^{204}Pb$ = 36.646, $^{207}Pb/^{204}Pb$ = 17.101 and $^{208}Pb/^{204}Pb$ = 36.593 with a precision of ±0.022, ±0.014 and ±0.038 (2SD), respectively. Sr and Nd isotope ratios were analysed in dynamic mode. Isotope fractionation was corrected using $^{86}Sr/^{88}Sr$ = 0.1194 and $^{146}Nd/^{144}Nd$ = 0.7219. Standard runs for Sr isotopes gave NBS987 (n = 16): 0.710299 (2SD = 0.000026) and all Sr isotope analyses were normalised to NBS987 = 0.710250. Standard runs for $^{143}Nd/^{144}Nd$ gave La Jolla (n = 14): 0.511862 (2SD = 0.000024). Procedural blanks at this time were generally better than 0.2 ng, 0.1 ng and 0.04 ng for Sr, Nd, and Pb. Based on the newly obtained Ar-Ar ages presented herein (Table 3) as well as on geological maps of Ponikarov (1963) and K-Ar ages of Giannerini et al. (Giannerini et al., 1988; Mouty et al., 1992; Sharkov et al., 1994) the isotope data were age-corrected and used in figures (Table 2).

Based on thin section investigation and on K contents samples with unaltered groundmass and considerable amounts of plagioclase phenocrysts were chosen and prepared for Ar-Ar dating. For analyses the crushed sample material were sieved. The 250-500 µm fraction was used to separate 50 mg of goundmass and/or 5-10 mg of feldspars by picking under a binocular microscope, whereby single grain analyses were perfomed with feldspar minerals of the 500-1000 µm fraction. Prior to irridation and analysis the mineral separates were leached for 15 minutes with diluted HF in an ultrasonic bath, were washed efficiently with ultraclean water and dried at <50°C for 12 hours to make sure that only such mineral grains were used for dating, which are unaltered and free of inclusions. Matrix and mineral samples were irradiated using the FRG2 reactor at the GKSS Research Center (Geesthacht) for 7 days (Cd-liner). Irradiated groundmass and feldspar samples were reloaded into aluminum trays with multiple pans holding between 5 and 8 mg of matrix material, single plagioclase crystals respectively. The matrix samples were heated by incrementally increasing laser power output from 0.15 to 20 Watt from <350°C to >1800 °C until complete fusion. Software has controlled the scanning across the samples with preset patterns and a defocused laser beam, to more evenly heat the material. Automated step-heating was followed by final fusion at ~25 Watt with a focused beam to ensure complete degassing (m/z 40 and m/z 39 signals at blank level), and essentially evaporating the residual melt/glass sphere.

Table 1. Major (XRF) and trace element (XRF, ICP-MS) analyses of the Syrian samples.

Sample	SY-049	SY-050	SY-052	SY-053	SY-054	SY-057	SY-091	SY-092	SY-093	SY-094	SY-100	SY-101
Lat. [°N]	35°43`28``	35°43`28``	35°43`26``	35°43`26``	35°43`11``	35°43`11``	35°45`22``	35°45`22``	35°45`22``	35°45`22``	35°45`26``	35°45`29``
Long. [°E]	37°03`44``	37°03`44``	37°03`30``	37°03`30``	37°03`26``	37°03`26``	36°24`25``	36°24`25``	36°24`25``	36°24`25``	36°24`35``	36°24`38``
Elevation [m]	294	294	-	-	289	289	360	360	360	360	346	369
Rock type[+]	AB	AB	AB	AB	AB	AB	B	B	B	B	H	B
SiO_2 [wt.%]	45.49	45.34	46.19	46.39	42.85	44.19	40.10	41.12	40.96	40.82	46.71	44.42
TiO_2	2.47	2.22	2.40	2.17	2.02	2.10	3.10	3.04	3.01	3.12	2.62	2.92
Al_2O_3	13.65	13.73	13.87	13.99	12.84	13.55	12.96	13.40	12.91	13.11	12.78	14.39
$Fe_2O_3^T$	14.18	13.12	13.44	13.06	12.36	12.91	13.53	13.94	13.74	14.31	12.82	14.30
MnO	0.19	0.17	0.17	0.17	0.16	0.16	0.18	0.21	0.20	0.21	0.19	0.20
MgO	7.51	7.84	6.90	8.65	7.86	6.63	7.69	7.76	8.28	8.28	7.20	6.88
CaO	9.98	11.10	9.97	10.20	12.74	12.71	10.99	11.27	10.97	11.37	8.34	8.93
Na_2O	2.85	3.39	3.21	3.35	2.97	2.77	4.42	4.46	4.40	4.00	4.15	4.88
K_2O	0.90	0.98	1.06	0.98	0.89	0.91	0.80	1.05	0.97	0.82	2.30	0.99
P_2O_5	0.42	0.41	0.43	0.40	0.41	0.42	2.16	2.18	2.09	2.16	0.97	1.02
L.O.I.	2.92	2.18	2.23	1.14	5.23	4.29	2.44	2.05	1.43	2.72	1.57	1.94
Total	100.56	100.48	99.87	100.50	100.33	100.64	98.37	100.48	98.96	100.92	99.65	100.87
Mg-no.[++]	0.55	0.58	0.54	0.61	0.60	0.54	0.57	0.56	0.58	0.57	0.57	0.53
Li [ppm]	-	-	-	14.7	16.0	-	2.53	-	-	-	-	6.04
Sc	-	-	-	18.6	18.0	-	11.1	-	-	-	-	16.4
V	-	-	-	-	-	-	135	-	-	-	-	190
Cr	283	276	261	302	270	264	125	215	216	209	204	122
Co	-	-	-	55.1	50.3	-	36.7	-	-	-	-	50.5
Ni	233	233	234	227	195	218	97.5	146	149	138	107	105
Cu	-	-	-	60.7	76.0	-	32.6	-	-	-	-	43.4
Zn	125	108	119	103	97.6	107	104	132	133	138	141	138
Ga	-	-	-	-	-	-	-	-	-	-	-	26.4
Rb	12	13	14	12.7	11.7	10	8.05	13	14	10	33	9.33
Y	-	-	-	17.5	17.0	-	28.2	-	-	-	-	26.9
Cs	-	-	-	0.211	0.151	-	0.434	-	-	-	-	0.325
Sr	631	592	626	979	613	626	2216	2228	2133	2232	1085	1986
Ba	474	302	-	203	1089	436	1413	932	-	884	-	417
Zr	254	240	199	142	133	244	325	729	468	739	390	354
Hf	-	-	-	4.10	3.92	-	7.82	-	-	-	-	6.48
Nb	-	-	-	26.8	24.1	-	114	-	-	-	-	75.5
Ta	-	-	-	1.83	1.64	-	5.84	-	-	-	-	4.33
Pb	-	-	-	2.35	2.80	-	4.84	-	-	-	-	3.52
Th	-	-	-	2.70	2.72	-	9.65	-	-	-	-	5.05
U	-	-	-	0.883	1.30	-	2.79	-	-	-	-	1.53
La	-	-	-	21.7	21.6	-	115	-	-	-	-	53.6
Ce	-	-	-	44.6	43.9	-	216	-	-	-	-	107
Pr	-	-	-	5.44	5.31	-	24.2	-	-	-	-	11.9
Nd	-	-	-	22.8	22.0	-	89.0	-	-	-	-	46.0
Sm	-	-	-	5.30	5.05	-	15.4	-	-	-	-	9.22
Eu	-	-	-	1.77	1.65	-	4.66	-	-	-	-	3.29
Gd	-	-	-	5.29	5.03	-	12.3	-	-	-	-	7.84
Tb	-	-	-	0.757	0.728	-	1.62	-	-	-	-	1.04
Dy	-	-	-	4.13	4.01	-	7.63	-	-	-	-	5.20
Ho	-	-	-	0.739	0.726	-	1.26	-	-	-	-	0.890
Er	-	-	-	1.85	1.81	-	2.93	-	-	-	-	2.14
Tm	-	-	-	0.241	0.241	-	0.351	-	-	-	-	0.296
Yb	-	-	-	1.49	1.49	-	2.02	-	-	-	-	1.66
Lu	-	-	-	0.208	0.210	-	0.278	-	-	-	-	0.209

[+] Rock type after TAS: B - basanite, AB - alkali basalt, T - tholeiite, H - hawaiite, PT - phonotephrite, F - foidite, std. - standard.

[++] Mg-no. = Mg/(Mg + Fe2+), assuming FeO = $0.85Fe^T$. n.d. - not detected.

Table 1. (continued)

Sample	SY-103	SY-104	SY-105	SY-106	SY-107	SY-108	SY-109	SY-111	SY-112	SY-113	SY-114	SY-134
Lat. [°N]	35°45`24``	35°45`40``	35°45`40``	35°45`40``	35°45`50``	35°45`50``	35°47`29``	35°47`29``	35°46`01``	35°35`46``	35°35`56``	34°45`38``
Long. [°E]	36°24`31``	36°21`38``	36°21`38``	36°21`38``	36°21`42``	36°21`42``	36°19`30``	36°19`30``	36°21`36``	36°23`45``	36°24`19``	36°40`14``
Elevation [m]	337	381	(381)	(381)	264	(264)	150	150	250	224	365	502
Rock type[+]	B	B	B	AB	B	B	B	B	B	B	B	AB
SiO_2 [wt.%]	41.12	42.42	43.40	44.10	43.27	43.42	41.92	42.90	42.27	42.73	41.87	46.15
TiO_2	3.35	3.11	3.00	2.93	2.94	2.79	3.28	3.24	3.19	3.52	3.05	2.25
Al_2O_3	13.30	13.65	13.91	14.03	13.47	13.34	13.43	13.92	13.37	13.65	13.12	15.21
$Fe_2O_3^T$	14.21	13.79	13.55	13.61	13.31	12.93	13.08	13.04	13.70	14.12	13.84	13.09
MnO	0.18	0.19	0.17	0.18	0.17	0.17	0.19	0.18	0.18	0.18	0.20	0.17
MgO	8.40	8.34	8.32	8.40	8.28	8.73	7.84	7.71	8.59	8.05	9.27	6.77
CaO	10.70	10.46	10.05	9.91	9.95	10.21	9.60	9.56	10.36	9.71	10.48	11.17
Na_2O	4.54	4.39	3.64	3.08	3.19	3.62	3.52	3.96	4.55	3.89	3.96	2.83
K_2O	1.75	0.97	1.64	1.57	1.60	1.56	1.31	1.30	1.09	1.54	1.67	0.65
P_2O_5	1.98	1.81	1.48	1.41	1.37	1.24	1.54	1.58	1.91	1.24	1.63	0.31
L.O.I.	1.15	1.17	1.20	0.96	1.21	1.97	4.56	3.38	1.03	1.28	0.89	0.97
Total	100.68	100.30	100.36	100.18	98.76	99.98	100.27	100.77	100.24	99.91	99.98	99.57
Mg-no.[**]	0.58	0.58	0.59	0.59	0.59	0.61	0.58	0.58	0.59	0.57	0.61	0.55
Li [ppm]	5.22	-	-	3.04	-	-	5.4	-	-	5.69	2.56	-
Sc	16.1	-	-	18.5	-	-	15.0	-	-	17.1	12.1	-
V	208	-	-	180	-	-	178	-	-	209	131	-
Cr	173	194	193	190	219	195	132	137	177	140	147	210
Co	51.2	-	-	51.2	-	-	42.9	-	-	47.0	38.2	-
Ni	141	162	171	163	158	190	111	132	156	140	118	100
Cu	44.4	-	-	44.8	-	-	36.9	-	-	33.9	44.3	-
Zn	125	123	114	114	125	117	123	127	124	120	101	105
Ga	24.0	-	-	22.7	-	-	23.3	-	-	24.3	-	-
Rb	13.1	12	21	18.6	30	24	20.8	22	22	15.0	20.3	5
Y	27.3	-	-	26.5	-	-	25.4	-	-	25.0	27.6	-
Cs	0.301	-	-	0.372	-	-	0.468	-	-	0.401	0.326	-
Sr	2122	1797	1615	1631	1542	1496	1923	1617	1906	1230	1610	469
Ba	776	767	788	662	-	-	643	741	755	477	677	-
Zr	337	598	540	252	335	322	298	568	634	296	265	152
Hf	5.75	-	-	4.51	-	-	6.11	-	-	6.04	6.84	-
Nb	107	-	-	79.7	-	-	88.9	-	-	77.2	81.1	-
Ta	4.64	-	-	3.58	-	-	4.78	-	-	4.24	4.86	-
Pb	5.20	-	-	4.46	-	-	4.52	-	-	3.99	5.39	-
Th	6.90	-	-	5.86	-	-	5.43	-	-	5.93	6.62	-
U	1.97	-	-	1.67	-	-	1.54	-	-	1.59	1.87	-
La	96.3	-	-	71.5	-	-	65.3	-	-	56.8	75.4	-
Ce	184	-	-	136	-	-	132	-	-	110	147	-
Pr	19.3	-	-	14.5	-	-	14.6	-	-	12.0	17.3	-
Nd	70.6	-	-	53.5	-	-	55.8	-	-	45.6	67.2	-
Sm	12.2	-	-	9.67	-	-	10.5	-	-	8.96	12.6	-
Eu	3.99	-	-	3.24	-	-	3.61	-	-	3.10	4.04	-
Gd	9.60	-	-	8.10	-	-	9.02	-	-	8.03	10.7	-
Tb	1.17	-	-	1.04	-	-	1.15	-	-	1.05	1.47	-
Dy	5.42	-	-	5.01	-	-	5.47	-	-	5.24	7.29	-
Ho	0.894	-	-	0.871	-	-	0.899	-	-	0.879	1.24	-
Er	2.11	-	-	2.12	-	-	2.09	-	-	2.10	2.93	-
Tm	0.276	-	-	0.294	-	-	0.276	-	-	0.275	0.360	-
Yb	1.52	-	-	1.68	-	-	1.56	-	-	1.57	2.12	-
Lu	0.192	-	-	0.222	-	-	0.202	-	-	0.205	0.286	-

Table 1. (continued)

Sample	SY-135	SY-138	SY-139	SY-141	SY-142	SY-143	SY-144	SY-145	SY-150	SY-151	SY-152	SY-154
Lat. [°N]	34°43`02``	34°42`21``	34°41`25``	34°41`04``	34°43`21``	34°45`21``	34°46`00``	34°47`21``	34°48`02``	34°48`02``	34°48`40``	34°50`29``
Long. [°E]	36°37`27``	36°34`58``	36°31`55``	36°28`02``	36°27`56``	36°26`59``	36°26`22``	36°24`45``	36°24`28``	36°24`28``	36°23`25``	36°22`02``
Elevation [m]	(503)	557	526	562	628	785	731	947	823	(840)	974	1022
Rock type[+]	AB	AB	AB	AB	B	H	B	H	AB	B	B	PT
SiO_2 [wt.%]	44.97	46.05	47.21	46.94	42.84	44.87	44.94	46.64	44.00	44.43	43.24	48.35
TiO_2	2.94	2.91	2.18	2.58	3.74	3.19	3.13	2.32	3.19	3.08	2.72	2.16
Al_2O_3	15.53	16.11	15.97	16.34	13.95	15.15	16.03	15.37	14.53	14.30	13.78	17.94
$Fe_2O_3^T$	13.72	12.84	12.96	13.75	14.82	13.57	13.21	12.56	13.81	13.39	13.60	11.64
MnO	0.18	0.16	0.17	0.16	0.17	0.18	0.18	0.18	0.17	0.17	0.18	0.23
MgO	5.67	4.87	6.86	5.56	8.77	7.21	6.13	7.24	8.52	8.64	10.87	3.00
CaO	10.89	10.24	10.12	10.45	9.09	9.14	9.59	9.36	9.05	8.61	10.91	6.65
Na_2O	2.75	2.66	3.11	3.02	3.67	4.16	3.87	3.94	3.28	3.86	3.31	5.34
K_2O	1.00	1.10	0.63	0.73	0.75	0.87	1.87	1.26	0.94	1.74	1.02	1.98
P_2O_5	0.73	0.65	0.29	0.40	0.66	0.65	0.79	0.49	0.71	0.68	0.84	1.62
L.O.I.	1.69	1.51	0.11	0.35	1.20	1.65	0.22	0.07	1.45	0.23	0.00	1.37
Total	100.07	99.10	99.61	100.28	99.66	100.64	99.96	99.43	99.65	99.13	100.47	100.28
Mg-no.[**]	0.49	0.47	0.55	0.49	0.58	0.55	0.52	0.57	0.59	0.60	0.65	0.38
Li [ppm]	-	5.91	-	-	-	-	5.30	-	6.27	-	5.60	9.60
Sc	-	17.4	-	-	-	-	18.8	-	14.3	-	20.0	5.05
V	-	-	-	-	-	-	209	-	-	-	-	-
Cr	148	73.0	197	166	244	209	104	152	188	187	366	n.d.
Co	-	37.9	-	-	-	-	44.8	-	48.3	-	56.2	18.6
Ni	67	40.0	74	70	226	153	67.3	103	166	173	212	11.0
Cu	-	45.9	-	-	-	-	55.2	-	41.6	-	62.4	7.56
Zn	119	109	98	105	106	101	105	102	100	97	103	130
Ga	-	24.1	-	-	-	-	24.9	-	20.3	-	20.9	25.0
Rb	13	11.4	7	8	15	40	19.0	13	14.7	15	12.1	19.3
Y	-	28.8	-	-	-	-	22.5	-	22.6	-	25.9	32.2
Cs	-	0.087	-	-	-	-	0.212	-	0.502	-	0.262	0.378
Sr	861	848	485	569	857	847	980	690	904	858	835	1967
Ba	-	290	314	259	392	422	326	325	318	445	356	724
Zr	259	186	142	222	342	374	259	280	185	336	160	434
Hf	-	4.60	-	-	-	-	5.17		4.48	-	3.79	7.85
Nb	-	36.9	-	-	-	-	47.9		38.7	-	47.8	123
Ta	-	2.12	-	-	-	-	2.69		2.14	-	2.40	6.64
Pb	-	2.06	-	-	-	-	3.13		3.10	-	2.95	1.96
Th	-	2.64	-	-	-	-	3.29		3.25	-	4.54	6.73
U	-	0.600	-	-	-	-	1.03		0.942	-	1.26	2.05
La	-	31.2	-	-	-	-	35.4		33.0	-	42.2	89.7
Ce	-	62.9	-	-	-	-	74.1		64.8	-	77.5	183.0
Pr	-	8.16	-	-	-	-	8.55		7.65	-	8.81	19.2
Nd	-	34.1	-	-	-	-	34.4		31.0	-	34.9	70.5
Sm	-	7.47	-	-	-	-	7.29		6.71	-	7.21	11.9
Eu	-	2.44	-	-	-	-	2.57		2.23	-	2.35	3.75
Gd	-	7.08	-	-	-	-	6.66		6.33	-	6.80	9.71
Tb	-	1.00	-	-	-	-	0.903		0.878	-	0.953	1.24
Dy	-	5.50	-	-	-	-	4.58		4.75	-	5.15	6.43
Ho	-	1.00	-	-	-	-	0.783		0.830	-	0.914	1.13
Er	-	2.54	-	-	-	-	1.89		2.03	-	2.28	2.86
Tm	-	0.335	-	-	-	-	0.258		0.259	-	0.289	0.375
Yb	-	2.00	-	-	-	-	1.48		1.52	-	1.74	2.28
Lu	-	0.281	-	-	-	-	0.194		0.209	-	0.239	0.320

Table 1. (continued)

Sample	SY-155	SY-156	SY-157	SY-158	SY-160	SY-161	SY-163	SY-165	SY-170	SY-173	SY-174	SY-282
Lat. [°N]	34°52`07``	34°53`11``	34°55`18``	34°55`31``	34°55`17``	34°55`17``	34°55`17``	34°58`13``	34°57`03``	34°55`16``	34°42`28``	35°05`46``
Long. [°E]	36°20`46``	36°20`37``	36°21`51``	36°21`56``	36°28`22``	36°28`22``	36°28`22``	36°33`29``	36°44`49``	36°44`32``	36°37`53``	36°14`41``
Elevation [m]	997	931	(500)	688	439	455	-	400	405	447	528	1118
Rock type[+]	AB	AB	B	B	AB	AB	B	AB	AB	T	AB	B
SiO_2 [wt.%]	45.30	46.35	46.67	42.33	46.32	46.54	41.58	47.40	47.47	47.94	44.87	39.70
TiO_2	2.41	2.45	2.80	3.39	2.50	2.44	3.56	2.15	2.07	2.31	2.10	2.89
Al_2O_3	14.19	16.07	16.75	13.63	14.79	14.57	13.72	16.00	14.73	14.37	15.16	11.76
$Fe_2O_3^T$	13.50	13.92	12.68	13.82	13.87	13.80	13.63	13.01	13.63	11.78	12.44	13.68
MnO	0.18	0.17	0.18	0.17	0.17	0.17	0.17	0.16	0.17	0.16	0.16	0.20
MgO	11.11	7.66	5.57	10.13	7.71	7.96	7.07	5.57	8.92	5.77	6.55	9.83
CaO	9.29	9.57	7.53	10.19	9.55	9.43	10.23	10.56	9.07	10.40	12.29	11.71
Na_2O	3.44	3.46	4.56	3.02	3.22	3.06	4.14	3.38	3.11	2.73	2.94	4.12
K_2O	0.90	0.75	2.07	1.37	1.05	1.06	1.77	0.71	0.69	0.71	0.67	1.14
P_2O_5	0.59	0.45	0.95	0.82	0.46	0.44	0.96	0.35	0.28	0.34	0.31	2.27
L.O.I.	0.00	0.00	0.10	0.13	0.05	0.09	1.93	0.59	0.00	2.02	1.81	0.90
Total	100.91	100.85	99.86	99.00	99.69	99.56	98.76	99.88	100.14	98.53	99.30	98.20
Mg-no.[**]	0.66	0.56	0.51	0.63	0.56	0.57	0.55	0.50	0.60	0.53	0.55	0.63
Li [ppm]	5.55	-	5.60	-	5.00	-	-	-	5.26	-	5.99	8.34
Sc	21.1	-	15.9	-	16.4	-	-	-	17.5	-	20.1	12.1
V	-	-	161	-	-	-	-	-	-	-	-	-
Cr	364	127	65.7	259	284	267	122	164	328	151	193	326
Co	56.7	-	40.9	-	48.2	-	-	-	55.3	-	44.3	47
Ni	255	96	61.3	161	151	167	113	62	224	58	83.0	195
Cu	91.5	-	41.2	-	43.6	-	-	-	56.2	-	50.1	47.4
Zn	92.4	107	104	101	111	116	114	101	107	97	95.0	123
Ga	-	-	23.3	-	21.8	-	-	-	21.0	-	21.1	21.5
Rb	7.86	9	19.9	14	13.5	14	21	10	8.33	8	7.69	32.6
Y	20.7	-	26.4	-	21.4	-	-	-	22.4	-	22.4	34.6
Cs	0.120	-	0.232	-	0.186	-	-	-	0.067	-	0.137	0.536
Sr	634	623	1146	1001	560	554	1082	488	393	488	428	2593
Ba	198	213	365	659	243	446	810	342	169	-	146	753
Zr	147	236	327	235	134	168	336	166	124	165	119	334
Hf	4.00	-	5.93	-	3.53	-	-	-	3.22	-	3.09	6.17
Nb	25.4	-	60.5	-	27.3	-	-	-	16.3	-	16.4	118
Ta	1.55	-	3.29	-	1.72	-	-	-	0.985	-	0.960	5.52
Pb	2.32	-	3.53	-	1.55	-	-	-	1.23	-	1.70	5.51
Th	2.52	-	4.24	-	2.07	-	-	-	1.37	-	1.39	11.0
U	0.796	-	1.36	-	0.583	-	-	-	0.271	-	0.370	3.25
La	27.6	-	44.3	-	21.3	-	-	-	13.7	-	13.5	114
Ce	54.7	-	89.3	-	42.9	-	-	-	30.6	-	30.0	217
Pr	6.51	-	10.0	-	5.30	-	-	-	4.06	-	4.00	22.3
Nd	26.5	-	38.8	-	22.6	-	-	-	18.0	-	17.4	82.3
Sm	5.79	-	7.80	-	5.19	-	-	-	4.58	-	4.47	14.7
Eu	1.96	-	2.72	-	1.76	-	-	-	1.54	-	1.53	4.40
Gd	5.79	-	6.87	-	5.22	-	-	-	4.79	-	4.70	12.2
Tb	0.828	-	0.946	-	0.763	-	-	-	0.721	-	0.721	1.52
Dy	4.65	-	4.91	-	4.27	-	-	-	4.29	-	4.27	7.52
Ho	0.858	-	0.894	-	0.782	-	-	-	0.812	-	0.814	1.25
Er	2.17	-	2.24	-	1.95	-	-	-	2.07	-	2.11	2.92
Tm	0.287	-	0.318	-	0.256	-	-	-	0.277	-	0.286	0.358
Yb	1.81	-	1.88	-	1.57	-	-	-	1.69	-	1.78	2.05
Lu	0.258	-	0.251	-	0.216	-	-	-	0.239	-	0.251	0.274

Table 1. (continued)

Sample	SY-283	SY-284	SY-285	SY-286	SY-287	SY-288	SY-290	SY-291	SY-294	SY-296	SY-298	SY-300
Lat. [°N]	35°05`46``	35°05`34``	35°05`34``	35°05`58``	35°05`58``	35°36`16``	35°36`37``	35°36`37``	35°34`35``	35°34`48``	35°39`01``	35°55`23``
Long. [°E]	36°14`41``	36°12`33``	36°12`33``	36°11`22``	36°11`22``	36°48`22``	36°53`21``	36°53`21``	37°02`07``	37°03`17``	36°55`10``	39°16`20``
Elevation [m]	1118	1043	1043	(1042)	(1042)	532	(500)	(500)	431	453	(388)	371
Rock type[+]	B	B	B	B	B	AB	H	AB	AB	H	AB	F
SiO_2 [wt.%]	39.03	42.06	42.52	41.68	40.50	45.11	45.02	44.87	47.41	47.12	45.01	38.84
TiO_2	2.88	2.87	2.71	2.65	2.57	2.17	2.60	1.91	2.34	2.59	1.97	3.24
Al_2O_3	11.52	13.15	13.14	12.78	12.67	13.52	13.94	13.57	13.93	15.60	13.73	10.24
$Fe_2O_3^T$	13.76	12.40	12.49	12.88	12.33	12.30	12.88	12.60	12.80	11.67	12.67	14.08
MnO	0.20	0.16	0.17	0.17	0.16	0.16	0.15	0.16	0.16	0.18	0.16	0.18
MgO	10.67	10.01	10.02	10.32	10.60	7.26	7.02	7.22	6.76	5.24	7.29	14.04
CaO	11.80	10.84	10.51	10.83	12.78	10.90	9.53	11.05	9.97	10.09	11.25	11.14
Na_2O	3.57	3.85	3.93	4.03	2.98	3.51	4.05	3.35	3.32	3.68	3.14	4.04
K_2O	0.90	1.74	1.57	1.11	0.65	1.20	1.64	0.90	1.03	1.27	0.88	1.34
P_2O_5	2.18	1.08	1.30	1.46	1.45	0.49	0.50	0.37	0.45	0.59	0.47	1.03
L.O.I.	2.25	0.72	0.40	0.42	2.07	2.10	1.51	2.91	2.02	0.57	2.18	0.88
Total	98.76	98.88	98.76	98.33	98.76	98.72	98.84	98.91	100.19	98.60	98.75	99.05
Mg-no.[**]	0.64	0.65	0.65	0.65	0.67	0.58	0.56	0.57	0.55	0.51	0.57	0.70
Li [ppm]	-	-	5.62	6.45	-	-	9.79	7.26	-	6.82	-	2.50
Sc	-	-	12.2	19.2	-	-	12.8	13.3	-	19.3	-	13.1
V	-	-	-	207	-	-	-	-	-	-	-	163
Cr	301	280	298	284	251	259	188	267	290	72.3	256	323
Co	-	-	47.4	56.6	-	-	48.8	52	-	37.7	-	51.1
Ni	222	215	228	247	237	229	181	248	187	47.7	228	260
Cu	-	-	53.7	56.4	-	-	52.6	52.5	-	54.3	-	42.5
Zn	127	106	114	112	102	106	127	106	116	101	109	111
Ga	-	-	21.8	22.2	-	-	24.6	20.1	-	-	-	-
Rb	17	34	16.7	25.6	33	19	17.4	9.93	14	17.5	17	11.6
Y	-	-	24.3	24.8	-	-	19.5	17.9	-	23.9	-	23.5
Cs	-	-	0.195	0.557	-	-	0.294	0.124	-	0.380	-	0.276
Sr	1772	1190	1362	1527	1522	593	711	534	693	810	627	1029
Ba	966	779	634	722	946	711	369	584	-	353	752	338
Zr	394	306	265	278	346	187	193	122	193	173	167	278
Hf	-	-	5.39	5.50	-	-	4.89	3.14	-	5.09	-	7.50
Nb	-	-	83.1	95.2	-	-	35.4	22.6	-	34.2	-	66.3
Ta	-	-	4.29	4.72	-	-	2.20	1.35	-	2.37	-	4.39
Pb	-	-	4.32	4.21	-	-	2.57	2.12	-	2.99	-	5.96
Th	-	-	7.35	9.06	-	-	2.34	1.83	-	2.86	-	6.05
U	-	-	2.22	2.70	-	-	0.511	0.538	-	0.925	-	2.05
La	-	-	69.2	84.8	-	-	23.4	17.6	-	30.3	-	57.3
Ce	-	-	125	156	-	-	50.1	36.9	-	66.1	-	118
Pr	-	-	13.4	16.1	-	-	6.30	4.58	-	8.37	-	14.6
Nd	-	-	49.8	58.6	-	-	26.8	19.2	-	35.4	-	58.8
Sm	-	-	9.11	10.5	-	-	6.28	4.53	-	7.72	-	12.1
Eu	-	-	2.83	3.33	-	-	2.09	1.49	-	2.49	-	3.79
Gd	-	-	7.80	8.78	-	-	5.95	4.42	-	7.36	-	10.3
Tb	-	-	1.01	1.12	-	-	0.823	0.651	-	1.03	-	1.41
Dy	-	-	5.13	5.55	-	-	4.23	3.65	-	5.48	-	6.73
Ho	-	-	0.877	0.933	-	-	0.716	0.667	-	0.988	-	1.08
Er	-	-	2.11	2.25	-	-	1.66	1.67	-	2.46	-	2.40
Tm	-	-	0.267	0.287	-	-	0.203	0.218	-	0.324	-	0.279
Yb	-	-	1.56	1.67	-	-	1.20	1.34	-	1.96	-	1.57
Lu	-	-	0.215	0.223	-	-	0.161	0.186	-	0.281	-	0.208

Table 1. (continued)

Sample	SY-301	SY-303	SY-305	SY-307	SY-311	SY-312	SY-314	SY-315	SY-316	SY-317	SY-318	SY-319
Lat. [°N]	35°55`31``	35°55`31``	35°45`12``	35°49`14``	36°31`34``	36°32`19``	36°31`44``	36°31`16``	36°34`56``	36°37`09``	35°23`58``	35°24`47``
Long. [°E]	39°16`12``	39°16`12``	40°45`23``	40°49`27``	40°51`19``	40°51`38``	40°49`04``	40°48`12``	40°32`00``	40°24`14``	40°04`07``	40°02`01``
Elevation [m]	346	346	-	306	430	-	357	310	386	406	280	-
Rock type[+]	F	F	AB	AB	AB	F	AB	AB	AB	AB	AB	AB
SiO_2 [wt.%]	39.08	39.15	44.34	44.95	45.87	39.55	45.17	45.25	44.14	43.51	43.65	44.29
TiO_2	3.19	3.19	2.83	2.53	2.53	3.48	2.59	2.57	2.46	2.28	2.62	2.62
Al_2O_3	10.15	10.13	13.14	12.60	11.86	10.34	12.08	11.98	13.85	13.77	11.51	11.50
$Fe_2O_3^T$	14.04	14.07	12.18	12.81	13.11	15.41	13.35	13.30	13.68	13.09	13.31	13.19
MnO	0.19	0.19	0.16	0.16	0.17	0.19	0.17	0.17	0.18	0.17	0.17	0.17
MgO	14.62	14.73	8.56	10.82	10.76	11.68	10.75	11.11	9.15	8.78	11.38	10.91
CaO	11.01	10.92	11.37	10.34	9.99	10.59	10.08	10.17	9.69	10.70	10.49	10.33
Na_2O	4.48	4.47	2.82	2.93	2.86	4.28	3.18	3.09	3.17	2.41	3.09	3.53
K_2O	1.49	1.36	1.28	0.98	1.06	1.76	1.16	1.16	1.06	0.83	1.21	1.18
P_2O_5	1.01	1.00	0.48	0.40	0.58	1.12	0.60	0.57	0.48	0.44	0.64	0.65
L.O.I.	0.00	0.00	1.70	0.55	1.54	0.51	0.47	0.32	0.75	2.85	0.36	0.15
Total	99.26	99.21	98.86	99.07	100.33	98.91	99.60	99.69	98.61	98.83	98.43	98.52
Mg-no.[**]	0.71	0.71	0.62	0.66	0.66	0.64	0.65	0.66	0.61	0.61	0.67	0.66
Li [ppm]	5.63	6.94	7.62	-	-	8.00	-	-	6.69	7.39	9.16	6.10
Sc	17.9	13.0	22.4	-	-	13.9	-	-	21.1	20.1	17.7	14.6
V	252	-	270	-	-	-	-	-	237	-	-	-
Cr	427	493	303	381	334	285	325	348	250	294	358	361
Co	64.7	65.9	54.1	-	-	62.3	-	-	61.0	55.0	59.1	56.1
Ni	344	386	175	264	298	292	282	312	235	227	312	276
Cu	59.5	52.0	67.2	-	-	59.3	-	-	63.2	58.5	65.6	58.2
Zn	117	126	101	107	129	158	129	123	110	99.3	120	112
Ga	22.3	23.5	23.3	-	-	27.7	-	-	22.9	-	22.8	22.0
Rb	14.7	11.8	16.3	11	12	12.3	13	15	9.28	8.70	15.2	13.1
Y	21.3	22.9	17.2	-	-	26.8	-	-	19.2	16.9	23.3	20.9
Cs	0.214	0.175	0.327	-	-	0.206	-	-	0.123	0.217	0.446	0.265
Sr	1114	1085	798	637	706	1253	781	713	696	650	814	761
Ba	295	293	320	320	-	248	-	-	1048	207	248	222
Zr	266	300	168	178	225	410	245	236	197	182	202	191
Hf	5.92	6.16	4.14	-	-	8.53	-	-	4.20	4.96	5.00	4.68
Nb	66.4	68.3	31.9	-	-	67.9	-	-	21.3	20.4	43.1	41.0
Ta	3.96	4.02	2.07	-	-	4.30	-	-	1.30	1.53	2.58	2.44
Pb	1.94	2.94	3.04	-	-	3.84	-	-	2.30	2.34	3.57	3.04
Th	4.28	4.83	2.86	-	-	5.46	-	-	1.71	2.04	4.01	3.46
U	1.79	1.60	0.491	-	-	1.99	-	-	0.600	0.791	1.05	1.23
La	50.9	50.8	26.8	-	-	57.3	-	-	23.4	21.6	34.4	31.8
Ce	107	104	57.8	-	-	121	-	-	52.9	48.1	70.8	65.8
Pr	12.3	12.4	6.85	-	-	14.7	-	-	6.41	6.01	8.65	7.93
Nd	48.7	49.5	27.8	-	-	60.0	-	-	26.3	25.1	35.3	32.5
Sm	9.96	10.0	5.98	-	-	12.4	-	-	5.76	5.55	7.79	7.12
Eu	3.22	3.11	2.04	-	-	3.89	-	-	2.00	1.81	2.49	2.30
Gd	8.61	8.69	5.43	-	-	10.6	-	-	5.57	5.34	7.13	6.54
Tb	1.11	1.10	0.746	-	-	1.35	-	-	0.751	0.758	0.966	0.880
Dy	5.29	5.43	3.88	-	-	6.47	-	-	3.91	4.07	5.02	4.58
Ho	0.846	0.874	0.672	-	-	0.990	-	-	0.690	0.732	0.855	0.772
Er	1.89	1.92	1.64	-	-	2.12	-	-	1.71	1.78	2.00	1.81
Tm	0.223	0.220	0.211	-	-	0.234	-	-	0.234	0.236	0.250	0.223
Yb	1.23	1.20	1.26	-	-	1.23	-	-	1.36	1.47	1.45	1.29
Lu	0.156	0.159	0.169	-	-	0.152	-	-	0.184	0.206	0.196	0.173

Table 1. (continued)

Sample	SY-321	SY-324	NE 01	NE 02	NE 03	NE 05	NE 06	NE 07	NE 08	NE 09	NE 10	NE 11
Lat. [°N]	35°38`10``	35°39`09``	36°39`30``	36°39`37``	36°41`29``	36°59`48``	37°01`15``	37°00`44``	36°59`57``	36°58`12``	36°59`17``	37°05`35``
Long. [°E]	39°48`02``	39°28`20``	40°24`37``	40°24`43``	40°25`07``	40°31`45``	41°35`01``	41°37`59``	41°44`19``	41°48`24``	41°50`32``	42°05`26``
Elevation [m]	239	-	388	386	399	533	456	453	437	431	441	581
Rock type[+]	B	B	AB	AB	AB		AB	AB	AB	AB	AB	AB
SiO_2 [wt.%]	42.67	43.80	44.54	44.96	44.71		45.09	46.63	46.06	45.63	47.55	47.86
TiO_2	3.56	3.15	2.37	2.37	2.40		1.61	1.81	1.82	2.22	1.79	2.10
Al_2O_3	12.21	12.52	13.59	13.75	13.69		13.90	14.30	14.38	13.38	14.87	14.60
$Fe_2O_3^T$	14.86	13.94	13.29	13.34	13.38		12.99	12.73	12.32	12.89	13.01	11.92
MnO	0.17	0.18	0.17	0.17	0.17		0.16	0.16	0.16	0.16	0.16	0.15
MgO	10.40	10.08	9.75	9.85	9.62		7.21	8.78	8.27	8.81	8.34	6.58
CaO	9.84	10.80	9.72	9.68	9.71		11.32	9.99	10.85	9.96	8.74	10.32
Na_2O	3.02	3.16	2.81	3.02	3.16		3.05	3.13	3.28	3.37	3.44	3.32
K_2O	1.23	1.16	1.07	1.06	1.09		0.57	0.77	0.77	1.09	0.92	0.90
P_2O_5	0.55	0.53	0.45	0.43	0.45		0.24	0.30	0.33	0.34	0.25	0.31
L.O.I.	0.09	0.77	0.51	0.43	0.29		2.69	0.42	0.98	1.04	0.11	0.76
Total	98.60	100.09	98.27	99.06	98.66		98.83	99.02	99.22	98.89	99.18	98.82
Mg-no.[**]	0.62	0.63	0.63	0.63	0.63		0.56	0.62	0.61	0.61	0.60	0.56
Li [ppm]	7.80	-	-	7.75	7.67	6.17	9.77	7.97	8.80	10.4	8.90	-
Sc	19.2	-	-	20.5	20.9	19.5	20.1	20.1	19.9	17.5	17.9	-
V	-	-	-	246	253	276	219	203	214	216	181	-
Cr	311	358	273	280	278	307	284	270	288	267	236	249
Co	60.3	-	-	58.5	59.1	62.8	54.3	56.6	51.7	55.5	54.5	-
Ni	243	266	264	257	255	234	210	215	196	238	215	122
Cu	70.0	-	-	61.0	61.0	61.7	67.1	61.4	61.9	70.2	69.6	-
Zn	112	115	106	109	111	109	110	109	99.1	117	117	101
Ga	-	-	-	28.2	27.2	29.0	30.7	24.5	44.4	34.9	28.9	-
Rb	12.2	18	10	10.2	10.5	10.8	9.48	7.43	7.97	17.7	13.4	13
Y	16.5	-	-	18.4	18.5	17.7	17.7	15.8	16.9	18.1	17.0	-
Cs	0.120	-	-	0.147	0.249	0.217	0.195	0.080	0.161	0.694	0.478	-
Sr	797	777	629	633	623	560	502	460	534	543	525	482
Ba	185	-	1113	185	155	196	244	135	564	305	156	376
Zr	194	228	228	200	200	159	133	104	130	172	165	167
Hf	5.56	-	-	5.00	4.96	4.39	3.56	2.92	3.44	4.62	4.45	-
Nb	32.5	-	-	22.2	22.2	25.0	20.6	8.74	18.2	31.7	28.6	-
Ta	2.47	-	-	1.37	1.36	1.50	1.00	0.521	0.865	1.84	1.73	-
Pb	2.52	-	-	1.98	2.00	1.51	2.38	1.46	1.98	2.63	2.24	-
Th	2.86	-	-	2.00	1.99	1.91	2.46	1.33	2.60	2.69	2.25	-
U	0.897	-	-	0.662	0.754	0.649	0.594	0.464	0.619	0.802	0.672	-
La	28.3	-	-	22.8	22.8	18.6	19.2	12.1	20.2	20.2	15.9	-
Ce	61.9	-	-	51.1	50.9	41.7	38.6	27.5	39.1	42.8	34.5	-
Pr	7.74	-	-	6.45	6.45	5.50	4.66	3.61	4.62	5.39	4.43	-
Nd	32.7	-	-	27.0	26.9	23.8	19.3	15.7	19.1	22.7	19.0	-
Sm	7.14	-	-	6.01	6.02	5.70	4.58	3.97	4.45	5.34	4.58	-
Eu	2.39	-	-	1.99	1.99	1.90	1.55	1.39	1.54	1.77	1.54	-
Gd	6.56	-	-	5.57	5.57	5.34	4.59	4.09	4.47	5.13	4.55	-
Tb	0.863	-	-	0.803	0.816	0.785	0.700	0.626	0.671	0.768	0.689	-
Dy	4.35	-	-	4.33	4.34	4.15	3.97	3.55	3.76	4.17	3.84	-
Ho	0.721	-	-	0.769	0.774	0.736	0.727	0.661	0.700	0.748	0.701	-
Er	1.67	-	-	1.88	1.89	1.83	1.85	1.70	1.78	1.85	1.77	-
Tm	0.207	-	-	0.244	0.244	0.231	0.249	0.220	0.234	0.249	0.237	-
Yb	1.18	-	-	1.45	1.46	1.43	1.51	1.41	1.44	1.51	1.46	-
Lu	0.161	-	-	0.204	0.205	0.201	0.218	0.205	0.205	0.204	0.207	-

Table 1. (continued)

Sample	NE 12	NE 13	NE 14	NE 15	BHVO-1	BR
Lat. [°N]	37°07`15``	37°12`10``	37°16`56``	36°59`25``		
Long. [°E]	42°07`23``	42°09`34``	42°11`42``	41°53`35``		
Elevation [m]	510	475	506	446		
Rock type[+]	AB	AB	AB	AB	std.	std.
SiO_2 [wt.%]	46.18	45.97	47.67	47.05	49.67	
TiO_2	1.75	1.72	1.92	1.67	2.77	
Al_2O_3	14.37	14.19	14.40	14.25	13.70	
$Fe_2O_3^T$	12.85	13.20	12.96	12.83	12.35	
MnO	0.16	0.16	0.16	0.16	0.17	
MgO	7.32	8.11	9.68	8.35	7.21	
CaO	10.68	10.02	10.03	9.81	11.38	
Na_2O	2.79	3.24	3.40	3.33	2.41	
K_2O	0.65	0.84	0.93	0.74	0.53	
P_2O_5	0.24	0.28	0.32	0.25	0.28	
L.O.I.	1.13	0.76	1.24	0.43		
Total	98.12	98.49	102.71	98.87	100.34	
Mg-no.[++]	0.57	0.59	0.64	0.60		
Li [ppm]	9.52	10.2	8.23	8.89	-	11.4
Sc	21.7	18.4	18.7	19.8	-	19.9
V	232	185	203	208	-	217
Cr	282	235	294	266	292	353
Co	53.9	55.8	57.2	53.2	-	54.6
Ni	178	214	236	198	155	249
Cu	53.7	66.2	51.7	55.0	-	65.9
Zn	107	115	109	106	105	149
Ga	26.8	30.4	30.9	26.1	-	34.9
Rb	9.55	10.4	11.4	11.6	10	45.6
Y	18.1	17.4	16.9	16.8	-	27.4
Cs	0.128	0.219	0.238	0.080	-	0.743
Sr	438	498	571	412	400	1229
Ba	165	219	233	168	285	1058
Zr	118	145	148	110	202	267
Hf	3.23	3.82	3.94	3.07	-	5.90
Nb	12.0	23.0	25.2	10.5	-	105
Ta	0.671	1.25	1.28	0.576	-	5.58
Pb	1.93	2.02	2.17	2.37	-	4.42
Th	1.70	2.04	2.54	1.92	-	10.6
U	0.554	0.533	0.634	0.325	-	2.48
La	13.5	16.8	20.5	14.1	-	79.8
Ce	29.9	36.1	41.0	30.6	-	151
Pr	3.88	4.60	4.99	3.89	-	16.8
Nd	16.8	19.6	20.4	16.6	-	64.3
Sm	4.20	4.68	4.73	4.01	-	12.0
Eu	1.46	1.55	1.61	1.41	-	3.55
Gd	4.35	4.59	4.60	4.13	-	9.94
Tb	0.677	0.705	0.693	0.646	-	1.29
Dy	3.91	3.89	3.85	3.71	-	6.37
Ho	0.744	0.720	0.694	0.689	-	1.07
Er	1.92	1.82	1.72	1.79	-	2.53
Tm	0.258	0.240	0.231	0.245	-	0.307
Yb	1.62	1.49	1.40	1.52	-	1.80
Lu	0.232	0.215	0.196	0.215	-	0.241

Table 2. Sr, Nd, and Pb isotopic compositions of selected Syrian lavas.

	isotopic compositions							age corrected isotopic compositions					
Sample	$^{87}Sr/^{86}Sr$	(2s)	$^{143}Nd/^{144}Nd$	(2s)	$^{206}Pb/^{204}Pb$	$^{207}Pb/^{204}Pb$	$^{208}Pb/^{204}Pb$	Age* [m.y.]	$^{87}Sr/^{86}Sr_T$	$^{143}Nd/^{144}Nd_T$	$^{206}Pb/^{204}Pb_T$	$^{207}Pb/^{204}Pb_T$	$^{208}Pb/^{204}Pb_T$
SY-053	0.705086	(9)	0.512902	(9)	18.950	15.605	38.745	5.00	0.70508	0.512897	18.93	15.60	38.73
SY-101	0.703588	(11)	0.512960	(9)	19.082	15.598	38.799	3.50	0.70359	0.512957	19.07	15.60	38.78
SY-103	0.703158	(10)	0.512904	(6)	19.054	15.614	38.816	3.50	0.70316	0.512901	19.04	15.61	38.80
SY-109	0.703638	(12)	0.512882	(12)	18.806	15.613	38.611	1.84	0.70364	0.512881	18.80	15.61	38.60
SY-113	0.703159	(11)	0.512989	(6)	18.986	15.600	38.758	1.84	0.70316	0.512987	18.98	15.60	38.75
SY-138	0.703321	(10)	0.512904	(17)	19.080	15.652	39.016	5.14	0.70332	0.512899	19.07	15.65	39.00
SY-150	0.703095	(10)	0.512929	(13)	18.716	15.604	38.522	5.14	0.70309	0.512924	18.70	15.60	38.51
SY-152	0.703148	(11)	0.512927	(13)	18.946	15.607	38.732	5.14	0.70314	0.512922	18.93	15.61	38.71
SY-157	0.703064	(9)	0.512948	(7)	18.868	15.601	38.656	5.14	0.70306	0.512944	18.85	15.60	38.64
SY-160	0.703256	(10)	0.512910	(13)	18.966	15.631	38.847	8.00	0.70325	0.512903	18.94	15.63	38.81
SY-174	0.703454	(15)	0.512874	(13)	18.848	15.649	38.826	5.14	0.70345	0.512869	18.84	15.65	38.81
SY-285	0.703231	(9)	0.512901	(12)	19.352	15.627	39.139	5.37	0.70323	0.512897	19.33	15.63	39.11
SY-286	0.703219	(11)	0.512934	(4)	19.403	15.617	39.126	5.37	0.70322	0.512930	19.37	15.62	39.09
SY-290	0.703323	(11)	0.512938	(16)	18.880	15.611	38.694	5.00	0.70332	0.512933	18.87	15.61	38.68
SY-291	0.703651	(11)	0.512896	(6)	18.922	15.620	38.761	5.00	0.70365	0.512891	18.91	15.62	38.75
SY-296	0.703482	(13)	0.512861	(15)	18.945	15.631	38.814	5.00	0.70348	0.512857	18.93	15.63	38.80
SY-303	0.703040	(12)	0.512971	(13)	19.024	15.586	38.712	0.50	0.70304	0.512970	19.02	15.59	38.71
SY-305	0.703893	(9)	0.512870	(13)	18.920	15.621	38.771	2.86	0.70389	0.512868	18.92	15.62	38.76
SY-312	0.703019	(9)	0.512961	(12)	19.073	15.600	38.749	0.40	0.70302	0.512960	19.07	15.60	38.75
SY-316	0.703700	(10)	0.512919	(15)	19.056	15.609	38.722	2.00	0.70370	0.512917	19.05	15.61	38.72
SY-318	0.703674	(11)	0.512946	(5)	18.994	15.635	38.820	1.22	0.70367	0.512945	18.99	15.63	38.82
SY-319	0.703385	(11)	0.512929	(13)	18.971	15.602	38.696	1.22	0.70338	0.512928	18.97	15.60	38.69
NE 02	0.703476	(10)			19.216	15.609	38.861	2.00	0.70348		19.21	15.61	38.85
NE 03	0.703323	(23)			19.220	15.628	38.919	2.00	0.70332		19.21	15.63	38.91
NE 05	0.703378	(13)			19.246	15.610	38.996	2.00	0.70338		19.24	15.61	38.99
NE 06	0.704143	(15)			18.924	15.629	38.785	2.00	0.70414		18.92	15.63	38.78
NE 07	0.703949	(15)			18.980	15.605	38.915	2.00	0.70395		18.97	15.60	38.91
NE 08	0.703942	(18)			18.986	15.608	38.946	2.00	0.70394		18.98	15.61	38.94
NE 09	0.704092	(10)			18.975	15.645	38.955	2.00	0.70409		18.97	15.64	38.95
NE 10	0.704357	(11)			18.909	15.617	38.846	2.00	0.70435		18.90	15.62	38.84
NE 12	0.704270	(12)			19.071	15.685	39.025	2.00	0.70427		19.07	15.69	39.02
NE 13	0.704071	(12)			19.003	15.613	38.899	2.00	0.70407		19.00	15.61	38.89
NE 14	0.704072	(16)			19.050	15.607	38.979	3.92	0.70407		19.04	15.61	38.96
NE 15	0.704290	(13)			18.973	15.716	39.094	2.00	0.70429		18.97	15.72	39.09

*correction age depends on geological map of Ponikarov et al. (1963), K-Ar ages of Sharkov et al. (1994), Mouty et al. (1992) and Giannerini et al. (1988), and Ar-Ar data presented herein

Table 3. Incremental heating and single-particle total fusion $^{40}Ar/^{39}Ar$ analyses on groundmass separates and plagioclase phenocrysts from Syrian volcanic rocks.

Matrix step-heating			**Age spectrum plateau age**				**Total gas age**	**Inverse isochron analysis**			
Sample	Mass [µg]	Analysis type	Age ± 1s [Ma]	^{39}Ar %	MSWD	n (N)	Age ± 1s [Ma]	Age ± 1s [Ma]	$^{40}Ar/^{36}Ar$ intercept ± 1s		MSWD
SY-028	6668	HR-IHA	**11.84 ± 0.12**	57.2	1.0	9(20)	12.20 ± 0.11	12.15 ± 0.16	299.3	± 4.2	2.10
SY-041	4912	HR-IHA	**12.27 ± 0.17**	53.9	0.52	7(20)	15.0 ± 0.2	12.56 ± 0.42	305.3	± 2.1	7.10
SY-060	7350	HR-IHA	**19.41 ± 0.09**	83.4	1.01	14(20)	20.80 ± 0.43	18.74 ± 0.33	300.7	± 1.2	0.66
SY-113	5075	HR-IHA	**1.84 ± 0.09**	79.1	0.57	14(20)	2.27 ± 0.11	1.80 ± 0.09	302.4	± 1.0	1.27
SY-151	5248	HR-IHA	**5.14 ± 0.08**	70.1	1.8	11(20)	5.18 ± 0.11	5.06 ± 0.14	296.9	± 2.1	1.69
SY-203	5704	HR-IHA	3.40 ± 0.09	100	1.0	20(20)	3.37 ± 0.11	3.28 ± 0.15	299.4	± 3.3	0.84
SY-203 (rpt.)	6690	HR-IHA	3.21 ± 0.08	100	1.5	20(20)	3.28 ± 0.11	3.03 ± 0.23	300.5	± 5.0	1.45
		Combined	**3.30 ± 0.06**								
SY-224	4852	HR-IHA	**4.19 ± 0.12**	83.7	0.82	14(20)	4.61 ± 0.16	3.83 ± 0.32	298.4	± 1.7	1.54
SY-234	7173	HR-IHA	***4.27 ± 0.25***	*35.9*	*1.8*	*7(20)*	*5.99 ± 0.31*	*1.20 ± 0.37*	*301.3*	*± 0.5*	*1.52*
SY-283	6239	HR-IHA	***11.70 ± 1.40***	*38.1*	*1.4*	*5(20)*	*13.8 ± 0.8*	*10.1 ± 2.6*	*304.1*	*± 2.1*	*18.9*
SY-284	7697	HR-IHA	**5.36 ± 0.15**	93.5	0.85	15(20)	6.52 ± 0.19	3.79 ± 0.21	299.2	± 0.3	0.81
SY-305	4810	HR-IHA	**2.86 ± 0.15**	70.1	1.2	12(20)	3.26 ± 0.17	3.12 ± 0.25	295.5	± 2.7	2.91
SY-314	7416	HR-IHA	**0.40 ± 0.10**	95.3	1.4	14(20)	0.73 ± 0.15	0.02 ± 0.19	298.6	± 0.9	1.49
NE 14	7098	HR-IHA	**3.92 ± 0.26**	80.8	0.85	12(20)	4.80 ± 0.33	3.12 ± 0.55	298.5	± 1.2	1.81

Feldspar single-crystal total fusion		**Mean apparent age**			**Total gas age**	**Inverse isochron analysis**			
Sample	Analysis type	Age ± 1s [Ma]	MSWD	n (N)	Age ± 1s [Ma]	Age ± 1s [Ma]	$^{40}Ar/^{36}Ar$ intercept ± 1s		MSWD
SY-038	MSP-TF	**11.14 ± 0.43**	1.14	13(13)	11.12 ± 0.46	9.81 ± 2.02	298.8	± 4.8	1.19
SY-206	MSP-TF	**1.82 ± 0.54**	0.40	11(11)	2.32 ± 0.72	0.58 ± 2.26	299.0	± 6.0	0.40
SY-267	MSP-TF	**5.67 ± 0.05**	1.08	12(12)	5.67 ± 0.05	5.55 ± 0.15	303.1	± 7.4	1.07

HR-IHA = High-resolution incremental heating analyses; MSP-TF = multiple single-particle total fusions. Rpt. = duplicate step-heating analyses on same sample. Combined = weighted average of duplicate runs. Reported 40Ar/39Ar dates are weighted age estimates and errors (1s) including uncertainties in the J value (~0.08%). MSWD = Mean Square Weighted Deviates for plateau ages and inverse isochrons calculated for N-2 df. N = total number of heating steps. n = number of heating steps in plateau comprising percent fraction of cumulative 39Ar release. Boldface: accepted ages based on single incremental heating analysis plateaus or weighted means from two duplicate runs. Oblique: results rejected because of plateau size deficiency or disturbed spectra.

Incremental heating $^{40}Ar/^{39}Ar$ age determinations were carried out on microcrystalline groundmass separates and plagioclase phenocrysts using an Ar-ion laser combined with a MAP-216 mass spectrometer at the Leibnitz Institut für Meereswissenschaften in Kiel, Germany. The mass spectrometer is equipped with a Baur-Signer-type ion source, a Johnston electron multiplier, and an ultra-clean gas cleanup line (~600 cc; Zr-Al getters; liquid nitrogen cold trap). Ion beam currents were measured with the electron multiplier at m/z = 36 to 40 and half-mass baselines with an 7.5 digit integrating HP multimeter. Peak heights were regressed to inlet time. The peak decay typically being less than 10% during the analyses. Average extraction line blanks are determined as $2x10^{17}$ mol at m/z = 36 and $4x10^{16}$ mol at m/z = 40. Mass discrimination was monitored using air-fused zero age basaltic glass and pipette air samples (1.0083 ± 0.0006 amu). Correction factors for interferring neutron reactions on Ca and K were determined from co-irradiated CaF_2 and K_2SO_4 salt crystals ($^{36}Ca/^{39}Ca$ = 0.445±0.005, $^{37}Ca/^{39}Ca$ = 1006±7, $^{38}K/^{39}K$ = 0.0168, $^{40}K/^{39}K$ = 0.004±0.002). $^{40}Ar/^{39}Ar$ ages were measured relative to the flux monitor standard TCR sanidine (27.92 Ma; Duffield and Dalrymple, 1990), uncertainties for the J-values being estimated as ± 0.08% (1Sigma). Incremental heating plateau ages (and single-particle mean apparent ages) were calculated as weighted mean (Taylor, 1982) and initial $^{40}Ar/^{36}Ar$ isotope ratios and isochron ages as least squares fit with correlated errors (York, 1969) applying the decay constants of Steiger and Jäger (1977). We analysed 13 samples from Syria using $^{40}Ar/^{39}Ar$ incremental heating techniques. From three more samples (SY-206, SY-267 and SY-038) plagioclase feldspar phenocrysts were analysed by single-crystal fusion. Results are compiled in Table 3 and are displayed in age plateau diagrams in Figure 3.2.

3.4 Results

3.4.1 $^{40}Ar/^{39}Ar$ mineral and whole rock ages and spectra

Most of the high-resolution incremental heating analyses yield well-defined age plateaus, with numerous consecutive gas release steps in the mid temperature range comprising a significant fraction (>50%) of the cumulative ^{39}Ar yield and apparent ages identical within error (2Sigma; excluding uncertainties in the J-value, Fig. 3.2). Frequently, elevated apparent ages at the edges of the spectra and systematically higher total gas (“K-Ar”) ages demonstrate the efficiency of the incremental heating procedure in selectively releasing low-, medium-, and high-temperature argon reservoirs (alteration products with or without ^{39}Ar recoil, Ar release from primary K-bearing mineral phases (i.e. plagioclase), and mafic high-temperature mineral phases with inherited excess ^{40}Ar, i.e. clinopyroxene and olivine, respectively).

Matrix analyses SY-234, SY-283, and SY-314 and feldspar analysis SY-206 show not well defined spectra but are included to demonstrate the limits of the analytical approach (Fig. 3.2; SY-206 not shown). Matrix analyses SY-234 and SY-283 display acceptable single-step precisions, but the overall spectra are strongly disturbed in the high-temperature gas release region,

which yields apparent ages ($^{40}Ar/^{39}Ar$ ratios) significantly higher than the small medium-temperature plateau intervals, being most likely derived from groundmass clinopyroxene with initial $^{40}Ar/^{36}Ar$ ratios >295.5 (Fig. 3.2). Matrix SY-314 and feldspars SY-206, in turn, are very young (several 100,000 years), and neither sample mass (K-content) nor irradiation parameters are suitable for argon isotope analyses with decent precisions.

Inverse isochron analysis of the entire incremental heating data sets yields isochrons with acceptable mean square weighted deviates for all samples except SY-041 and SY-283 (Table 3). Isochron ages that are generally identical to the plateau ages within 1? or 2? uncertainties, but also yield virtual initial $^{40}Ar/^{36}Ar$ ratios slightly higher than atmosphere (296 to 305), reflecting either (a) systematically elevated initial $^{40}Ar/^{36}Ar$ ratios in most samples, or (b) counterclockwise tilting of the isochron (mixing) lines from low-temperature, high-atmosphere gas releases due to secondary mineral and ^{39}Ar recoil. Isochron ages, however, are not systematically younger than the plateau ages, as would be expected from counterclockwise rotation (Table 3). Moreover, the flatness and extent of the plateau regions reflect homogeneous Ar sources with respect to radiogenic and other Ar isotope components throughout most spectra. Therefore, the virtual initial $^{40}Ar/^{36}Ar$ ratios >295.5 are considered to be artifacts and the plateau ages are considered superior to isochron ages.

A duplicate incremental heating analysis with varied sample mass and heating schedule was carried out on matrix sample SY-203. The analyis gave plateau ages identical within error (3.40±0.09 Ma vs. 3.21±0.08 Ma), which are combined into an inverse-variance weighted mean age of 3.30±0.06 Ma (Fig. 3.2, Table 3).

3.4.2 Sr, Nd, and Pb isotopes

In the following our data of the Syrian part of the Harrat Ash Shamah (HAS) will be combined with published data (Barberi et al., 1980; Giannerini et al., 1988; Altherr et al., 1990; Mouty et al., 1992; Stein and Hofmann, 1992; Mor, 1993; Nasir, 1994; Sharkov et al., 1994; Weinstein et al., 1994; Tarawneh et al., 2000; Ilani et al., 2001; Bertrand et al., 2003; Shaw et al., 2003;) from the remaining parts of this large volcanic field. The Syrian samples recovered further north than the HAS are also supplemented by published volcanic data (Giannerini et al., 1988; Mouty et al., 1992; Sharkov et al., 1994; Butler et al., 1997; Sharkov et al., 1998; Bertrand et al., 2003) (Fig. 3.1b). The northern Syrian lavas display large variations in $^{87}Sr/^{86}Sr$ and $^{143}Nd/^{144}Nd$ isotope compositions with most of them lying on a negative correlation. Only a few lavas trend to high $^{87}Sr/^{86}Sr$, whereby $^{143}Nd/^{144}Nd$ ratios remain constant at around 0.5129 (Fig. 3.3a). Compared with the northern Syrian group the HAS lavas show less extreme isotopic variation. Both groups overlap with volcanic rocks from Yemen and Saudi Arabia and largely with lavas from the Afar region (i.e. lavas erupted in Ethiopia and Djibouti). However, the Afar lavas with the highest $^{3}He/^{4}He$ isotope composition have significantly higher $^{87}Sr/^{86}Sr$ and lower

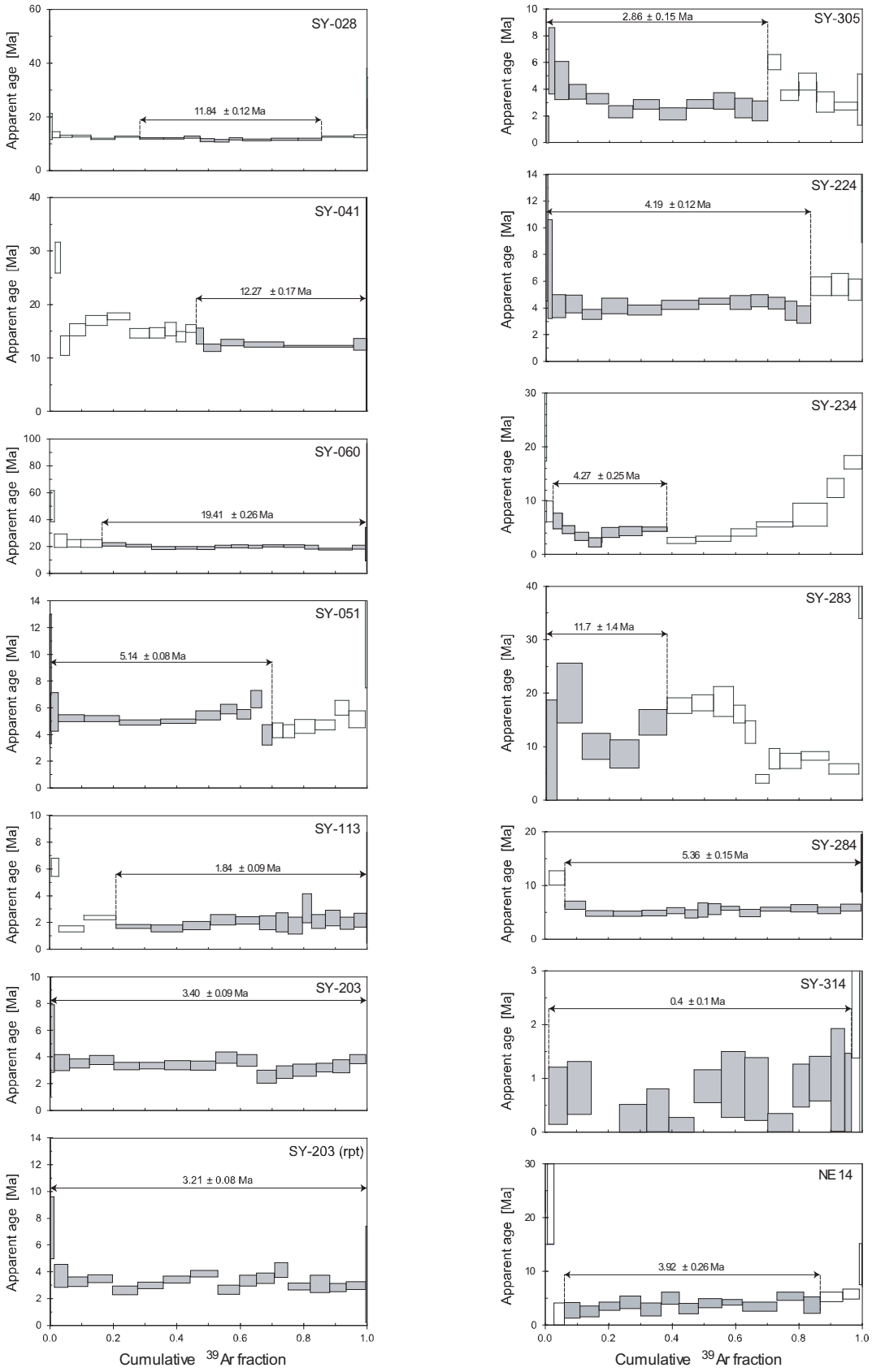

Fig. 3.2. Microcrystalline groundmass $^{40}Ar/^{39}Ar$ incremental heating analyses. Reported $^{40}Ar/^{39}Ar$ dates are weighted age determinates and errors of the plateau fractions at the 1σ confidence level including 0.08% standard deviation in the J-value. Plateau ranges and ^{39}Ar fractions as indicated. All samples were analysed using Taylor Creek Rhyolite TCR sanidine (27.92 Ma; Duffield and Dalrymple, 1990) as irridiation standard.

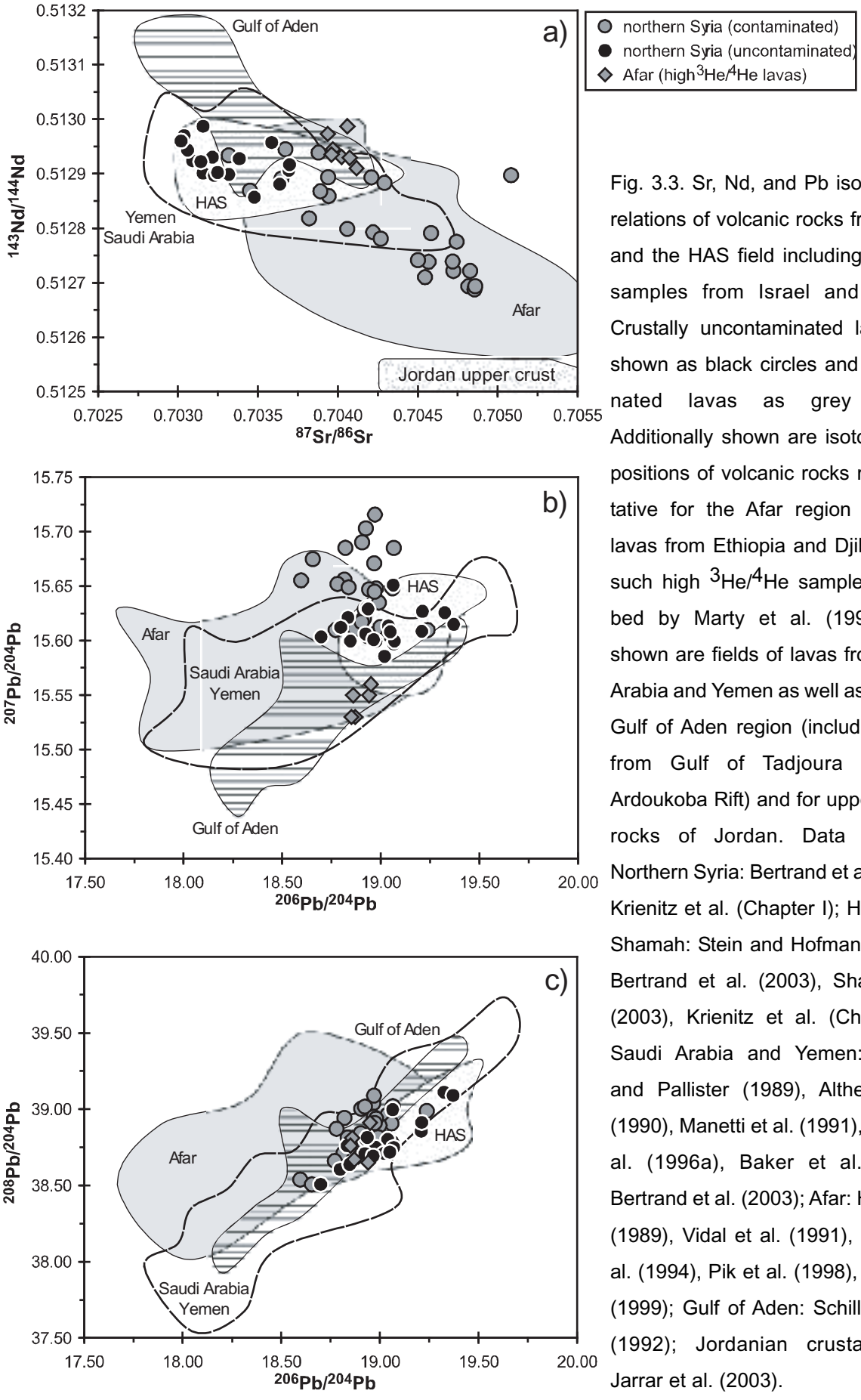

Fig. 3.3. Sr, Nd, and Pb isotope correlations of volcanic rocks from Syria and the HAS field including volcanic samples from Israel and Jordan. Crustally uncontaminated lavas are shown as black circles and contaminated lavas as grey circles. Additionally shown are isotope compositions of volcanic rocks representative for the Afar region including lavas from Ethiopia and Djibouti and such high $^{3}He/^{4}He$ samples described by Marty et al. (1996). Also shown are fields of lavas from Saudi Arabia and Yemen as well as from the Gulf of Aden region (including lavas from Gulf of Tadjoura and the Ardoukoba Rift) and for upper crustal rocks of Jordan. Data sources: Northern Syria: Bertrand et al. (2003), Krienitz et al. (Chapter I); Harrat Ash Shamah: Stein and Hofmann (1992), Bertrand et al. (2003), Shaw et al. (2003), Krienitz et al. (Chapter II); Saudi Arabia and Yemen: Hegner and Pallister (1989), Altherr et al. (1990), Manetti et al. (1991), Baker et al. (1996a), Baker et al. (1997), Bertrand et al. (2003); Afar: Hart et al. (1989), Vidal et al. (1991), Deniel et al. (1994), Pik et al. (1998), Pik et al. (1999); Gulf of Aden: Schilling et al. (1992); Jordanian crustal rocks: Jarrar et al. (2003).

$^{207}Pb/^{204}Pb$ compared to all Syrian lavas whereas volcanic rocks of the Gulf of Aden region generally trend to higher $^{143}Nd/^{144}Nd$ (Fig. 3.3a).

All Syrian lavas yield a restricted range of $^{206}Pb/^{204}Pb$ between 18.60 and 19.50 when compared to lavas from other Afro-Arabian regions but they exhibit significant scatter in $^{207}Pb/^{204}Pb$ at a constant $^{206}Pb/^{204}Pb$ of about 19.00 (Fig. 3.3b). In contrast, the Syrian lavas show a relatively small variation in $^{208}Pb/^{204}Pb$ and a broad positive correlation can be observed with $^{206}Pb/^{204}Pb$ in the HAS and Syrian lavas (Fig. 3.3c). The Syrian lavas overlap with samples from Saudi Arabia and Yemen, the Gulf of Aden, and the Afar region but generally range to higher $^{206}Pb/^{204}Pb$ compositions and some have significantly higher $^{207}Pb/^{204}Pb$ than the lavas form the other regions. The HAS lavas trend to slightly higher $^{206}Pb/^{204}Pb$ compared to the northern Syrian lavas (Fig. 3.3c). In a plot of $^{206}Pb/^{204}Pb$ versus $^{87}Sr/^{86}Sr$ most of the north Syrian lavas as well as the HAS lavas show a large range of Sr isotopic compositions at $^{206}Pb/^{204}Pb$ between 18.80 and 19.10 (Fig. 3.4a). North Syrian lavas with $^{87}Sr/^{86}Sr$ <0.7035 exhibit a positive correlation between Sr and Pb isotopic compositions. Syrian lavas with high $^{206}Pb/^{204}Pb$ have relatively high $^{143}Nd/^{144}Nd$ whereas lavas with low Nd isotope ratios also have low $^{206}Pb/^{204}Pb$. A negative correlation of some of the Syrian samples is also observed in the HAS group trending from most radiogenic $^{206}Pb/^{204}Pb$ to compositions characterised by Gulf of Aden lavas with highest $^{143}Nd/^{144}Nd$ but lowest $^{206}Pb/^{204}Pb$ ratios (Fig.

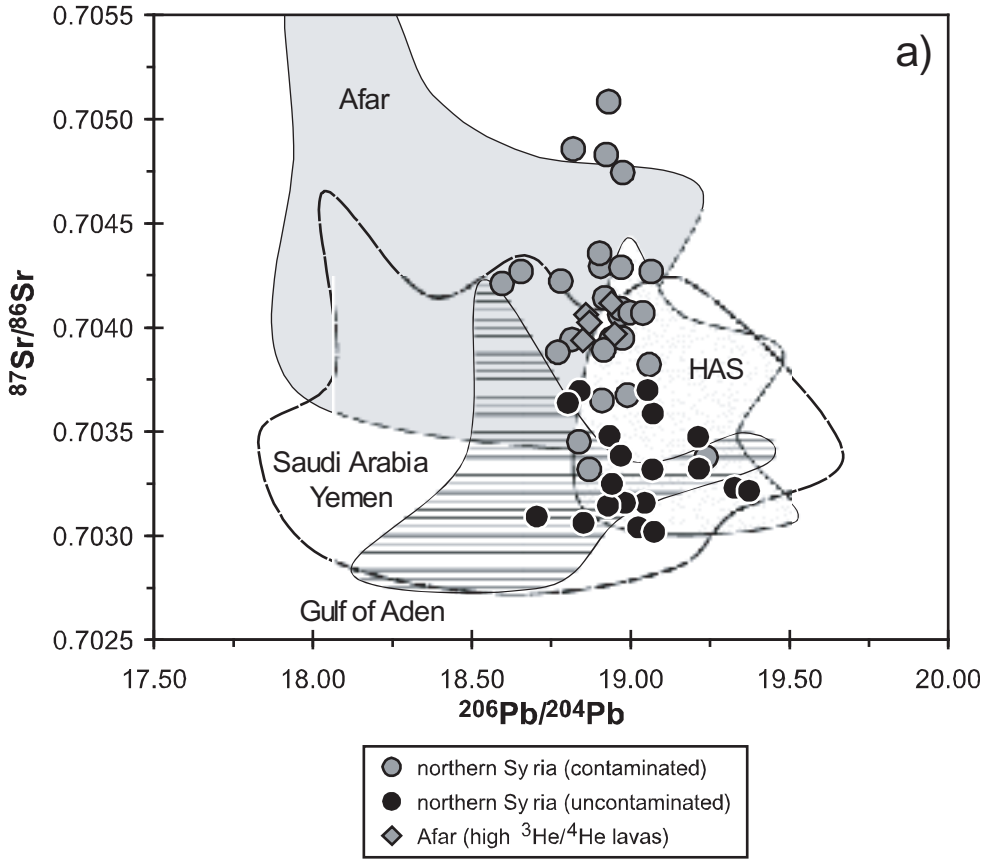

Fig. 3.4. Diagrams of (a) $^{87}Sr/^{86}Sr$ and (b) $^{143}Nd/^{144}Nd$ versus $^{206}Pb/^{204}Pb$. Data sources as in Figure 3.3.

3.4b).

3.3 Discussion

3.3.1 Temporal implications on volcanism

The new $^{40}Ar/^{39}Ar$ ages of Syrian lavas recovered from locations nearby previous dated regions (Mouty et al., 1992) yield explicit younger ages. We interpret that these old K-Ar ages of 130 Ma and 90 Ma (Mouty et al., 1992) are probably caused by the analysis of altered sample material. In the following discussion we will focus on the episodes of volcanic activity occurring during the last 35 Ma in the

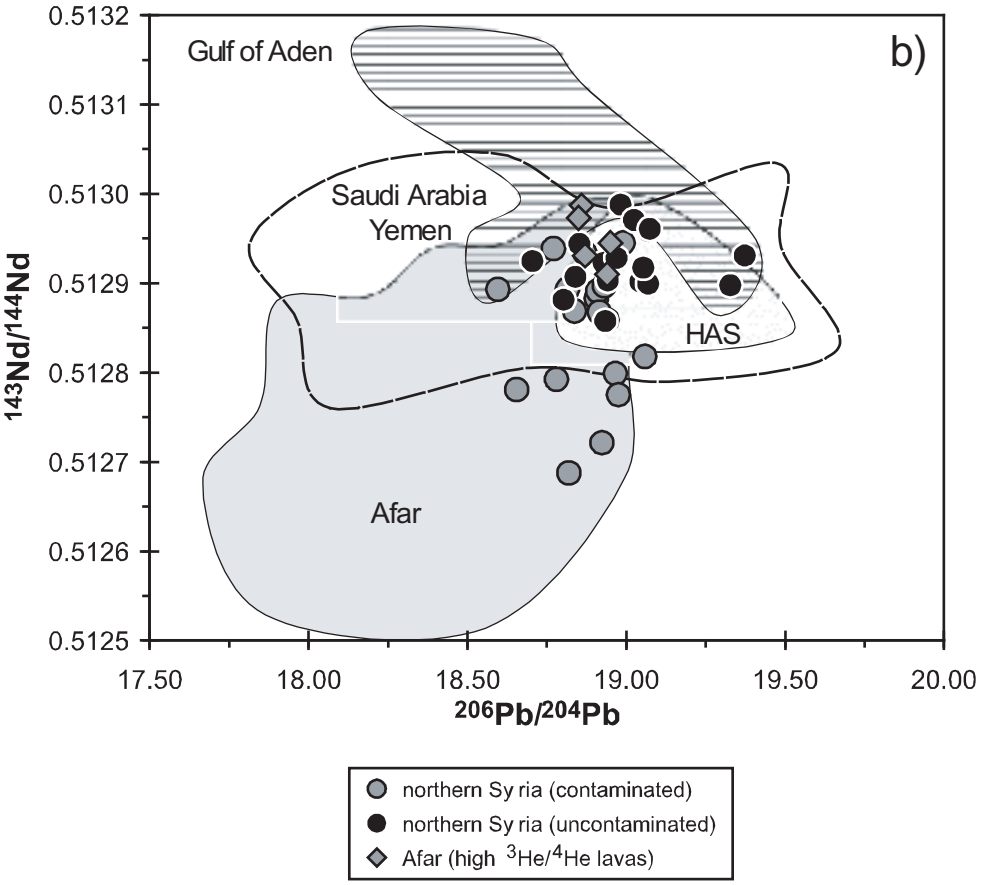

Fig. 3.4. continued

Afro-Arabian region.

The oldest volcanism (<16 Ma) in Syria is restricted to the western part of the country near the Dead Sea transform fault, whereas at later times volcanic activity in the vicinity of the Dead Sea fault system and in the region of the HAS volcanic has been rather periodic (Figs. 3.1 and 3.5a). Krienitz et al. (Chapter II) have shown that volcanism in the HAS is consistent with magma generation in a pulsing mantle plume regime. The temporal and spatial distribution of volcanic activity in Syria can be attributed to minor extension at the Dead Sea transform fault system accompanied by the inflow of plume material along preexisting weak zones of the continental lithosphere. Interestingly the magmatic activity in the northeastern parts of the country is restricted to the youngest magmatic phase (4 Ma – 0 Ma) and thus may indicate the northward migration of the plume mantle material (Fig. 3.5a).

Figure 3.3b shows a compilation of K-Ar and Ar-Ar ages of lavas from the Afro-Arabian area together with major tectonic events. Concidering the whole Afro-Arabian region the timing of volcanism reveals a progressive south to north decrease for the commencing volcanic activity.

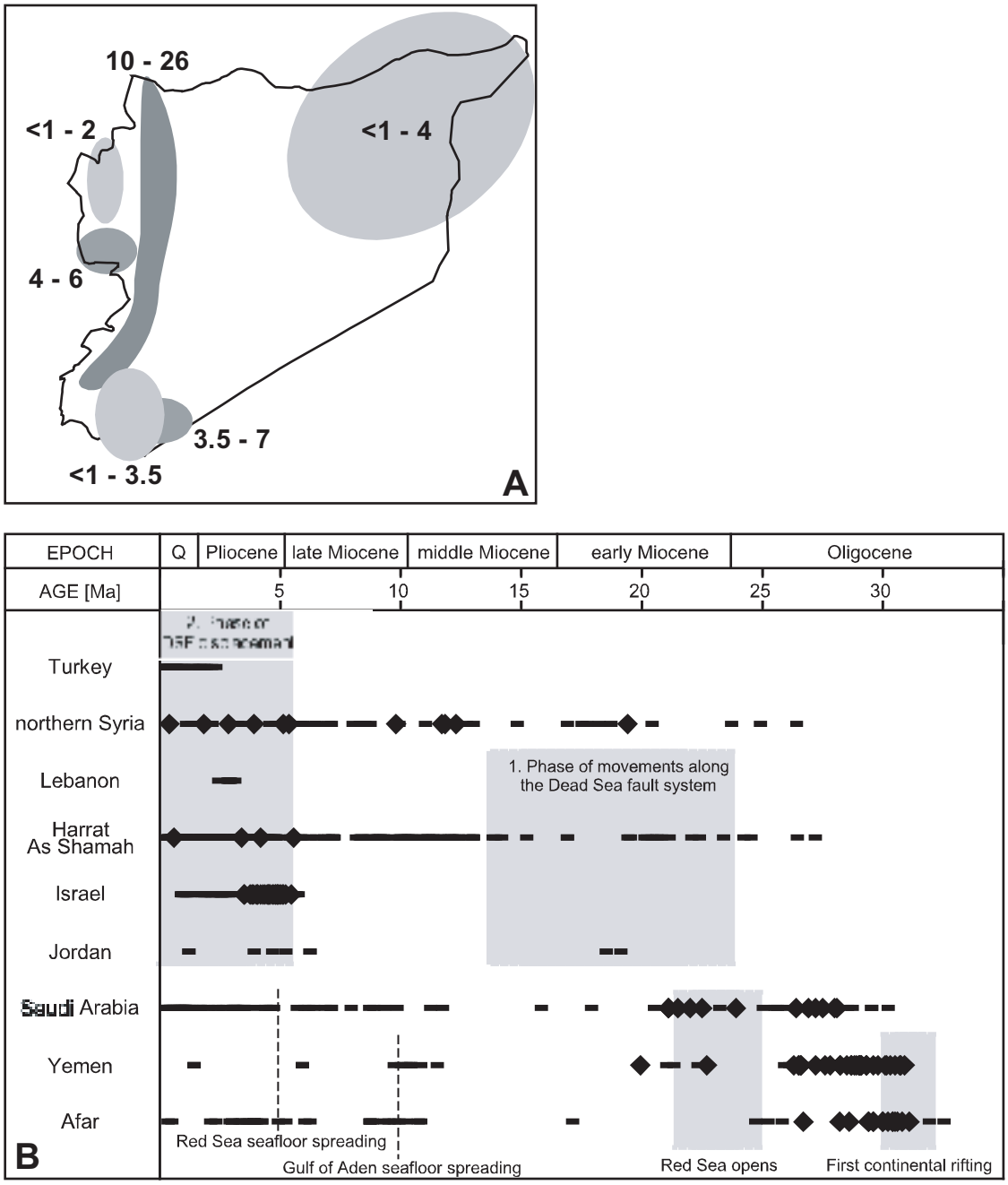

Fig. 3.5. (a) Sketch of Syria. Grey fields denote the spatial distribution of volcanic rocks together with age information. Numbers give ages in Ma. (b) Radiometric ages of volcanic rocks of the Afar region and the western Arabian edge correlated with major tectonic events in the Afro-Arabian area. K-Ar ages are given by rectangles and Ar-Ar ages are denoted by diamonds. Data sources: Harrat Ash Shamah and northern Syria: as noted in the text; Turkey: Capan et al. (1987), Notsu et al. (1995), Rojay et al. (2001); Lebanon: Mor (1993); Israel: Heimann and Ron (1993), Heimann et al. (1996); Jordan: Barberi et al. (1980), Heimann et al. (1996); Saudi Arabia: Camp and Roobol (1989), Hegner and Pallister (1989), Altherr et al. (1990), Camp et al. (1991), du Bray et al. (1991), Sebai et al. (1991); Yemen: Manetti et al. (1991), Baker et al. (1996a); Afar: Hart et al. (1989), Hofmann et al. (1997).

Accompanied by first continental rifting volcanism started in Ethiopia and Yemen circa 31 Ma ago (Ukstins et al., 2002) indicating the arrival of the Afar plume head (Hofmann et al., 1997). The northward migration of volcanism with time appears to be a reflection of the flattening of the Afar plume head and indicate continuing plume flow underneath Arabia. These observation support the model of Camp and Roobol (1992) about the northward channelling of hot mantle material. With respect to the more precise Ar-Ar ages of lavas and assuming that the Afar plume contributed to the earliest volcanism which is recognised along the western Arabian plate from Yemen (~31 Ma) over 2,500 km to northern Syria (~19 Ma) an average flow velocity of the plume material of about 21 cm/a can be calculated (Fig. 3.5b). This calculated mantle flow velocity of the plume material is somewhat lower compared to the Hawaiian plume with vertical upwelling rates of up to 34 cm/a on the plume axis (Watson and McKenzie, 1991). After a phase of relative volcanic quietness between roughly 16 Ma and 13 Ma, the renewal of volcanic activity comprises the whole Afro-Arabian area, whereby a northward migration of volcanism cannot be observed. The similarity of the onset of volcanism is taken as evidence for the relation of this volcanism to movements along the Red Sea and the begin of Gulf of Aden sea floor spreading (Cochran, 1981; Hempton, 1987; Brew et al., 2001) (Fig. 3.5b). Since the last 5 to 6 Ma enhanced volcanism in the Afro-Arabian area can also be recognised corresponding to the second phase of movements along the Dead Sea fault and the commencing ocean floor spreading in the Red Sea (Girdler and Styles, 1974; Hempton, 1987; Girdler, 1990) (Fig. 3.5b). However, although the volcanic activity is, in some respects, passively induced by extensional processes due to movements along major plate boundaries, the spatial and temporal variations of volcanism imply a plume influence in the northern Arabian region (Fig. 3.5b).

The contribution of the Afar plume northwards over a distance more than 2,500 km exceeds the predicted dimensions (~2,000 km in diameter) of flattened plume heads (Griffiths and Campbell, 1990) and also the distribution of the Afar plume with an radius of 1,000 km as proposed by Schilling et al. (1992) and Marty et al. (1996) based on Sr, Nd, Pb, and He isoptopes in lavas (Fig. 3.1a) On the other hand Hopp et al. (2004) argued on the basis of Ne and He isotopes that the influence of the Afar plume can be traced to the northern parts of the Red Sea and thus over a distance of about 1,800 km (Fig. 3.1a). This dimension resembles our suggested range of the plume influence and agrees with the model of Camp and Roobol (1992) that the evolution of the Afro-Arabian dome is a consequence of northwards directed flow of hot mantle material probably generated in the Afar region (Fig. 3.1a).

3.5.2 Mantle sources contributing to the continental Afro-Arabian volcanism

Since magmas in continental regions can be affected by the assimilation of crustal material the evaluation of primary mantle source characteristics has to include the elimination of these contamination effects. To identify crustally contaminated magmas the Ce/Pb and Nb/U ratios of lavas can be used. Average Ce/Pb ratios of 25±5 and Nb/U ratios of 47±10 are characteristic for lavas

erupted at mid-ocean ridges and for ocean island basalts (Hofmann et al., 1986), and, in fact, appear typically for lavas directly derived from the Earth's mantle. In contrast, crustal rocks exhibit significantly lower Ce/Pb and Nb/U ratios, but generally are characterised by high SiO_2 contents, radiogenic $^{87}Sr/^{86}Sr$ and unradiogenic Nd isotopic compositions. As illustrated in figure 3.4a the broad negative correlation of Sr and Nd isotopes, most notably shown by the northern Syrian rocks, trend to crustal compositions exemplarily displayed by Jordanian upper crustal rocks with high $^{87}Sr/^{86}Sr$ and low $^{143}Nd/^{144}Nd$ (Jarrar et al., 2003). In the following discussion we will disregard the Nb/U ratios, because of the mobile behaviour of U, and the Sr isotope compositions, because of its sensitivity to possible alteration processes. Instead we will focus on those lavas yielding Ce/Pb ratios >20 and $^{143}Nd/^{144}Nd$ compositions that lie above 0.51280.

The variable isotope compositions of uncontaminated Syrian lavas imply that three mantle sources were involved in magma genesis (Figs. 3.3 and 3.4). One mantle component identified has low $^{143}Nd/^{144}Nd$ (~0.51280) at relatively low Sr isotope ratios (<0.702) and high Pb isotope compositions ($^{206}Pb/^{204}Pb$ ~19.5, $^{207}Pb/^{204}Pb$ ~15.65, $^{208}Pb/^{204}Pb$ ~39.75) (Figs. 3.3 and 3.4). The low $^{143}Nd/^{144}Nd$ ratios indicate a time integrated enrichment of Nd relative to Sm in the source region and thus this end member is relatively enriched in light rare earth elements with respect to an asthenospheric mantle source represented by Gulf of Aden lavas with low Sr and high Nd isotope ratios (Schilling et al., 1992) (Figs. 3.3a and 3.4b). The slightly higher Sr isotope ratios of the Syrian lavas relative to asthenospheric magmas imply higher Rb/Sr ratios of the source region for this mantle component. The component with radiogenic Pb isotopic composition occurs in lavas from north- and southwestern Arabia and from Afar and is also present in lavas from the Gulf of Aden, i.e. from oceanic crust (Schilling et al., 1992; Baker et al., 1996b; Stewart and Rogers, 1996) (Figs. 3.3 and 3.4). Based on oxygen isotope variations in mineral separates of Yemen lavas that exceed the range observed in peridotites from the continental lithospheric mantle Baker et al. (2000) take into consideration that crustal contamination was an important process in the magma genesis and call the inferred role of an enriched lithospheric mantle contributing to volcanism at the Afro-Arabian triple junction into question (Hart et al., 1989; Vidal et al., 1991; Chazot and Bertrand, 1993; Deniel et al., 1994). As we can rule out crustal contamination this end member probably reflects either a lithospheric component or represent a mantle plume. Based on the spatial distribution of lavas with high $^{206}Pb/^{204}Pb$ ratios in western Arabia and due to the absence of this high Pb signature in lavas erupted in the central Red Sea area, these lavas being directly derived from the astenosphere, this mantle component could reflect plume mantle. In our opinion, the fact that this mantle component can be observed in oceanic magmas rules out a continental lithospheric origin. Moreover, the elevated topography in the region of the Aden ridge, where lavas with high $^{206}Pb/^{204}Pb$ were erupted, indicates that hot material is present underneath the Aden region, causing uplift. This is contrary to the hypothesis of Bertrand et al. (2003) attributing this mantle component to the subcontinental lithosphere and interpreting its occurrence in the Gulf of Aden as a remnant part of this lithosphere, which was isolated during extension. Our assumption, however, is supported by seismic

tomography indicating hot mantle material in the Aden region (Daradich et al., 2003) and thus preferentially points to a mantle plume origin of the high Pb signature.

In the Arabian area there are no indications for other mantle plumes but the Afar plume, thus this plume may account for the high Pb isotope ratios in lavas (Fig. 3.1a). Based on Sr, Nd, and Pb isotope compositions the high $^{206}Pb/^{204}Pb$ isotope end member has been attributed to the Afar plume (Schilling et al., 1992; Vidal et al., 1991; Deniel et al., 1994). In contrast, Baker et al. (1996b) and Pik et al. (1999) propose a less radiogenic $^{206}Pb/^{204}Pb$ composition for the plume than the observed high $^{206}Pb/^{204}Pb$ ratios of about 19.5 and attribute this end member to another mantle component. However, the composition of the Afar plume is better constrained considering $^{3}He/^{4}He$ ratios. Marty et al. (1996) stated that Ethiopian lavas with high $^{3}He/^{4}He$ ratios probably reflect undegassed material of the lower mantle. This assumption is assisted by seismic tomography, whereby the Afar hotspot may represent a deep seated mantle plume (Ritsema and Allen, 2003; Montelli et al., 2004). Strikingly the high $^{3}He/^{4}He$ lavas have $^{206}Pb/^{204}Pb$ compositions of about 18.8 (Pik et al., 1999), too low to account for the observed isotopic variations in the Syrian lavas (Figs. 3.3b, 3.3c and 3.4). Moreover, the Ethiopian lavas also have higher $^{87}Sr/^{86}Sr$ for a given $^{143}Nd/^{144}Nd$ (Pik et al., 1999) compared to lavas from Syria (Fig. 3.3a). Thus, this lower mantle component of the Afar plume is can not contribute to Syrians volcanism.

Griffiths and Campbell (1990) noticed that mantle plumes originating from the core/mantle boundary contain a high percentage of entrained material of the overlying upper mantle. If recycled enriched components were stored at upper mantle depths, as it is proposed in the model of Marty et al. (1996) for the evolution of the Ethiopian plume (i.e. the Afar plume), the entrainment process would lead to distinct isotopic signatures in magmas when compared to the initial material rising from the lower mantle. Thus, the plume composition would be heterogeneous and the radiogenic Pb isotope compositions in lavas could be explained by this entrained proportion of the upper mantle. Thus, in our opinion the relatively enriched mantle end member with high $^{206}Pb/^{204}Pb$ ratios represents plume mantle and is associated with the Afar mantle plume. The increasing $^{206}Pb/^{204}Pb$ ratios of the HAS lavas over the past 13 Ma therefore imply an increasing Afar plume influence in the northern Arabian region (Fig. 3.6). This agrees with the proposal of Camp and Roobol (1992) that a period of uplift and magmatism is controlled by active mantle upwelling concentrated along the major axis (MMN line) of the Arabian dome in Saudi Arabia (Fig. 3.1a).

The second end member involved in magma genesis of northern Arabian lavas has low $^{87}Sr/^{86}Sr$ (~0.7030), high $^{143}Nd/^{144}Nd$ (~0.5130) and is characterised by relative unradiogenic Pb isotope ratios (Figs. 3.3 and 3.4). It has been shown that mid ocean ridge tholeiites erupted in the Gulf of Aden and also in the central parts of the Red Sea probably represent the asthenosphere in these regions (Altherr et al., 1988; Eissen et al., 1989; Schilling et al., 1992; Haase et

al., 2000). Based on the similar Sr, Nd, and Pb isotope compositions of the Syrian HAS lavas and Red Sea basalts, Krienitz et al. (Chapter II) proposed that the HAS lavas could have been formed from an incompatible element-enriched asthenospheric source. The trend of the Syrian lavas towards isotopic compositions of the Gulf of Aden lavas with high $^{143}Nd/^{144}Nd$ and low $^{87}Sr/^{86}Sr$ as well as the similar isotope composition of the northern Syrian and the HAS lavas therefore suggests that the second end member probably reflects an asthenospheric mantle

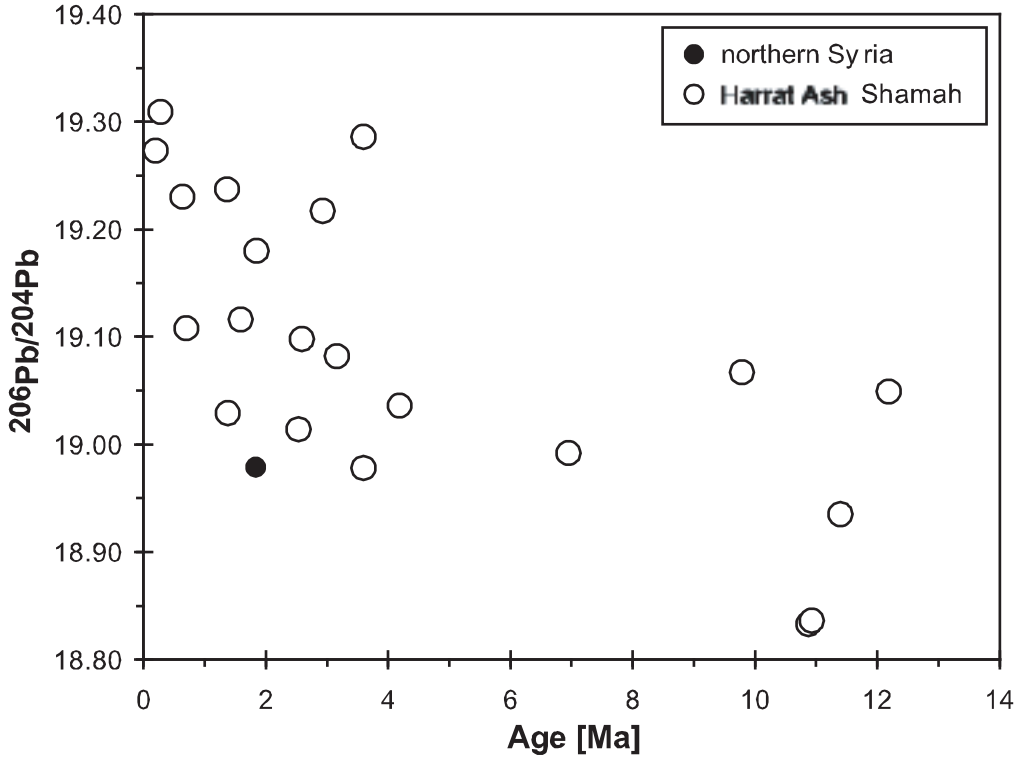

Fig. 3.6. K-Ar and Ar-Ar ages versus $^{206}Pb/^{204}Pb$ for northern Syrian and HAS lavas. The time intervall considered is 14 Ma and the data illustrated include only such samples with Ce/Pb >20 and/or $^{143}Nd/^{144}Nd$ >0.51280. Data sources as in Figure 3.3 and 3.4.

component in northern Arabia (Figs. 3.3 and 3.4).

A third mantle component identified is defined by Sr isotope ratios of ~0.7038 and $^{143}Nd/^{144}Nd$ of about 0.5129 (Figs. 3.3 and 3.4). This mantle component has $^{207}Pb/^{204}Pb$ ratios of ~15.6 for a given $^{206}Pb/^{204}Pb$ of ~18.7 and is present in those Gulf of Aden regions that were interpreted by Schilling et al. (1992) to be in a nascent state of extension (i. e. Gulf of Tadjoura and Ardoukoba rift zone). Because of the low $^{207}Pb/^{204}Pb$ ratios for a given $^{206}Pb/^{204}Pb$ and high $^{87}Sr/^{86}Sr$ ratios of the high $^{3}He/^{4}He$ Afar lavas a contribution of this Afar plume component can be ruled out. Furthermore, the entrained upper mantle proportion of the Afar plume has too radiogenic $^{206}Pb/^{204}Pb$ compared to this end member. Both high $^{143}Nd/^{144}Nd$ ratios and low Sr isotope ratios of Gulf of Aden lavas, which represent the asthenosphere in the Afro-Arabian region, and the absence of the third component in the central parts of the Gulf of Aden argue against an asthenospheric origin of this mantle component. Based on Sr, Nd, and Pb isotope signatures Schilling et al. (1992) interpreted that this end member probably represents a continen-

tal lithospheric component. Because the northern Syrian and HAS lavas trend to compositions similar to these lithosphere influenced lavas of the Gulf of Aden region, the third component probably reflects a continental lithospheric signature in northern Arabian magmatism.

3.3.3 The melting regime in the Afro-Arabian region

In order to determine the mantle melting processes in the Afro-Arabian region we compare fractionation-corrected compositions of uncontaminated lavas, i.e. those within the range of mantle compositions in terms of Ce/Pb and with $^{143}Nd/^{144}Nd$ >0.51280. The used fractionation correction scheme based on the SiO_2 contents is similar to the approach of Klein and Langmuir (1987)

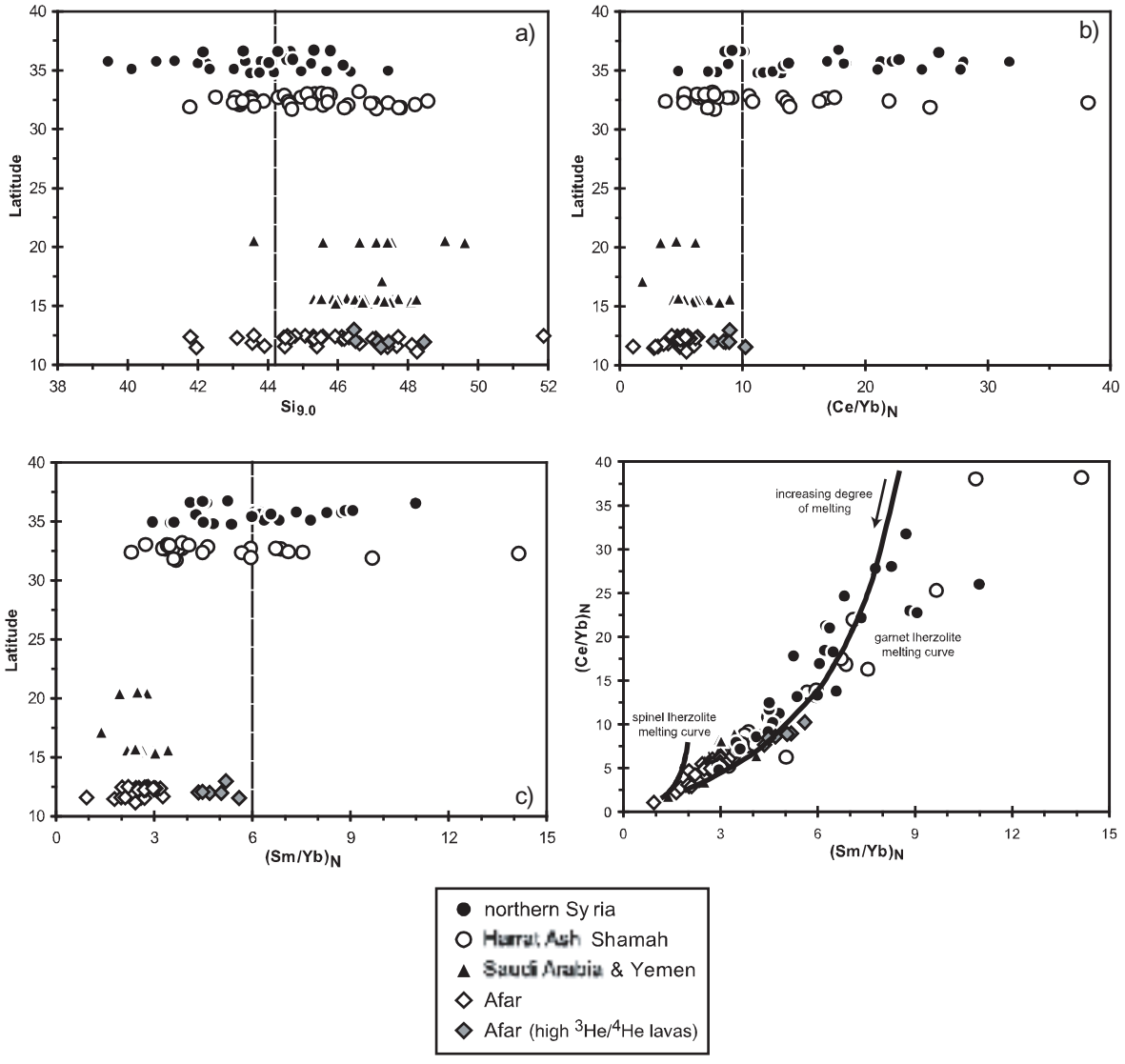

Fig. 3.7. Diagrams of (a) $Si_{9.0}$, (b) chondrite-normalised Ce/Yb, (c) Sm/Yb ratios of lavas versus latitude, and (d) chondrite-normalised Sm/Yb versus Ce/Yb ratios of Arabian and Afar lavas. Exemplarily shown are melting curves of garnet and spinel lherzolites. The compositions of lavas considered include only such samples with MgO >5 wt.%, Ce/Pb >20, and/or $^{143}Nd/^{144}Nd$ > 0.51280. The fractionation correction scheme on the SiO_2 contents is similar to the approach of Klein and Langmuir (1987). Chondrite composition used for normalising is from McDonough and Sun (1995). Data sources as in Figure 3.4.

and includes only lavas with MgO >5 wt.%. It is apparent from figure 3.7a that the SiO_2 concentrations of the Syrian lavas are lower than most of the Saudi Arabian and Afar lavas. Since the SiO_2 concentrations of primitive melts are mainly controlled by melting pressure - decreasing pressures resulting in increasing SiO_2 (Hirose and Kushiro, 1993) - rather than by the degree of melting, the variations in $Si_{9.0}$ suggests that the maximum depths at which melting occured decreases southward along western Arabia. Moreover, if only Afar lavas with high $^3He/^4He$ ratios are taken into account (Marty et al., 1996) this gradient in melting depths can be traced further into the Afar region (Fig. 3.7a).

The chondrite normalised Ce/Yb and Sm/Yb ratios of northern Arabian lavas show large variations and trend to higher ratios compared to Saudi Arabian, Yemen and Afar lavas with low chondrite-normalised Ce/Yb (<10) and Sm/Yb (<6) (Figs. 3.7b and c). These differences may depend on variable mantle source compositions and/or variations in the degree of melting. Since distribution coefficients in garnet are higher for the heavy REEs than for the middle and light ones, melting of a garnet facies mantle results in a strong fractionation of the HREEs and can produce large variations in the LREE/HREE ratios and also in the MREE/LREE ratios. In contrast, melting of a spinel-peridotite would not produce such a strong fractionation of the HREEs and thus would lead to minor variations. The highly variable REE ratios of northern Arabian lavas displayed in Figures 3.7b to 3.7d therefore indicate residual garnet in the source region and thus the generation from a garnet peridotite at high pressures. Krienitz et al. (Chapter II) calculated pressures of melt formation corresponding to depths of 100 to 150 km and have shown that the wide range of REE ratios in the lavas from the Syrian part of the HAS field are caused by melting of garnet bearing mantle sources. Lavas from southern Arabia and Afar have fractionated HREEs being generally lower than northern Arabian lavas indicating either relative minor amounts of garnet in their source regions or larger degrees of melting or both. Baker et al. (1997) have pointed out that the REE patterns of Yemen lavas are produced by mixing of small melt fractions generated in a predominantly garnet peridotite facies mantle with larger degree melts of a spinel peridotite mantle source. We interpret the REE ratios to be to a minor extent controlled by source compositions, i. e. by variable amounts of garnet in the mantle source regions of the Arabian and Afar lavas, whereby the amount of garnet generally should be larger in the north than in the south (Figs. 3.7b to d).

The low SiO_2 contents in lavas are coupled with high Ce/Yb and Sm/Yb ratios suggesting a relation between the extent and depths of melt formation (Figs. 3.7a to c). The commencing melting process probably took place at greater depths with minor degrees of melting in the northern Arabia region compared to other Afro-Arabian regions. This assumption agrees with the conclusions of Shaw et al. (2003) that melt formation in Jordan took place at deeper levels than in Yemen where intraplate volcanism clearly displays the influence of a mantle plume (Baker et al., 1997).

Extensive melting of mantle material at a potential temperature of 1280°C can only occur when the stretchting factor of the lithosphere is in the range between 2 and 5 (McKenzie and Bickle, 1988; White and McKenzie, 1989). Camp and Roobol (1992) calculated a local stretching factor for the lithosphere beneath Saudi Arabia of only ~1.0 and Krienitz et al. (Chapter II) calculated stretching factors for the lithosphere in northwestern Arabia of 1.3 to 1.6. Theses factors are too low to account for melt generation and cannot explain the observed differences in the melting regime in the Afro-Arabian region. Alternatively melting may occur if the source region contains minor amounts of volatiles lowering the solidus or if the temperature is hotter than the average potential mantle temperature of 1280°C. Volatiles are stored in mineral phases such as amphibole or phlogopite in the upper mantle, whereby Le Roex et al. (2001) noticed that amphibole is neither a stable phase under mantle plume nor under asthenospheric mantle conditions. Based on similar isotopic and incompatible trace element signatures of Yemen lavas and amphibole-bearing lithospheric mantle xenoliths Baker et al. (1997) proposed that volcanism in western Yemen appears to be induced by lithospheric extension resulting in melting of shallow mantle that was hydrated due to the influence of the Afar plume. In this context and on the basis of variable isotope and trace element compositions of Syrian HAS lavas Krienitz et al. (Chapter II) proposed that the magmas were generated by both a volatile- and incompatible element-enriched mantle and by a mantle plume with a maximum excess temperature of 180°C. However, the melt formation rather appears to be controlled by elevated mantle temperatures in a mantle plume beneath the Arabian region. This is supported by the elevated topography of these regions, by elevated geotherms calculated on the basis of mantle xenoliths (McGuire and Bohannon, 1989; Snyder et al., 1993; Nasir and Safarjalani, 2000; Al-Mishwat and Nasir, 2004) and heat flow measurements (Gettings, 1981) as well as by seismic tomography (Daradich et al., 2003). The isotopic relations observed in the lavas also suggest that a mantle plume is involved in the magma genesis of northern Arabian lavas enforcing our hypothesis. In summary, the data are consistent with a mainly temperature controlled melting regime that varies from deep mantle melting with low extents of partial melting in northern Arabia to relatively shallower melt formation with larger melt proportions in southern Arabia and Afar.

3.6 Conclusion

The new geochemical and isotope data as well as $^{40}Ar/^{39}Ar$ ages of lavas from the northwestern Arabian plate in Syria and their relation to volcanism along western Arabia and the Afar region demonstrate the far scale influence of the Afar mantle plume to the north. The isotopic record of crustally uncontaminated Syrian lavas implies that asthenospheric, lithospheric and plume mantle sources contribute to their magma genesis, whereby the plume end member can be related to a entrained upper mantle component of the Afar plume containing recycled and enriched material. Variable fractionation corrected SiO_2 contents and REE ratios of crustally uncontaminated Arabian and Afar lavas indicate variations in the extent of melting as well as in

the depths of melt formation varying from relatively shallow but high degree melting in the south to increasingly deeper regions and lower extents of partial melting in the north. This is consistent with a northward directed plume flow regime from the Afar region, where the continuing plume inflow resulted in relatively shallow melt generation accompanied by large extents of melt formation. Further support of this model is given by the age progressive onset of volcanic activity to the north since the arrival of the Afar plume in Ethiopia and Djibouti some 30 Ma ago.

Aknowledgements

This study is part of M.-S.K.´s dissertation and was funded by the Deutsche Forschungsgemeinschaft (DFG) under grant HA 2568/5. We thank H. Baier, H. Blaschek, D. Garbe-Schönberg, K. Kißling, and P. Rengers for their help during the analytical work.

References

Al-Mishwat, A.T. and Nasir, S.J., 2004. Composition of the lower crust of the Arabian Plate: a xenolith perspective. Lithos, 72: 45-72.

Altherr, R., Henjes, K.F. and Baumann, A., 1990. Asthenosphere versus lithosphere as possible sources for basaltic magmas erupted during formation of the Red Sea; constraints from Sr, Pb and Nd isotopes. Earth and Planetary Science Letters, 96: 269-286.

Altherr, R., Henjes-Kunst, F., Puchelt, H. and Baumann, A., 1988. Volcanic activity in the Red Sea axial trough-evidence for a large mantle diapir? Tectonophysics, 150: 121-133.

Baker, J.A. et al., 2000. Resolving crustal and mantle contributions to continental flood volcanism, Yemen; constraints from mineral oxygen isotope data. Journal of Petrology, 41: 1805-1820.

Baker, J.A., Menzies, M.A., Thirlwall, M.F. and Macpherson, C.G., 1997. Petrogenesis of Quaternary intraplate volcanism, Sana'a, Yemen; implications for plume-lithosphere interaction and polybaric melt hybridization. Journal of Petrology, 38: 1359-1390.

Baker, J.A., Snee, L.W. and Menzies, M.A., 1996a. A brief Oligocene period of flood volcanism in Yemen; implications for the duration and rate of continental flood volcanism at the Afro-Arabian triple junction. Earth and Planetary Science Letters, 138: 39-55.

Baker, J.A., Thirlwall, M.F. and Menzies, M.A., 1996b. Sr-Nd-Pb isotopic and trace element evidence for crustal contamination of plume-derived flood basalts; Oligocene flood volcanism in western Yemen. Geochimica et Cosmochimica Acta, 60: 2559-2581.

Barberi, F. et al., 1980. Recent basaltic volcanism of Jordan and its implications on the geodynamic history of the Dead Sea shear zone. In: A. Carrelli (Editor), Geodynamic evolution of the Afro-Arabian rift system. Atti dei Convegni Lincei, Accademia Nazionale dei Lincei. Accademia Nazionale dei Lincei, Rome, Italy, pp. 667-683.

Bertrand, H., Chazot, G., Blichert-Toft, J. and Thoral, S., 2003. Implications of widespread high-μ volcanism on the Arabian Plate for Afar mantle plume and lithosphere composition. Chemical Geology, 198: 47-61.

Best, J.A., Barazangi, M., Al, S.D., Sawaf, T. and Gebran, A., 1990. Bouguer gravity trends and crustal structure of the Palmyride mountain belt and surrounding northern Arabian Platform in Syria. Geology, 18: 1235-1239.

Bohannon, R.G., Naeser, C.W., Schmidt, D.L. and Zimmermann, R.A., 1989. The timing of uplift, volcanism, and rifting peripheral to the Red Sea; a case for passive rifting? Journal of Geophysical Research, 94: 1683-1701.

Brew, G., Barazangi, M., Al-Maleh, A.K. and Sawaf, T., 2001. Tectonic and Geologic Evolution of Syria. GeoArabia, 6: 573-616.

Brew, G. et al., 1997. Basement depth and sedimentary velocity structure in the northern

Arabian platform, eastern Syria. Geophysical Journal International, 128: 617-631.
Butler, R.W.H., Spencer, S. and Griffiths, H.M., 1997. Transcurrent fault activity on the Dead Sea transform in Lebanon and its implications for plate tectonics and seismic hazard. Journal of the Geological Society of London, 154: 757-760.
Camp, V.E. and Roobol, M.J., 1989. The Arabian continental alkali basalt province; Part I, Evolution of Harrat Rahat, Kingdom of Saudi Arabia; with Suppl. Data 89-04. Geological Society of America Bulletin, 101: 71-95.
Camp, V.E. and Roobol, M.J., 1992. Upwelling asthenosphere beneath western Arabia and its regional implications. Journal of Geophysical Research, 97: 15,255-15,271.
Camp, V.E., Roobol, M.J. and Hooper, P.R., 1991. The Arabian continental alkali basalt province: Part II. Evolution of Harrats Khaybar, Ithnayn, and Kura, Kingdom of Saudi Arabia. Geological Society of America Bulletin, 103: 363-391.
Campbell, I.H. and Griffiths, R.W., 1990. Implications of mantle plume structure for the evolution of flood basalts. Earth and Planetary Science Letters, 99: 79-93.
Capan, U.Z., Vidal, P. and Cantagrel, J.M., 1987. K-Ar, Nd, Sr and Pb isotopic study of Quaternary volcanism in Karasu Valley (Hatay), N-end of Dead Sea rift zone in SE-Turkey. Yerbilimleri, 14: 165-178.
Chazot, G. and Bertrand, H., 1993. Mantle Sources and Magma-Continental Crust Interactions During Early Red Sea-Gulf of Aden Rifting in Southern Yemen: Elemntal and Sr, Nd, Pb Isotope Evidence. Journal of Geophysical Research, 98: 1819-1835.
Cochran, J., 1981. The Gulf of Aden: structure and evolution of a young ocean basin and continental margin. Journal of Geophysical Research, 86: 263-288.
Daradich, A., Mitrovica, J.X., Pysklywec, R.N., Willett, S.D. and Forte, A., M, 2003. Mantle flow, dynamic topography, and rift-flank uplift of Arabia. Geology, 31: 901-904.
Deniel, C., Vidal, P., Coulon, C., Vellutini, P.-J. and Piguet, P., 1994. Temporal evolution of mantle sources during continental rifting: The volcanism of Djibouti (Afar). Journal of Geophysical Research, 99: 2853-2869.
du Bray, E.A., Stoeser, D.B. and McKee, E.H., 1991. Age and petrology of the Tertiary As Sarat volcanic field, southwestern Saudi Arabia. Tectonophysics, 198: 155-180.
Duffield, W.A. and Dalrymple, G.B., 1990. The Taylor Creek Rhyolite of New Mexico; a rapidly emplaced field of lava domes and flows. Bulletin of Volcanology, 52: 475-487.
Eissen, J.P. et al., 1989. Petrology and geochemistry of basalts from the Red Sea axial rift at 18 degrees North. Journal of Petrology, 30: 791-839.
El-Isa, Z.H., Mechie, J., Prodehl, C., Makris, J. and Rihm, R., 1987. A crustal structure study of Jordan derived from seismic refraction data. Tectonophysics, 138(2-4): 235-253.
Garbe-Schönberg, C.-D., 1993. Simultaneous determination of thirty-seven trace elements in twenty-eight international rock standards by ICP-MS. Geostandards Newsletter, 17: 81-97.
Gettings, M.E., 1981. A heat flow profile across the Arabian Shield and Red Sea. Eos, Transactions, American Geophysical Union, 62: 407.
Giannerini, G., Campredon, R., Feraud, G. and Abou, Z.B., 1988. Deformations intraplaques et volcanisme associe; exemple de la bordure NW de la plaque Arabique au Cenozoique Translated Title: Intraplate deformation and associated volcanism; example of the northwestern edge of the Arabian Plate during the Cenozoic. Bulletin de la Societe Geologique de France, Huitieme Serie, 4: 937-947.
Girdler, R. and Styles, P., 1974. Two stage Red Sea floor spreading. Nature, 247: 1-11.
Girdler, R.W., 1990. The Dead Sea transform fault system. Tectonophysics, 180: 1-13.
Griffiths, R.W. and Campbell, I.H., 1990. Stirring and structure in mantle starting plumes. Earth and Planetary Science Letters, 99: 66-78.
Guba, I. and Mustafa, H., 1988. Structural control of Young basaltic fissure eruptions in the plateau basalt area of the Arabian Plate, northeastern Jordan. Journal of Volcanology and Geothermal Research, 35: 319-334.
Haase, K.M., Muehe, R. and Stoffers, P., 2000. Magmatism during extension of the lithosphere; geochemical constraints from lavas of the Shaban Deep, northern Red Sea. Chemical Geology, 166: 225-239.
Hart, W.K., WoldeGabriel, G., Walter, R.C. and Mertzman, S.A., 1989. Basaltic Volcanism in Ethiopia: Constraints on Continental Rifting and Mantle Interactions. Journal of Geophysical Research, 94: 7731-7748.
Hegner, E. and Pallister, J.S., 1989. Pb, Sr, and Nd isotopic characteristics of Tertiary Red Sea

Rift volcanics from the central Saudi Arabian coastal plain. Journal of Geophysical Research, 94: 7749-7755.
Heimann, A. and Ron, H., 1993. Geometric changes of plate boundaries along part of the northern Dead Sea Transform; geochronologic and paleomagnetic evidence. Tectonics, 12: 477-491.
Heimann, A., Steinitz, G., Mor, D. and Shaliv, G., 1996. The Cover Basalt Formation, its age and its regional and tectonic setting; implications from K-Ar and $^{40}Ar/^{39}Ar$ geochronology. Israel Journal of Earth-Sciences, 45: 55-71.
Hempton, M.R., 1987. Constraints on Arabian Plate motion and extensional history of the Red Sea. Tectonics, 6: 687-705.
Hirose, K. and Kushiro, I., 1993. Partial melting of dry peridotites at high pressures; determination of compositions of melts segregated from peridotite using aggregates of diamond. Earth and Planetary Science Letters, 114: 477-489.
Hofmann, A.W., Jochum, K.P., Seufert, M. and White, W.M., 1986. Nb and Pb in oceanic basalts; new constraints on mantle evolution. Earth and Planetary Science Letters, 79: 33-45.
Hofmann, C. et al., 1997. Timing of the Ethiopian flood basalt event and implications for plume birth and global change. Nature, 389: 838-841.
Hopp, J., Trieloff, M. and Altherr, R., 2004. Neon isotopes in mantle rocks from the Red Sea region reveal large-scale plume-lithosphere interaction. Earth and Planetary Science Letters, 219: 61-76.
Ilani, S. et al., 2001. New K-Ar ages of basalts from the Harrat Ash Shaam volcanic field in Jordan: Implications for the span and duration of the upper-mantle upwelling beneath the western Arabian plate. Geology, 29: 171-174.
Jarrar, G., Stern, R.J., Saffarini, G. and Al-Zubi, H., 2003. Late- and post-orogenic Neoproterozoic intrusions of Jordan: implications for crustal growth in the northernmost segment of the East African Orogen. Precambrian Reseach, 123: 295-319.
Klein, E.M. and Langmuir, C.H., 1987. Global correlations of ocean ridge basalt chemistry with axial depth and crustal thickness. Journal of Geophysical Research, 92: 8089-8115.
Kumar, M.R., Ramesh, D.S., Saul, J., Sarkar, D. and Kind, R., 2002. Crustal structure and upper mantle stratigraphy of the Arabian shield. Geophysical Research Letters, 29: 83/1 - 83/4.
Le Roex, A.P., Spath, A. and Zartmann, R.E., 2001. Lithospheric thickness beneath the southern Kenya Rift: implications from basalt geochemistry. Contributions to Mineralogy and Petrology, 142: 89-106.
Manetti, P. et al., 1991. Magmatism of the eastern Red Sea margin in the northern part of Yemen from Oligocene to present. Tectonophysics, 198: 181-202.
Marty, B., Pik, R. and Gezahegn, Y., 1996. Helium isotopic variations in Ethiopian plume lavas; nature of magmatic sources and limit on lower mantle contribution. Earth and Planetary Science Letters, 144: 223-237.
McBride, J.H. et al., 1990. Seismic reflection structure of intracratonic Palmyride fold-thrust belt and surrounding Arabian Platform, Syria. AAPG Bulletin, 74: 238-259.
McDonough, W.F. and Sun, S.S., 1995. The composition of the Earth. Chemical Geology, 120: 223-253.
McGuire, A.V. and Bohannon, R.G., 1989. Timing of mantle upwelling; evidence for a passive origin for the Red Sea Rift. Journal of Geophysical Research, 94: 1677-1682.
McKenzie, D. and Bickle, M.J., 1988. The volume and composition of melt generated by extension of the lithosphere. Journal of Petrology, 29: 625-679.
Montelli, R. et al., 2004. Finite-Frequency Tomography Reveals a Variety of Plumes in the Mantle. Science, 303: 338-343.
Mor, D., 1993. A time-table for the Levant volcanic province, according to K-Ar dating in the Golan Heights, Israel. Journal of African Earth Sciences, 16: 223-234.
Mouty, M., Delaloye, M., Fontignie, D., Piskin, O. and Wagner, J.J., 1992. The volcanic activity in Syria and Lebanon between Jurassic and Actual. Schweizerische Mineralogische und Petrographische Mitteilungen = Bulletin Suisse de Mineralogie et Petrographie, 72: 91-105.
Nasir, S., 1994. Geochemistry and petrogenesis of Cenozoic volcanic rocks from the northwestern part of the Arabian continental alkali basalt province, Jordan. Africa Geoscience Review, 1: 455-467.

Nasir, S. and Safarjalani, A., 2000. Lithospheric petrology beneath the northern part of the Arabian Plate in Syria: evidence from xenoliths in alkali basalts. Journal of African Earth Sciences, 30: 149-168.

Notsu, K., Fujitani, T., Ui, T., Matsuda, J. and Ercan, T., 1995. Geochemical features of collision-related volcanic rocks in central and eastern Anatolia, Turkey. Journal of Volcanology and Geothermal Research, 64: 171-192.

Pik, R. et al., 1998. The northwestern Ethiopian Plateau flood basalts: Classification and spatial distribution of magma types. Journal of Volcanology and Geothermal Research, 81: 91-111.

Pik, R., Deniel, C., Coulon, C., Yirgu, G. and Marty, B., 1999. Isotopic and trace element signatures of Ethiopian flood basalts; evidence for plume-lithosphere interactions. Geochimica et Cosmochimica Acta, 63: 2263-2279.

Ponikarov, V.P., Protasevich, L., Maximov, A. and Tkachev, G., 1963. Geological map of Syria 1:200 000. V.O. Technoexport, Russian Federation, Moscow.

Ritsema, J. and Allen, R.M., 2003. The elusive mantle plume. Earth and Planetary Science Letters, 207: 1-12.

Rojay, B., Heimann, A. and Toprak, V., 2001. Neotectonic and volcanic characteristics of the Karasu fault zone (Anatolia, Turkey): The transition zone between the Dead Sea transform and the East Anatolian fault zone. Geodinamica Acta, 14: 197-212.

Sandvol, E. et al., 1998. Lithospheric seismic velocity discontinuities beneath the Arabian Shield. Geophysical Research Letters, 25: 2873-2876.

Schilling, J.G., Kingsley, R.H., Hanan, B.B. and McCully, B.L., 1992. Nd-Sr-Pb isotopic variations along the Gulf of Aden; evidence for Afar mantle plume-continental lithosphere interaction. Journal of Geophysical Research, 97: 10,927-10,966.

Searle, M.P., 1994. Structure of the intraplate eastern Palmyride fold belt, Syria. Geological Society of America Bulletin, 106: 1332-1350.

Sebai, A. et al., 1991. $^{40}Ar/^{39}Ar$ dating of alkaline and tholeiitic magmatism of Saudi Arabia related to the early Red Sea rifting. Earth and Planetary Science Letters, 104: 473-487.

Seber, D. et al., 1993. Upper crustal velocity structure and basement morphology beneath the intracontinental Palmyride fold-thrust belt and north Arabian platform in Syria. Geophysical Journal International, 113: 752-766.

Sengör, A.M.C. and Burke, K., 1978. Relative timing of rifting and volcanism on Earth and its tectonic implications. Geophysical Research Letters, 5: 419-421.

Sharkov, E.V. et al., 1998. New data on the geochronology of upper Cenozoic plateau basalts from the northeastern periphery of the Red Sea Rift area (northern Syria). Doklady Earth Sciences, 358: 19-22.

Sharkov, Y.V. et al., 1994. Geokhronologiya pozdnekaynozoyskikh bazal'tov Zapadnoy Sirii Translated Title: Geochronology of late Cenozoic basalts in western Syria. Petrologiya, 2: 385-394.

Shaw, J.E., Baker, J.A., Menzies, M.A., Thirlwall, M.F. and Ibrahim, K.M., 2003. Petrogenesis of the Largest Intraplate Volcanic Field on the Arabian Plate (Jordan): a Mixed Lithosphere-Asthenosphere Source Activated by Lithospheric Extension. Journal of Petrology, 44: 1657-1679.

Snyder, G.A. et al., 1993. Petrogenesis of garnet pyroxenite and spinel peridotite xenoliths of the Tell-Danun alkali basalt volcano, Harrat as Shamah, Syria. International Geology Review, 35: 1104-1120.

Steiger, R.H. and Jäger, E., 1977. Subcommission on geochronology; convention on the use of decay constants in geo- and cosmochronology. Earth and Planetary Science Letters, 36: 359-362.

Stein, M. and Hofmann, A.W., 1992. Fossil plume head beneath the Arabian lithosphere? Earth and Planetary Science Letters, 114: 193-209.

Stewart, K. and Rogers, N., 1996. Mantle plume and lithosphere contributions to basalts from southern Ethiopia. Earth and Planetary Science Letters, 139: 195-211.

Tarawneh, K. et al., 2000. Dating of the Harrat Ash Shaam Basalts Northeast Jordan (Phase 1). Hashemite Kingdom of Jordan, Natural Resources Authority; Geol. Surv. Isr. Rep. GSI/2/2000: 59.

Taylor, J.R., 1982. An Introduction to Error Analysis. University Science Books, Mill Valley, CA, 270 pp.

Ukstins, I.A. et al., 2002. Matching conjugate volcanic rifted margins; ^{40}Ar / ^{39}Ar chrono-

stratigraphy of pre- and syn-rift bimodal flood volcanism in Ethiopia and Yemen. Earth and Planetary Science Letters, 198: 289-306.
Vidal, P. et al., 1991. Changes of mantle sources in the course of a rift evolution: The Afar case. Geophysical Research Letters, 18: 1913-1916.
Walley, C.D., 1998. Some outstanding issues in the geology of Lebanon and their importance in the tectonic evolution of the Levantine region. Tectonophysics, 298: 37-62.
Watson, S. and McKenzie, D., 1991. Melt Generation by Plumes: A Study of Hawaiian Volcanism. Journal of Petrology, 32: 501-537.
Weinstein, Y., Navon, O. and Lang, B., 1994. Fractionation of Pleistocene alkali-basalts from the northern Golan Heights, Israel. Israel Journal of Earth-Sciences, 43: 63-79.
White, R. and McKenzie, D., 1989. Magmatism at rift zones; the generation of volcanic continental margins and flood basalts. In: W.P. Leeman and J.G. Fitton (Editors), Special section on Magmatism associated with lithospheric extension. Journal of Geophysical Research. American Geophysical Union, Washington, DC, United States, pp. 7685-7729.
York, D., 1969. Least squares fitting of a straight line with correlated errors. Earth and Planetary Science Letters, 5: 320-324.